ENHANCING BIO-PHARMACEUTICAL PROPERTIES OF POORLY SOLUBLE ANTI-MALARIAL DRUGS BY FORMULATING AMORPHOUS FORMS WITH BIOCOMPATIBLE EXCIPIENTS

KUMARAN LETCHMANAN

NATIONAL UNIVERSITY OF SINGAPORE

2015

ENHANCING BIO-PHARMACEUTICAL PROPERTIES OF POORLY SOLUBLE ANTI-MALARIAL DRUGS BY FORMULATING AMORPHOUS FORMS WITH BIOCOMPATIBLE EXCIPIENTS

KUMARAN LETCHMANAN

(B. Eng., UNIVERSITY OF MALAYSIA PAHANG, MALAYSIA)

A THESIS SUBMITTED

FOR THE DEGREE OF DOCTOR OF PHILOSOPHY

DEPARTMENT OF CHEMICAL AND BIOMOLECULAR ENGINEERING

NATIONAL UNIVERSITY OF SINGAPORE

2015

DECLARATION

I hereby declare that this thesis is my original work and it has been written by me in its entirety. I have duly acknowledged all the sources of information which have been used in the thesis.

This thesis has also not been submitted for any degree in any university previously.

Kumaran Letchmanan

5th November 2015

ACKNOWLEDGEMENT

First of all, I would like to take this opportunity to express my sincere gratitude to my supervisor, Prof. Reginald Tan and my co-supervisor, Dr. Shen Shoucang and team leader, Dr. Ng Wai Kiong, for their advice and patient guidance throughout my candidature.

This study has been carried out at the Institute of Chemical and Engineering Sciences (ICES), Agency for Science, Technology and Research (A*STAR), Singapore and supported by the Chemical and Biomolecular Engineering Department, National University of Singapore. I am very grateful for the provision of financial support for this study in the form of the project grant R-279-000-329592 from GlaxoSmithKline (GSK) and the Science and Engineering Research Council of A*STAR, Singapore. I also very much appreciate the guidance from Dr. Keith Carpenter, Executive Director of ICES throughout the candidature. I also like to thank Dr. Simon Black for giving me very useful advice in my research work.

The colleagues and fellow students at the ICES and NUS have been most supportive to me. I would like to extend my gratitude to Dr. Ron Lim Tau Yee and Dr. Kwek Jin Wang for their invaluable support in analytical studies. I also wish to thank Ms. Vanessa Joanne Xavier for her generous assistance in cell culture work. I also like to thank Mr. Jose Varghese Parambil, my wife, Rajaletchumy and my family members for their constant help and support.

TABLE OF CONTENTS

SUMMARY

Oral administration is one of the most common and preferred route of drug delivery due to easy administration, manufacturing flexibility and cost-effectiveness. However, the bioavailability and clinical efficacy of oral dosage forms can be hampered by the poor aqueous solubility and dissolution of their drug content, especially for those drugs listed under the Biopharmaceutical Classification System (BCS) Class II. Enhancing the solubility of poorly water-soluble drugs is an important challenge encountered by pharmaceutical companies. In formulation, the amorphization of crystalline compounds via formulation of solid dispersions using mesoporous carriers and transglycosylated food additives have been applied to enhance the dissolution rate and aqueous solubility of poorly water-soluble drugs.

This thesis focuses on formulating amorphous solid dispersions to enhance the biopharmaceutical properties of two antimalarial drugs widely used in artemisinin-based combination therapies (ACTs): artemisinin (ART) and mefloquine (MFQ). Since ART is a vital component in ACTs, priority has been given to the formulation of ART solid dispersions. All the carriers were preliminarily tested with ART to identify suitable excipients and to optimize storage conditions. The carrier that exhibited a superior performance in improving the biopharmaceutical properties with adequate storage stability was then used to formulate the solid dispersion of MFQ and followed by combination of ART/MFQ.

Solid dispersions of ART were prepared by using porous activated carbon (AC), mesoporous silica (SBA-15), α-glucosyl hesperidin (Hsp-G) and α-glucosyl stevioside (Stevia-G) via co-spray drying. The characterization of the powder samples entailed analysis of surface area and pore volume analyzer (BET), thermogravimetric analysis (TGA), differential scanning calorimetry (DSC), powder X-ray diffractometry (PXRD), scanning electron microscopy (SEM) and transmission electron microscopy (TEM). The drug release profiles were investigated by using flow-through cell (USP IV) and *in vitro* dissolution tester (USP II). The physicochemical stability of the samples was investigated for 6-months under various storage conditions: desiccators (25 °C/18% RH), Activ-vial® (25 °C), open pan (25 °C/75% RH), Activ-vial® (40 °C) and open pan (40 °C/75% RH). In addition, the biocompatibility of SBA-15 was investigated by *in vitro* cytotoxicity study using Caco-2 cells after 24-hours incubation.

The formulated amorphous samples exhibited an enhanced dissolution rate and supersaturation as compared with untreated drugs. Interestingly, ART formulated with the functionalized food additives showed an initial burst with approximately 100% of drug release within 5 min. Although ART formulated with mesoporous materials showed slower dissolution as compared with ART formulated with functionalized food additives, the dissolution rate is nonetheless superior to that of untreated drugs. On the other hand, AC/ART was unable to provide acceptable chemical stability during storage periods. Meanwhile, ART formulated with SBA-15 and food additives exhibited better storage stability for 6-months, except under extreme conditions of 40 ºC or

75% RH. Moreover, the results of cytotoxicity with more than 90% of cell survival rate indicated good biocompatibility of SBA-15 and ART/SBA-15 formulations. Additionally, SBA-15 exhibited better drug loading capacity as compared with food additives. The drug loading of SBA-15 reached as high as 50 wt% with retention of the amorphous drug form whereas only 9.1 wt% drug loading for Hsp-G and Stevia-G. Thereafter, SBA-15 with superior performance compared with other carriers as regards drug loading, drug release and stability was chosen as the carrier to formulate solid dispersions of ART and MFQ. Moderate storage conditions such as desiccators (25 °C/18% RH) and Activ-vial® (25 °C) were used for stability tests, in which formulation with SBA-15 was expected to have good physicochemical stability.

In conclusion, this work has demonstrated the potential applications of mesoporous materials and functionalized food additives in amorphization and stabilization of poorly water-soluble antimalarial drugs (ART and MFQ) through spray drying. This study could provide a practical reference in evaluating the *in vitro* drug behaviors and in elucidating the physicochemical stability of ART and ART/MFQ combination, which have rarely been reported.

NOMENCLATURE

Symbol	Description
C_b	Concentration of compound in the bulk medium
C_s	Saturated solubility of the compound at the particle–media interface
D	Diffusion coefficient of the compound in the medium
H	Hour
Min	Minute
M	Mass of compound dissolved in time t
P_c	Supercritical pressure
S	Surface area
S_{BET}	BET Specific surface area
T_m	Melting point
T_g	Glass transition temperature
T_c	Supercritical temperature
V_{pore}	Total pore volume
A	Specific surface area

Greek letters	Description
2θ	2-Theta scale
P	Density
B	Beta
A	Alpha
pKa	Acid dissociation constant
log *P*	Partition coefficient

ABBREVIATION

Abbreviation	Description
AC	Activated carbon
ACT	Artemisinin-based combination therapy
API	Active pharmaceutical ingredient
ART	Artemisinin
ASES	Aerosol solvent extraction system
BET	Brumauer-Emmett-Teller
BJH	Barrett-Joyner-Halenda
BCS	Biopharmaceutical Classification System
CD	Cyclodextrin
CMC	Critical micelle concentration
DMEM	Dulbecco's Modified Eagle Medium
DOSY	Diffusion-ordered spectroscopy
DSC	Differential scanning calorimetry
e.g.	Exempli gratia (for example)
EPN	Evaporative precipitation of nanosuspension
et al.	Et alia (and others)
FDC	Fixed-dose combination
FOMC	Fibrous ordered mesoporous carbon
GAS	Gas antisolvent precipitation
GI	Gastrointestinal
HIV	Human immunodeficiency virus
HPH	High-pressure homogenization
HPLC	High performance liquid chromatography

ICH	International Conference on Harmonization
i.e.	Id est (that is)
IUPAC	International Union of Pure and Applied Chemistry
KFC	Karl Fisher Coulometric
LEI	Lower electron image
MCM-41	Mobil Composition of Matter No. 41
MFQ	Mefloquine
NCEs	New chemical entities
PBS	Phosphate buffered saline
PCA	Precipitates by compressed antisolvent
PEG	Polyethylene glycol
PLH	Pranlukast hemihydrate
P.M.	Physical mixture
PRR	Parasite reduction ratio
PVP	Polyvinylpyrrolidone
PXRD	Powder X-ray Diffraction
RESS	Rapid expansion of supercritical solutions
RH	Relative humidity
SAS	Supercritical antisolvent
SBA-15	Santa Barbara Amorphous 15
S.D.	Standard deviation
SDS	Sodium dodecyl sulphate
SEDS	Solution enhanced dispersion by supercritical fluids
SEI	Secondary electron imaging
SEM	Scanning electron microscopy
SP	Sulphadoxine-pyrimethamine

TBA	Tertiary butanol
TEOS	Tetraethyl orthosilicate
TEM	Transmission electron microscopy
TGA	Thermogravimetric analysis
UMCS	Uniform mesoporous carbon spheres
WHO	World Health Organization

LIST OF FIGURES

LIST OF TABLES

Chapter 1 Introduction

1.1 Research Background

Oral administration is one of the most common and preferred routes of drug delivery due to easy administration, manufacturing flexibility and cost-effectiveness (Bobe et al., 2011, Savjani et al., 2012, Saharan et al., 2009). However, the bioavailability and clinical efficacy of oral dosage forms are mainly hampered by their poor aqueous solubility and dissolution, especially for those active pharmaceutical ingredients (APIs) listed under the Biopharmaceutical Classification System (BCS) class II (Skolnik et al., 2010, Heng et al., 2010, Shono et al., 2010). The solubility of BCS class II drugs in gastric and intestinal fluids plays a vital role in determining their bioavailability and therapeutic effects, since these drugs have a good absorption and permeation across the intestinal lumen (Ahuja et al., 2007, Uchiyama et al., 2010a). The administrated APIs need to be dissolved in the gastrointestinal tract in order to be absorbed across the intestinal mucosa and reach the circulatory system. Limited solubility of APIs may result in insufficient and variable absorption, which will lead to unacceptable bioavailability and inadequate clinical efficacy (Limnell et al., 2011a).

Contemporary approaches to drug discovery and development have caused an increase in the number of poorly water-soluble drug candidates in the past few decades (Lipinski et al., 1997, Van Speybroeck et al., 2009). In today's market, approximately 40% of the drugs listed under the U.S.

Pharmacopoeia and 50% of the new chemical entities (NCEs) suffer from poor bioavailability due to low aqueous solubility, since the solubility is a deciding factor for *in vivo* absorption (Ahuja et al., 2007, Shen et al., 2010). The extremely low water-solubility of drugs often necessitate the application of high doses of APIs in order to achieve a desired therapeutic plasma concentration (Tozuka et al., 2011), which may concomitantly lead to side effects such as gastric discomfort, nausea, vomiting and dizziness (Shen et al., 2010). Endeavors to enhance the solubility of these therapeutic agents are associated with rapid drug absorption, which eventually improves the bioavailability and reduces clinically relevant doses (Sugano et al., 2007, Sigfridsson et al., 2009, Van Eerdenbrugh et al., 2010).

Numerous pharmaceutical formulation techniques have been employed to overcome the delivery barriers of BCS class II drugs, including modification of the crystal forms (Singh et al., 2010, Lim et al., 2012), complexation (ElShaboury, 1990, Cserháti et al., 1996, Jiang et al., 2012b, Pitha et al., 1986, Sigurðoardóttir and Loftsson, 1995), solubilization by surfactants (Bajaj et al., 2011, Singh et al., 2010), micro- and nano-sizing (da Costa et al., 2012, Gupta and Sehrawat, 2011, Rasenack et al., 2003), nanoemulsions (Kotta et al., 2012), co-crystallization (Shiraki et al., 2008), polymeric micellations (Kutty and Feng, 2013), liposomes (Chen et al., 2009) and co-solvency (Singh et al., 2010, Vemula et al., 2010). To date, however, the number of simple and effective oral formulations of BCS class II drugs developed using the above techniques that have achieved marketed

applications is limited. Therefore, it is essential to explore new types of formulation approaches with market values.

Among these techniques, more attention is given to amorphization to circumvent the problem of poor aqueous solubility and slow dissolution rate of water-insoluble drugs (Paudel et al., 2013). The amorphous forms possesses improved wettability (Liu et al., 2010b) and reduced particle size (Gupta and Sehrawat, 2011), which increases the total surface area per unit volume of drug particles exposed to the dissolution medium compared with the corresponding crystalline forms (Sharma and Jain, 2011). Furthermore, the active sites of drug molecules which would strongly interact with each other in a crystalline structure would be exposed to the environment in amorphous particles. Therefore, the binding energy between molecules in amorphous particles is relatively weak, necessitating minimum energy to break them. This confers upon the amorphous form a higher solubility and dissolution rate than the crystalline form (Yoshioka and Aso, 2007).

Unfortunately, amorphization may lead to poor physicochemical stability of the drug molecules over the designated shelf-life. This can affect the biopharmaceutical properties and the performance of the amorphous drugs, especially during the administration, processing and storage periods (Zhang et al., 2009a). In drug development, physical and chemical stability is a vital factor that determines the success of any drug candidate and is influenced by factors such as molecular mobility, particle size, temperature, humidity and

pH. Therefore, formulating dosage form with an acceptable shelf-life is a major challenge faced during amorphization process.

The confinement of drugs in mesoporous carriers via spray drying is considered as one of the most effective techniques to enhance the supersaturation and physical stability of poorly water-soluble drugs. Pore size, pore topology and surface interactions are the most important parameters that can change the thermodynamics and crystallization kinetics of amorphous drugs to improve their physical stability (Rengarajan et al., 2008). For example, it is feasible to form amorphous drugs if the ratio of pore diameter to the molecular size of an API is not more than 20 (Sliwinska-Bartkowiak et al., 2001) and the re-crystallization of amorphous particles can be completely suppressed if the pore diameter of a carrier is lower than a certain critical pore diameter (Prasad and Lele, 1994). In addition, immobilization of drug molecules on the surface of pore walls due to a strong interaction (hydrogen bonds) between drug molecules and pore walls can lower the crystallization kinetics of amorphous drugs (Arndt et al., 1997).

Since Vallet-Regi et al. (2000) used MCM-41 as a novel drug delivery system, there has been growing interest in employing mesoporous materials especially mesoporous silica in drug delivery systems. Statistics show that over 3400 research papers related to mesoporous and drug delivery have been published in the Web of Science up to 2014, thereby illustrating the importance of the mesoporous materials in medical applications. Kinnari et al. (2011) compared the performance of different mesoporous silicon (between

thermally oxidized and thermally carbonized) and non-ordered mesoporous silica (between Syloid AL-1 and Syloid AL-244) as drug carriers for a hydrophobic drug, itraconazole. The effect of surface chemistries, pore volumes, surface areas and particle sizes of the mesoporous carriers on the degree of drug loading, dissolution behavior and physicochemical stability of itraconazole was investigated. Furthermore, Limnell et al. (2011b) performed a similar study using ordered and non-ordered mesoporous silica to evaluate the loading efficiency and the rate of drug release of indomethacin by comparing three drug loading methods: immersion, rotavapor and fluid bed loading. The results showed that the drug release properties of the delivery system were affected by the pore size and particle size of mesoporous silica. Moreover, surface modification of mesoporous materials played a significant role in altering the mechanism of drug release. Zeng et al. (2005) reported organic modification of MCM-41 with aminopropyl groups via solvothermal process for controlling drug delivery of aspirin. The release properties of this delivery system were found to be a function of the quantity of aminopropyl groups on the pore walls and of the ordered structure of mesoporous materials.

Among the diverse mesoporous materials, SBA-15 synthesized by non-ionic polymer surfactants has attracted much attention as a drug delivery matrix for both rapid and controlled release (Rahmat et al., 2010, Limnell et al., 2011a). The growing interest in this material for drug delivery is mainly due to its important features such as uniform pore size distribution, tunable pore diameter, thick pore walls, large pore volume and specific surface area enriched with silanol groups (Van Speybroeck et al., 2009, Mellaerts et al.,

2010). The ordered mesoporous structures of SBA-15 that can be adjusted in the range of 5−30 nm allow encapsulation and release of larger drug molecules in a more reproducible and predictable manner compared with microporous materials, which can only adsorb small molecules up to 2 nm (Rahmat et al., 2010). Moreover, the large pore volumes (0.8–1.3 cm^3/g) and specific surface areas (600–1000 m^2/g) of SBA-15 are essential for drug delivery as these features enable stronger adsorption with greater drug loading (Van Speybroeck et al., 2009, Limnell et al., 2011a). It has been reported that the drug loading of SBA-15 can reach up to 50% (w/w) with the drug particles remaining in an amorphous form (Shen et al., 2010, Shen et al., 2011). The higher payload of drug is critical to minimize the wastage of matrix and to reduce the size of formulations. The silanol functional groups on the surface of pore walls of silica are useful in immobilizing the drug molecules through hydrogen bonds. Thus, SBA-15 microparticles can potentially provide better encapsulation and immobilization of drug molecules and play a profound role in providing physical stability to the amorphous drugs.

Limnell et al. (2011a) studied ordered mesoporous silica MCM-41 and SBA-15 microparticles as devices for the delivery of indomethacin. The physicochemical stability of indomethacin-loaded MCM-41 and SBA-15 samples was investigated after three-months of storage at 30 °C and 56% RH. The drug release studies were performed using USP dissolution paddle method at pH 1.2 and 6.8, mimicking gastrointestinal fluids. Although the physical stability of the samples was found to be satisfactory and rapid drug release was observed after storage, some impairment was observed in their chemical

stability. Shen et al. (2010) investigated the mesoporous SBA-15 submicron particles as a drug delivery system to enhance the dissolution properties and physical stability of ibuprofen and evaluated the drug release profile of the formulated ibuprofen in powder and tablet forms. No significant difference between these two forms was observed and the release profiles exhibited a pronounced initial burst release of 100% and outstanding stability when subjected to stress test conditions of 40°C/75% RH in open pans for 12-months. Meanwhile, Van Speybroeck et al. (2009) scrutinized the dissolution enhancement of 10 poorly water-soluble compounds using SBA-15. The physical stability of the samples was analyzed using differential scanning calorimetry (DSC) after being stored at 25°C/52% RH for 6-months. All the SBA-15 formulations present in amorphous form showed enhanced dissolution compared with their crystalline counterparts. Importantly, the enhanced pharmaceutical performance of all the formulations was retained during the 6-months storage period. These results suggest that SBA-15 can be applied as a promising carrier to enhance the biopharmaceutical properties of a variety of poorly soluble drugs.

Apart from mesoporous silica, activated carbon is another attractive and versatile porous material that can be used as a drug carrier. Activated carbon is an industrially available cost-effective porous carrier that can be synthesized on a large scale and has been used extensively in drug delivery systems, especially for oral administration. Porous carbon has attracted as much attention as mesoporous silica, due to its highly ordered structures, large pore volume, extended specific surface area, strong adsorption capacity and

tunable pore diameters, which are capable of extensive drug loading (Wang et al., 2011a, Zhao et al., 2012a, Zhao et al., 2012b). Typically, the conventional activated carbon has specific volume and surface area in the range of 0.1–0.5 cm^3/g and 10–2000 m^2/g, respectively (Hu and Srinivasan, 2001). Additionally, activated carbon possesses special features like low density, high thermal conductivity, good electrical conductivity, mechanical stability and ease of handling (Zhu et al., 2011, Wang et al., 2011b). As compared with mesoporous silica, porous carbon is highly tolerant to an aqueous environment, more resistant to structural changes by hydrolytic effects and chemically stable under non-oxidizing conditions (Zhu et al., 2011). Moreover, carbon materials are generally considered as inert substances that are safe and nontoxic (Zhao et al., 2012a, Zhao et al., 2012b).

Niu et al. (2013) evaluated the applicability of mesoporous carbon as a novel drug carrier to enhance the dissolution and bioavailability of fenofibrate intended for oral administration. Mesoporous carbon was synthesized by the co-assembly of phenol resin, TEOS and Pluronic F127, followed by carbonization and silica removal. Fenofibrate was loaded onto mesoporous carbon using incipient wetness impregnation and solvent and melting methods. Besides enhancing the dissolution rate, mesoporous carbon was found to improve the oral bioavailability of the drug without any irritation to the intestinal mucosa compared with fenofibrate commercial capsules. Wang et al. (2011b) synthesized magnetic Fe-containing mesoporous carbon through incipient wetness impregnation method without using any solvent. Investigation of the release behavior from the material demonstrated that the

release rate of ibuprofen increased with the degree of loading. It is evident that there are advantages of activated carbon in various applications compared with other porous materials. However, to the best of our knowledge, very few studies have reported the improvement of dissolution rate and bioavailability of poorly water-soluble drugs using porous carbon as a vehicle.

Besides mesoporous materials, formulations of amorphous solid dispersions using transglycosylated food additives have recently attracted much attention, since these pharmaceutical excipients are relatively safe and cost-effective (Uchiyama et al., 2010b, Uchiyama et al., 2010a). Among them, α-glucosyl hesperidin (Hsp-G) and α-glucosyl stevioside (Stevia-G) are particularly noteworthy as potential drug carriers, considering their high solubility augmented by transglycosylation (Kometani et al., 1996, Kometani et al., 1999, Kometani et al., 2008). Hsp-G is the transglycosylation product of hesperidin (a flavonoid also referred to as vitamin P in citrus fruits), of which the solubility is improved by 300 fold (approximately 0.2 kg/L) compared with that of the original hesperidin. It is used as a drug carrier due to its unique properties such as its superior solubility and the absence of toxicity to Caco-2 cells (Uchiyama et al., 2010a, Tozuka et al., 2011). Moreover, it has significant anti-inflammatory, hypotensive and analgesic effects (Uchiyama et al., 2010b). On the other hand, Stevia-G is the transglycosylation product of Stevia, (a herb belonging to the *Compositea* family) (Uchiyama et al., 2010b), of which the solubility is estimated to be approximately 3.2 kg/L. Stevia-G has been used as a sweetener and sugar substitute for more than 20 years [Uchiyama et al., 2010b]. It has also been reported to have the ability to

regulate blood glucose levels of rats by enhancing insulin secretion (Chen et al., 2005).

Numerous studies have been published on the applications of Hsp-G and Stevia-G as potential drug carriers with an impressive improvement in dissolution rates and supersaturation. For example, Uchiyama et al. (2010b) found that treatment of two poorly water-soluble drugs, flurbiprofen and probucol, with Hsp-G and Stevia-G contributed to elevated dissolution rates (up to 3 fold and 1000 fold respectively compared with the untreated drugs) and thereby enhanced bioavailability. Tozuka et al. (2011) investigated the application of Hsp-G in nanoparticle formation of glibenclamide by dry grinding in a vibrational ball mill. The effectiveness of the ground mixtures were analyzed by *in vitro* and *in vivo* studies. The formulated glibenclamide/Hsp-G nanoparticles exhibited marked improvement in the dissolution profile and a significantly higher rate of decline in blood glucose levels of rat compared with untreated glibenclamide. Uchiyama et al. (2011b) demonstrated the ability of Hsp-G to improve both the dissolution and absorption properties of pranlukast hemihydrate (PLH) using high-pressure homogenization (HPH) processing without using organic solvent. Compared with untreated PLH crystals, HPH-processed PLH/Hsp-G (1:10 w/w) exhibited enhancement in the following parameters: a 2.5-fold increment for apparent solubility and 3.9-fold for C_{max}.

Artemisinin (ART), also known as *qinghaosu*, is a BCS class II drug with low solubility and high permeability which used in malarial treatment

(Shahzad et al., 2012). This antimalarial drug was selected as the model compound for the first part of the research, in which ART was formulated with mesoporous materials and with functionalized food additives. To the best of our knowledge, there have hitherto been no reports on the application of these two types of carriers for antimalarial drugs. Pharmacologically, ART possesses the most rapid action against *Plasmodium falciparum* and *Plasmodium vivax* (Shahzad et al., 2012, Sahoo et al., 2010). It has a worldwide demand and is recommended by the World Health Organization, due to its low toxicity and high efficiency in attacking malaria parasites, such as multidrug resistant and cerebral strains (Ngo Thu et al., 1996, Thu Hoa et al., 1997, Ferreira et al., 2013). However, ART suffers from a number of drawbacks such as poor solubility and a short half-life. The poor solubility of ART in water (48 µg/mL at 37°C) and blood (Shahzad et al., 2012, Ferreira et al., 2013, Sahoo et al., 2011b) translates into poor bioavailability despite the excellent permeability across intestinal membranes. The short half-life and high first pass metabolism of ART may also cause incomplete clearance of malaria parasites (Sahoo et al., 2011b). In order to address these problems, several techniques have been discovered to improve the performance and the efficiency of ART, especially for enhancing the solubility and bioavailability. Sahoo and coworkers reported the dissolution enhancement of ART by using modified multi-fluid nozzle pilot spray dryers (Sahoo et al., 2011a, Kakran et al., 2011), with maltodextrin (Sahoo et al., 2009), polyethylene glycol (PEG) and polyvinylpyrrolidone (PVP) as hydrophilic carriers (Sahoo et al., 2010, Sahoo et al., 2011b). Van Nijlen et al. (2003) used supercritical fluid

technology with PVPK25 as a excipient whereas Wong and Yuen (2001) used β-cyclodextrin and γ-cyclodextrin to formulate solid dispersion of ART. All these formulations of solid dispersions have shown remarkable results in solubility enhancement compared with untreated ART crystals. Even though a number of studies have reported the solubility enhancement of ART, based on our knowledge, no studies have hitherto been published regarding the physicochemical stability of the amorphous solid dispersions of ART.

MFQ (IUPAC nomenclature: R, S-erythro-et-2-piperidyl-2, 8-bis (trifluoromethyl)-4 quinolinemethanol hydrochloride) is a 4-quinolinemethanol derivative. It is an orally administrated antimalarial drug, which is a highly effective against multidrug-resistant strains of *Plasmodium* species (Rao and Murthy, 2002). It was used as the model drug to co-formulate solid dispersions with ART and a selected carrier for combination therapy in the second part of this study. MFQ is slightly soluble in water (1.8 mg/mL) at room temperature and highly lipophilic (log P = 3.9), leading to variation in oral absorption. MFQ is a weak base with pKa of 8.6 and classified as a BCS class II or IV drug because of its low solubility and the lack of permeability data (Strauch et al., 2011, Lindenberg et al., 2004). Yadav et al. (2010) investigated the effects of co-crystallization on the physicochemical properties of MFQ. Different types of co-crystals exhibited augmented dissolution rate and supersaturation with adequate physical stability for 6-months of storage at 30 °C/65% RH. du Plessis et al. (2014) reported an improved therapeutic index with decreased toxicity and unchanged

in vivo bioavailability by incorporating MFQ with a lipid-based drug delivery system using Pheroid vesicles.

Both the drugs are BCS class II antimalarial drugs widely used in artemisinin-based combination therapies (ACTs). ART, despite its short half-life, possesses a rapid action, which is vital to the initial anti-parasite effect against *Plasmodium* whereas MFQ, despite its slow action, possesses a long half-life, which is vital to preventing recurrence and resistance against the antimalarial drugs (White, 2004). ART has been combined with naphthoquine as a product called ARCO® whereas MFQ has been combined with artesunate as a product called *Artequin*™. However, no single commercial products contain the combination of ART and MFQ.

To the best of our knowledge, only a very limited number of reports on the *in vitro* dissolution and solubility enhancement of antimalarial drugs have been published. In addition, no study on these aspects of ACTs using mesoporous carriers has been reported. More details on ACTs will be provided in Section 2.2.

All the solid dispersions of ART and MFQ were formulated via spray drying due to the advantages of this technique compared with other drug loading techniques. Spray drying is a single-stage process that produces solid dispersions in a dry and powdered form. The use of spray drying therefore reduces the mass and energy consumption by minimizing secondary manufacturing steps such as micronization and milling (Boersen, 1990, Ameri

and Maa, 2006). More details about the applications and important features of spray dying will be provided in Section 2.7.2.3.

1.2 Hypothesis and Research Objectives

It is hypothesized that both the mesoporous carriers and functionalized food additives are able to amorphize the crystalline ART and MFQ by encapsulating them during co-spray drying. The amorphization with a reduction in particles size is expected to enhance the drug release profile of the drugs. In addition, these carriers are also expected to confer acceptable physicochemical stability to the amorphous forms.

This thesis focuses on formulating amorphous solid dispersions to enhance the biopharmaceutical properties of two widely used antimalarial drugs for ACTs. The amorphization of these drugs was achieved by encapsulating the drug particles in porous and/or biocompatible carriers via co-spray drying. The excipients used include two mesoporous carriers (activated carbon and SBA-15) and two functionalized food additives (Hsp-G and Stevia-G). Since ART and ART derivatives are vital components in ACTs, priority has been given to the formulation of ART solid dispersions. The carriers were first tested with ART to identify suitable excipients and optimal storage conditions. This was followed by the formulation of solid dispersions of the ART/MFQ drug combination. The objectives of this research are as follows:

I. To formulate amorphous solid dispersions of ART and ART/MFQ combination drugs and to identify suitable carriers for dosage forms.

II. To enhance the biopharmaceutical properties such as aqueous solubility, dissolution rate and physicochemical stability of the formulated solid dispersions.

III. To develop a suitable method and identify optimal storage conditions to stabilize the amorphous solid dispersions of ART and MFQ.

IV. To elucidate the physicochemical properties of the formulated solid dispersions.

1.3 Organization of Thesis

This thesis comprises of nine chapters. Chapter 1 provides a brief introduction and research background of formulation of solid dispersions for oral drug delivery systems, especially on improving the dissolution rate of poorly water-soluble drug via nano-confinement by using mesoporous carriers and via encapsulation into functionalized food additives. Therein, the objective of our research work is defined.

Chapter 2 can be separated into 2 sections; the first section outlines a brief literature review about malaria including life cycle of malaria parasites, complications of malaria, current challenges in malaria treatments and ACTs. The second section outlines the current challenges in drug development and oral delivery systems. It also includes recent approaches to enhance the dissolution rate of poorly water-soluble drug such as micronization, inclusion

complexation, solubilization by surfactants and modification of the crystal forms; and formulation strategies including hot-melt extrusion, lypophillization and supercritical fluid and spray drying.

Chapter 3 describes the material and experimental procedures used in this study. The synthesis of mesoporous silica via hydrolysis is was summarized. The formulation methods including spray drying, physical mixture, cryo- and ball-milling employed to generate solid amorphous forms were outlined. It also includes different types of characterization procedures, *in vitro* drug release, physicochemical stability evaluation and cytotoxicity study.

Chapter 4 and Chapter 5 present experimental results and discussion of the ability of mesoporous materials as drug carriers to enhance the solubility and storage stability of ART. Chapter 6 describes the formulation of solid dispersions of ART using functionalized food additives as carriers whereas Chapter 7 introduces the biopharmaceutical enhancement work of ACTs by using SBA-15, ART and MFQ.

Conclusions are drawn in Chapter 8 to summarize all the important results presented in the preceding chapters and future research work of this PhD is recommended in Chapter 9. A list of publications stemming out from this study and achievements are given in Appendices.

Chapter 2 Literature Review

2.1 Malaria

Parasitic infections remain one of the major causes of mortality in many tropical and subtropical areas around the globe. Among the different species of parasites, the parasitic protozoan belonging to the genus *Plasmodium* causes the vector-borne infectious disease, malaria. Malaria is the most important parasitic disease and biggest infectious killer of human beings (Ridley, 2002). It is a major public health and economic burden in third-world countries and has therefore become a tropical disease of the first priority for the World Health Organization (WHO) (Ridley, 2002, Snow et al., 2005, Yang et al., 2011, Liu et al., 2010a). Malarial infections in human beings are caused by five species of the genus *Plasmodium*; most cases are caused by either *P. falciparum* or *P. vivax* and the rest of the infections caused by caused by *P. ovale*, *P. malariae* and *P. knowlesi* (Trampuz et al., 2003, Kantele and Jokiranta, 2011). *P. falciparum* is the most virulent and lethal form that is responsible for the most serious form of the disease and fatal cases, resulting in rapid deterioration of the patient's condition with concomitant development of life-threatening complications (De Donno et al., 2012, Guerin et al., 2002). Malaria is transmitted in 97 countries inhabited by roughly 3.3 billion people, of whom 1.2 billion are from Africa and Southeast Asia. Approximately 500 million clinical cases and 2–3 million of death cases are reported annually, accounting for about 4–5% of total fatalities in the world. More than 81% of malaria cases and 91% of malaria deaths occur in Africa, wherein most

victims are children under 5 years of age and pregnant women (Yaméogo et al., 2012, Wells et al., 2013). The severity of the situation is reflected in the estimation that one person (usually a child) dies every 12 s as a consequence of this infection (Ajibade and Kolawole, 2008, Marconi et al., 2004). In the following sections, symptoms of disease and the treatment methods are discussed.

2.1.1 Life Cycle of *Plasmodium Falciparum*

Malaria is transmitted to humans by the bite of infected female *Anopheles* mosquitoes (the definitive host) while feeding on human blood (Cloete et al., 2012). The life cycle of *P. falciparum* is provided in Figure 2.1.

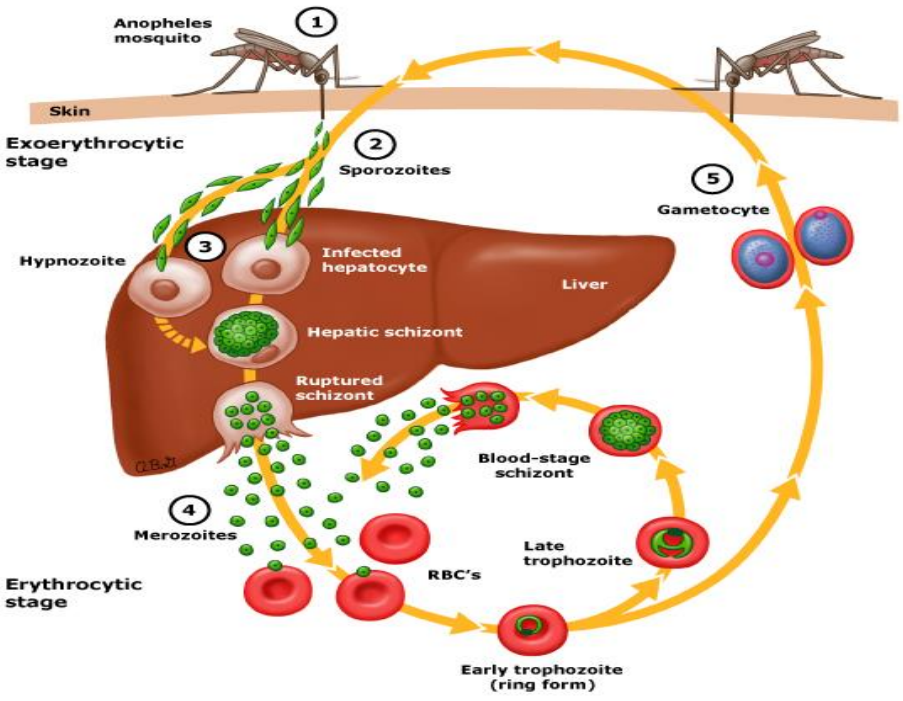

Figure 2.1 Lifecycle of *P. falciparum* in the human host and in the *Anopheles* mosquito (Breman J.G. et al., 2014).

The asexual stage of the cycle begins when microscopic motile infective forms of sporozoites in the saliva of the mosquitoes are inoculated into the bloodstream of a vertebrate host such as a human. Within days, the sporozoites travel through the blood vessels, enter hepatocytes and begin to divide asexually into thousands of exoerythrocytic merozoites (tissue schizogony). For *P. vivax* and *P. ovale* infections, some schizonts may remain dormant as hypnozoites in the liver for-weeks to years (depending on the geographic origin) before causing clinical relapses that characterize these infections; for *P. falciparum,* no such hypnozoites are produced. Once the merozoites leave the liver, they invade erythrocytes and develop into early trophozoites, which are ring-shaped, vacuolated and uninucleated. Upon division, the trophozoites are called schizonts, consisting of many daughter merozoites (blood schizogony). Eventually, infected erythrocytes are lysed, releasing the merozoites into the bloodstream, which subsequently invade other erythrocytes; thus the infective cycle of schizogony begins anew. The duration of each cycle is about 48 hours for *P. falciparum*, *P. vivax* and *P. ovale*, 72 hours for *P. malariae* and 24 hours for *P. knowlesi* (White et al., 2014). In non-immune humans, the infection is amplified by about 20-fold each cycle (Simpson et al., 2002). After several cycles, some of the merozoites develop into the non-multiplying and longer-life sexual form (immature gametocytes), which are the precursors of male and female gametes and cause no symptoms, but are infective for mosquitoes. These gametocytes are crucial for perpetuating the life cycle of the parasite. When a fertilized female mosquito bites an infected person, the gametocytes are taken up by it and thereafter

reproduce sexually, forming ookinete and then oocyst in the mosquito midgut. The oocyst bursts and liberates thousands of infective sporozoites, which migrate to the insect's salivary glands to await inoculation of the next vertebrate host to initiate another life cycle. The entire cycle can take roughly 1-month (White et al., 2014, Greenwood et al., 2005).

2.1.2 Complications of Malaria

The clinical symptoms of malaria are primarily due to the rupture of schizonts and the destruction of erythrocytes. Illness starts when the number of total asexual parasites in the circulation reaches approximately 100 millions. Malaria can have a gradual or fulminant course with nonspecific symptoms (Murphy and Oldfield, 1996). Usually the symptoms for malaria infections appear within 8 to 25 days after the mosquito bite (possibly longer in the case of a patient who has taken antimalarial prevention medication). The presentation of malaria often resembles those of common viral infections, potentially leading to delayed diagnosis. The majority of patients experience fever, chills, headaches and diaphoresis; other common symptoms include back and muscular pain, dizziness, malaise, myalgia, convulsion, abdominal pain, hemoglobin in the urine, nausea, vomiting, jaundice, mild diarrhea and dry cough. Clinical assessment also depends on signs such as tachycardia, jaundice, pallor, orthostatic hypotension, hepatomegaly and splenomegaly (Taylor et al., 2010, Malaria, 2014).

Serious complications of malaria may still develop notwithstanding clinical responses to initial treatment and eradication of parasitemia, due to

delayed cytokine release. Patients with severe malaria should be treated in an intensive care unit. Some of the example of the complications in patients with severe malaria are hypoglycemia, hypotension and shock, hematologic abnormalities (Trampuz et al., 2003) as well as neurologic (Warrell et al., 1982, Brewster et al., 1990), pulmonary (Gachot et al., 1995) and renal (Prakash et al., 1996) complications

Though malaria is a major cause of death, for which the number of mortalities is as high as that for human immunodeficiency virus (HIV) infections, effort and financial resources allocated to the research on malaria is much lower compared with that on HIV infections. For example, in 2013, malaria-associated deaths totaled up to approximately 1 million whereas HIV-associated deaths totaled up to 1.5 million. However, the money spent on malaria research was $US42 per malaria-associated death compared $US3270 per HIV/AIDS-associated death. The reason for the scant attention or interest devoted to the research on malaria is that the infection is predominantly localized in poor countries (Nosten and Brasseur, 2002). In addition, the cost of the treatment is another major problem in treating malaria. The complete diagnosis and treatment of malaria costs about $US2 to 3 per patient, which will be financially untenable for African countries considering that the expenditure per person for health is only around $US5 to 7 per year (Nosten and Brasseur, 2002). This causes the Africans to depend on self-medication through the unregulated private and informal drug sectors. A large portion of antimalarial medicines sold in Africa is believed to be substandard medicines (i.e. those genuine ones with 80% or less of the listed active ingredient that fail

to meet quality specifications) and counterfeit medicines (i.e. those spurious ones that are "fraudulently mislabeled with respect to identity and/or source") (Snow et al., 1992, Newton et al., 2011, Cockburn et al., 2005, Bate et al., 2008) The low quality of drugs and the poor access to public health facilities translate into the failure of properly treating malaria and contribute to the spread of antimalarial drug resistance; these, in turn, increase morbidity and mortality (Newton et al., 2011).

2.1.3 Emergence of Resistance

The emergence and spread of drug-resistant strains of *P. falciparum* is another obstacle in malaria treatment in the 21st century. The first cases of drug-resistant malaria were documented during World War II, in which patients showed reduced efficacy to the prophylactic antimalarial drug, mepacrine (Atebrine). Since then, drug resistance has continued to characterize malaria treatment and has currently developed against all classes of antimalarial drugs (Sa et al., 2011). Chloroquine is one of the earliest and most effective drug discovered in the 1940s to control malaria. However, towards the end of the 1960s, treatment failures of chloroquine were reported almost simultaneously in South America and Southeast Asia (Western Cambodia and the Thailand–Myanmar) and then in Africa in the late 1970s, which have caused millions of deaths (Sa et al., 2011, Dondorp et al., 2009, Phyo et al., 2012). At present, this drug has become ineffective in most of *P. falciparum* malaria-endemic areas and has been almost removed from modern malaria treatment due to the widespread resistance. The resistance to a

drug develops through spontaneous genetic mutations, which are a function of the number of individual parasites in a given population. For instance, in any malaria patient, the probability of resistance-conferring mutations is higher when the parasite biomass is the largest during the acute phase of the infection (White, 1997). Drug resistance and the relative increase in the probability of carrying gametocytes lead to a slower clinical and parasitological recovery, anaemia and ultimately an increase in mortality, especially among children and pregnant women. Therefore re-treatment, sometimes warranting more expensive drugs is required (Ekvall et al., 1998, Trape et al., 1998).

Factors that contribute to the development of drug resistance are (1) total number of parasites exposed to the drug; (2) concentration of the drug to which the parasites are exposed; (3) pharmacokinetic and pharmacodynamic properties of the drug; (4) degree of resistance conferred by mutations; (5) degree of premunition in the host; (6) exposure of the parasites to other drugs for which no resistance has arisen; (7) monotherapy; (8) usage of counterfeit drugs; (9) extensive use and misuse of drugs; (10) intensity of transmission; and (11) population immunity or population movements (Wernsdorfer, 1994, Nosten and Brasseur, 2002). Meanwhile, the consequences of the emerging resistance are summarized in Figure 2.2. The length of half-life of antimalarial drugs also plays an important role in determining the development of resistance. The long half-life of antimalarial drugs, such as mefloquine and sulphadoxine-pyrimethamine (SP), are meritorious in affording effective single-dose treatment and in preventing infection for weeks. However, this feature is also detrimental in exerting drug pressure on the parasites for an

undesirably long time even after their concentration has fallen below the critical threshold (Watkins et al., 1997). Such overly long exposure to the drugs may induce the development of resistance among the parasites (Keating, 2012).

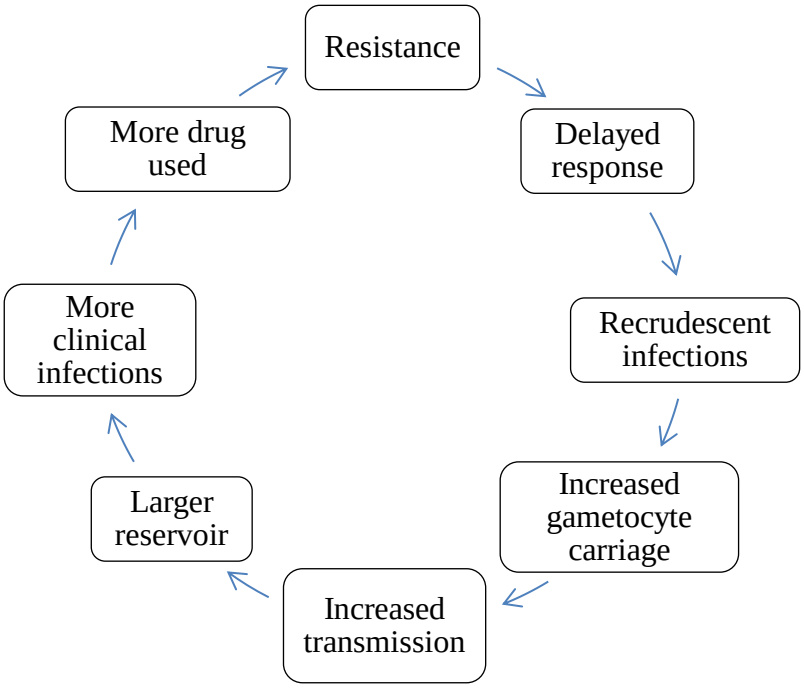

Figure 2.2 The 'vicious cycle' of antimalarial drug resistance (Wernsdorfer, 1994, Nosten and Brasseur, 2002).

2.2 Artemisinin-based Combination Therapies (ACTs)

Combination therapies have paved the way in preventing and delaying the emergence and spread of drug resistance. The idea of drug combinations is not novel since the principle has been used for highly drug-resistant diseases such as HIV/AIDS, tuberculosis and cancers (Montaner et al., 1999). For malaria, some of the examples of the earliest combination therapies are quinine-tetracycline, sulfadoxine-pyrimethamine, pyrimethamine-dapsone,

atovaquone-proguanil, quinine-tetracycline and mefloquine-pyrimethamine/sulfadoxine (White, 1999b, White and Olliaro, 1996, White, 1998). Unfortunately, resistance has emerged to all these combinations for the following reasons: a lack of activity on the sexual stage of the parasite cycle in the host; linked modes of action of compounds that are susceptible to the same parasite mutations; existing resistance to one of the compounds; mismatched pharmacokinetic properties of the compounds; and the slow action (low parasite reduction ratio) on the parasites.

Artemisinin-based combination therapies (ACTs) have subsequently been proposed and approved as a new approach due to their efficacy and ability to lower malaria incidence (some examples of ACTs are presented in Table 2.1). ACTs have shorter parasite and fever clearance times compared with chloroquine. The addition of artemisinin derivatives to combination therapies has shown a remarkable double effect of preventing the emergence and spread of drug resistance and of interrupting the transmission of *P. falciparum* (Nosten et al., 2000, White, 1999b, Price, 2000, White, 1999a). In the event that some parasites have survived the double actions of the therapies, the probability of transmission is still low. Therefore, the combined actions of drugs in ACTs result in a faster clinical and parasitological recovery (Nosten et al., 1994). ACTs were pioneered in Southeast Asia, the most studied and used of which is the combination of artesunate-mefloquine. Interestingly, this combination was shown to stop the progression of resistance to mefloquine (Brockman et al., 2000). By 2005, 43 countries have adopted

ACTs as their first or second line drugs, most of them being in sub-Saharan Africa (Table 2.2) (Mutabingwa, 2005, Attaran et al., 2004).

Table 2.1 Examples of artemisinins (ART derivatives are underlined) and partner drugs in ACTs and their half-life ($t_{1/2}$) (Eastman and Fidock, 2009)

Antimalarial combination drug	$t_{1/2}$ of artemisinin derivatives	$t_{1/2}$ of partner drugs
Artemether-lumifantrine (Coartem)	~ 3 h	4-5 days
Artesunate-mefloquine	< 1 h	14-21 days
Artesunate-amodiaquine	< 1 h	9-18 days
Dihydroartemisinin-piperaquine	45 min	~ 5-weeks
Artesunate-pyronaridine	< 1 h	16 days
Artemisinin-naphthoquine	2-3 h	10 -17 days

Table 2.2 Countries that have adopted ACTs as the first or second line drugs (Mutabingwa, 2005)

Continent	Country	First line	Second line
Africa	Burundi, Cameroon, Eq. Guinea, Gabon, Ghana, Madagascar, ST&P, Sierra Leone, Liberia, South Sudan, Zanzibar	Artesunate-amodiaquine	
	Angola, Benin, Comoros, Ethiopia, Kenya, Mali, Namibia, Niger, Nigeria, South Africa, Tanzania, Uganda, Zambia	Artemether-lumifantrine (Coartem)	
	Mozambique, North Sudan	Artesunate-sulfadoxine/ pyrimethamine	
	Code d'Ivoire, Mozambique, North Sudan, ST&P, Zanzibar		Artemether-lumifantrine (Coartem)
Asia	Cambodia, Thailand	Artesunate-mefloquine	
	Bangladesh, Bhutan, Laos, Myanmar	Artemether-lumifantrine (Coartem)	
	Indonesia	Artesunate-amodiaquine	
	Afghanistan, India, Iran, Tajikistan	Artesunate-sulfadoxine/ pyrimethamine	
	Vietnam	Combination of dihydroartemisinin, piperaquine, trimethoprim and primaquine	
	Papua New Guinea		Artesunate-sulfadoxine/ pyrimethamine

Continent	Country	First line	Second line
	Philippines		Artemether-lumifantrine (Coartem)
South America	Ecuador, Peru	Artesunate-sulfadoxine/pyrimethamine	
	Bolivia, Peru	Artesunate-mefloquine	
	Guyana, Suriname	Artemether-lumifantrine (Coartem)	

In order to have a better performance in combating malaria, the component drugs in ACT must have certain characteristics (Nosten and Brasseur, 2002). However, none of the previous and current combination therapies meets all these criteria, except artemether-lumefantrine combination, which is the closest. The characteristics of an "ideal" antimalarial combination are:-

i. Modes of action: The modes of action of component drugs on the parasite must be unrelated.

ii. Onset of action and parasite reduction ratio (PRR): At least one rapid-acting component drug must be used in the combination and exhibit the highest possible parasite reduction ratio of no less than 10^4.

iii. Pharmacological profile: The co-administration of the drugs must not result in detrimental drug-drug interactions.

iv. Duration of treatment: The total duration of the dosing regimen must be sufficiently short for patients' adherence, i.e. it must at most be only 3-day long.

v. Elimination half-life and duration of action: One of the components must be present in the circulation after the 2 cycles of exposure to the fast-acting drug, i.e. the elimination half-life of the partner drug must be longer than that of the fast-acting one.

vi. Toxicological profile: The tolerability must be good with reasonably acceptable toxicity.

vii. Spectrum of action: The combination must have pharmacological activity against all stages of the parasite, including gametocytes.

viii. Dosage formulation: The relative proportions of the drugs in combination must be fixed, i.e. formulated in the same tablet.

ix. Economic consideration: The therapeutic regime must be financially viable for all patients.

Artemisinin and its derivatives have a rapid parasite clearance rate (Adjuik et al., 2004). Despite its short half-life, it is vital to the initial anti-parasite effect against *Plasmodium*. The gametocytocidal effect of artemisinins on the parasite in the early developmental stages reduces the viability of gametocytes, thereby controlling the overall malaria transmission and lowering the infectivity of mosquitoes. Treating early cases of uncomplicated malaria with rapidly acting artemisinins is able to thwart the progression to severe cases and reduce mortality rates (Barnes and White, 2005, Adjuik et al., 2004). Complementing this, the partner drug(s) should

have a slow action with a long half-life, which is vital to the prevention of recurrence and resistance to the antimalarial drugs.

Though artemisinin is the parent compound and economical to produce from the plant *Artemisia annua*, more attention has been given to its derivatives produced from bio-synthesis such as artemether, artesunate and dihydroartemisinin. Artemisinin derivatives are preferred as a potent antimalarial in ACTs over artemisinin itself due to the poor aqueous solubility and the resultant poor oral bioavailability of artemisinin (Lapenna et al., 2009). Artemisinin has not been widely deployed in ACTs, except for artemisinin-naphthoquine (ARCO®), which is the only available commercial oral delivery ACT product that contains artemisinin (Hombhanje et al., 2009, Hombhanje and Huang, 2010). Even though antimalarial drugs are administrated via oral and intravenous routes, the oral administrations are much preferred and most commonly used especially in poor countries due to easy administration and cost-effectiveness. Most of the ACT products available in the market are manufactured for oral administration. Some of the examples of malaria pharmaceutical products classified according to the Global Fund Quality Assurance Policy are listed in Table 2.3. Therefore, enhancing the solubility of artemisinin (especially oral dosage forms) by using cost-effective and simple steps is essential to reduce the overall manufacturing cost. In the next section of literature review, more details will be provided on these aspects: oral drug delivery, Biopharmaceutical Classification Systems, the mechanism and principle of dissolution, solubility enhancement, examples of drug loading methods and available porous carriers.

Table 2.3 List of ACT products classified according their dose and dosage forms and manufacturers (Anonymous, 2015)

ACT products	Dose	Dosage form	Supplier/ Manufacturer(s)
Amodiaquin + Sulfadoxine/Pyrimethamine	150 mg + 500 mg/25 mg	Tablet (Co-Blistered)	Guilin Pharmaceuticals
Artemether + Lumefantrine	20 mg+120 mg	Tablet (FDC)	Novartis Pharma Ajanta Pharma Cipla Ltd. Laboratories Ltd.
Artemether + Lumefantrine	20 mg + 120 mg	Dispersible tablets (FDC)	Ajanta Pharma Novartis Pharma
	40 mg + 240 mg	Tablet (FDC)	Mylan Lab
Artesunate + Mefloquine	200 mg + 250 mg	Tablet (Co-Blistered)	Mepha
	25 mg+50 mg 100 mg+200 mg	Tablet (FDC)	Cipla Ltd.
Artesunate + Sulfadoxine/ Pyrimethamine	50 mg+ 500 mg/25 mg	Tablet (Co Blistered)	Guilin Pharmaceuticals
Piperaquine tetraphosphate + Dihydroartemisinin	160 mg+20 mg 320 mg+ 40 mg	Film coated Tablet	Sigma-tau Industrie Farmaceutiche Riunite SpA
Artesunate + Amodiaquine	50 mg + 150 mg	Tablet (Co-Blistered)	Pharmaceutical Co. Ltd.
	50 mg + 153 mg		Cipla Ltd. Laboratories Ltd
	67.5 mg + 25 mg	Tablet (FDC)	Ajanta Pharma Cipla

[a] Fixed-dose combination

2.3 Oral Drug Delivery

Medical drugs can be administered by various routes into the human body depending on the desired effects, the therapeutical medications, the type and pathophysiology of the disease and the physicochemical properties. Drugs can be either delivered directly to the target organ or tissue affected by the disease or given systematically to target the infected organ on which it can exert its therapeutic effect. Knowledge on the possible methods of drug delivery is vital in achieving the best therapeutic benefits from any drug. Oral (Agrawal et al., 2014), intravenous (Lalatsa et al., 2015), pulmonary (Patton and Byron, 2007), transdermal (Lee et al., 2015), ocular (Ahuja et al., 2015) and nasal routes (Illum, 2002) are some routes of administration, each with its own advantages and disadvantages, as summarized in the Table 2.4 (excluding oral administration which will be discussed extensively subsequently).

Table 2.4 Advantages and disadvantages of different routes of drug administration

Route	Advantages	Disadvantages
Rectal	-Affords good absorption – the haemorrhoidal veins drain directly into the inferior vena cava, avoiding hepatic first-pass metabolism	-May not be suitable after rectal or anal surgery -May be stigmatized and not be accepted by patients
Subcutaneous or intramuscular	-Affords good absorption, especially for drugs with a low oral bioavailability -Exhibits rapid onset of action -Can have very long duration of action depending on formulations, e.g. depot antipsychotics and contraceptives -Can be formulated as controlled depot release -Can be used for most therapeutic molecules	-May exhibit unpredictable absorption if peripheries are poorly perfused -Causes pain and bruises and may cause fear amongst patients -May lead to noncompliance amongst patients out of fear -May lead to higher risks of infection
Intravenous	-Exhibits dependable and reproducible effects -Can be used for drug administration in life threatening situations -Exhibits rapid onset of action – the entire administered dose reaches the systemic circulation immediately -Affords accurate dose-titration against clinical response -Affords up to 100% bioavailability -Can be used for most therapeutic molecules	-May be more expensive and labor intensive than other routes -May lead to distress amongst patients -May lead to higher risks of infection -May be difficult for patient to self-administer -May afford only a short duration of action -May cause local reactions e.g. thrombophlebitis and tissue necrosis and other severe adverse effects e.g. organ toxicity

Route	Advantages	Disadvantages
Topical/ Transdermal	-Affords easy and non-invasive drug delivery -Affords patient satisfaction -Results in fewer side-effects due to direct delivery to the skin -Bypasses first-pass degradation	-May not be suitable for drugs of high molecular weight or that are poorly lipid soluble due to poor transdermal absorption -May lead to slow absorption, as dependent on skin conditions and locations -May lead to potential use of the wrong dose (e.g. creams) by patients
Inhalation	-Affords rapid absorption due to the huge surface area of the respiratory endothelia -Allows targeted action lungs with low levels of systemic absorption by means of bronchodilators and inhaled steroids	-May yield inconsistent delivery and bioavailability due to patient-to-patient variations in techniques of using inhalers and the size of drug particles generated

Oral administration represents the most extensively used mode of drug delivery; for instance, more than billions of aspirin tablets are consumed worldwide annually (Kermode, 2004). The multifarious merits of this route form the rationale underlying the fact that the majority of small drug molecules are designed for oral administration. It is by far the most dominant and convenient route that offers portability, flexibility and control over dosing schedules, simplicity for self-administration and systemic delivery; all incorporated in one tablet or capsule along with the non-invasive nature of administration (Brayden and O'Mahony, 1998, Park et al., 2011, Goldberg and Gomez-Orellana, 2003). In addition, it offers convenience for chronic therapy and effectiveness in dealing with specific diseases (Bromberg, 2008, Yamanaka and Leong, 2008). From the perspective of the manufacturing industry, another merit of the orally administered drugs is their less stringent sterility constraints. From the perspective of clinical practice, compared with parenteral delivery, oral administration can suppress the risk of disease transmission and reduces the overall treatment cost (Gaucher et al., 2010, Ruenraroengsak et al., 2010).

Despite the numerous benefits, oral drug delivery has its own drawbacks. With regard to the gastrointestinal (GI) tract, orally administered drugs must survive in the harsh environment, transit through the chemical and enzymatic GI liquids, cross the mucous layer and the epithelia before being absorbed. This route is therefore limited by the complex interplay between the physicochemical properties of the drug and the physiological processes; the repercussion is that the bioavailability may be compromised. Bioavailability

refers to the extent and rate at which a drug reaches the systemic circulation after administration, depending on aqueous solubility, drug permeability, dissolution rate, first-pass metabolism, pre-systemic metabolism and susceptibility to efflux mechanisms (Savjani et al., 2012). For intravenously administered drugs, a bioavailability of 100% can be expected; for those drugs otherwise administered, especially orally delivered ones, a poor bioavailability is often observed. The undesirably low bioavailability of oral drugs are mainly influenced by the low mucosal penetration inherent to the physicochemical properties of the drug; restricted drug permeability at specific GI regions; poor dissolution rate in intestinal fluids corresponding to a low aqueous solubility; gastric emptying and intestinal motility; and drug degradation before absorption due to drug instability within the microenvironment of GI tract (Ponchel and Irache, 1998). The Biopharmaceutical Classification System (BCS) is a scientific framework to classify active pharmaceutical ingredients according to their solubility and permeability, which are essential in predicting bioavailability (Shugarts and Benet, 2009) (refer in Section 2.4).

In addition, the inability of oral drug administration route to deliver large therapeutic molecules is also a concern. Considering that the rate of absorption depends on the molecular size, macromolecules such as proteins, vaccines or nucleic acids encounter intestinal barrier limits more frequently than small molecules (Agrawal et al., 2014). Besides, oral drug delivery fails to meet advanced therapeutic needs such as targeting. Also, the immediate release of certain oral dosage forms has also been found to be associated with toxicity and side effects (Goldberg and Gomez-Orellana, 2003).

2.4 Biopharmaceutical Classification System (BCS)

The Biopharmaceutical Classification System (BCS) was introduced by Amidon et al. (1995) to correlate physicochemical properties of the drug to absorption and bio-performance after oral administration. It plays a vital role in the designing of formulations and in the understanding the physicochemical and biopharmaceutical properties of drugs. The BCS divides active substances into four classes, i.e. class I to class IV (Figure 2.3). Permeability is measured based on the rate of mass transfer of a drug substance across the human intestinal membrane; a drug is considered highly permeable when the extent of intestinal absorption is more than 90% of the administered dose. Solubility is measured based on the rate at which solid drug or drug in a formulation passes into solution; a drug is considered highly soluble when the highest strength is soluble in less than 250 mL of aqueous media at 37 ºC and pH range of 1.0–7.5. The volume estimate of aqueous media is derived from typical bioequivalence study protocols that prescribe the administration of a drug product to fasting human volunteers with about 250 mL of water (Kawabata et al., 2011, Yu et al., 2002).

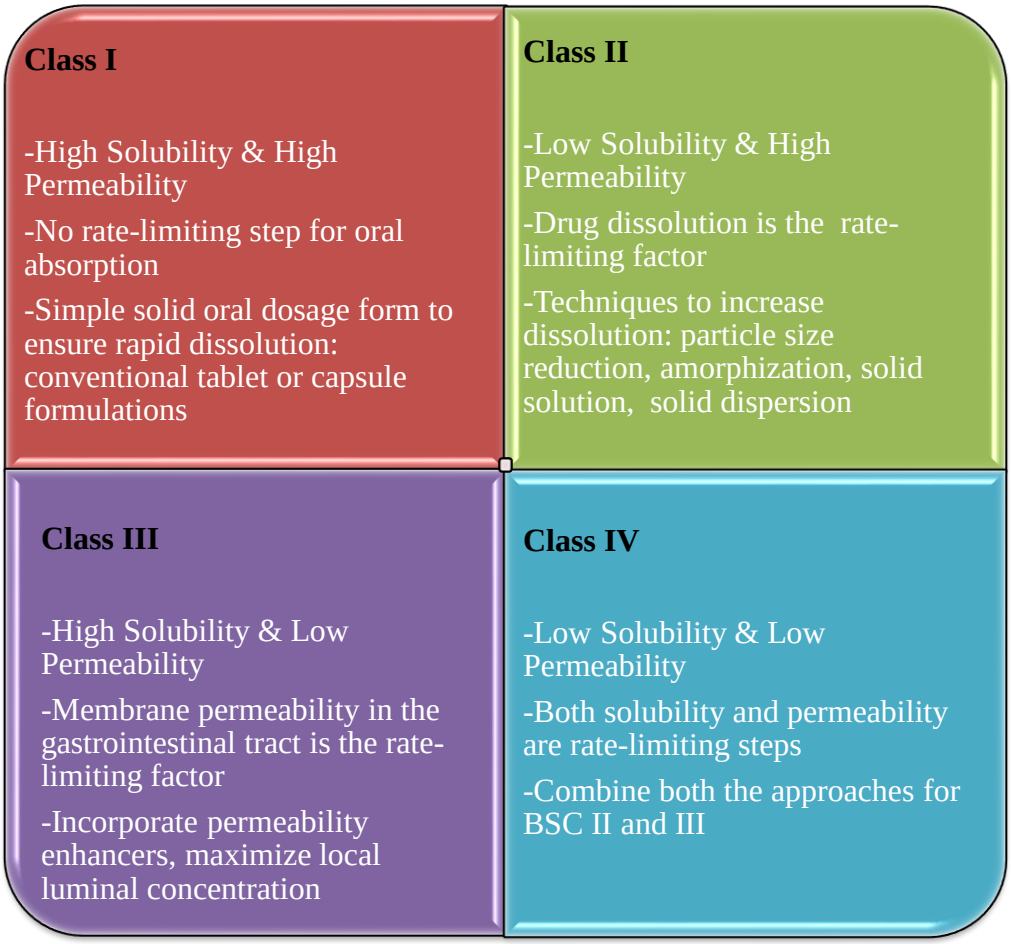

Figure 2.3 The Biopharmaceutical classification system (BCS) and the techniques to overcome limitations of each class (Kawabata et al., 2011).

The BCS class II drugs are of specific interest, because the number of poorly water-soluble compounds are rapidly increasing in drug discovery and approximately 40% of the world's top oral drugs are classified as BCS class II and class IV compounds (Lipinski et al., 1997). Artemisinin (Shahzad et al., 2012), lumefantrine, mefloquine, pyrimethamine and doxycycline are example of APIs that classified under BCS class II and sometime may classified under both BCS class II and IV due to lack of permeability data (Lindenberg et al., 2004). The permeability of BCS class II drugs across the intestinal membranes is fast; hence the absorption will mainly be determined by the dissolution rate

of the drug in the GI fluids. As a result, a small increase in the dissolution rate can result in a drastic increase in the bioavailability (Lobenberg and Amidon, 2000). As the drug is exposed in the intestine, the dissolution profile will influence the concentration profile along the intestines and absorption will occur for a much longer time, which can contribute to an improved bioavailability (Amidon et al., 1995, Kawabata et al., 2011). Therefore, enhancement in solubility and dissolution will translate into an enhancement in bioavailability; the challenge remains that how the dissolution rate of BCS class II drugs can be augmented.

2.5 Solubility and Dissolution Rate

Solubility is the maximum concentration of a drug that can dissolve in a certain quantity of solvent or solution under specific conditions of temperature, pH and pressure (Lachman et al., 1986). A solution is said to be saturated if its concentration equals the equilibrium concentration, sub-saturated if its concentration is lower than the equilibrium concentration and super-saturated if its concentration exceeds the equilibrium concentration. Different classifications of solubility are summarized in Table 2.5 (Savjani et al., 2012) and factors affecting the solubility of a drug are summarized in Table 2.6. In comparison with solubility, dissolution (Figure 2.4) refers to the transfer of molecules or ions from a solid state into a solution, which depends on temperature and the relative affinity between molecules of the solid substance and solvent.

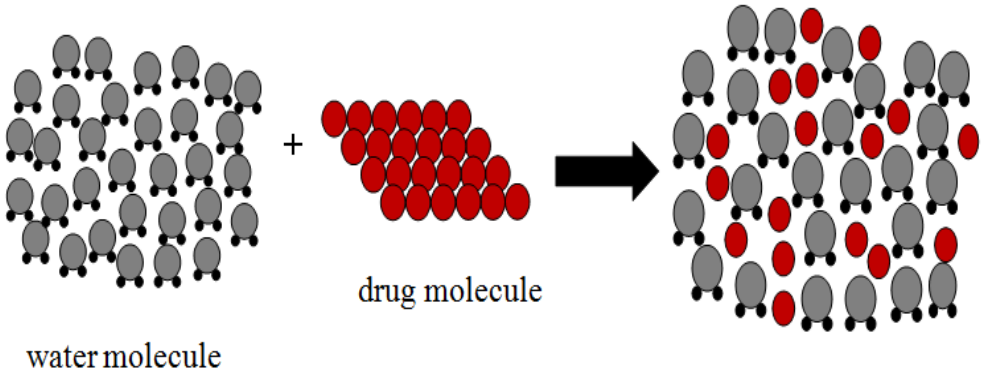

Figure 2.4 Scheme of solubilization.

Both dissolution and solubility are important parameters that influence and determine the bioavailability of dosage forms, especially for orally administrated BCS class II drugs. The rate-limiting step to achieve *in vivo* absorption and bioavailability of BCS class II drugs is their solubility and dissolution rate since these drugs have rapid diffusion across the gut walls; therefore enhancing the solubility will improve the drug absorption and drug bioavailability. Solubility is important to accomplish the required concentration of a drug in the systemic circulation for acceptable pharmacological responses and therapeutic effectiveness (Alavijeh et al., 2005, Kamble et al., 2014). The drugs need to be dissolved in the gastrointestinal tract and present in the form of an aqueous solution at the absorption site to be distributed and absorbed across the intestinal mucosa and reach the circulatory system (Limnell et al., 2011a). Therefore, poor solubility of orally administrated drug has a low saturation solubility which is typically correlated with a low dissolution rate causing inadequate and variable bioavailability. The application of drugs with insufficient solubility causes increase in dosage and frequency of administration to reach the desired

therapeutic plasma concentration. High dosage and repeated administration may then lead to occurrence of side effects (Daughton and Ruhoy, 2013, Savjani et al., 2012). Hence, drugs with poor solubility face many development challenges which lead not only to increased developmental cost and time but also results in higher risks of failure during discovery, formulation development and generic development, since the solubility affects both pharmacokinetics and pharmacodynamics properties.

Table 2.5 Classification of drugs according to their solubility (Takagi et al., 2006)

Descriptive term	Parts of solvent required for one part of solute	Solubility range (mg/mL)
Very soluble	< 1	≥ 1,000
Freely soluble	From 1 to 10	100–1,000
Soluble	From 10 to 30	33–100
Sparingly soluble	From 30 to 100	10–33
Slightly soluble	From 100 to 1,000	1–10
Very slightly soluble	From 1,000 to 10,000	0.1–1
Practically insoluble	≥10,000	< 0.1

Table 2.6 Factors affecting the solubility of a drug (Murdande et al., 2010b)

Factors	Remarks
Nature of solute and solvent	The solubility of substances can be influenced by their nature such as their ability to form hydrogen bond, the strength of the bonds, polarizability and ionization potential.
Particle size	Smaller particle size increases surface-area-to-volume ratio, which will result in greater contact and interaction with the solvent. Since interactions between the solute and the solvent takes place at only the surface of each particle, a larger surface area will mean that dissolution occurs more rapidly. For very small particle sizes, the solubility will be a function of particle dimension, resulting in higher equilibrium solubility.
Molecular size	The solubility of the substance is inversely proportional to the molecular size. Generally, solubility decreases with an increase in molecular weight and molecular size since larger molecules are more difficult to be solvated by solvent molecules.
Temperature	As temperature rises, more energy will be provided to the dissolution process and increase the motion of solvent and solute particles. This generally increases the solubility.
Pressure	Pressure has no effect on solids and liquid solutes, but influences the solubility of gas. An increase in pressure increases the solubility of gaseous solutes.
Polarity	Polar solutes will dissolve in polar solvents and non-polar solutes will dissolve in non-polar solvents. The phenomena are due to intermolecular forces such as dipole-dipole interactions and van der Waals force.
Polymorphism	Different polymorphs will have different physical properties and molecular arrangements. Metastable forms will have higher solubility compared with stable forms. Generally the range of solubility differences between polymorphs is only within 2-3 fold due to relatively small differences in free energy.

2.6 Solubility Enhancement Techniques

According to recent studies, more than one-third of the drugs listed under the U.S. Pharmacopoeia and half of the new chemical entities (NCEs) developed in the pharmaceutical industry have poor bioavailability because of their biopharmaceutical properties such as poor aqueous solubility and dissolution (Ahuja et al., 2007, Shen et al., 2010). Enhancing the solubility of BCS class II drugs is a major challenge for formulation scientists to a successful drug development (Sugano et al., 2007, Sigfridsson et al., 2009, Van Eerdenbrugh et al., 2010). Numerous pharmaceutical formulation techniques have been reported to overcome the delivery barriers of poorly water-soluble drugs; however, the number of simple and effective techniques that have achieved marketed applications is limited. Therefore, it is essential to explore new types of formulation approaches with market values. Recently, more attention has been given to amorphization technique by confining drug particles in mesoporous carriers via spray drying to circumvent the poor supersaturation and storage stability of poorly water-soluble drugs (Rengarajan et al., 2008). There has been growing interest in employing mesoporous materials especially mesoporous silica and mesoporous carbon in drug delivery systems for both rapid and controlled drug release (Rahmat et al., 2010, Limnell et al., 2011a). Common approaches utilized for achieving higher drug bioavailability/solubility such as particle size reduction, inclusion complexation, modification of the crystal forms and solid dispersions are discussed further in this section.

2.6.1 Particle Size Reduction

According to the modified Noyes-Whitney relationship [equation (a)] (Noyes and Whitney, 1897), the dissolution rate of drugs can be related to the particle size. Reducing the particles size of a coarse drug powder by applying considerable shear forces will increases the surface area per unit volume ratio of drugs, which in turn augments the interaction between the drug and the solvent, thereby improving the dissolution rate. However, this is not suitable for drugs having a high dose number because it does not influence the saturation solubility of the drug (Blagden et al., 2007). Examples of particle size reduction techniques include micronization (2−5 μm) (Rasenack and Muller, 2002) and nanonization (200–500 nm) (Keck and Muller, 2006) using hammer mills, rotor stator colloid mills, ball mills, air-jet mills, comminution and spray drying. Meanwhile nanosuspensions are produced by homogenization and wet milling process (Rabinow, 2004).

$$\frac{dM}{dt} = \frac{DS\,(C_s - C_b)}{h} \qquad \text{(a)}$$

where,

M = mass of compound dissolved in time t; D = diffusion coefficient of the compound in the medium; S = surface area; h = thickness of the stagnant film layer; C_s = saturated solubility of the compound at the particle–media interface; and C_b = concentration of compound in the bulk medium.

Rasenack et al. (2003) have studied the effect of micronization on a poorly water-soluble drug, ECU-01 (a low molecular enzyme-inhibitor with

anti-inflammatory properties). The dissolution rate of micronized ECU-01 (mean particles size = 1 µ) was 93% after 20 min while that of the untreated crystals (mean particles size = 20 µ) was only 4% after 20 min. Table 2.7 shows examples of samples prepared by particle size reduction methods..

Table 2.7 Examples of samples (solid dispersions) prepared by particle size reduction methods

Drug	Technique	References
Cilostazol	Hammer -mill, jet-mill and spray-dryer	(Jinno et al., 2006)
Cilostazol	Supercritical antisolvent (SAS)	(Kim et al., 2007)
Fenofibrate, Ibuprofen, Sulfamethoxazole and Itraconazole	Wet milling	(Bhakay et al., 2011)
Creatine and Ibuprofen	Rapid Expansion of Supercritical Solution (RESS)	(Hezave et al., 2010) and (Charoenchaitrakool et al., 2000)
Fenofibrate	Micronization , co-grinding and spray drying	(Vogt et al., 2008a)
EMD 57033	Co-grinding	(Vogt et al., 2008b)
Danazol	Aqueous dispersion of nanoparticulate danazol, danazol-hydroxypropyl-β-cyclodextrin complex; aqueous suspension of conventional danazol particles	(Liversidge and Cundy, 1995)

2.6.2 Inclusion Complexation

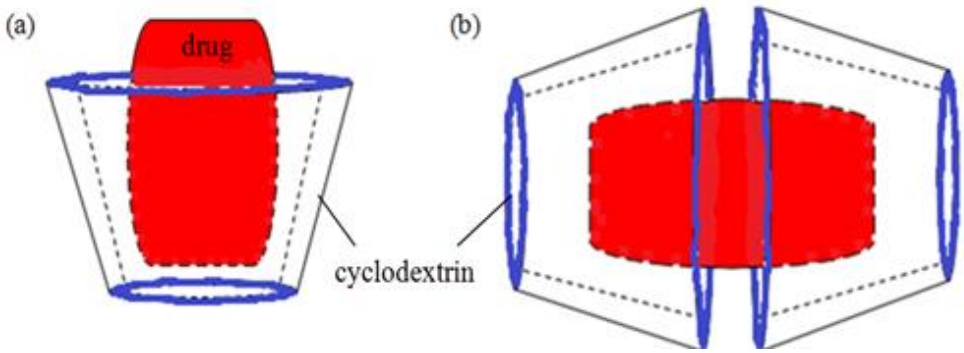

Figure 2.5 Schematic diagram for inclusion complexes using cyclodextrin with drug/carrier ratio of (a) 1:1 (w/w) and (b) 1:2 (w/w).

Inclusion complexes are another common method to enhance the stability, wettability, aqueous solubility, membrane permeability, dissolution rate and bioavailability of poorly water-soluble oral or parenteral drugs (Park, 2006). Inclusion complexes are formed by insertion of the non-polar region of a drug molecule (known as the 'guest') into the cavity of another group of molecules (known as the 'host') to form a stable association (ElShaboury, 1990). The most commonly used complexing ligand is cyclodextrin (CD) (Figure 2.5); α-CD, β-CD and γ-CD are three naturally occurring CDs (Uekama et al., 1998). Other complexing ligands include apart from caffeine, urea, polyethylene glycol, N-methylglucamide. Derivatives of β-cyclodextrin such as hydroxypropyl-β-cyclodextrin are widely used in pharmaceutical formulations. CDs are non-reducing, crystalline and water-soluble compounds made up of sugar molecules, bound together in a donut-shaped ring (cyclic oligosacharides) that have a non-polar cavity and a hydrophilic external surface (Jiang et al., 2012b, Pitha et al., 1986). The polar exterior of the cyclodextrin (due to the presence of hydroxyl groups on the molecule) renders

them water-soluble and the hydrophobic cavity provides a microenvironment for inclusion of non-polar molecules (which reduces the contact of the hydrophobic drug molecules with water) (Uekama et al., 1998). Complexation relies on relatively weak forces such as London forces, hydrogen bonding and hydrophobic interactions. Slightly water-soluble drugs such as phenobarbitone, diazepam, prednisolone and spironoiactone have been found to form inclusion complexes with β-CD in different molar ratios. These drugs that are produced in the tablet dosage form with spray dried lactose exhibit better mechanical properties and enhanced dissolution rate of up to 6-10 fold (ElShaboury, 1990). Various technologies are applied for the preparation of the inclusion complexes of poorly water-soluble drugs with cyclodextrins (Table 2.8).

Table 2.8 Examples of samples (solid dispersions) prepared by inclusion complexation

Carrier	Drug	Approaches	References
Hydroxypropyl -β- CD	Ketorolac	Kneading method	(Nagarsenker et al., 2000)
β- CD	Meloxicam	Milling	(Bandarkar and Vavia, 2011)
β - CD	Scutellarin	Lyophilization/ Freeze drying technique	(Cao et al., 2005)
2-Hydroxypropyl -β- CD	Naproxen	Co-precipitation, solvent evaporation, freeze-drying and kneading	(Lee and Lee, 1995)
β- CD	Carvedilol	Microwave irradiation	(Wen et al., 2004)
Maltosyl-β-CD	N-type Ca^{2+} channel blocker ONO-2921	Four-Fluid Nozzle Spray drying	(Ozeki et al., 2012)
β- CD	Artemisinin	Spray drying	(Balducci et al., 2013, Sahoo et al., 2009)
β- CD	Naringenin	Solvent evaporation method	(Semalty et al., 2014)
β-CD or hydroxypropyl-β-CD	Piroxicam	Freeze drying and the spray drying	(Bouchal et al., 2014)
β- CD	Diosmin	Kneading technique	(Anwer et al., 2014)

2.6.3 Co-Solvency

Co-solvency or solvent blending (Figure 2.6) is a process in which the solubility of a poorly water-soluble drug is improved by changing the polarity of water by adding one or more water-miscible solvents. The mixture thus formed, in which the drug has a good solubility, is known as co-solvents (Strickley, 2004). Co-solvency is a suitable approach for highly crystalline and lipophilic drugs that have a high solubility in a solvent mixture. The system works by reducing the interfacial tension between the aqueous solution and the hydrophobic solute. Co-solvency is one of the most widely used techniques for the oral and parenteral routes because it is simple to produce and evaluate; ethanol, glycerin, sorbitol, polyoxyethylene glycols, PEG 300 and propylene glycol are the most frequently used low-toxicity co-solvents (Table 2.9) (Yalkowsky and Rubino, 1985, Pan et al., 2001).

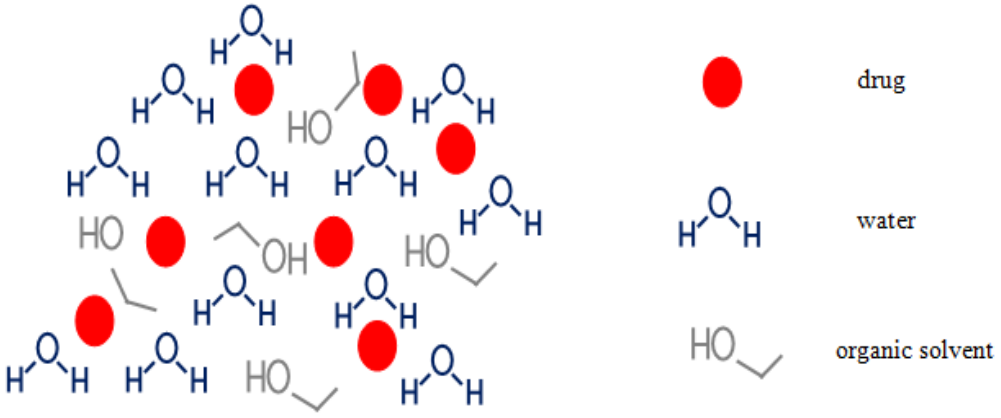

Figure 2.6 Schematic diagram for co-solvent formation.

Table 2.9 Examples of samples (solid dispersions) prepared by co-solvency

Drug	Co-solvents	References
Gliclazide, glyburide, glipizide, glimepiride, repaglinide, pioglitazone and roziglitazone.	Polyethylene Glycol 400, polyethylene Glycol 8000, propylene glycol, glycerol, ethanol and propylene glycol + Ethanol (1:1 v/v)	(Seedher and Kanojia, 2009)
Famotidine	Liquid co-solvent: ethanol and polyethylene glycol 400	(Matsuda et al., 2011)
Risperidone	Transcutol	(Shakeel et al., 2014)
Daidzein	Propylene glycol	(Zeng et al., 2014)
Rapamycin	Polyethylene Glycol 400/ethanol, glycerol/ethanol, propylene glycol, glycerol formal, transcutol P	(Sun et al., 2011)
Hydrocortisone , sulfanilamide, acetophenetidine, benzocaine, indomethacin, thymol and ibuprofen	Polar solvents: methanol, ethanol and propanol; Less polar solvents: N-methyl pyrrolidone, tetraglycol and labrasol.	(Miyako et al., 2010)
phenytoin	Surfactants: sodium dodecyl sulfate, Tween 80; Co-solvents: dimethylacetoamide, ethanol, polyethylene glycol 400, glycerol	(Kawakami et al., 2006)

2.6.4 Surfactants

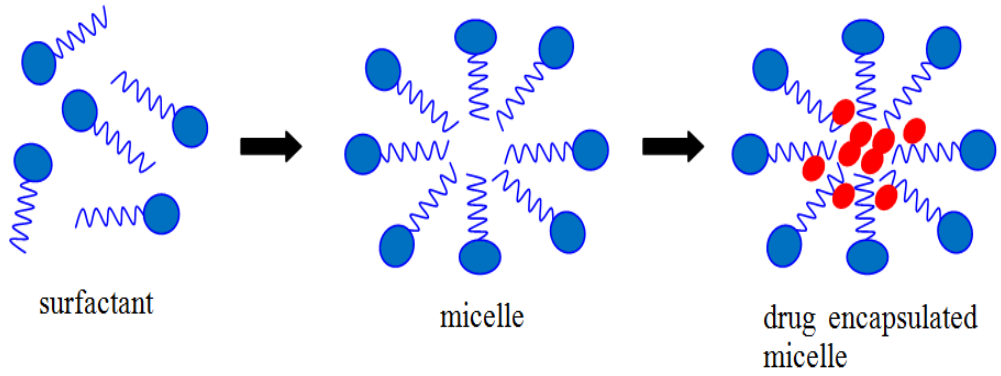

Figure 2.7 Schematic diagram for micelle formation and drug encapsulation.

Surface active agents (surfactants) are molecules with both a non-polar (hydrophobic) region, of which hydrocarbons are a major portion and a polar (hydrophilic) region. Depending on their charge characteristics, surfactants can be divided into four classes: anionic (i.e. the hydrophilic group is negatively charged, e.g. sodium lauryl sulphate and potassium laurate); cationic (i.e. the hydrophilic group is positively charged, e.g. cetrimide, benzalkonium chloride); zwitterionic (i.e. the molecule is both negatively and positively charged, e.g. N-dodecyl-N, N-dimethylbetaine); nonionic (i.e. the hydrophile carries no charge but derives its water-solubility from highly polar groups such as hydroxyl or polyoxyethylene groups, e.g. Spans, Tweens, polysorbates, polyoxyethylated castor oil, polyoxyethylated glycerides and lauroyl macroglycerides) (Kawakami et al., 2006, Kawakami et al., 2004). Surfactants are used to form micelles to improve the solubility and wettability of hydrophobic drugs by entrapping the poorly soluble drugs in the hydrophobic core (Figure 2.7) and lowering the surface tension between the drug and the solvent (Torchilin, 2001, Jones and Leroux, 1999). They can also

be used to stabilize drug suspensions and micro-emulsions and increase the rate of disintegration of drugs into finer particles (Schreier et al., 2000, Yu et al., 1998). The micelles are formed when the surfactant concentration exceeds their critical micelle concentration (CMC), which depends upon the surfactant itself and the ionic strength of the media (Dutt, 2003). This process, known as micellization, is a widely used alternative for the dissolution of poorly soluble drugs which generally results in enhanced solubility (Desai et al., 2003, Liu et al., 2004, Desai and Park, 2004). Gliclazide, glyburide, glimepiride, glipizide, repaglinide, pioglitazone and rosiglitazone are examples of poorly water-soluble drugs of which the solubility is enhanced by micellar solubilization (Seedher and Kanojia, 2008).

2.6.5 Modification of the Crystal Forms

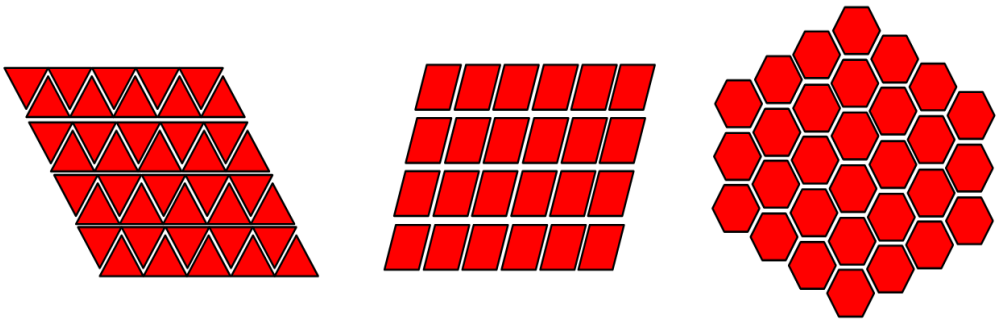

Figure 2.8 Schematic diagram of crystalline structure in different polymorphs.

Modification of the crystalline form of a drug is another method to improve the solubility of poorly water-soluble drugs. Polymorphism is the ability of a drug substance to exist in more than one crystalline form (Figure 2.8). Different polymorphs of the same drug will have identical chemical properties but may show variations in physical properties such as solubility,

melting point, density, texture and stability (Singh et al., 2010, Datta and Grant, 2004, Grunenberg et al., 1996). Identifying the desired polymorph of a drug before formulation is important to ensure a sufficiently reasonable solubility and dissolution rate. It can be done by controlling the crystallization process to favor the creation of amorphous or metastable forms of a drug possessing higher free energies. Compared with metastable forms and amorphous forms, the most stable polymorph has the least amount of free energy and, consequently, the lowest solubility. The dissolution rate of different solid forms of a given drug, in descending order, is as follows: amorphous (highest), metastable and stable (lowest) (Hammond et al., 2007). For example, indomethacin normally exists in 2 polymorphs which are α- and γ-indomethacin. The γ-indomethacin which is more thermodynamically stable, has a lower solubility in water compared with the α-indomethacin, which is in a metastable form (Lim et al., 2012). Chloramphenicol palmitate (Aguiar et al., 1967), sulfameter (Khalafallah et al., 1974), phenylbutazone (Pandit et al., 1984), amobarbital (Kato and Kohketsu, 1981), celecoxib (Lu et al., 2006), rifaximin (Viscomi et al., 2008) are some examples of drugs thus formulated. However, the stability of the amorphous and metastable forms is still a problem to address unless stabilizers intended to inhibit crystal growth of the stable form are incorporated in the formulation.

2.6.6 Solid Dispersions

Solid dispersion is a a useful pharmaceutical technique to enhance the dissolution, aqueous solubility, absorption and therapeutic efficacy of

formulated drugs. A solid dispersion refers to a solid containing one or more active ingredients in an inert carrier or matrix in a solid state. The matrices refer to amorphous or crystalline water-soluble carriers where the hydrophobic drugs can be dispersed molecularly or in amorphous or crystalline forms depending on drug-carrier interactions and drug loading (Akbuga et al., 1988, Okonogi et al., 1997). The concept of solid dispersion was first recognized by Sekiguchi and Obi to overcome the poor dissolution or solubility and the low bioavailability of lipophilic drugs (Sekiguchi and Obi, 1961). Solid dispersions can produce non-molecular level mixing (eutectic) or molecular level mixing (solid solution) products. According to the properties of the carrier and molecular arrangement of the drug within the carrier matrix, solid dispersions can be classified into 6 categories (Table 2.10) which involves 3 generations (Figure 2.9). Detailed literature reviews about these solid dispersions are available in works by Leuner and Dressman (2000) and Vasconcelos et al. (2007).

The enhancement of the dissolution by solid dispersions is influenced by different mechanisms: (1) a reduction in particle size with a resultant increase in the total surface area per unit volume of drug particles that is exposed to the dissolution medium; (2) an augmented saturation concentration around smaller particles compared with larger particles; (3) improved wettability of a drug by its direct contact with the hydrophilic matrix; (4) a reduction in the lattice energy due to changes in polymorphs or amorphization or reduced crystallinity; and (5) an increase in the porosity of drug particles; and (6) an elevated solubilizing effect of the carriers.

The selection of carriers for the formulation of solid dispersions is critical since it determines the physicochemical properties and stability of the drug. The chosen carrier should ideally possess these features: high solubility in not only water but also a variety of solvents with rapid dissolution properties; ability to enhance the aqueous solubility of the drug; biocompatibility, lack of toxicity and pharmacological inertness; thermal stability with a low melting point for the melt method; chemical compatibility with the drug and only weakly bonded with the drug. Different classes of water-soluble carriers such as surfactants, sugars and polymers are employed to formulate solid dispersions using techniques including melting (fusion) method, solvent method, or fusion solvent-method (Table 2.11). Spray drying, a solvent method that is of interest in this research, will be discussed extensively in Section 2.7.2.3. Gris-PEG® is a commercially available solid dispersion of griseofulvin and polyethylene glycol 8000 (carrier). Other carriers such as nanoparticles, microcapsules, microspheres are also widely used in this process.

Table 2.10 Classification of solid dispersion subtypes according to the physical form of the drug and the carrier

Type	Solid Dispersion	Drug	Carrier	Total No. of Phases	Physical Drug Stability
1	Eutectic mixture	C	C	2	Stable
2	Solid amorphous suspension	A	C	2	Unstable; risk of crystallization
3	Solid solution	M	C	1	Stable (below crystalline solubility) and Unstable (above crystalline solubility); risk of crystallization
4	Glass suspension	C	A	2	Stable
5	Glass amorphouss uspension	A	A	2	Unstable; risk of crystallization
6	Glass solution	A	A	1	Unstable; risk of phase-separation and of crystallization

A- Amorphous
C- Crystalline
M- Molecularly dispersed

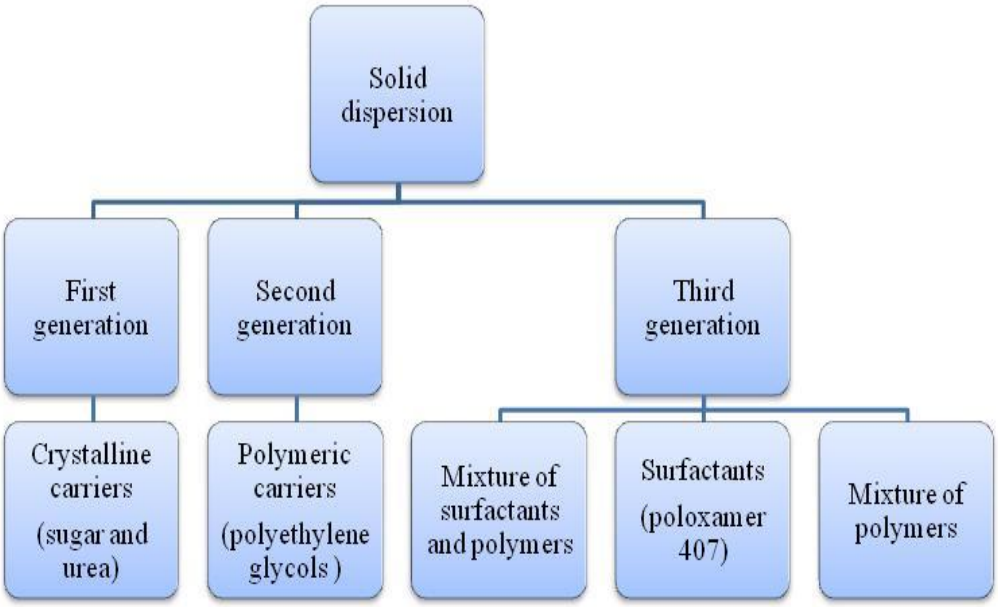

Figure 2.9 Generations of solid dispersions.

Table 2.11 Types of water-soluble excipients employed as carriers to formulate solid dispersions

Carriers	API	Preparation of solid dispersion	References
Poloxamers	Desloratadine	Melting method/ fusion method	(Kolasinac et al., 2012)
Polyethylene Glycol 4000 (PEG)	Rofecoxib	Melting method/ fusion method	(Liu and Desai, 2005)
Polyvinylpyrrolidone (PVP)	Griseofulvin	Ball milling	(Al-Obaidi et al., 2013)
Hydroxypropylmethyl cellulose acetate succinate	Griseofulvin	Ball milling	(Al-Obaidi et al., 2013)
Polyvinylpyrrolidone K-30	Loratadine	Spray drying and rotary evaporation	(Frizon et al., 2013)
Hydroxypropylmethyl cellulose (HPMC)	Felodipine	Physical mixing and hot melt mixing	(Sarode et al., 2014)
Hydroxypropylcellulose (HPC)	Aripiprazole	Nanomilling and co-precipitation	(Abdelbary et al., 2014)
Polyvinyl caprolactam graft copolymer, soluplus and vinylpyrrolidone-vinyl acetate copolymer grades, Kollidon VA64 (VA64) and Plasdone S630 (S630)	Indomethacin and famotidine	Hot -melt extrusion	(Maniruzzaman et al., 2013)
PEG 6000, Myrj 52, Lactose, Sorbitol, Dextrin and Eudragit® E100	Indomethacin	Co-evaporation and Melting method/ fusion method	(Valizadeh et al., 2004)

Despite the promising dissolution enhancement and simplicity of solid dispersion techniques, challenges in formulation methods and manufacturing, problems associated with the reproducibility of physicochemical properties, poor predictability of solid dispersion behavior, stability and scale-up have limited the solid dispersions from achieving commercial market values (Serajuddin, 1999, Dahlberg et al., 2008, Leuner and Dressman, 2000). Solid dispersions are thermodynamically less stable and tend to re-crystallize due to mechanical stress during the processing period and temperature and humidity stress during the storage period (Pokharkar et al., 2006, Vasanthavada et al., 2004, Vasconcelos et al., 2007). Most of the hygroscopic carriers tend to absorb moisture from humid surroundings. The resultant alteration in the molecular mobility of drug particles may promote re-crystallization and phase separation, thereby hampering storage stability of amorphous and metastable crystalline pharmaceuticals, potentially resulting in decreased solubility and dissolution rate with aging (Sharma and Jain, 2011, Johari et al., 2005, Vasconcelos et al., 2007). In view of this, formulating solid dispersions by confining drug particles in mesoporous carriers present a better solution for the poor stability of the amorphous forms. Some details of nano-confinement have been discussed in introduction (Section 1.1); and more detailed literature regarding mesoporous materials especially mesoporous silica will be provide in next section

2.6.6.1 Mesoporous materials

Mesoporous materials are highly porous solids characterized by a uniform pore shape and a narrow pore size distribution. According to the IUPAC classification, porous materials can be classified into three main categories, depending on their pore size: pores with a diameter smaller than 2 nm are referred to as micropores, those between 2–50 nm as mesopores and those larger than 50 nm as macropores (Sing et al., 1985). The term of nanopore is also sometimes used to describe mesopores.

Ordered mesoporous materials possess outstanding properties compared with other porous materials, including: (1) high surface area, high porosity and high pore volume; (2) well-defined pore sizes and shapes with a narrow pore-size distribution; (3) adjustable pore size in the range of 2−30 nm; (4) highly ordered pore structures at the nanometer level; (5) presence of micropores in the amorphous walls; (6) diversity of structures, wall compositions and pore shapes; (7) high thermal and hydrothermal stability; (8) availability of different controllable regular morphologies on scales ranging from nanometers to micrometers (Zhao et al., 2012, Charnay et al., 2004, Kapoor et al., 2009, Vinu et al., 2005).

The discovery of MCM-41 (M41S family), the first mesoporous material, in 1992 by Mobil scientists heralded the beginning of ordered-mesoporous-material synthesis and application (Kresge et al., 1992, Wan and Zhao, 2007). Since then, mesoporous materials have attracted research interest and much progress has been accomplished in aspects such as elucidating the

formation mechanism, synthesizing mesoporous materials with large pore sizes (up to 30 nm) and generating mesoporous materials in different structures (lamellar, cubic and 2D- and 3D-hexagonal phases) (Figure 2.10) and forms (films, fibers, spheres and monoliths) (Hartmann, 2005, Stein, 2003, Meynen et al., 2009). To date, the ordered mesoporous materials and their synthesis methods have become a 'hot' research area in the discipline of material science worldwide.

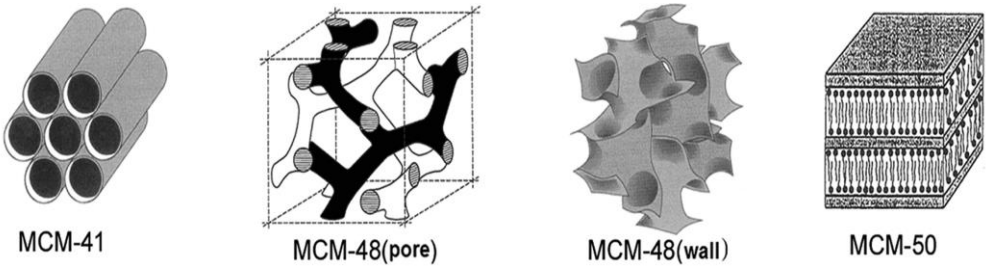

Figure 2.10 Structures for first synthesized mesoporous materials (M41S family)

Mesoporous materials have practical application in areas such as adsorption, separation, purification of gas and liquid, catalysis and also been used as semiconductors, optics components, sensors, materials for environmental protection and so on (Xu et al., 2009, Igarashi et al., 2007, Perez-Quintanilla et al., 2006, Bhatnagar and Sillanpaa, 2010). With specific regard to drug delivery, mesoporous materials have also offered much promising potential (Manzano and Vallet-Regi, 2010, Wang, 2009). For example, improved dissolution of poorly soluble drugs either rapid release or sustained release of active pharmaceutical ingredients (APIs) through the encapsulation of drug particles into nano-sized carriers.

The successful development of a mesoporous drug carrier involves the production of the porous material, the design of the appropriate surface chemistry and the characterization of the properties of the carrier and the drug loaded in the pores. There are several types of mesoporous materials are available, such as mesoporous carbon, polymers and various metal oxides (Ahola et al., 2000, Kortesuo et al., 2000, Unger et al., 1983). Among them, silicon-based materias sucha as porous silicon (PSi) and porous silica are the most studied mesoporous materials in drug delivery applications. More literature of the applications of mesoporous carriers in dissolution enhancement is provided in Table 2.12. The characteristics of porous silica render it suitable for different purposes: its relatively inert nature makes it a perfect host for guest species and its structural features afford improved molecular accessibility and rapid mass transport (Zhao et al., 1998, Ambrogi et al., 2007, Heikkila et al., 2007, Charnay et al., 2004).

2.6.6.1.1 Mesoporous silica

The first mesoporous silica was synthesized with amphiphilic triblock copolymers in 1998 by Zhao et al (Zhao et al., 1998). These materials are named SBA-X (Santa Barbara Amorphous) where X is a number denoting a specific pore structure and surfactant, e.g. SBA-15 has hexagonally ordered cylindrical pores synthesized with P123 as a surfactant while SBA-16 has spherical pores arranged in a body-centred cubic structure synthesized with F127. Other families of mesoporous silica are MSU (Bagshaw et al., 1995), KIT (Ryoo et al., 1996) and FDU (Yu et al., 2000) which are synthesized

under various conditions with different surfactants. Among these mesoporous silica, the SBA-series has attracted considerable interest for various applications, chief amongst which is the most extensively studied SBA-15, which is the subject of attention in this thesis (Zhao et al., 1998). In the following sections are summarized more details of SBA-15 including syntheses, structures, formation mechanisms and applications.

2.6.6.1.1.1 Santa Barbara Amorphous-15 (SBA-15)

SBA-15 is a mesoporous silica (SiO_2) characterized by hexagonally arranged cylindrical pores, with the pore size being tuneable between 4–26 nm and the length of the pores ranging from approximately 200 nm to several microns (Zhao et al., 1998, Zhang et al., 2004). Around each mesopore is a microporous network called the corona (Impéror-Clerc et al., 2000, Ryoo et al., 2000), which originates from trapped hydrophilic chains of the surfactants (Kruk et al., 2000, Ruthstein et al., 2003). This network underlies the interconnection of the mesopores with each other, affording its hexagonal structure (Figure 2.11) and high surface area of SBA-15.

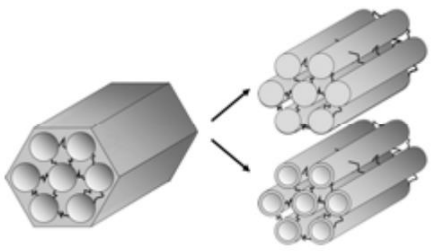

Figure 2.11 The structure of mesoporous silica SBA-15 (to the left) and its replica in form of rods (top right) and straws (bottom right).

The meritorious features of SBA-15 render it ideal for a diverse array of applications. Its narrow pore size distribution makes it a suitable candidate as molecular sieves and as templates for producing nanoparticles and other mesoporous structures. Its large specific surface area (500–1000 m^2/g) contributes to its being an ideal substrate for catalysts and mesoreactors where chemical reactions take place in the pores. Besides that, by proper functionalization of the silica walls, catalytic reactions can be realized at the surfaces. Examples of the usage of SBA-15 as a host for catalysts are: incorporation of Ti for hydrogen storage and photovoltaic applications (Das et al., 2010), addition of FeW for hydrotreating heavy gas oil and storage of methanol (Boahene et al., 2011). Furthermore, SBA-15 can be used as a template for anode or cathode materials for batteries (Procházka et al., 2009, Xi et al., 2005). SBA-15 is also exploited in solar cell applications, both as a template for incorporation of titanium or cobalt nanoparticles (Lachheb et al., 2011, Ding et al., 2005) and as a scattering layer for improving the cell efficiency (Yang and Zheng, 2012).

With specific regard to dosage form design, mesoporous silica has been shown to be an excellent carrier for poorly water soluble drugs (Slowing et al., 2008). The delivery of such drugs by means of mesoporous silica can resolve many problems associated with these molecules. In general, for poorly soluble drugs, an enhanced release rate can be achieved either by reducing the drug particle size or by changing in the physical state of loaded drugs (meta-stable or amorphous forms) via confining the drugs into mesopores (Salonen et al., 2008). In the latter, the use of mesoporous silica not only augments the

release rate but also efficiently stabilizes the state of the drug. In addition, SBA-15 with large specific surface areas and total pore volumes provides a high capacity to absorb drug molecules into their pore structures, thereby achieving a high extent of drug loading. The high applicability of this method to a wide variety of poorly soluble drugs (Van Speybroeck et al., 2009) also means that it is conveniently unnecessary to tune the carrier according to the properties of the drug, provided that the drug is chemically compatible with the carrier. Other potential benefits of the carrier are as follows: ensuring a sustained release resulting from attachment of molecules onto the surface and diffusion limitations; potentially protecting drug molecules from enzymatic degradation prior to release since the pores are inaccessible to enzymes; and ease of practical use (the loading of the carrier is uncomplicated, at least on a laboratory scale and can be performed at room temperature).

2.6.6.1.1.2 Syntheses of Mesoporous Silica

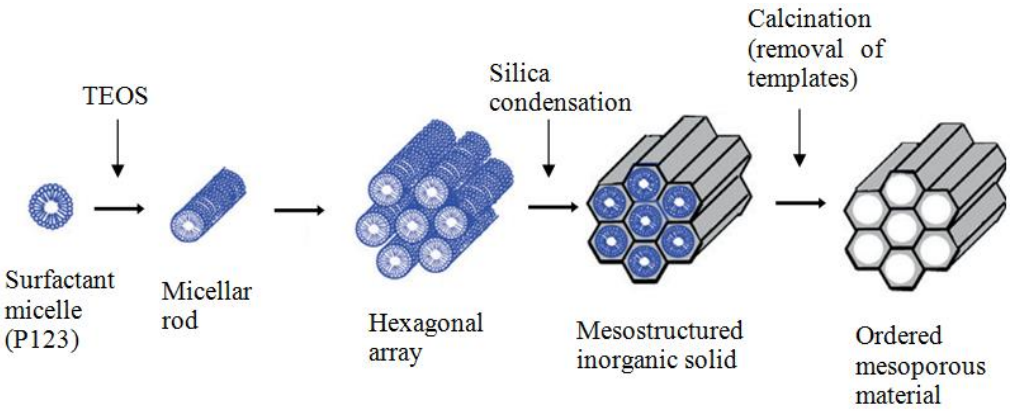

Figure 2.12 Possible synthesis pathway for the synthesis of hexagonal silica

The core principle of synthesis of all the mesoporous materials is almost the same. It involves a sol–gel process (Figure 2.12), in which surfactants or other species are used as templates in the presence of an acidic or basic synthesis medium. The nature of the templates may be cationic, anionic, neutral, multiple charges, multiple alkyl chains and polymer surfactants while the temperatures may vary from room temperature to approximately 150 ºC. The structures and compositions of materials are also extended, including silica-based materials: FSM-16, SBA-1, SBA-2, SBA-6, SBA-8, SBA-11, SBA-12, SBA-16, FDU-n, disordered HMS, MSU-n, KIT-1 and so on.

There are four main steps in the preparation of SBA-15. The first step is the synthesis of the mesoporous structure using a block copolymer and a silica precursor. The surfactants are added to a homogeneous, acidic solution containing distilled water and HCl. In some cases, the addition of surfactants may be preceded by that of swelling agents. For SBA-15, the triblock

copolymer P123 is used as the surfactant. The P123 forms spherical micelles in the solution. Upon addition of silica precursor, it penetrates into the core of the micelles due to their hydrophobic properties. The hydrolyzed precursors then diffuse into the corona and adsorb onto the P123, followed by polymerization beginning in the core/corona interface and subsequently in the corona. The polymerization in the core/corona region is simultaneous with respect to the elongation of the micelles whereas the polymerization in the pure corona is associated with the precipitation of flocs. When the silica precursor is polymerized on the PEO chains, the water content in this area is decreased. This changes the polarity resulting in a reduced curvature of the micelle and hence, the micelles, now elongated from spheres to cylinders, arrange themselves in a hexagonal pattern while the silica walls are built.

The second step is the hydrothermal treatment at a higher temperature after the formation of SBA-15. Through hydrothermal treatment, the properties of the final products such as pore size, micropore volume and surface area can be tuned. After the establishment of the hexagonal structure, the PEO chains are trapped into the silica network (Ruthstein et al., 2003, Galarneau et al., 2001), which subsequently are the source from which the micropores in the final product are formed. With increasing temperature, the PEO chains becomes more hydrophobic and retract from the silica wall and migrate into the more hydrophobic core of the micelles. The results of this are threefold: an increased pore size, reduced microporosity and surface area and reduced shrinkage of the silica walls upon calcination. The effect of hydrothermal treatment is illustrated in Figure 2.13. By increasing the

hydrothermal treatment temperature from 35 to 130 ˚C, it is possible to increase the mesopore size by several nanometers. Significant changes are observed above 60 ˚C (Galarneau et al., 2001). wherethe microporosity and surface area are decreased. At 130 ˚C, no micropores remain and all surface originates from the mesopores. The unit cell parameter is however nearly constant for calcinated samples with hydrothermal treatment temperature above 60 ˚C; therefore, during the increase of mesopore size, the wall thickness decreases, the wall becomes denser and the microporosity is lost (Galarneau et al., 2001, Impéror-Clerc et al., 2000). A similar effect, but not as pronounced, is observed by prolonging the hydrothermal treatment time.

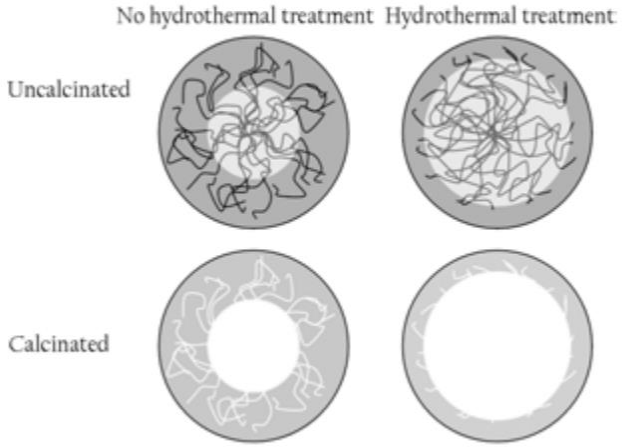

Figure 2.13 The effect of the hydrothermal treatment.

Filtration and washing the samples are the third step followed by the fourth and final step is the removal of the surfactants most often done by calcination. Calcination is the most common way to remove the surfactants from SBA-15. During the process, which is performed in air, the material is heated to 550 ˚C and this temperature is held for 5 h before the material is cooled down to room temperature. Most of the surfactants decompose between

150–250 ˚C and at this stage the hexagonal structure retains its size. Above 300 ˚C water is released and the rest of the polymers are combusted and the hexagonal framework is decreased probably due to condensation in the framework and closure of micropores (Kleitz et al., 2003). During the shrinkage of the hexagonal structure, the mesopore volume is decreased but the micropore volume remains almost constant (Bérubé and Kaliaguine, 2008).

Table 2.12 The application of mesoporous carriers in dissolution enhancement of poorly water-soluble drugs reported in literature. The BET surface area (S_{BET}), pore diameter, pore volume and particle size of the carriers as well as the drug loading used in each study are provided.

Mesoporous carrier	S_{BET} (m^2/g)	Pore diameter (Å)	Pore volume (cm^3/g)	Particle size (μm)	Morphology	Drug	Loading (wt%)	BCS	References
MCM-41	996	39	0.70	1.0	Oval	Carvedilol	25.0	II	(Hu et al., 2012b)
	1028	27	0.73	–	–	Fenofibrate	20.0		(Van Speybroeck et al., 2010a)
	1200	33	1.00	–	–	Ibuprofen	41.0		(Andersson et al., 2004)
	768-1157	25-36	0.85-1.01	–	–	Ibuprofen	11.0–34.0		(Horcajada et al., 2004)
	1063	26	0.72	<38.0	–	Ibuprofen	11.7		(Heikkilä et al., 2007)
	850	34	0.62	10.0–50.0	Spheres	Ibuprofen	2.5– 37.1		(Charnay et al., 2004)
	920	34	0.78	<125.0	Irregular clusters	Indomethacin	27.0		(Limnell et al., 2011b)

Mesoporous carrier	S_{BET} (m^2/g)	Pore diameter (Å)	Pore volume (cm^3/g)	Particle size (µm)	Morphology	Drug	Loading (wt%)	BCS	References
SBA-15	629	73	0.83	–	Fibrous- rod-like sub-particles	Celecoxib	–	II	(Zhao et al., 2012a)
	866	70	1.10	–	–	Ezetimibe	17.9		(Kiekens et al., 2012)
	518/862	44/73	0.41/1.03	–	–	Fenofibrate	20.0/ 40.0		(Van Speybroeck et al., 2010a)
	607	72	0.90	–	–	Glibenclamide indomethacin	22.5 19.3		(van Speybroeck et al., 2011)
	625	69	1.07	~50.0	Rod-like particle	Ibuprofen	102.0		(Heikkilä et al., 2007)
	734	60	1.05	0.5– 1.0	Spheres	Ibuprofen	50.0		(Shen et al., 2010)
	487-618	78- 81	0.62-1.05	13.8	Irregular shapes	Itraconazole	19.1		(Vialpando et al., 2011)
	844	73	0.85	0.2– 1.0	Randomly oriented building	Itraconazole	21.3		(Mellaerts et al., 2008)

Mesoporous carrier	S_{BET} (m^2/g)	Pore diameter (Å)	Pore volume (cm^3/g)	Particle size (μm)	Morphology	Drug	Loading (wt%)	BCS	References
					blocks			II	
	918	113	1.15	~0.05/1.0–2.0	Clustered sheets	Telmisartan	27.5		(Zhang et al., 2012)
	636/664	76/83	0.81/0.83	0.2– 1.0	–	Carbamazepine Cinnarizine Danazol Griseofulvin Ketoconazole Nifedipine Phenylbutazone	22.5 20.7 20.9 19.7 20.4 20.7 19.8		(Van Speybroeck et al., 2009)
Spherical mesoporous silica	963-1283	25	0.56-0.72	0.5– 1.0	Spheres	Ibuprofen	21.3–24.3		(Xu et al., 2009)
Syloid 244	311	190	1.42	2.5– 3.7	Irregular clusters	Indomethacin	28.9		(Limnell et al., 2011b)
Syloid AL- 1	683	32	0.13	6.5– 8.1	Spheres	Itraconazole	21.0/25.1		(Kinnari et al., 2011)
Syloid AL-244	311	190	1.42	2.5– 3.7	Spheres	Itraconazole	21.9/32.8		(Kinnari et al., 2011)

Mesoporous carrier	S_{BET} (m^2/g)	Pore diameter (Å)	Pore volume (cm^3/g)	Particle size (μm)	Morphology	Drug	Loading (wt%)	BCS	References
APTES modified SBA- 15	458-860	78/86	0.70-1.20	–	–	Ibuprofen	16.9–37.2	II	(Song et al., 2005)
SBA-16	541	43	0.34	2.0– 3.0	Spheres	Carvedilol	25.0		(Hu et al., 2012b)
PSi	254	129	1.33	<38.0	–	Ibuprofen	36.8		(Limnell et al., 2007)
TCPSi	248	–	0.87	<38.0	–	Antipyrine Ibuprofen Ranitidine.HCl Furosemide	53.4 30.4 13.2 41.3	I II III IV	(Salonen et al., 2005)
	246	151	0.96	<38.0	–	Ibuprofen	30.9	II	(Limnell et al., 2007)
	282	110	0.86	<38.0	–	Ibuprofen	41.5		(Heikkilä et al., 2007)
	253	129	1.06	25.0–75.0	Angular structures	Itraconazole	11.3		(Kinnari et al., 2011)
AnnTCPSi	59	465	0.63	<38.0	–	Ibuprofen	39.6		(Limnell et al., 2007)

Mesoporous carrier	S_{BET} (m^2/g)	Pore diameter (Å)	Pore volume (cm^3/g)	Particle size (μm)	Morphology	Drug	Loading (wt%)	BCS	References
TOPSi	321	88	0.54	13.6	Irregular shape with sharp edges	Indomethacin	5.6	II	(Wang et al., 2010)
TOPSi	226	91	0.73	25.0–75.0	Angular structures	Itraconazole	11.2		(Kinnari et al., 2011)
TOPSi	222	85.3	0.62	<38.0	–	Ibuprofen	36.5		(Limnell et al., 2007)
AnnTOPSl	71.5	407	0.67	<38.0	–	Ibuprofen	30.9		(Limnell et al., 2007)
Mesoporous carbon	1069-1457/ 722-938	38-60/44-70	1.02-1.49/0. 87-1.09	5.0– 40.0	Spherical/ fibrous	Lovastatin	25.6–36.3		(Zhao et al., 2012b)
Carbon	722-938	44-70	0.87-1.09	0.5– 0.8/ 5.0– 40.0	Fibrous- rod-like sub-particles	Celecoxib	28.5–37.5		(Zhao et al., 2012a)
Magnetic mesoporous carbon	667-1471	33-34	0.75-0.98	–	–	Ibuprofen	18.0–30.0		(Wang et al., 2011b)

Mesoporous carrier	S_{BET} (m^2/g)	Pore diameter (Å)	Pore volume (cm^3/g)	Particle size (μm)	Morphology	Drug	Loading (wt%)	BCS	References
NFM-1	793	26	0.40	10.2	Rod -type	Atazanavir	28.2	II	(Xia et al., 2012)
AMS-6	847	43	0.80	9.4	Spheres	Atazanavir	31.5		(Xia et al., 2012)
STA-11	847	79	0.85	9.9	Spheres	Atazanavir	32.8		(Xia et al., 2012)
TiO2 (ATMT)	109	300–400	0.15	0.2	Spheres	Carvedilol	23.9		(Jiang et al., 2012a)
TiO2 (APMT)	364	20–30	0.20	0.3	Cotton-like spheres	Carvedilol	22.8		(Jiang et al., 2012a)
Hydroxycarbonate apatite	98-122	<35	0.11-0.18	0.2– 0.3	Clustered sheet	Carvedilol	22.5–48.7		(Zhao et al., 2012c)
TUD-1	453	46	0.57	<38.0	–	Ibuprofen	49.5		(Heikkilä et al., 2007)
COK- 2	445 - 652	81- 91	0.55 - 1.05	19.0	Irregular shapes	Itraconazole	18.1		(Vialpando et al., 2011)

2.7 Methods of Preparation of Solid Dispersions

Solid dispersions can be formulated through thermal and solvent methods. The former includes fusion method, solvent evaporation and hot-melt extrusion whereas the latter includes supercritical fluid technology, lypophillization and spray drying. Provided in the following section are a short summary of the fusion method, hot-melt extrusion, supercritical fluid method and lypophillization and detailed explanations of spray drying, i.e. the technique of interest in this study.

2.7.1 Thermal Methods

2.7.1.1 Fusion/Melting Method

The fusion method entails the dissolution of drugs in molten carriers in rubbery state by direct heating for incorporation into the matrix. Processes such as ice bath agitation, spreading on plates placed over dry ice, immersion in liquid nitrogen, spraying the hot melt on a cold surface and storage in desiccators are used to cool and solidify the melted mixture. The resultant sample is crushed, pulverized and sieved (Chiou and Riegelma.S, 1971). The combination of sulfathiazole and urea as a matrix was the first solid dispersion prepared by the fusion method for pharmaceutical applications. Poly (ethylene glycol), poly (vinyl pyrrolidone), mannitol and poloxamers are types of matrices commonly used in the fusion method because of their low melting point (Sharma and Jain, 2011, Leuner and Dressman, 2000). Several

modifications such as hot-melt extrusin, melt agglomeration and Meltrex™ were introduced to overcome the limitations encountered by this technique.

2.7.1.2 Hot-Melt Extrusion

Hot-melt extrusion is a method similar to the fusion method but there is an additional mechanical process applied to the molten mixture of drug, carrier and plasticizer under controlled conditions of temperature and shear forces. The co-melts are mixed, homogenized using transport screws and extruded through a die to form tablets, pellets, sticks and sheets for implants, ophthalmic inserts, or oral dosage forms (Crowley et al., 2007, Breitenbach, 2002). One of the important parameters for hot-melt extrusion technique is the operating temperature, which can be determined by the melting points (T_m) of drug and of crystalline carrier or glass transition temperature (T_g) of the amorphous carrier. Knowledge of the optimal operating temperature is critical to not only preventing degradation of the drug during this process but also ensuring that the carrier(s) are sufficiently softened (less viscous) so that it can flow through the extruder (Forster et al., 2001b). Additives such as surfactants (Tween® 80) are widely used as plasticizers to decrease the T_m or T_g of carriers and the operating temperature to enable the flow of the mixture through the extruder (Ghebremeskel et al., 2007). Two categories of carriers widely used in hot-melt extrusion are the synthetic polymeric carriers and the carbohydrate carriers. Examples of synthetic polymeric carriers include PVP K30, PVPVA 64 and EudragitR E100 (polymethacrylates) whereas examples of carbohydrate carriers include cyclodextrin (CD) derivatives and

hydroxypropylmethylcellulose (Forster et al., 2001a, He et al., 2010, Fu et al., 2010). Although hot-melt extrusion has some disadvantages as a fusion method, this technique offers continuous production which is suitable for large scale productions (Leuner and Dressman, 2000).

2.7.2 Solvent Methods

2.7.2.1 Supercritical Fluid Method

Supercritical fluid method is another technique used for formulating solid dispersion and for particle size reduction. Supercritical fluid exists as a single fluid phase with both liquid and gas physicochemical behaviors: the liquid-like characteristic is exploited for the dissolution of the solute whereas the gas-like characteristic is exploited for the rapid precipitation of solutes. Carbon dioxide is the most common supercritical fluid used because of its low supercritical temperature (T_c=31.1°), low supercritical pressure (P_c=73.8 bar), inertness, nontoxic and non-flammable nature, cost-effectiveness and environmentally friendly properties (recyclable after processing) (Lim et al., 2012). The relatively low T_c and P_c allow easy processing which is suitable for pharmaceutical products (Yasuji et al., 2008). Even nitrous oxide, water, methanol, ethanol, ethane and propane are also used as supercritical fluids for a variety of applications. There are two categories of supercritical drying in which the supercritical fluid plays different roles: as a solvent and as an anti-solvent (Subramaniam et al., 1997). When the supercritical fluid is used as a solvent, the drugs are dissolved in it and the precipitation of drug or solid

dispersion is obtained by reducing the pressure and/or the temperature [known as rapid expansion of supercritical solutions (RESS)]. The main disadvantage of this method is that both the drug and the carrier have to be soluble in supercritical CO_2 which may not be invariably feasible for many drug and carrier combinations (Matson et al., 1987). Conversely, when the supercritical fluid is used as an anti-solvent, a common organic solvent is used to dissolve both the drug and the carrier, followed by the saturation of the solution with supercritical CO_2 to precipitate the drug and the carrier (Sharma and Jain, 2011, Leuner and Dressman, 2000). In this technique, the drug and carrier should not be soluble in the mixture of supercritical fluid and organic solvent; and the organic solvent should be miscible with the supercritical fluid. Among the methods in which the supercritical fluid serves as an anti-solvent include gas antisolvent precipitation (GAS), precipitates by compressed antisolvent (PCA), supercritical antisolvent (SAS), aerosol solvent extraction system (ASES) and solution enhanced dispersion by supercritical fluids (SEDS) (Pasquali et al., 2008).

2.7.2.2 Lyophilization

Lyophilization or freeze-drying is an alternative method to replace the drying and solvent evaporation process in order to prepare solid dispersions. In this technique, the drug and the carrier are dissolved in a common solvent, which is then subjected to freezing and sublimation to produce a lypophilized molecular dispersion. It consists of three sequential steps: freezing, primary drying and secondary drying. In freezing, samples that consist of the drug, the

carrier and the solvent system are solidified (Abdelwahed et al., 2006). The frozen solvents are then removed from the sample by sublimation (primary drying) and the remaining unfrozen solvents are removed by diffusion/desorption (secondary drying) to produce the final product with a sufficiently low moisture or solvent content. Lyophilization is advantageous in two aspects: the drugs undergo minimal thermal stress during formulation; and the risk of phase separation is reduced once the solution is vitrified. The disadvantage, however, is that more complex co-solvent systems are required due to the low solubility of lipophilic compounds in water. Furthermore, the choices of organic solvents to be used in lyophilization are very limited because most organic solvents have a low freezing point. Ideal co-solvents for lyophilization, therefore, are those with a high vapor pressure for high sublimation rate and a high melting point to allow convenient freezing (Sharma and Jain, 2011, Leuner and Dressman, 2000). Therefore, organic solvents such as tertiary butanol (TBA) and 2-methyl-2-propanol which fulfill such criteria are widely used in this process (Van Drooge et al., 2004).

2.7.2.3 Spray Drying

Spray drying is a widely applied and effective technique to convert aqueous or organic solutions into dry materials with distinct properties required for various applications. The spray dryer was discovered and developed in the 1940s to reduce the weight and volume of food products for transportation during World War II (Shahidi and Han, 1993, Gouin, 2004). Intensive research and development in the last few decades have rendered

spray drying a highly competitive and widely applicable technology in the pharmaceutical, chemical and food industries. The range of product applications produced predominantly by spray drying continues to expand, among which are dairy products, detergents and dyes (R. P. Patel et al., 2009).

Spray drying is a continuous process in which a fluid feed will be transformed into dried particles by spraying the feed into a hot drying medium such as air or nitrogen, where the evaporation of the organic solvent or water gives rise to solid microparticles (Billon et al., 2000). The feed can be in the form of solutions, emulsions or suspensions which contain a drug, a carrier and sometimes additives. The final products can be in the form of powders, granules or agglomerates, depending on the parameters of the spray dryer and the physicochemical properties of the final products (Ré, 2006). Important parameters that affect the morphology, yield, physicochemical characteristics and amount of residual solvent of the final products include the following: feed rate of the solution, flow rate of the atomizing air, inlet temperature and flow rate of the drying gas (Dobry et al., 2009, Esposito et al., 2000, Cabral-Marques and Almeida, 2009, Nekkanti et al., 2009). Detailed correlations of these parameters for optimization of the instrument settings are provided in Table 2.13.

Table 2.13 Optimization of the process settings of spray drying

Dependence	Parameter						
	Aspirator rate	Air humidity	Inlet temperature	Spray air flow	Feed rate	Solvent instead of water	Concentration
Outlet temperature	Less heat loss based on total inlet of energy	More energy stored in humidity	Direct proportion	More cool air to be heated up	More solvent to be evaporated	Less heat of energy of solvent	Less water to be evaporated
Particle size	–	–	–	More energy for fluid dispersion	More fluid to disperse	Less surface tension	More remaining product
Final humidity of product	Lower partial pressure of evaporated water	Higher partial pressure of drying air	Lower relative humidity in air	–	More water leads to higher particle pressure	No water in feed leads to very dry product	Less water evaporated, lower partial pressure
Yield	Better rate of separation in cyclone	More humidity can lead to sticking product	Eventually dryer product prevent sticking	–-	Depends on applicatio n	No hygroscopic behavior leads to easier dying	Bigger particles lead to higher separation

Various types of spray dryers are available for current applications, among which are single-stage and two-stage spray dryers, horizontal and vertical spray dryers and fluidized spray dryers. Spray dryers are used based on the type of applications and the properties of samples; for example, two-stage spray dryers are used for heat-sensitive samples whereas vertical spray dryers are suitable for both fat and non-fat samples (R. P. Patel et al., 2009). Spray dryers can be divided into two designs: open-cycle and close-cycle (or inert loop). In the open-cycle design, the air used as a heating medium and the aqueous solution as a feeding medium are discharged into the atmosphere after use; in the close-cycle design, inert gases such as nitrogen are used as a drying medium and the organic solvents as a feeding medium is re-cycled after use (R. P. Patel et al., 2009, Ré, 2006).

The four fundamental steps involved in spray drying are atomization, mixing, evaporation and separation (Thybo et al., 2008, Paudel et al., 2013). Spray drying starts with the atomization of a liquid feed into a spray of fine droplets, which are then mixed with a heated gas stream (typically air or nitrogen gas), allowing the liquid to evaporate, leaving behind the dried solids of a similar size and shape depending on the form of atomized droplets. The drying continues until the desired moisture content is achieved in the sprayed particles. Finally, the dried powder is separated from the gas stream and collected (Boersen, 1990, Ameri and Maa, 2006).

In atomization, the fluid streams will be broken down into fine droplets by applying force or pressure to increase the surface area per volume ratio of

the streams. The size of the droplets depends on the flow rate, viscosity, solid content and surface tension of the feed. Smaller particles will have a larger surface-to-volume ratio which affords a better evaporation rate, so that the particles can be dried more rapidly and efficiently. Several types of atomizers are available for spray drying, such as rotary atomizer, ultrasonic atomizer, pressure nozzle and single and two-fluid nozzles (Paudel et al., 2013). Choosing the right atomizer is critical to yield products of a high quality and with the desired properties such as particle size, shape and density. There are a number of aspects that determine the selection of atomizers such as the properties of the liquid to be processed and the specifications required for the final product.

The atomized fluid streams will come across with the heated air from the air disperser for evaporation to take place. The mixing and evaporation processes must occur immediately after atomization to prevent the droplets from sticking on the walls of the dryer. The 3 types of configuration to mix the heated air with the atomized droplets are the concurrent configuration (suitable for commodity chemicals), the counter-current configuration (suitable for products that need heat treatment) and the mixed-flow configuration (suitable for thermally stable products).

Drying or evaporation is a crucial part of spray drying process because it will determine the quality of the final products. Evaporation begins once the droplets come into contact with the heated air and continues until the fluid can diffuse from the inner part to the surface of the solids. The dimensions of the

drying chamber play a crucial role in evaporation of the droplets, by providing sufficient contact time between the droplets and hot air to prevent direct contact between the droplets and the heated chamber walls. It is substantially important to prevent the droplets from coming into contact with and sticking to the walls before they have been dried. Once the products are dried into the powder form, the fine powder will be collected by using a cyclone separator, while the used drying gas and medium is treated to fulfil environmental requirements followed by exhaustion of the gas to the atmosphere or, in some cases, re-circulated to the system.

Spray drying has garnered much attention as it exhibits multifarious advantages compared with other conventional methods. Such useful features render it a promising technique in formulating various types of products in the pharmaceutical, chemical and food industries (Takeuchi et al., 2005, Moretti et al., 2001), including heat-resistant and heat-sensitive drugs, organic or non-organic excipients, water-soluble and water-insoluble drugs and hydrophilic and hydrophobic polymers (Ré, 2006). Some of the advantages offered by spray drying are:

i. It has demonstrated reproducibility and reliability under production conditions and enabled the possible control of particles size and drug release.
ii. A wide range of spray drying designs is available to meet diverse product specifications. Various types of feeds can be dried instantaneously into fine, homogeneous and often amorphous powder

with a large surface (Sahoo et al., 2009). Feed concentration, nozzle feed rate and inlet air temperature of the drying gas play vital roles in determining the particles characteristics; thus sample properties can be controlled by optimizing these critical parameters (Paudel et al., 2013).

iii. Feeds with different viscosities such as solutions, slurries, pastes, gels, suspensions or melt forms can be spray dried as long as the feeds can be pumped (Ré, 2006).

iv. Spray drying presents as a technique in which different types of powder samples can be handled with negligible degradation; for instance, heat-sensitive or heat-resistant samples can be spray dried with the retention of the properties and quality of the final products. The rapid evaporation of liquid from atomized droplets entails only low particle temperatures, which minimize heat damage or degradation under optimal conditions (Ståhl et al., 2002, Ré, 2006).

v. In terms of economic considerations, spray drying is able to reduce mass and energy consumption because dried final products in micron-sized powders can be produced within a single processing step and additional secondary manufacturing steps such as micronization and milling could be minimized (Boersen, 1990, Ameri and Maa, 2006).

In next section, some of the important formulation techniques that have been used to enhance the biopharmaceutical and physicochemical properties of various types of antimalarial drugs will be discussed.

2.8 Formulations of Antimalarial Drugs

Enhancing the bioavailability and therapeutic efficacy of antimalarial drugs (especially artemisinin) is a major concern and challenge encountered by pharmaceutical industries. Various approaches have therefore been used to improve their performance and the efficiency. For example, Lapenna et al. (2009) have investigated not only the micellar solubilization capacity of sodium dodecyl sulphate (SDS) for artemisinin and curcumin but also the potentially useful combination of the surface activity and antioxidant properties of the binary system of SDS and octanoyl-6-O-ascorbic acid (ASC8) for artemisinin. Quantitative analysis measurements by diffusion-ordered spectroscopy (DOSY) and 1H-NMR revealed two findings: firstly, the solubility of artemisinin and curcumin increased as a function of the concentration of SDS; secondly, the incorporation of ASC8 enhanced the molecular stability. Gahoi et al. (2012) reported elevated antimalarial activity of lumefantrine by nanopowder formulation through wet-milling using DYNO MILL with HPMC E3 and Tween 80 as dispersing agents. This formulation technique afforded nanoparticles of lumefantrine with a mean size of 251 nm. It was found that the nanopowder exhibited an enhanced dissolution rate and *in vivo* antimalarial activity with an IC_{50} 175-fold lower than untreated lumefantrine.

Balducci et al. (2013) studied the efficiency of formulation of microparticles of artemisinin/β-cyclodextrin via co-spray drying in enhancing the dissolution rate and bioavailability of oral dosage forms of artemisinin.

The co-spray dried microparticles were able to increase the apparent solubility of artemisinin by approximately six-fold and its dissolution rate (in 10 min) by 60% compared with untreated artemisinin. Yang et al. (2009) reported a similar study, but, instead of artemisinin and β-cyclodextrin, they used artemether and hydroxypropyl-β-cyclodextrin. The results have shown that the apparent bioavailability was enhanced by 1.81-fold compared with untreated artemether due to an increase in water-solubility. Shahzad et al. (2012) evaluated the effectiveness of solid dispersions of artemisinin by three different formulation methods: physical mixtures using glass mortar and pestle, solid dispersions via solvent evaporation and lyophilization. Samples with different drug ratios were prepared with the hydrophilic polymer polyvinylpyrrolidone (PVP). The dispersions of artemisinin with PVP improve the pharmaceutical properties of ART including solubility and permeability in this descending order: lyophilisation > solvent evaporation > physical mixtures. The solubility of lyophilized artemisinin, which was found to be PVP-dependent, was increased by up to 4-, 5- and 8-fold in water, in PBS and in methanol, respectively.

Additional examples from the literature regarding the formulation techniques are summarized in Table 2.14. Despite the number of studies reporting solubility and bioavailability enhancement techniques of antimalarial drugs, to the best of our knowledge, there have been very few studies regarding the physicochemical stability of antimalarial drugs, especially artemisinin. Knowledge of the long-term storage stability of drugs is essential in order to understand their performance for long periods and their shelf-life.

Therefore, characterization of the physicochemical stability of artemisinin in single dosage forms and combination dosage forms are the major aim of this study.

Table 2.14 Formulation approaches to enhance the solubility and bioavailability of antimalarial drugs.

Antimalarial drugs	Solubility enhancement techniques	References
Mefloquine	Co-crystallization by using solution crystallization method	(Yadav et al., 2010, Shete et al., 2013)
	Preparation of microparticles by co-acervation method using Eudragit E (polymer) and sodium hydroxide (precipitant)	(Shah et al., 2008)
Artemisinin and curcumin	Liposomal delivery systems via film hydration method using poly(ethylene glycol)-2000 distearoylphosphatidylethanolamine	(Isacchi et al., 2012)
α-(2-Piperidyl)-3,6-bis(trifluoro methyl)-9-phenanthrene methanol	Formation of drug salts by hydrophilic counterions	(Agharkar et al., 1976)
Curcumin	Micellization using Camel Beta-casein	(Esmaili et al., 2011)
	Formation of complexation with phosphatidyl choline	(Gupta and Dixit, 2011)
	Formation of solid dispersion by solvent evaporation technique using cellulose acetate	(Wan et al., 2011)
	Microemulsions using oil, surfactant and co-surfactant	(Hu et al., 2012a)
Artemisinin	Formation of artemisinin-polyethylene glycol liposomes according to film-hydration method	(Isacchi et al., 2011)

Antimalarial drugs	Solubility enhancement techniques	References
	Formation of microparticles by co-spray drying ART with polyethylene glycol (PEG) via modified multi-fluid nozzle pilot spray drier	(Sahoo et al., 2011b)
	Inclusion complex with β-CD by evaporative precipitation of nanosuspension (EPN) method	(Kakran et al., 2011)
	Micronization and formation of solid dispersions with PVPK25 and supercritical fluid technology	(Van Nijlen et al., 2003)
	Micronization via a Rapid Expansion of Supercritical Solutions (RESS) method	(Yu et al., 2012a)

2.9 Latest Outlook of Formulations of Poorly Water-Soluble Drugs

Although existing sophisticated approaches have circumvented the drawbacks of poorly water-soluble drugs and improved the absorption of the active substances, these approaches are often inefficient due to inadequate drug delivery for most formulations and yet to progress to broad clinical application. Numerous new approaches have been proposed from time to time to overcome the limitation and inefficiency of currently available drug delivery systems. The global market for advanced drug delivery systems amounted to $134.3 billion in 2008 and rose to $139 billion in 2009 and to $196.4 billion in 2014. Examples of novel drug delivery approaches are summarized as follows (Bernkop-Schnurch and Kast, 2001).

Combinations of two or more formulation strategies in a single device have become increasingly attractive. For example, mucoadhesive polymers chemically bound to an enzymatic inhibitor of peptidases have been synthesized to afford and improve oral delivery of peptides and proteins (Bernkop-Schnurch and Kast, 2001).

Intestinal patches are another novel oral delivery method to address shortcomings of poorly-absorbed molecules, such as peptides and proteins. These patches with combination of different features into a single drug delivery platform possess multiple advantages compared with other polymeric systems. Using such patches minimizes the dilution and loss of drugs into luminal fluids by creating a reservoir containing an elevated drug concentration with unidirectional drug release (Martin and Grove, 2001).

Nanotechnology, characterized by the technology of using carriers on the nanoscale, is another technique that enhances oral drug delivery and overcomes the associated demerits including poor solubility, stability and biocompatibility of drugs (Agrawal et al., 2014). Nanotechnology has been used to improve oral delivery of anticancer drugs across the gastrointestinal barrier by virtue of their extremely small size and their appropriate surface-coating to escape from the recognition by P-glycoprotein (P-gp) (Wang et al., 1996). Moreover, oral administration of nanoparticles encapsulated agent control the drug releases to slow breakdown of the polymer over a period of time such as nanoparticles made of poly (ε-caprolactone) (Carrio et al., 1995, Calvo et al., 1996).

Chapter 3 Materials and Methods

3.1 Materials

Artemisinin (ART) was obtained from Junda Pharmaceuticals, Co. China, Mefloquine hydrochloride (MFQ-HCl) from Provizer Pharma, India and activated carbon (Norit Caspf) was obtained from Behn Meyer, Singapore. Meanwhile, α-glucosyl hesperidin (Hsp-G) and α-glucosyl stevioside (Stevia-G) was purchased from Toyo Sugar Refining Co., Ltd. Activ-vial® was supplied by CSP technologies, USA. Tri-block copolymer poly (ethylene oxide)-poly (propylene oxide)-poly (ethylene oxide), pluronics P123 (EO_{20}-PO_{70}-EO_{20}, MW: 5800) and tetraethyl orthosilicate (TEOS, 98%) were purchased from Sigma-Aldrich. Hydrochloric acid (HCl) was from Kanto Chemical Co. Inc., Japan and deionized water was acquired by reverse osmosis with a MilliQ system (Millipore, Roma, Italy). All other reagents and solvents used in the study were reagent grade and were used without further purification.

3.2 Synthesis of SBA-15

Ordered mesoporous silica, SBA-15, was synthesized via a rapid condensation process as reported by Shen et al. (2010, 2011). In the typical synthesis, Pluronic P123 was used as a template in acidic conditions and TEOS as a silica source. 4 g of Pluronic P123 was added to 150 g of an aqueous solution of HCl (2N) and stirred for 2 h at 40 ºC to completely

dissolve the Pluronic P123. Successively, to this acidic Pluronic P123 solution, 9 g of TEOS was added under vigorous stirring for 1 min, while maintaining the temperature. The hydrolysis of TEOS was then carried out at 40 ºC without stirring for 2 h. The mixture was transferred to a polypropylene bottle and aged in an oven at 100 ºC for 24 h under static conditions. The white solid obtained was then recovered through rinsing (deionized water) and filtering and then dried at 55 ºC for 12 h. Finally, the resulting white powder was heated from room temperature to 550 ºC at a heating rate of 2 ºC/min and calcined in air at 550 ºC for 6 h to eliminate the template molecules.

3.3 Synthesis of non-porous silica

Typically, 90.8 ml of ethanol was mixed with 15 ml of NH4OH (25 wt.%) aqueous solution. 5.2 ml of tetraethoxysilane (TEOS) or a mixture of TEOS and (3-aminopropyl)triethoxysilane (APTES) was introduced into the ammonia solution under sonication. The reaction was performed at room temperature under sonication for 30 min. The resultant solid was recovered by centrifugation and washed with ethanol twice to remove unreacted free silica precursors. The powder was vacuum dried at room temperature for subsequent characterization.

3.4 Spray Drying

The solid dispersions of ART and SBA-15 were formulated by using BÜCHI B-290 mini spray dryer (BÜCHI Labortechnik AG, Switzerland) that operated in inert loop mode with nitrogen purge flow. The inlet temperature

was maintained at 81 °C (slightly higher than the boiling point of ethanol, 78 °C). The resulting outlet temperature at the aforesaid operating condition was approximately 47–53 °C. In order to formulate ART/SBA-15 (1:1 w/w) samples , 2 g of ART was dissolved in 200 mL of ethanol (Fisher Scientific Ltd., UK), to which 2 g of SBA-15 was subsequently dispersed. The mixture was stirred overnight. The fine liquid suspension of SBA-15 and ART was fed to the spray dryer via a peristaltic pump at a feed rate of 6.0 mL/min and sprayed into the chamber from a nozzle with 406 μm diameter at a pressure of 0.12-0.15 MPa. Similarly, in order to formulate ART/MFQ/SBA-15 (1:2:3 w/w/w) samples, 2 g of ART, 4 g of MFQ and 6 g of SBA-15 were used. In the case of solid dispersions of ART/Hsp-G (1:10 w/w) and ART/Stevia-G (1:10 w/w), 2 g of ART was dissolved in 250 mL of mixture of ethanol/water (8:2 v/v), to which 20 g of Hsp-G or Stevia-G was subsequently added. The inlet temperature was 120 °C and the outlet temperature was 70–80 °C. All the samples were dried in desiccators with silica gel under reduced pressure for 1 day before characterization.

3.5 Physical Mixture

The physical mixtures (hereafter denoted by P.M.) were prepared by thoroughly mixing the components in a turbula mixer (Turbula® T2F) at 49 rpm for 30 min until a homogeneous mixture was obtained. All the P.M.s were characterized immediately after harvesting the samples from the glass vessels at the end of the mixing. Meanwhile, physical mixtures of ART/MFQ (1:2 w/w) were prepared by using simple mixing using spatula.

3.6 Surface Area and Pore Volume Analyzer

Nitrogen adsorption-desorption isotherms were measured by using Autosorb-6B gas adsorption analyzer (Quantachrome Instruments, Boynton Beach, FL) at -196 °C (77 K). Approximately 0.10 g of sample was used for each measurement. Prior to adsorption measurements, SBA-15 samples were degassed under vacuum at 200 °C while drug-loaded samples were outgassed at 40 °C under vacuum for 24 h to remove any residues and absorbed water. The temperature applied for the drug-loaded samples was kept low to avoid degradation of the drug during pre-treatment. The specific surface areas of the samples were assessed using the linear region of the Brunauer-Emmett-Teller (BET) plots. The total pore volume was estimated from the amount of N_2 adsorbed at a relative pressure of 0.95 P/P_o whereas mesopore size distributions were computed from the adsorption branch of N_2 adsorption-desorption isotherms by means of the conventional Barrett-Joyner-Halenda (BJH) approach. The primary mesopore volume was calculated with the BJH theory and micropore volume by t-plot analysis.

3.7 Powder X-ray Diffraction (PXRD)

The crystallinity of the formulated samples was characterized by powder X-ray diffraction (PXRD). The PXRD was performed using a D8-Advance (Bruker, Madison, WI) X-ray diffractometer in steps of 0.028° using monochromatized Cu Kα radiation (λ = 0.1542 nm) as X-ray source and scanned over an angular range from 5^o to 50^o (2θ). The measurement

conditions were as follows: target, Cu; filter, Ni; voltage, 40 kV; current, 10 mA; scanning speed, 2°/min. PXRD holders were used to support samples and all the measurements were performed at room temperature.

3.8 Differential Scanning Calorimetry (DSC)

The loaded powder samples were analyzed by using differential scanning calorimetry (DSC) to study the thermal behaviour of drug particles in the mesoporous silica. The DSC was performed concurrently using a SDT 2960 simultaneous TGA-DSC thermo-gravimetric analyzer (TA Instrument Co.). Samples of 10 mg were weighted directly into open platinum pans in each experiment, with an empty platinum pan being the control. Before each analysis, the sample pans were washed with ethanol and heated with flame jet to remove any residues. The samples were heated from room temperature to 170 °C under nitrogen purge flow at 100 mL/min with a heating rate of 10 °C/min. All data handling was performed using the Universal Analysis 2000 software package ((TA Instrument Co.).

3.9 Thermogravimetric analysis (TGA)

Thermogravimetric (TA instrument, TGA-Q500) analysis was conducted with an automatic analyzer to determine the drug loading of co-spray dried samples. Samples of 10 mg were used in each analysis. Weight changes of the samples were measured at the temperature range of 25–800 °C with a heating rate of 10 °C/min under a nitrogen purge flow of 40 mL/min. The loading of drug in mesoporous silica was determined by the weight loss.

3.10 Scanning Electron Microscopy (SEM)

The morphology of powder samples was examined by a high resolution scanning electron microscope (SEM, JSM-6700F, JEOL, Tokyo, Japan) operating at 5 keV in secondary electron imaging (SEI) and lower electron image (LEI) modes. Prior to analysis, samples were mounted on double-sided adhesive carbon tapes and coated with gold for 1 min in a sputter coater (Cressington Sputter Coater 208HR, UK).

3.11 Transmission Electron Microscopy (TEM)

The internal pore structures of SBA-15 and drug-loaded SBA-15 were observed by transmission electron microscopy (TEM). High resolution TEM images were taken by Tecnai F20 (G^2) (FEI, Philips Electron Optics, Holland) electron microscope at 200 kV. Prior to examination, powdered samples were deposited on a copper grid with Formvar carbon film.

3.12 Karl Fisher Coulometric (KFC)

Moisture contents of all formulations were determined using Karl Fisher coulometric titration (coulometric titration method, 831 KF Coulometer, Metrohm, Metrohm Ltd. Ch-9101 Herisau, Switzerland). Sample powders weighing 15 mg were added into a titration vessel containing Hydranal®-Coulomat AG reagent, following equilibration of the instrument. The drift value and the pause time were 20 µg/min and 4 min, respectively. Each sample was measured in triplicates (n=3) to ensure reproducibility.

3.13 Dissolution Test using Flow-Through Cell (USP IV)

Flow-through cell apparatus (Erweka Gmbh, D63150, Heusenstamm, Germany), representing the USP Apparatus 4 was used to study the dissolution rate of formulated samples. This apparatus can be operated as either an open loop or a close loop system. The former provides an infinite sink condition by a fresh medium continuously pumped through the samples whereas the latter provides a finite sink condition. In this research, the open loop system to maintain the infinite sink condition was used.

Although USP IV was initially introduced for slow and sustained release, the application of USP IV for immediate release has been approved by FDA (Yu, 2012b) and a large number of studies about the application of USP IV for rapid and burst release of poorly water soluble drugs have been reported (Heng et al., 2008, Nicklasson et al., 1991, Waehling et al., 2011, Emara et al., 2009, Emara et al.,2002, Okumu et al., 2008). This wide application of USP IV is mainly due to the advantages of this apparatus as compared with others. For example, variation in the dissolution profiles of USP I and II have been reported, as can be attributed to, firstly, coning or dead zones of the apparatus and, secondly, the propensity of nanoparticles to form aggregates and floating drug samples (especially crystalline drug particles) on the surface of the medium despite the use of wetting agents such sodium lauryl sulphate as and sodium dodecyl sulphate (Bhattachar et al., 2002). These effects are observed predominantly for those drugs that have poor wettability

such as artemisinin. These problems necessitate the application of a USP IV apparatus in order to achieve acceptable and reproducible results.

Compared with other USP dissolution apparatus, the USP IV is specially designed to have a small hold-up volume that helps to minimize spreading of drug particles to undefined sites of the apparatus. This feature is useful in the testing of drug powders, especially those with poor solubility and wettability, as spreading results in erratic and highly variable dissolution profiles (Langenbucher et al., 1989). The USP IV was found to be less dependent on the hydrodynamics and the amount of substance tested in each run, which generated a better overall reproducibility of the *in vitro* dissolution data. Some investigators have demonstrated that good *in vitro*/*in vivo* correlations can be established using the USP IV dissolution testing method (Derendorf et al., 1983, Aiache et al., 1987, Phillips et al., 1989). Some of the applications of USP IV for the investigation of rapid release of poorly water soluble drugs has been demonstrated in the studies below:

I. Bhattachar et al. (2002) studied the dissolution enhancement of Pfizer Compound PD198306 by investigating the impact of drug loading into a flow-through dissolution cells on dissolution rate.
II. Sunesen et al. (2005) have used USP IV to study the *in vitro*/*in vivo* correlations for a poorly soluble drug, danazol. The authors found out that the correlations with *in vivo* release of danazol under fasted and fed conditions can be obtained by using the USP IV flow-through dissolution method.

III. Heng et al. (2008) have compared the performance of four commonly used dissolution tester (the paddle, rotating basket and flow-through cell and a dialysis method) to identify a suitable dissolution method for cefuroxime axetil. Their results showed the flow-through cell to be unequivocally the most robust dissolution method for the nanoparticulate system. A substantial variability was found when the USP II method was used, probably due to insufficient reproducibility of the hydrodynamic conditions in the vessel and due to wetting problems caused by the physical nature of cefuroxime axetil.

IV. Nicklasson et al. (1991) have evaluated the *in vitro* dissolution of phenacetin crystals by comparing the USP IV method with the USP II. The USP IV method shows less variation compared with the USP II method. The USP IV was also found to generate faster *in vitro* dissolution rates for phenacetin than those found with the USP II method, probably caused by steeper concentration gradients at the vicinity of the crystals and by the better ability to uniformly wet the phenacetin crystals.

However, some of the limitations of USP IV also cant be overlooked. For example, the possibility of the dissolved drug to re-crystallize in the sample holder due to the minute amount of dissolution medium passing through the drug samples. In addtion, the possibility of the undissolved inorganic carrier particles to form a cake (under PTFE membrane filters), which can block the flow of dissolution medium as well as the diffusion of the

dissolved drugs. Therefore the dissolution test was conducted by using both USP II (Section 3.14) and USP IV.

The equipment was fitted with cells of internal diameter (i.d.) of 12.0 mm. A glass bead with an i.d. of 6 mm were placed at the bottom of the cone to prevent a jet of fluid from back flowing and glass beads with 1 mm i.d were placed inside the dissolution chamber to generate a laminar flow. The tests were performed in an open loop system to maintain sink condition with fresh solvent from the reservoir continuously passing through the cell at 37.0 ± 0.5 ºC pumped using a peristaltic pump at a rate of 8 mL/min. Different amount of samples used in each dissolution test are shown in Table 3.1. Each of the samples were mixed or sandwiched with 1 g of glass beads (i.d. 1 mm) and placed inside the dissolution chamber. PTFE membrane filters (pore size 0.45 μm) were placed at the bottom and the top of the dissolution chamber to retain the undissolved samples. During the dissolution tests, the fluid passing through the cells was collected, the accumulated volume was weighed and the exact volume was calculated based on the density of water. Subsequently, 3 mL aliquots of the dissolution medium were withdrawn from the vessel at intervals of 5, 10, 15, 30, 60 and 120 min, filtered over PTFE membrane filters (pore size 0.45 μm). The drug concentration was determined by means of high performance liquid chromatography (HPLC, Agilent 1100 series). Based on the concentration and the volume of the collected samples at different time intervals, the exact amount of the dissolved drug was calculated. Drug release from the formulated solid dispersions was compared with that from their corresponding untreated crystalline drugs and physical mixtures. All

experiments were performed in triplicates (n=3) and the results were registered as an average with standard deviation.

Table 3.1 Amounts of samples used for dissolution test under sink condition

Sample	Weight of sample (mg)	Weight of ART (mg)	Weight of MFQ (mg)	Weight of excipient (mg)
ART	10	10	–	–
Spray dried ART	10	10	–	–
MFQ	20	–	20	–
ART/MFQ (1:2 w/w)	30	10	20	–
ART/AC (1:1 w/w)	20	10	–	10
ART/SBA-15 (1:1 w/w)	20	10	–	10
ART/Hsp-G (1:10 w/w)	110	10	–	100
ART/Stevia-G (1:10 w/w)	110	10	–	100
ART/MFQ/SBA-15 (1:2:3 w/w/w)	60	10	20	30

3.14 Dissolution Test using *In Vitro* Dissolution Tester (USP II)

The supersaturation of ART and MFQ was established under non-sink condition by using an *in vitro* dissolution tester, USP II, Agilent 708-DS Dissolution Apparatus. The total amount of samples used in this study was equivalent to 200 mg of ART and 400 mg of MFQ. Drug release from the SBA-15 formulations was compared with that from the corresponding

crystalline drugs. The amount of samples used in each dissolution test is shown in Table 3.2. Each of the samples was mixed with 800 mg of cornstarch and pressed to a tablet (i.d. 13 mm) at a pressure of 75 MPa to characterize the drug release profile. The tests were executed in 900 mL of distilled water (D.I water) at 37 ± 0.5 ºC with a paddle speed of 100 rpm. Subsequently, 3 mL aliquots of the dissolution medium were withdrawn from the vessel at interval of 5, 10, 15, 30, 60 and 120 min and replaced by fresh dissolution medium. The collected samples were filtered over PTFE membrane filters (pore size 0.45 μm).

In addition, USP II also was used to quantify the dissolution rate (under sink condition) of SBA-15 related samples as a comparison and also to study the dissolution of samples after 6-months of storage. Tablets of samples with an amount equivalent to 50.0 ± 1.0 mg ART and 100.0 ± 1.0 mg MFQ and 800 mg of cornstarch were used in this set of experiment.

Table 3.2 Amounts of samples used for dissolution test under non-sink condition

Sample	Weight of sample (mg)	Weight of ART (mg)	Weight of MFQ (mg)	Weight of excipient (mg)
ART	200	200	–	–
MFQ	400	–	400	–
ART/MFQ (1:2 w/w)	600	200	400	–
ART/AC (1:1 w/w)	400	200	–	200
ART/SBA-15 (1:1 w/w)	400	200	–	200
ART/Hsp-G (1:10 w/w)	2200	200	–	2000
ART/Stevia-G (1:10 w/w)	2200	200	–	2000
ART/MFQ/SBA-15 (1:2:3 w/w/w)	1200	200	400	600

3.15 Chemical and Physical Stability

Physical and chemical stability tests of spray dried solid dispersions at controlled temperature and relative humidity (RH) were conducted based on the procedures from the International Conference on Harmonization (ICH)-ICH Q1A (R2). The samples were tested for 3- and 6-months under different storage conditions: open pan inside desiccators (25 ºC/18% RH); open pan (25 ºC/75% RH); open pan (40 ºC/75% RH); Activ-Vial® (25 ºC) and Activ-Vial® (40 ºC). The Activ-vial® consists of a flip-top closed vial with integrated

molecular sieve sleeves that prevent moisture by providing a greater moisture adsorptive capacity than ordinary silica gel. The physical stability of all the samples was analyzed using PXRD; the chemical stability was investigated using HPLC.

3.16 *In vitro* cytotoxicity

The *in vitro* cytotoxicity tests of the ART, SBA-15 and solid dispersions were evaluated by the standard flow-cytometric technique on human colon carcinoma (Caco-2) cells. Caco-2 cells were cultured using the Dulbecco's Modified Eagle Medium (DMEM) supplemented with 10% phosphate buffered saline (PBS) and 1% penicilline-streptomycin solution in 75-cm^2 culture flasks. Cells were cultivated in an incubator at 37 ºC with 5% carbon dioxide. Prior to each test, the cells were washed with PBS, trypsinized, pelleted at 1500 rpm for 5 min and re-suspended in DMEM. The cells were seeded in 12 well plates (Costar, IL, USA) at 5×10^5 cells/well (1 mL) and incubated for 24 h. Then, the medium was replaced with sample suspensions at different concentrations and incubated for 24 h. After incubation, the wells were washed with PBS to remove excess particles and the cells were then harvested with trypsin solution. After being centrifuged at 1500 rpm for 5 min, the pellets were re-suspended in PBS. In order to distinguish cellular debris and living cells in the flow cytometeric analysis, Caco-2 cells were further stained with propidium iodide (PI, Becton Dickinson, Franklin Lakes, NJ, USA). The dead cells were measured using a FACSCalibur with CellQuest software (BD Biosciences, San Jose, CA). The data were derived from a

minimum of 10,000 events per sample measurement. Each sample was tested in triplicates (*n*=3). Untreated cells were used as controls.

3.17 Method of Analysis

The concentration of ART was measured by HPLC (Agilent 1100 series) equipped with Eclipse XDB C18 (150 mm × 4.6 mm (i.d.) × 5 μm) (Eka Chemicals AB, Sweden) column (Stringham et al., 2009, Liu et al., 2010a). The mobile phase consisted of 50% of ultrapure water and 50% acetonitrile (HPLC grade). The flow rate was maintained at 1.0 mL/min and the UV detector was operated at a wavelength of 210 nm. Drug content was determined by calculating the peak area at 9.3 min. For MFQ, the concentration of the samples was measured by means of HPLC (Agilent 1100 series) equipped with Inertsil C8-3 (150 mm × 4.6 mm (i.d.) × 5 μm) (GL Sciences Inc., Tokyo, Japan) column (Lai et al., 2007). The mobile phase which consisted of MeOH, acetonitrile and 0.05 M KH_2PO_4 (55:9:35, v/v/v) adjusted to pH 3.9 with 0.5% orthophosphoric acid was filtered through a 0.2 μm nylon filter. The flow rate was maintained at 1.00 mL/min and the UV detector was operated at a wavelength of 284 nm. Drug content was determined by calculating the peak area at 6.8 min. All the measurements were carried out in triplicates (*n*=3) to ensure replicability.

3.18 Statistical analysis

Data were processed using Microsoft Excel 2003 software. Each sample was tested in triplicates and the mean ± standard deviation is reported. Two sample

comparisons of means were carried out using Student's t-test analysis and statistical significance was ascertained when the p value was less than 0.05.

Chapter 4 Formulation of Amorphous ART using Activated Carbon

ART was formulated into solid dispersions by using porous activated carbon (AC) to enhance its dissolution rate, supersaturation and physicochemical stability. AC was chosen as a drug carrier due its remarkable structural properties, biocompatibility and cost-effectiveness. It was expected that ART/AC would be able to form amorphous solid dispersions even at higher drug loading due to its high specific surface area, large pore volume and strong adsorption capacity. Therefore, solid dispersions of ART/AC at drug loadings from 25 wt% to 80 wt% were prepared by using co-spray drying (Figure 4.1) and their dissolution rate and solubility were investigated. Both moderate and stressed conditions were used to study the physicochemical stability of the formulated samples.

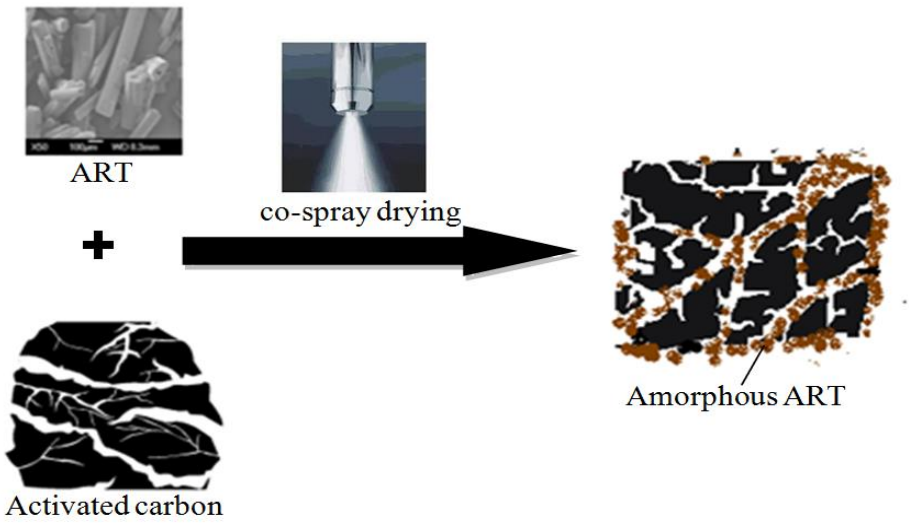

Figure 4.1 Schematic diagram of formulation of ART/AC solid dispersion via co-spray drying.

4.1 Surface Area and Pore Volume after Drug Loading

N_2 adsorption was conducted to understand the changes in pore structures of AC before and after co-spray dying with ART. The N_2 adsorption/desorption isotherms for ART/AC samples with different degrees of drug loading are presented in Figure 4.2. The changes in the surface area and total pore volume of AC are summarized in Table 4.1. The isotherm of AC is similar to the type IV isotherm with a clear hysteresis loop from a relative pressure of 0.04 to 1.0, indicating that most of the pores are in the mesoporous range. However, the pore size distribution of AC is not uniform (Figure 4.3) as compared with other reported activated carbons, such as uniform mesoporous carbon spheres (UMCS) and fibrous ordered mesoporous carbon (FOMC) (Zhao et al., 2012b). The amount of N_2 adsorbed onto AC was reduced drastically after co-spray drying with ART. The surface area and the total pore volume for the ART/AC (1:3 w/w) sample declined with respect to those of the AC-only samples, i.e. from 1364.1 to 478.6 m^2/g and from 1.45 to 0.48 cm^3/g, respectively.

The significant reduction in N_2 adsorption, alongside the decrease in the total pore volume and surface area of AC, suggested that most of the pore channels of AC were occupied by ART molecules after co-spray drying. The large surface area (1364.1 m^2/g) and pore volume (1.45 cm^3/g) of AC contribute to its high encapsulation capacity and drug loading efficiency. This is illustrated by the findings that about 90% of the ART used in each formulation of solid dispersions was encapsulated in the porous structures of

AC and that the final drug loading is close to the designated value (Table 4.2). Such features render porous AC a potential carrier for the drug delivery system.

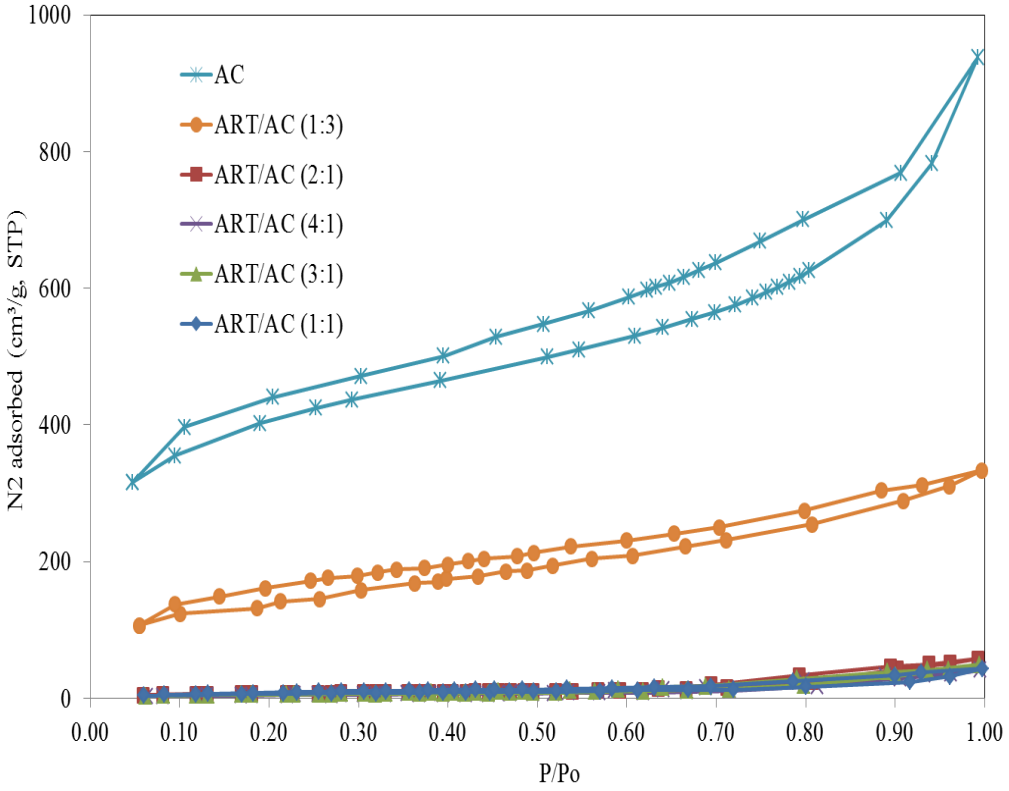

Figure 4.2 N_2 adsorption-desorption isotherms of AC before and after co-spray drying with ART.

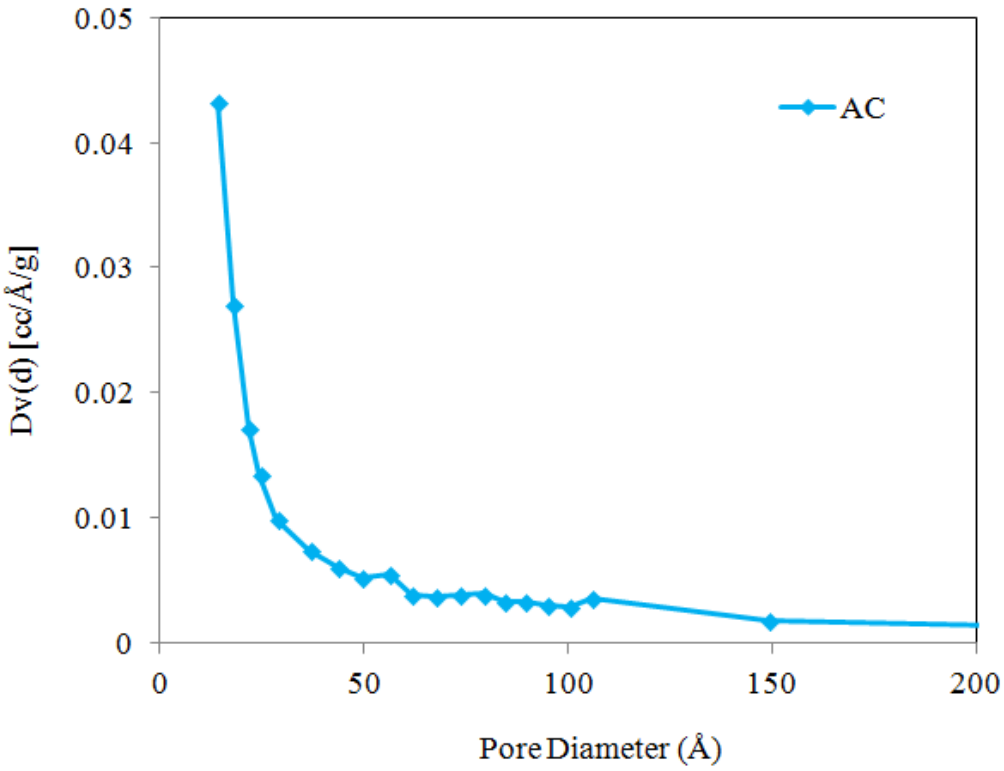

Figure 4.3 Pore size distribution of AC.

Table 4.1 Pore volume and surface area of AC before and after co-spray drying with ART

Sample	Surface area (S_{BET}) [m^2/g]	Total pore volume (V_{pore}) [cm^3/g]
AC	1364.1 ± 64.0	1.45 ± 0.23
ART/AC (1:3 w/w)	478.6 ± 40.5	0.48 ± 0.16
ART/AC (1:1 w/w)	24.4 ± 30.8	0.05 ± 0.04
ART/AC (2:1 w/w)	25.6 ± 13.9	0.08 ± 0.02
ART/AC (3:1 w/w)	19.8 ± 9.7	0.07 ± 0.02
ART/AC (4:1 w/w)	15.5 ± 12.8	0.05 ± 0.01

Data represent mean ± S.D., *n*=3

Table 4.2 Drug loading of ART in AC

Sample	Theoretical drug loading [wt%]	Drug Loading [wt%]	Drug Loading efficiency [%]
ART/AC (1:3 w/w)	25	23.6 ± 0.9	94.4 ± 3.6
ART/AC (1:1 w/w)	50	45.0 ± 2.8	90.0 ± 5.6
ART/AC (2:1 w/w)	67	64.9 ± 0.8	96.9 ± 1.2
ART/AC (3:1 w/w)	75	72.6 ± 1.0	96.8 ± 1.3
ART/AC (4:1 w/w)	80	79.6 ± 0.5	99.5 ± 0.6

Data represent mean ± S.D., *n*=3

4.2 Thermal Analysis

The thermal behavior of untreated ART and co-spray dried ART/AC at different weight ratios was analyzed by using DSC (Figure 4.4). The DSC curve of untreated ART is found to have an intense endothermic peak at 153.4 °C, with an enthalpy of fusion of 73.0 J/g (Table 4.3), similar to that reported by Kakran et al. (2011). In comparison, for drug-loaded samples, the

DSC curves are found to have endothermic peaks with a decreased intensity, each with a lower corresponding temperature. Amongst the drug-loaded samples, the ART/AC (2:1 w/w), ART/AC (3:1 w/w) and ART/AC (4:1 w/w) exhibited lower heat of fusion and their endothermic peaks are at 144.2, 147.3 and 149.4 °C, respectively, In addition, combination of two endothermic peaks can be observed for both the ART/AC (3:1 w/w) and ART/AC (4:1 w/w) samples which might be due to the presence of different polymorphs of ART. This is in good agreement with the results reported by Chan et al. (1997), whereby two types of polymorphs (orthorhombic and triclinic) have been observed. On the other hand, the ART/AC (1:3 w/w) and ART/AC (1:1 w/w) samples did not exhibited observable endothermic peaks.

The intense endothermic melting peak of ART at 153.4 °C shows the crystalline nature of the untreated ART. Since the heat of fusion is proportional to the crystallinity of the solid dispersions (Sahoo et al., 2011b), the decrease in endothermic peak intensity and heat of fusion of the drug-loaded samples indicates the reduction in crystallinity of ART upon its encapsulation into the pores of AC. The shift of endothermic peak temperatures of co-spray dried samples to lower values may be attributed to the interaction between ART and AC as proposed by Zhao et al. (2012a) and Shen et al.(2011). The absence of endothermic melting peak for ART/AC (1:3 w/w) and ART/AC (1:1 w/w) samples suggest that the ART adsorbed onto AC lacked crystalline structure and were hence in amorphous form. The amorphization of ART in the ART/AC samples could be attributed to the nano-confinement of ART in the pore of AC and rapid evaporation of organic

solvent during co-spray drying. During co-spray drying, the AC particles allow entrapment of the dissolved ART within the pores of AC through capillary condensation. This prevents the nucleation and growth of large ART crystals. The spray dried ART particles will remain in amorphous form in the confined pores of AC after the organic solvent was removed.

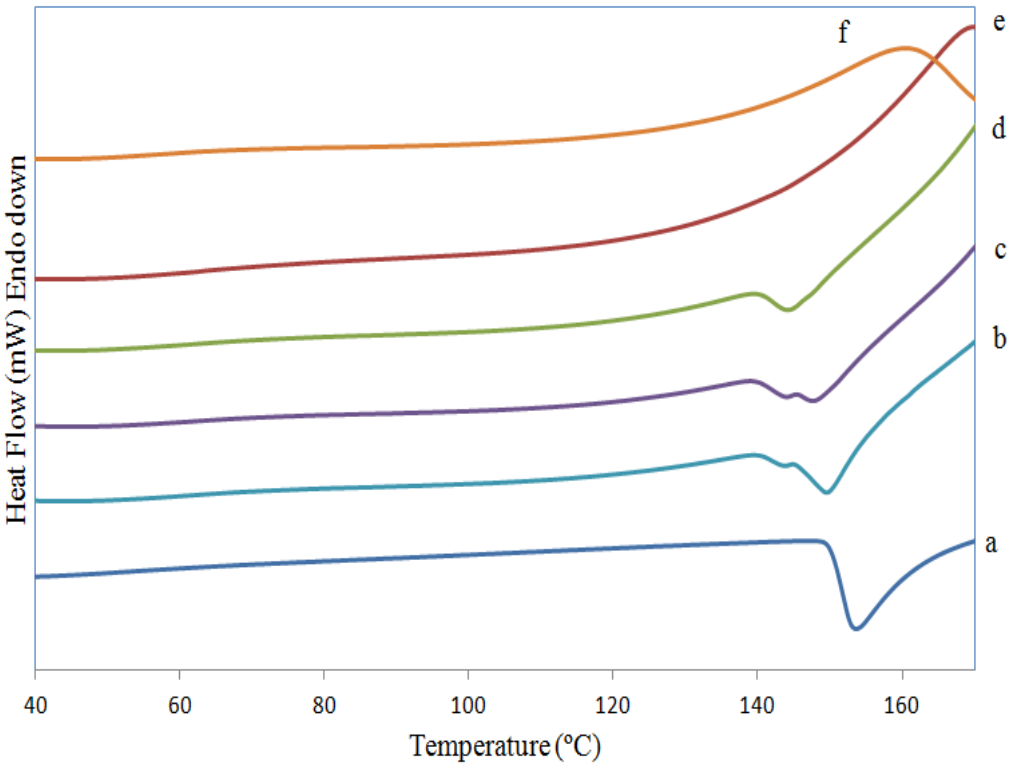

Figure 4.4 DSC curves of (a) untreated ART crystals, (b) ART/AC (4:1 w/w), (c) ART/AC (3:1 w/w), (d) ART/AC (2:1 w/w), (e) ART/AC (1:1 w/w) and (f) ART/AC (1:3 w/w).

Table 4.3 Melting temperatures (T_m) and heat of fusion (ΔH_f) of untreated ART and ART/AC solid dispersions

Sample	Melting Temperature, T_m (˚C)	Heat of Fusion, ΔH_f (J/g)	Percentage of crystallinity (%)
Untreated ART	153.4 ±2.8	73.0 ± 5.8	-
ART/AC (1:3 w/w)	-	-	-
ART/AC (1:1 w/w)	-	-	-
ART/AC (2:1 w/w)	144.2 ± 1.2	6.1 ± 1.6	8.6 ± 2.4
ART/AC (3:1 w/w)	147.3 ± 1.1	9.8 ± 0.8	13.8 ± 1.6
ART/AC (4:1 w/w)	149.4 ± 0.8	17.9 ± 4.5	24.6 ± 6.5

%Crystallinity was calculated based on the equation reported by Khanfar et al. (2013)
Data represent mean ± S.D., *n*=3.

4.3 Solid State

Figure 4.5 displays the PXRD patterns of ART and solid dispersions of ART/AC with different extents of drug loading. As anticipated, the untreated ART exhibited a highly crystalline nature with intense PXRD peaks. The untreated ART crystals show numerous distinct sharp peaks at 2θ values of 7.3°, 11.8°, 14.7° and 22.1°, indicating that the bulk ART is present in the orthorhombic crystal form (Kakran et al., 2011). In addition, ART that spray dried without AC retained the X-ray diffraction characteristic peaks as crystalline ART, even though the intensity of the peaks was decreased. This indicates, although the degree of crystallinity of ART decreased after spray drying, the polymorphic conversion and amorphization may not be feasible without presence of carriers. This signifies the role of AC as a carrier in amorphization of ART via co-spray drying.

The co-spray dried ART/AC samples showed less intense X-ray diffraction peaks compared with the untreated ART crystals. The intensity of the PXRD peaks decreases as both the drug loading and the crystallinity of ART decreased from ART/AC (4:1 w/w) to ART/AC (1:3 w/w). The flat PXRD pattern of ART/AC (1:3 w/w) and the weak diffraction peak of ART/AC (1:1 w/w) indicate that most of the ART entrapped in the pore structures are in the X-ray amorphous form. The presence of a small amount of crystals in ART/AC (1:1 w/w) could be detected by PXRD but not by DSC. The PXRD patterns of the other three solid dispersions (ART/AC > 1:1 w/w) are similar to that of untreated ART, especially the characteristic peak at 11.8°. This demonstrates the presence of partially crystalline ART in ART/AC solid dispersions.

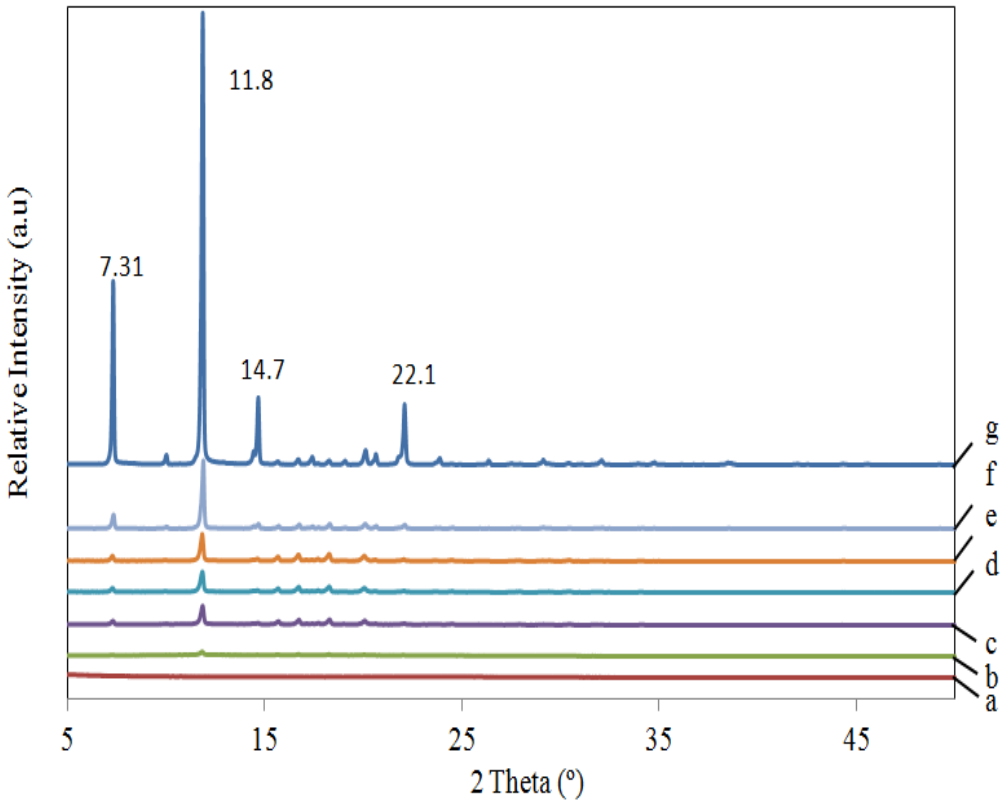

Figure 4.5 PXRD patterns of (a) ART/AC (1:3 w/w), (b) ART/AC (1:1 w/w), (c) ART/AC (2:1 w/w),(d) ART/AC (3:1 w/w), (e) ART/AC (4:1 w/w), (f) spray dried ART and (g) untreated ART crystals.

4.4 Morphology

The morphologies of all the unprocessed and processed samples were characterized by using SEM images as shown in Figure 4.6. Apparently, the crystalline nature of untreated ART could be seen clearly from Figure 4.6(a) and the crystalline form of ART did not change after co-spray dried without any excipients [Figure 4.6(b)]. Figure 4.6(a) and (b) also show the orthorhombic forms with prism and rod-like sub-particles of ART. The particle size of the spray dried ART (0.5–10 μm) is 100 times smaller than the untreated ART crystals (50–1000 μm). In this regard, Sahoo et al. (2010) have reported the reduction in particles size of ART to the range of 1−5 μm by

using a modified multi-fluid nozzle pilot spray dryer. However, the inlet temperature used in their study was 140 ºC, which is significantly higher than that used in the present work (81ºC). Figure 4.6(c) depicts the irregular shape with rough surfaces and sharp edges of AC. Such rough surfaces might be due to the presence of porous structures on the surface of AC. Mesoporous carbons with different structures have been reported in the literature. For example, Zhao et al. (2012a) have studied two types of mesoporous carbons, uniform mesoporous carbon spheres (UMCS) and fibrous ordered mesoporous carbon (FOMC) and found that the former has uniform and spherical structures whereas FOMC has fibrous structures.

Figure 4.6(d)-(h) illustrate the morphology of ART/AC solid dispersions with different extents of drug loading. When the ratio of ART/AC is below 1:1 w/w, as for ART/AC (1:3 w/w) [Figure 4.6(d)] and ART/AC (1:1 w/w) [Figure 4.6(e)], the morphology is similar to that of AC with sharp edges and rough surfaces, as most ART molecules were entrapped inside AC pores. In comparison, when the ratio of ART/AC increased to 2:1 w/w or above, as for ART/AC (2:1 w/w), ART/AC (3:1 w/w) and ART/AC (4:1 w/w) [Figure 4.6(f)-(h)], the morphologies were changed significantly. Additional particles with smooth edges were observed on the surface. With such extents of drug loading, the amount of ART exceeded the capacity of total pore volume of AC, thus part of ART remained on the external surface of AC to form surface particles after being co-spray dried.

Further inferences could be drawn by examining the morphology in SEM images. Firstly, the particle size of ART formed on the surface of AC was much smaller than that of raw and spray dried ART. During co-spray drying, the atomization of ART solution was affected by the presence of AC particles. The moving inorganic AC particles prevent the formation of large ART crystals. Secondly, the prism and rod-like structures of ART are not found in all of the four solid dispersions with AC, which could be attributed to the amorphization and decrease in the crystallinity of ART. This is in contrast to the observations of Sahoo et al. (2010) who reported the formation of solid dispersion of ART by using PVP and PEG as hydrophilic carriers via co-spray drying. The morphology of the formulated solid dispersions showed that PVP and PEG did not mix homogeneously with ART, resulting in free ART particles which were observed in the solid dispersions even at higher contents of PVP and PEG.

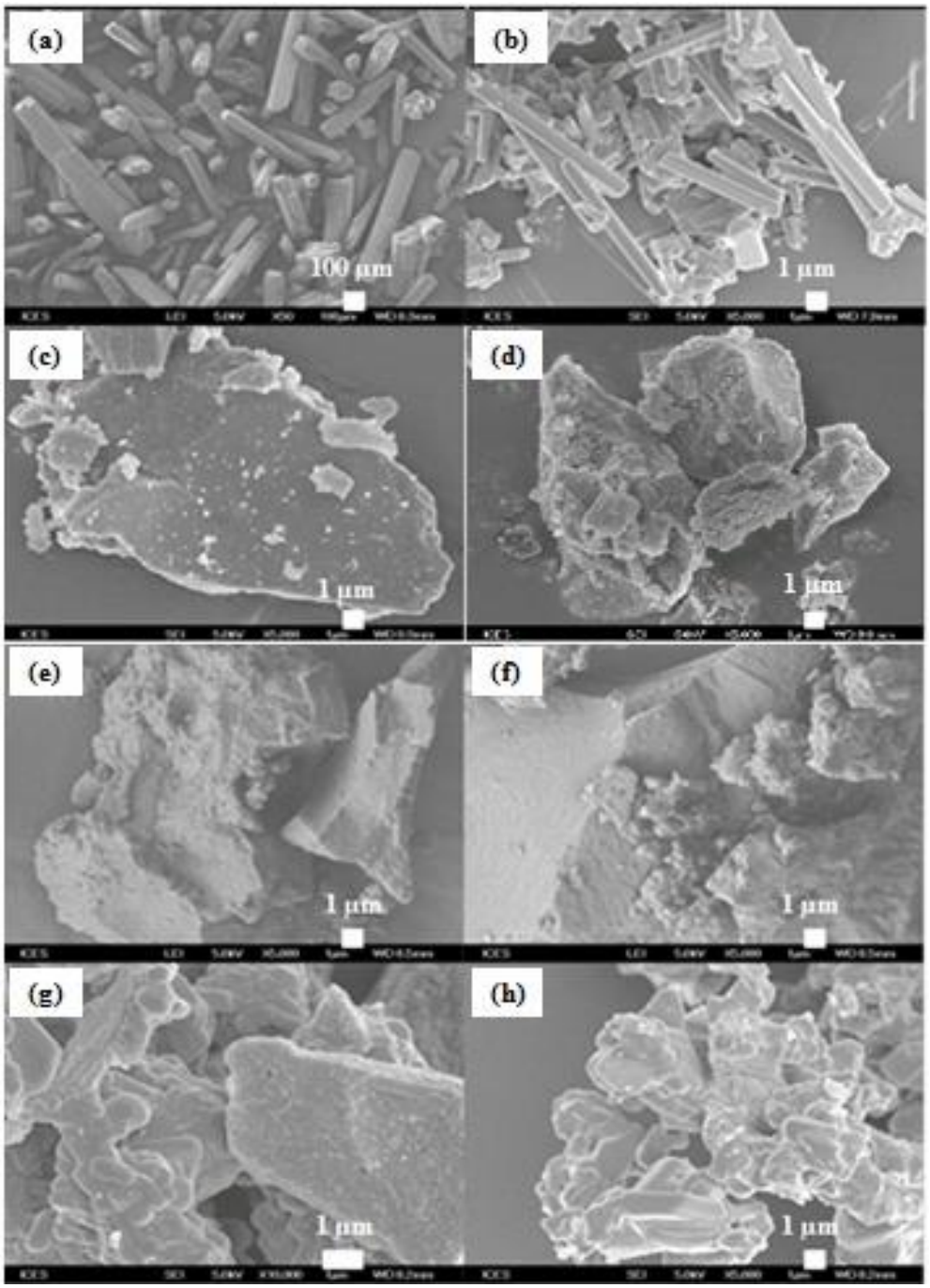

Figure 4.6 SEM images of (a) untreated ART, (b) spray dried ART crystal, (c) AC, (d) ART/AC (1:3 w/w), (e) ART/AC (1:1 w/w), (f) ART/AC (2:1 w/w), (g) ART/AC (3:1 w/w) and (h) ART/AC (4:1 w/w).

4.5 Dissolution Rate under Sink Condition

In vitro drug release studies of co-spray dried ART/AC samples were performed in order to demonstrate the significance of AC in improving the dissolution kinetics of ART. This dissolution study was performed using distilled water instead of simulated gastrointestinal fluids since ART is a neutral compound whose dissolution is not pH-dependent (Hoa et al., 1996). Figure 4.7 shows the *in vitro* dissolution profile of untreated ART and ART/AC solid dispersions with different drug loadings. Untreated ART crystals have a very poor dissolution rate in water, as indicated by a meager 26.7% of drug release of ART after 30 min. Furthermore, the dissolution rate of untreated ART was consistently low throughout the experiment and only 56.7% of the ART was dissolved after 120 min. Relative to untreated ART crystals, the physical mixtures of ART and AC are also found to have a poor drug release profile: only 26.9% and 41.5% of ART dissolved from P.M.-ART/AC (1:1 w/w) and P.M.-ART/AC (2:1 w/w), respectively, at the end of the dissolution test after 2 h. Physically mixing ART with AC appears to decrease the dissolution of the crystalline drug. This decrease might be due to the strong adsorption capacity of AC, which able to re-adsorb the dissolved ART. On the other hand, for the spray dried ART, the dissolution was observed to be 52.9% ($p < 0.05$) and 61.9% in 30 and 120 min, respectively. Similarly, the co-spray dried samples also [except ART/AC (1:3 w/w)] exhibited an improved dissolution rate compared with the untreated ART and with the physical mixtures. For the spray dried ART/AC samples, within the first 30 min, dissolution was observed to be approximately 61.7% ($p < 0.05$),

74.6% ($p < 0.05$), 82.1% ($p < 0.05$) and 87.5% ($p < 0.05$) of ART for ART/AC (1:1 w/w), ART/AC (2:1 w/w), ART/AC (3:1 w/w) and ART/AC (4:1 w/w), respectively, before equilibrium was attained. However, ART/AC (1:3 w/w) sample show very poor results throughout the dissolution process with approximately 15% of ART was dissolved. Similar type of study has been conducted by Wang et al. (2011a) whereby dissolution enhancement of ibuprofen by using ordered mesoporous carbon via solvent evaporation was reported and all the drug-loaded samples reach 60–70% drug release in one hour.

The dissolution improvement in spray dried ART can be attributed to the particle size reduction as suggested by the Noyes-Whitney equation (Noyes and Whitney, 1897). The SEM images in Figure 4.6 indicate that the particle size of ART was reduced significantly after being spray dried, resulting in augmented specific surface areas exposed to dissolution medium compared with their crystalline counterpart. This confirms the significance of particle size reduction on dissolution enhancement, as observed with other reported studies (Zhang et al., 2009b, Brion et al., 2009).

Several reasons underlie the dissolution enhancement of ART/AC solid dispersions compared with the untreated ART samples. Firstly, the rapid dissolution of ART from the solid dispersion with a lower extent of drug loading (ART/AC < 1:1 w/w) is contributed by the amorphous state of ART entrapped inside the porous structures as revealed by PXRD and DSC. The amorphous form of pharmaceutically active materials represents the most

energetic solid state, which provides the greatest advantage in terms of bioavailability and solubility (Hancock and Zografi, 1997). It has also been reported that the amorphization of drugs increases the molecular motion and reduces the binding energy of drug particles, subsequently resulting in the increases in dissolution rate (Zhao et al., 2012a). Secondly, in solid dispersions with a higher extent of drug loading (ART/AC > 1:1 w/w), ART will be in partially crystalline form, which distributed in two phases; ART entrapped in AC pore structures and ART remained on external surface. These partially crystalline ART particles are highly dispersed with reduced in crystallinity and particle size. Simultaneous decrease in crystallinity and particles size can remarkably enhance the dissolution rate of ART due to the increase in solubility and surface area of the particles in contact with the dissolution medium.

Although all the solid dispersions, except ART/AC (1:3 w/w), exhibited enhanced dissolution rate compared with the raw ART and physical mixtures, the total amount of drug dissolved at the end of the dissolution test still leaves room for improvement. The release of ART from solid dispersions achieved equilibrium after 30 min, with the systems failed to reach a 100% of drug release after 120 min. The total amount of ART dissolved before the attainment of equilibrium decreases with increasing amounts of AC in the solid dispersions. For example, about 90% of ART dissolved from the ART/AC (4:1 w/w), whereas only 15% and 60% ART dissolved from the ART/AC (1:3 w/w) and ART/AC (1:1 w/w) samples, respectively. Therefore, it can be deduced that the presence of AC might affect the total release of

ART prior to the equilibrium. The explanation for this lies in the large surface area and strong adsorption capacity of AC, onto which the dissolved drugs could re-adsorbed.

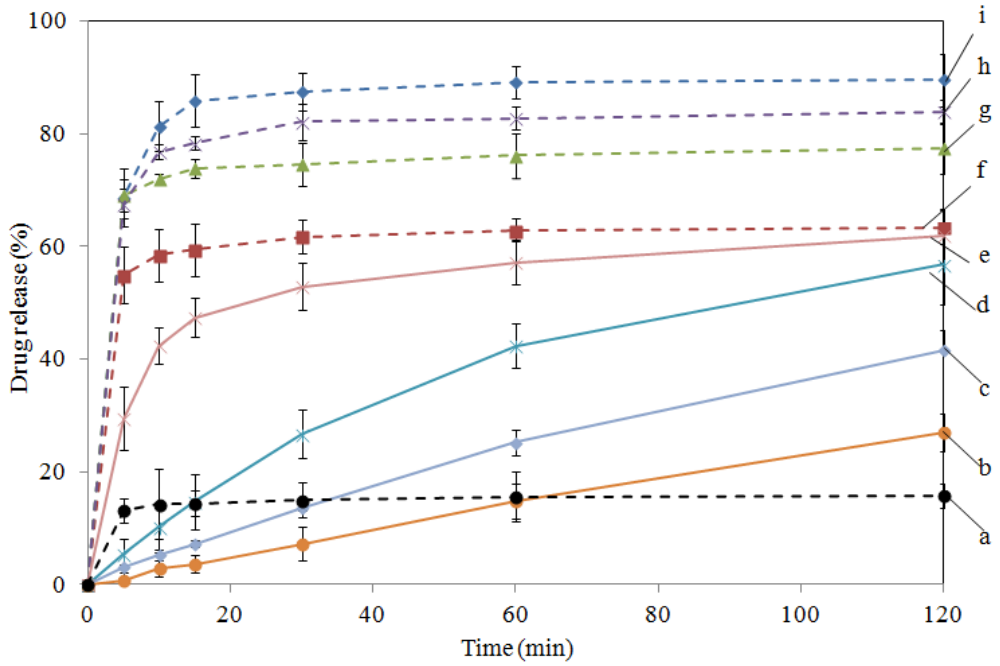

Figure 4.7 Dissolution profiles (sink condition) of (a) ART/AC (1:3 w/w), (b) P.M.-ART/AC (1:1 w/w), (c) P.M.-ART/AC (2:1 w/w), (d) untreated ART crystal, (e) spray dried ART, (f) ART/AC (1:1 w/w), (g) ART/AC (2:1 w/w), (h) ART/AC (3:1 w/w) and (i) ART/AC (4:1 w/w). n=3, $p < 0.05$ versus free ART.

4.6 Supersaturation under Non-Sink Condition

Dissolution profiles of ART/AC were examined under non-sink conditions to evaluate the supersaturation of ART. Figure 4.8 illustrates the *in vitro* dissolution profile (under non-sink condition) of untreated ART and ART/AC solid dispersions with different extents of drug loading**.** The amount of ART/AC used is equivalent to 200 mg of ART. The obtained supersaturation of ART (48.4 µg/mL) is almost similar to the reported literature value: 48 µg/mL (aqueous solubility of ART at 37 °C) (Ferreira et

al., 2013). The co-spray dried ART/AC dispersions enhanced the supersaturation of ART compared with the untreated ART. The ART/AC samples could achieve an apparent solubility of approximately 86–95 µg/mL ($p < 0.05$).

The amorphization and decrease in crystallinity and particle size of ART are the main factors for the enhancement of supersaturation of treated ART compared with that of the untreated ART. It has been reported that amorphous APIs are remarkably more soluble than their crystalline counterparts (Hancock and Parks, 2000). The improved supersaturation of amorphous APIs is due to the higher free energy and greater molecular motion of solids in the amorphous form compared with those in the crystalline form, which have undesirably higher lattice energy and lower solvation energy (Van den Mooter, 2012, Murdande et al., 2010a). This difference translates into the fact that no additional energy is required to solvate or hydrate the amorphous ART. In addition, the reduction in particle size also contributes to the solubility enhancement of ART. The particle size of all the four solid dispersions of ART/AC is much smaller than the untreated ART crystals. The amorphous ART which undergoes reduction in particles size will have a reduced radius of curvature that can contribute to improved supersaturation compared with the crystalline counterpart. The relationship between the particles size and supersaturation of amorphous solids is illustrated by the Ostwald-Freunlich equation (Ostwald, 1900, Freundlich, 1923).

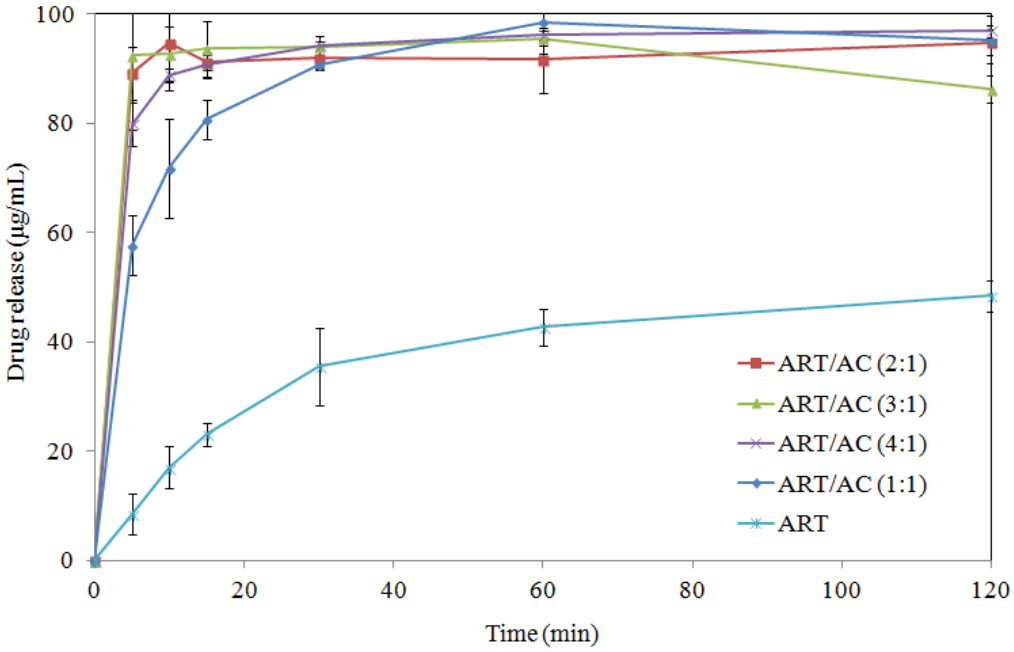

Figure 4.8 ART dissolution profiles using equivalent of 200 mg of untreated ART and formulated ART under sink conditions using USP II. *n*=3, $p < 0.05$ versus free ART.

4.7 Chemical Stability Evaluation

The chemical stability of amorphous ART under two different storage conditions was examined by using HPLC after 1-week and 3-months of storage. Samples of ART/AC (1:3 w/w), ART/AC (1:1 w/w) and ART/AC (4:1 w/w) were chosen for the chemical stability test with untreated ART and spray dried ART as controls. The untreated ART and spray dried ART could preserve more than 99% of drug without degradation after storage at 40 °C/75% RH in open pans for 12-months (Table 4.4), attesting to the chemical stability of crystalline drugs under stressed condition. However, the co-spray dried samples show poor chemical stability under both the stressed (40 °C/75% RH) and mild (25 °C/18% RH) conditions (Table 4.5). The samples started to degrade drastically within the first-week upon storage and

completely degraded after 3-months; with particle agglomeration and formation of sticky samples was observed. The poor chemical stability of treated ART might have been attributed to the amorphization of ART and the catalytic activity of AC. With regards to the catalytic activity, it can be surmised that the AC which is widely used as a catalyst for the decomposition of hydrogen peroxide (Aguinaco et al., 2011, Rey et al., 2011) could have accelerated the degradation of ART by reacting with peroxide bridge in ART molecules. Therefore, apart from the strong adsorption capacity of AC, the degradation of ART could be another reason for poor dissolution of the treated ART.

Table 4.4 Percentage of ART remained after stored at 40 ºC/75 %RH

Sample	% of ART after 12-months
ART	99.4 ± 1.6
Spray dried ART	98.8 ± 1.8

Data represent mean ± S.D., *n*=3

Table 4.5 Percentages of ART remaining in co-spray dried ART/AC after storage under 2 different storage conditions for 1-week and 3-months

Sample	Storage conditions	% of ART remaining	
		1-week	3-month
ART/AC (1:3 w/w)	Desiccators (25 °C/18% RH)	19.9 ± 0.1	0
	Open pan (40 °C/75% RH)	0	0
ART/AC (1:1 w/w)	Desiccators (25 °C/18% RH)	28.9 ± 0.8	0
	Open pan (40 °C/75% RH)	0	0
ART/AC (4:1 w/w)	Desiccators (25 °C/18% RH)	32.9 ± 1.4	0
	Open pan (40 °C/75% RH)	0	0

Data represent mean ± S.D., *n*=3

4.8 Conclusions

Confinement of ART into the pores of AC produced amorphous forms with reduced particle size. Co-spray drying of ART with AC at high drug loading (ART/AC > 1:1 w/w) led to the formation of partial crystalline ART with two different polymorphs. The amorphization or reduction in crystallinity and particle size reduction are the important factors that contributed to the enhancement in dissolution rate and supersaturation of ART. Although the untreated ART and spray dried ART remain chemically stable for 12-months of storage test, the formulated samples show poor chemical stability under stressed and moderate conditions within the first month of storage, which

might adversely affect the drug release of ART. The poor stability of formulated amorphous ART might have been due to the catalytic activity of AC.

Chapter 5 Nano-Confinement of ART in SBA-15

Activated carbon was replaced by ordered mesoporous silica, SBA-15 as a carrier to enhance the biopharmaceutical properties of ART. On the other hand, non-porous silica was used as a carrier to investigate the confinement of ART molecules inside the pore channels of SBA-15 and not on the external surface. The solid dispersions were formulated via co-spray drying (Figure 5.1) with drug loadings lesser than 50 wt% since crystalline particles were observed for ART/AC at drug loading above 50 wt%. Since the formulation of amorphous forms is the objective of this research, attention was devoted to samples with drug ratios below 50% w/w and samples with drug loading above 50% w/w were formulated as a control. Meanwhile, more storage conditions were used to test the stability of the formulated solid dispersions: desiccators (25 °C/18% RH), Activ-vial® (25 °C), open pan (25 °C/75% RH), Activ-vial® (40 °C) and open pan (40 °C/75% RH). Since the capability of SBA-15 to improve the physicochemical stability of different types of poorly water-soluble drugs has been reported previously, it was expected that the physicochemical stability of amorphous ART could be retained by SBA-15 especially under moderate storage conditions. Additionally, the biocompatibility of SBA-15 and ART/SBA-15 was investigated by *in vitro* cytotoxicity tests.

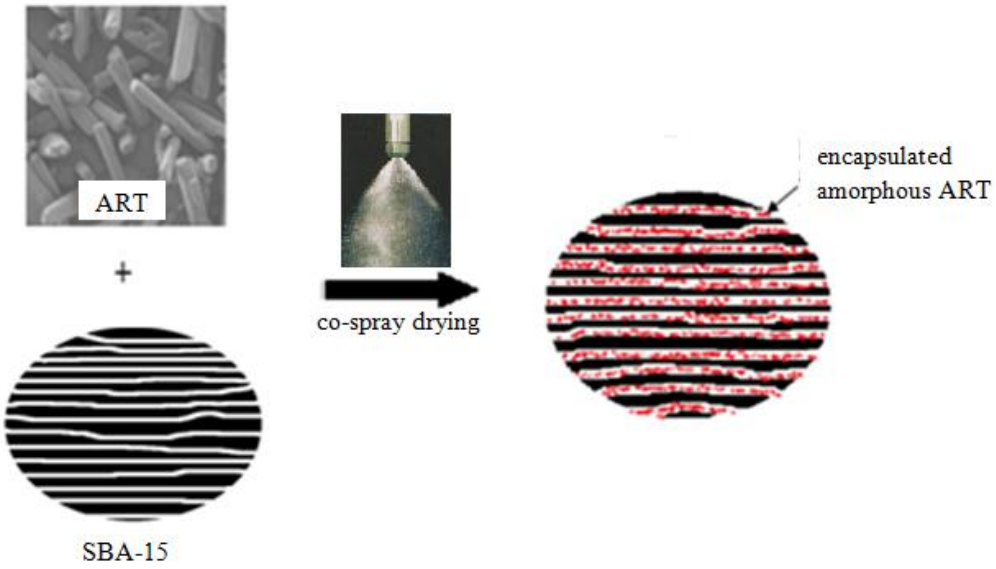

Figure 5.1 Schematic diagram of formulation of ART/SBA-15 solid dispersion via co-spray drying.

5.1 Changes to Pore Structure after Drug Loading

Figure 5.2 and Figure 5.3 display the nitrogen adsorption-desorption isotherms and pore size distributions of SBA-15 and co-spray dried ART/SBA-15 samples, respectively. Table 5.1 lists the average pore size (d), Brunauer-Emmett-Teller (BET) specific surface area (S_{BET}) and total pore volume (V_{pore}) of the samples. According to the International Union of Pure and Applied Chemistry (IUPAC) classification, SBA-15 and drug-loaded samples illustrate the typical type IV adsorption isotherm containing the H1 hysteresis loop in the range of P/P_0 at 0.50–0.77, associated with mesoporous materials (Wu et al., 2012). Furthermore, based on Barrett-Joyner-Halenda (BJH) analysis, SBA-15 has a uniform pore size distribution with a mean pore size of approximately 8.7 nm. The total pore volume and BET surface area of SBA-15 are 1.16 cm^3/g and 809.0 m^2/g, respectively.

Once co-spray dried with ART, the pore size of ART/SBA-15 (1:3 w/w) reduced to 7.3 nm together with a decline in the amount of N_2 adsorbed. Correspondingly, the surface area and the total pore volume decreased to 370.7 m^2/g and 0.63 cm^3/g respectively. With the loading increased to 1:1 w/w, a further reduction was observed in these three parameters: the total pore volume declined to 0.20 cm^3/g, the surface area reduced to 112.8 m^2/g and the pore diameter shrank to 6.4 nm. The reduction of pore diameter, pore volume and surface area of SBA-15 indicate that most of the mesoporous channels were occupied with ART molecules through co-spray drying. The narrowed hysteresis loop and the reduced amount of N_2 adsorbed suggest a limited size and number of pores after the encapsulation of ART. Moreover, the capillary condensation of the ART/SBA-15 samples shifted to lower relative pressures upon encapsulation of ART due to reduced pore size (Guo et al., 2013). Once the drug loading was increased to above 50 wt% [ART/SBA-15 (3:1 w/w)], the pore volume, surface area and N_2 adsorption of co-spray dried samples shrank to almost non-porous materials as pore channels were almost fully occupied.

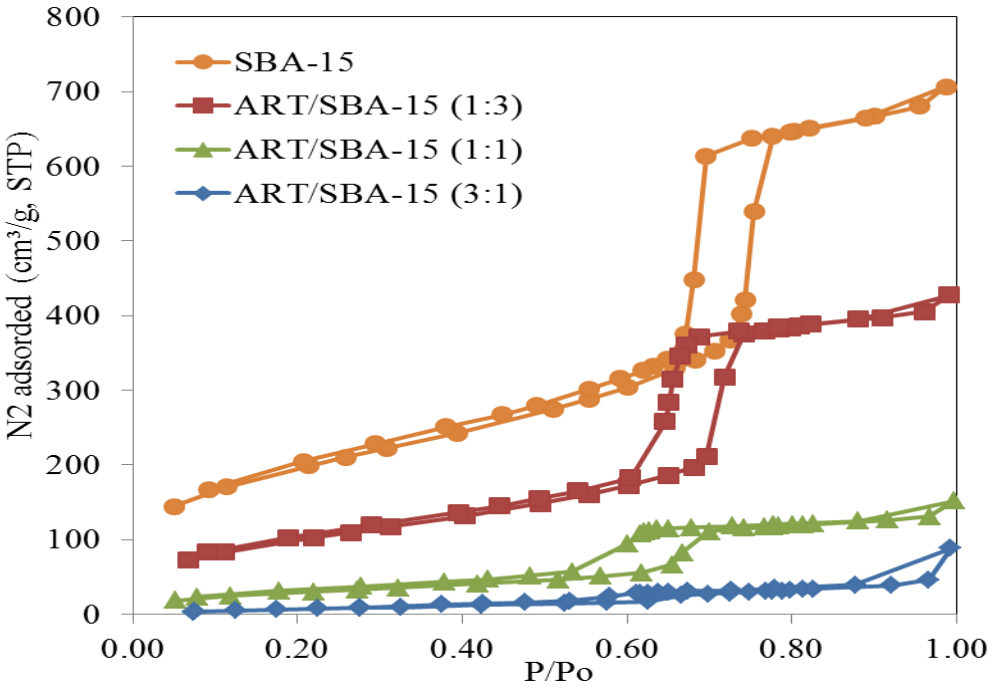

Figure 5.2 N_2 adsorption-desorption isotherms of SBA-15 before and after co-spray drying with ART.

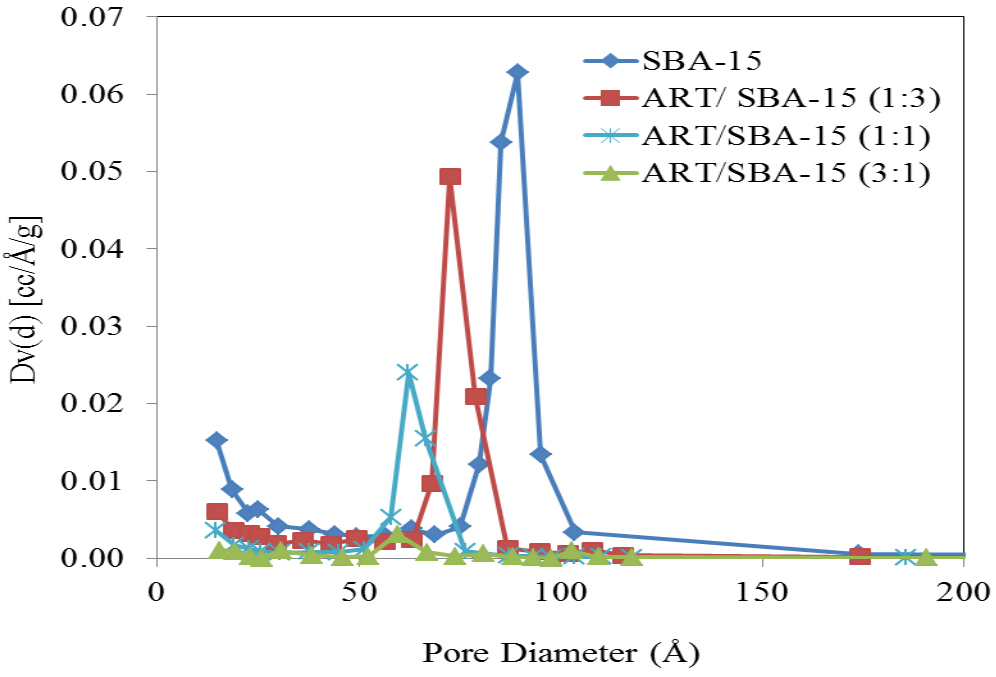

Figure 5.3 Pore size distribution of SBA-15 before and after co-spray drying with ART.

Table 5.1 Pore volume, surface area and average pore size of SBA-15 before and after co-spray drying with ART

Sample	Surface area (S_{BET}) [m^2/g]	Total pore volume (V_{pore}) [cc/g]	Average pore diameter (d) [nm]
SBA-15	809.0 ± 26.3	1.16 ± 0.04	8.70 ± 0.32
ART/SBA-15 (1:3 w/w)	370.7 ± 41.8	0.63 ± 0.04	7.34 ± 0.53
ART/SBA-15 (1:1 w/w)	112.8 ± 24.5	0.20 ± 0.04	6.40 ± 0.32
ART/SBA-15 (3:1 w/w)	36.6 ± 3.3	0.07± 0.01	4.60 ± 0.01

Data represent mean ± S.D., *n*=3

5.2 Drug Loading Efficiency

The encapsulation efficiency of SBA-15 was quantified by measuring the ART loading in the pore channels of SBA-15. ART-loaded samples weighing 5 mg were extracted with 50 mL of ethanol with stirring for 24 h, followed by filtration and analysis by HPLC. Table 5.2 outlines the drug loading efficiency of ART/SBA-15 samples at different drug ratios. The drug loading of ART/SBA-15 (1:3 w/w) and ART/SBA-15 (1:1 w/w) that represent the drug uptake by SBA-15 particles was 23.6 wt% and 48.8 wt% respectively. It is shown that more than 94% of ART in the designed formulation was loaded onto SBA-15. The obtained results are in agreement with results of thermal gravimetric analysis (TGA) (Figure 5.4). The high drug loading efficiency is mainly due to the high BET specific surface area and the

large pore volume of SBA-15, together with the efficiency of spray dying technique.

In addition, the nano-confinement of ART inside the pore channels of SBA-15 can be investigated by correlating the drug loading and the pore volume reduction of SBA-15. The pore volume reduction is approximately equal to the theoretical volume of ART used for formulation. For example, the drug loading based on HPLC results indicates that in 1 g of ART/SBA-15 (1:1) sample contained 0.488 g of ART and 0.512 g of SBA-15. Since the total pore volume of SBA-15 is 1.16 cm^3/g, the available pore volume in 1 g of ART/SBA-15 (1:1) for ART inclusion was $1.16 \times 0.512 = 0.59$ cm^3/g. Referring to the specific volume of ART (0.806 cm^3/g), the total volume that was able to be occupied by ART was $0.488 \times 0.806 = 0.39$ cm^3/g. Finally the calculated unoccupied pore volume of ART/SBA-15 (1:1) was $0.59 - 0.39 = 0.20$ cm^3/g. This calculated unoccupied pore volume of the sample is the same as the BET result (Table 5.1) measured by N_2 adsorption, indicating that most of the ART is inserted within the mesopores of SBA-15 and cause the reduction of pore volume.

Table 5.2 Drug loading of ART inside mesoporous silica

Sample	Theoretical drug loading [wt%]	Drug Loading [wt%]	Drug Loading efficiency [%]
ART/SBA-15 (1:3 w/w)	25	23.6 ± 1.2	94.4 ± 4.8
ART/SBA-15 (1:1 w/w)	50	48.8 ± 1.1	97.6 ± 2.2

Data represent mean ± S.D., *n*=3

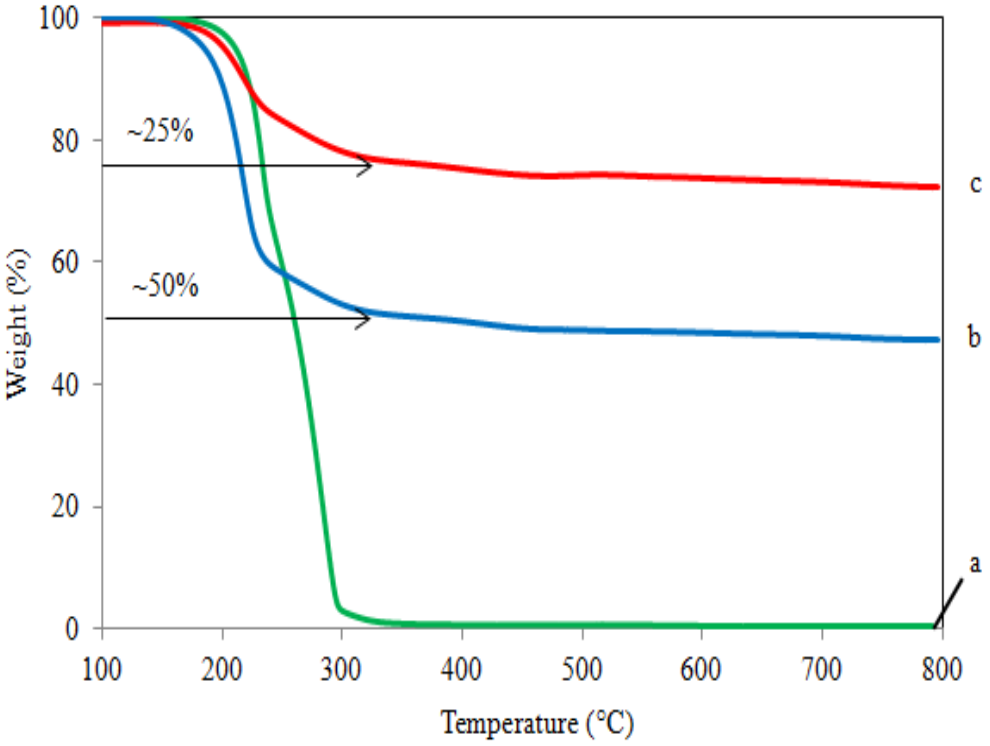

Figure 5.4 Thermograms of (a) untreated ART crystals, (b) ART/ SBA-15 (1:1 w/w) and (c) ART/ SBA-15 (1:3 w/w).

5.3 X-Ray Diffraction Analysis

The PXRD patterns of untreated ART, co-spray dried samples and physical mixtures are depicted in Figure 5.5. Intense PXRD peaks of untreated ART with 4 main characteristic peaks at 7.3°, 11.8°, 14.7° and 22.1° exemplify the typical reflections of the orthorhombic polymorphic form of ART as consistent with previous literature (Ambrogi et al., 2013). The co-spray dried ART/SBA-15 samples with drug loadig lower than 50 wt.% display PXRD patterns without observable peaks attributable to the crystalline ART, indicating that no crystalline ART was detected by X-ray diffraction. The physical state of ART is fundamentally changed from the crystalline form to the amorphous after co-spray dried with SBA-15. However, PXRD peaks assigned to crystalline ART were detected for ART/SBA-15 (3:1 w/w) sample, indicating ART could be re-crystallized and remained on the external surface once the pore volume was fully occupied at drug loading above 50 wt.%. Similarly, the physical mixtures of ART/SBA-15 also exhibited strong X-ray diffraction intensity with the same pattern of raw ART, since the physically mixed samples still exhibited completely crystalline forms.

The amorphization of ART is mainly due to the confinement of the drug within nano-sized pore channels of SBA-15 through capillary condensation and the subsequent rapid evaporation of the organic solvent during formulation (Planinšek et al., 2011), which prevent the nucleation and the formation of long-range ordered crystalline structures (Ambrogi et al., 2013). It has been reported in the literature that pore diameters smaller than

20 nm are able to restrict the nucleation of drug molecules (Planinšek et al., 2011, Shen et al., 2010). Since the pores of SBA-15 is in the range of 8–9 nm, those ART drug particles encapsulated within the pore channels are expected to be in the amorphous form.

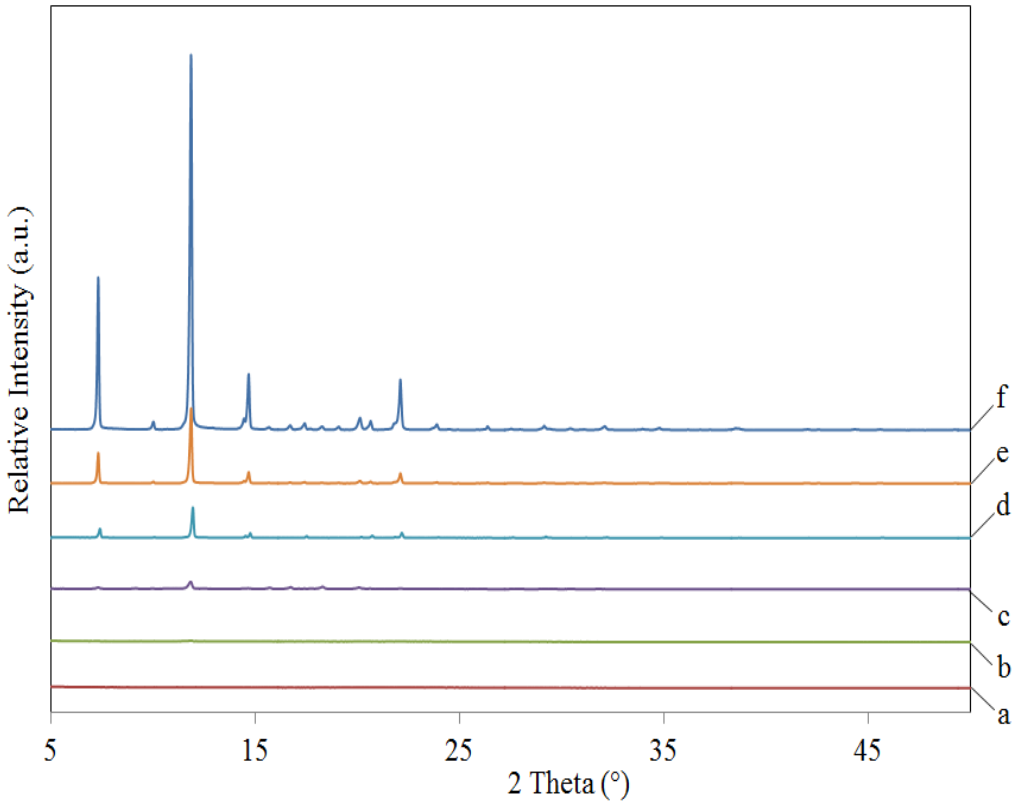

Figure 5.5 PXRD patterns of (a) ART/SBA-15 (1:3 w/w), (b) ART/ SBA-15 (1:1 w/w), (c) ART/SBA-15 (3:1 w/w), (d) P.M.-ART/SBA-15 (1:3 w/w), (e) P.M.-ART/SBA-15 (1:1 w/w) and (f) untreated ART crystals.

5.4 Characterization by DSC

The physical state of all the samples was further investigated by DSC analysis, in which an endothermic melting peak can indicate crystallinity of the drug as suggested by Zhang et al. (2011). DSC thermograms of untreated ART, co-spray dried ART/SBA-15 and physical mixtures of ART/SBA-15 are

depicted in Figure 5.6. A single sharp endothermic peak is observed for the untreated ART at 153.4 °C, corresponding to the intrinsic melting point of the crystalline phase of ART, with an endothermic enthalpy of 73.0 J/g. In contrast, less intense and slightly broader melting peaks were observed in the thermogram for the physical mixtures of ART/SBA-15 at temperature lower than 153.4 °C. Once ART was co-spray dried with SBA-15, no endothermic peaks corresponding to drug melting were observed, confirming the absence of ART crystals. This result provides further evidence that ART in co-spray dried ART/SBA-15 dispersions are in amorphous the form, which is in agreement with the PXRD results.

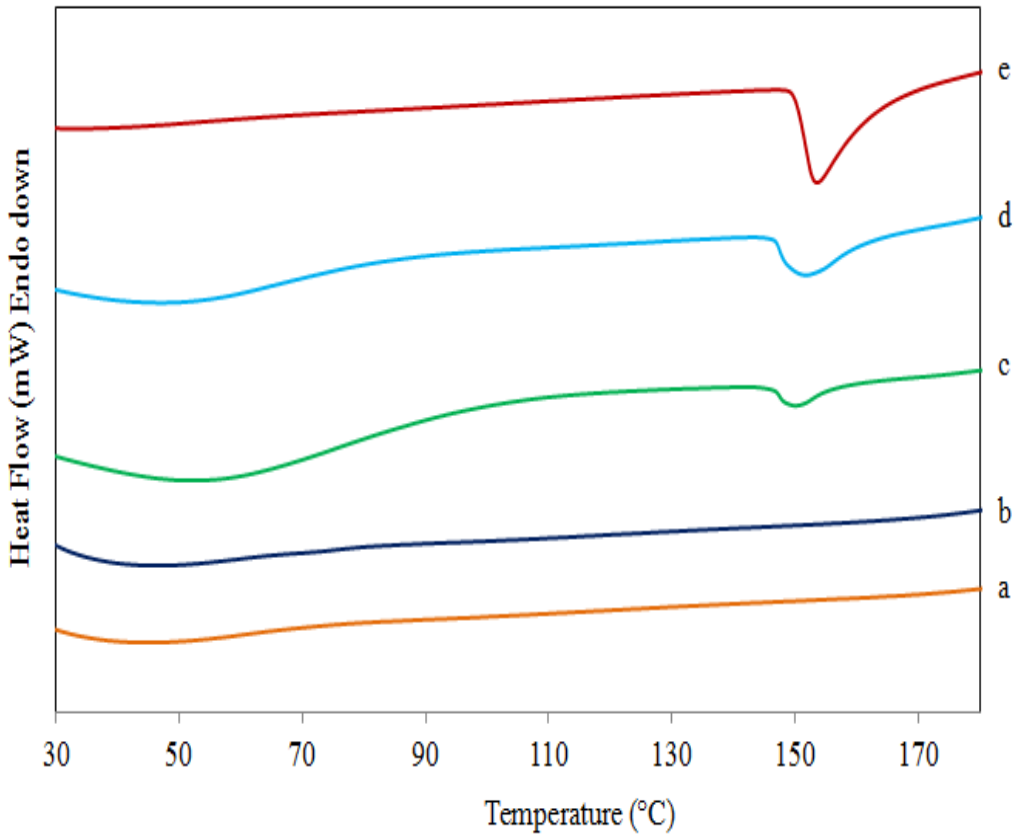

Figure 5.6 DSC curves of (a) ART/SBA-15 (1:3 w/w), (b) ART/SBA-15 (1:1 w/w), (c) P.M.-ART/SBA-15 (1:3 w/w), (d) P.M.-ART/SBA-15 (1:1 w/w) and (e) untreated ART crystals.

5.5 Morphology and Particle Size

Figure 5.7 shows the morphology and particle size of raw and spray dried ART, porous silica (SBA-15) and non-porous silica and co-spray dried samples. The crystalline nature of ART could be discerned from the untreated and spray dried ART [Figure 5.7(a) and (b)], in which both the particles are in an orthorhombic form with prism and rod-like shapes (Chan et al., 1997). Both the raw ART and spray dried ART exhibit particle size in the range of 50-1000 μm and 0.5-10 μm, respectively. Meanwhile, SBA-15 appears as aggregates of

spherical and spheroid shaped particles [Figure 5.7(c)] with a narrow particle size distribution (average size about 0.5–1 μm). It is noted that both the co-spray dried ART/SBA-15 (1:3 w/w) and ART/SBA-15 (1:1 w/w) exhibit the similar morphology as SBA-15 and no superficial drug crystals were observed [Figure 5.7(d) and (e)]. The retained morphologies and absence of additional particles on the external surfaces of the samples suggest that most of the ART particles are well-dispersed and encapsulated within the pore channels of the carrier. During co-spray drying, the presence of the SBA-15 particles prevent the nucleation and formation of large ART crystals, whereby the dissolved ART in liquid dispersion was quickly entrapped inside the pore channnels of SBA-15 through capillary condensation. These ART particles remain in amorphous the form within the confined pores of SBA-15 after the organic solvent was removed by rapid evaporation via spray drying (Zhao et al., 2012a). However, when the ratio of ART/SBA-15 increased to 3:1 w/w [Figure 5.7(f)], changes in the morphologies can be seen with additional particles with smooth edges were observed on the surface. With such extents of drug loading, the amount of ART exceeded the capacity of total pore volume of SBA-15 and part of ART remained on the external surface of SBA-15 to form surface particles after being co-spray dried.

On the other hand, ART was co-spray dried with non-porous silica at different drug loadings as a comparison in order to provide additional evidence to support that artemisinin could be confined within the pore channels of SBA-15. The total pore volume and specific surface area of non-porous silica are 0.012 cm^3/g and 6.39 m^2/g, respectively, which are very low

as compared with SBA-15. The morphologies and physical states of co-spray dried ART/non-porous silica have been shown in Figures 5.7 and 5.8, respectively. Apparently, the non-porous silica appeared to be in a uniform spherical form with particle size in the range of 0.3-0.6 μm. The sample of ART/non-porous-silica (1:9 w/w) shows morphology similar to that of raw non-porous silica. When the ART/non-porous-silica ratio was increased to 1:3 w/w and 1:1 w/w, changes in the morphologies with the presence of smooth edges and crystalline particles corresponding to ART crystals can be clearly observed. The results indicated that crystalline ART particles could be formed on the external surface of non-porous silica during co-spray drying as the drug carrier lacks pore channels to accommodate the drug molecules. These ART particles were not observed on the external surfaces of SBA-15 even after co-spray drying at the high ART/SBA-15 ratio of 1:1 w/w.

Additionally, it was found that the presence of crystalline particles can be detected by PXRD (Figure 5.8) for the co-spray dried ART/non-porous silica (1:9 w/w) samples. Samples with 1:3 w/w and 1:1 w/w of drug-to-carrier weight ratios showed even stronger X-ray diffraction intensity with the same pattern of raw ART (Figure 5.8). These results indicate that, even as low as 10 wt% of ART on surface on non-porous silica, ART could be re-crystallized and remained on the external surface of non-porous silica after being co-spray dried. In comparison, co-spray dried ART/SBA-15 showed amorphous PXRD patterns even at a high drug loading of 50 wt% (Figure 5.5), indicating that the ART molecules encapsulated inside the pore channels of SBA-15 after co-spray drying.

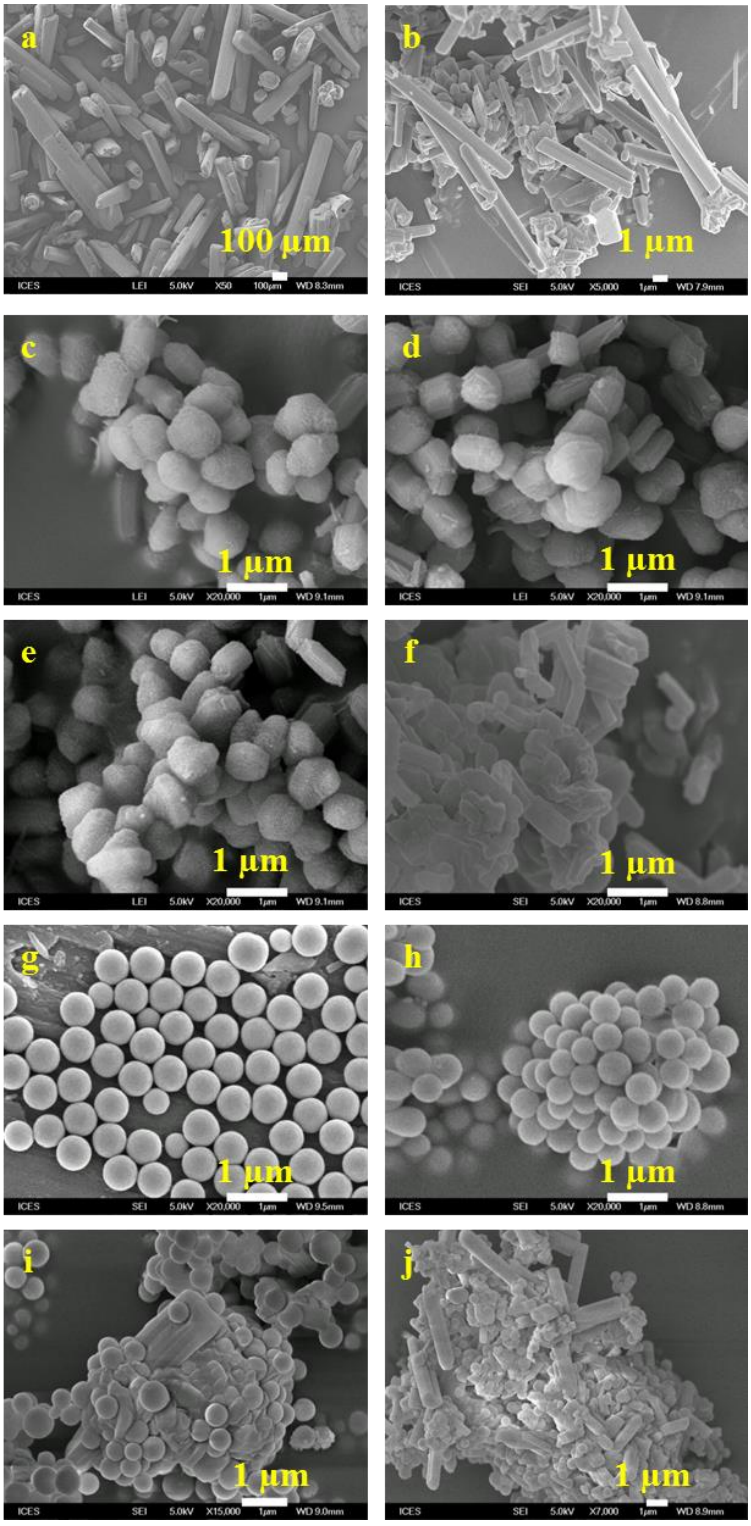

Figure 5.7 SEM images of (a) untreated ART, (b) spray dried ART, (c) SBA-15, (d) ART/SBA-15 (1:3 w/w), (e) ART/SBA-15 (1:1 w/w), (f) ART/SBA-15 (3:1 w/w) (g) non-porous silica, (h) ART/non-porous silica (1:9 w/w), (i) ART/non-porous silica (1:3 w/w) and (j) ART/non-porous silica (1:1 w/w)

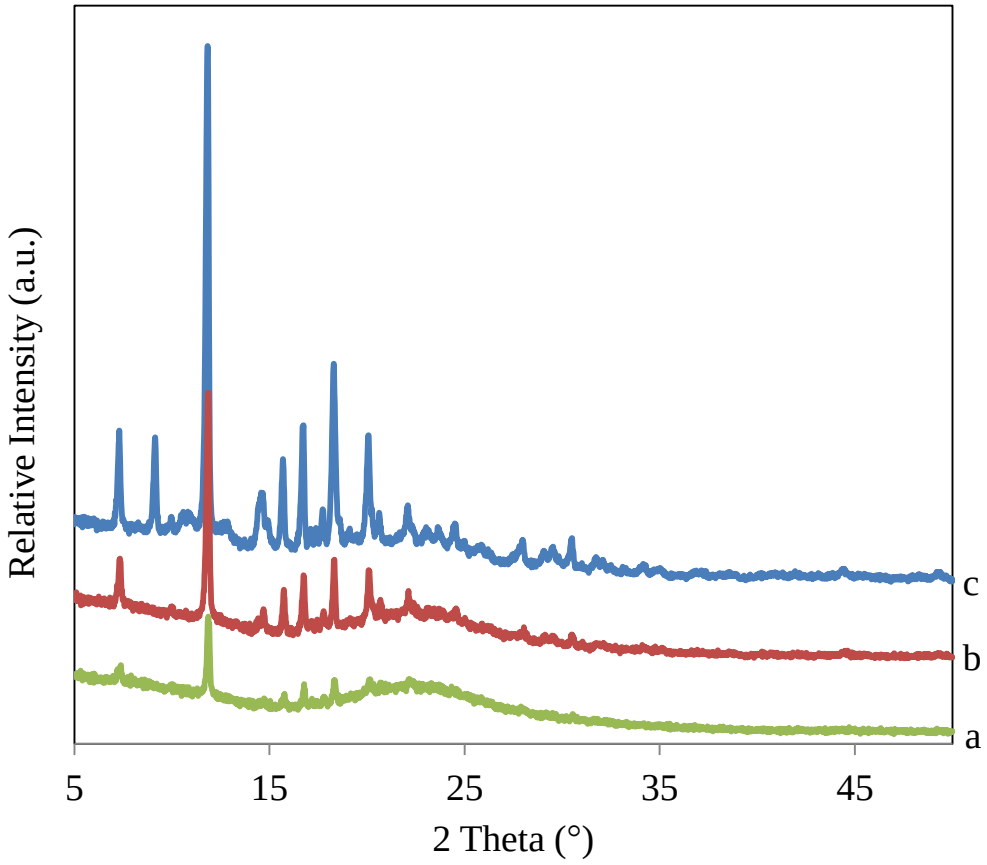

Figure 5.8 PXRD patterns of (a) ART/non-porous silica (1:9 w/w), (b) ART/non-porous silica (1:3 w/w) and (c) ART/non-porous silica (1:1 w/w)

5.6 Internal Pore Structure

TEM was used to reveal the internal mesoporous structural features of SBA-15 before and after loading as can be inspected in Figure 5.9. TEM images of SBA-15 clearly illustrate that the mean pore diameter of the cylindrical pore channels of mesoporous silica was uniform at approximately 8.7 nm, which is in agreement with the N_2 adsorption-desorption analysis. Moreover, the pore system of the SBA-15 is in a well-ordered hexagonal arrangement and straight lattice fringes were viewed along and perpendicular to the pore axis, confirming the existence of a two-dimensional hexagonal

structure of *p*6mm symmetry (Guo et al., 2013). The length of SBA-15 particle is in the range from 0.5–1 µm (Figure 5.9a). Figure 5.9b and c illustrate the unchanged appearance of SBA-15 pore channels and pore walls after loading with ART particles. This verifies that the drug encapsulation did not change the appearance and the internal pore structures of SBA-15. In addition, TEM investigation also indicated that no particles were observed to accumulate at pore openings of SBA-15 at drug loading equal or below 50 wt.%. This indicating that pore channels were not blocked by ART at the pore opening position to cause significant shrinkage of the pore volume after drug loading. As comparison, extra drug particles at outside of SBA-15 particles could be observed (indicated by red arrows) for sample with 75 wt.% drug loading formulated by same co-spray drying method (Figure 5.9d).

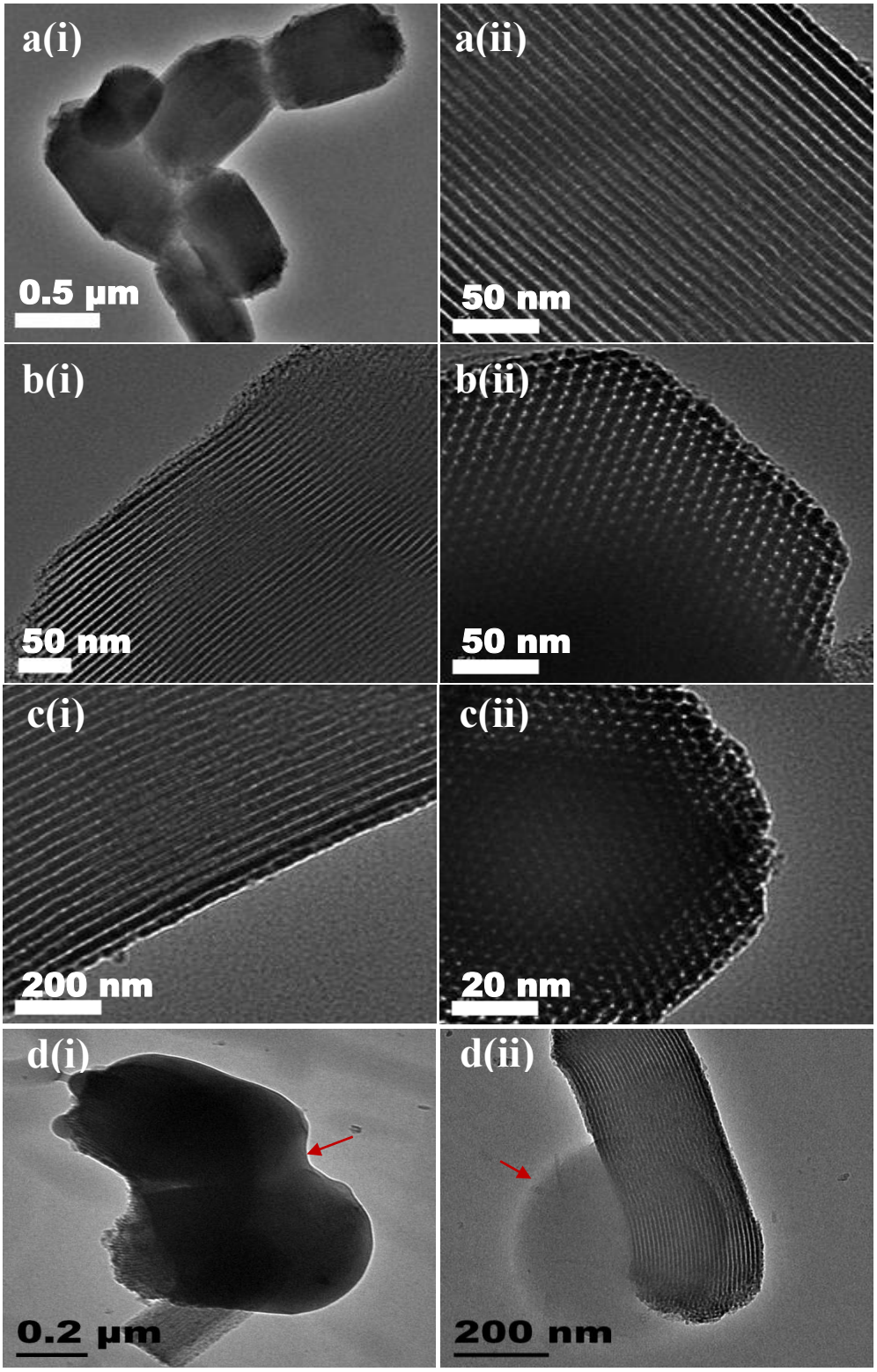

Figure 5.9 TEM images with different orientations of (a) SBA-15, (b) ART/SBA-15 (1:3 w/w), (c) ART/SBA-15 (1:1 w/w) and (d) ART/SBA-15 (3:1 w/w)

5.7 Dissolution Profile (Sink Condition)

The USP IV dissolution profiles are presented in Figure 5.10. The results indicate that the amount of drug released from co-spray dried ART/SBA-15 samples was much higher than other control samples of crystalline ART and ART/SBA-15 physical mixtures. Within the first 15 min of sampling time, the crystalline ART and the P.M.-ART/SBA-15 (1:1 w/w) and P.M.-ART/SBA-15 (1:3 w/w) achieved drug release of only 14.7%, 26.7% and 13.9%, respectively. The final accumulated amount of drug released from crystalline ART was only 56.7% after 2 h and that from the two physical mixtures was even lesser than the crystalline ART. The strong adsorption capacity of SBA-15 which able to re-adsorb the dissolved drug might contribute to the lower drug release from physical mixtures of ART/SBA-15 compared with crystalline drug. In comparison, the drug release from co-spray dried solid dispersions are markedly superior: by 15 min, an initial burst release of 57.0% ($p < 0.05$) and 63.8% ($p < 0.05$) of ART from ART/SBA-15 (1:3 w/w) and ART/SBA-15 (1:1 w/w), respectively, was observed; by 2 h, 82.9% ($p < 0.05$) and 95.0% ($p < 0.05$) of ART had been released from ART/SBA-15 (1:3 w/w) and ART/SBA-15 (1:1 w/w), respectively.

The dissolution studies for ART/SBA-15 based samples were conducted only for 2 hours even though not 100% of the drug released within 2 hours of dissolution. Since the gastric emptying rate is about 15−20 min, the first 20 min of dissolution is important and needs to be considered for oral

drug delivery (FDA, 1997). It is unlikely that the slower dissolution rate of ART/SBA-15 samples was due to the recrystallization of the dissolved drug in the sample holder due to the minute amount of dissolution medium passing through the drug samples (refer Section 6.5). More likely the samples required time to diffuse through the pore channels as SBA-15 with 2D porous channels is not dissolved in medium.

As comparison, the dissolution test was repeated using USP II (Figure 5.11) in order to determine the complete release of the loaded drug. Within the first 15 min, the crystalline ART and the P.M.-ART/SBA-15 (1:1 w/w) and P.M.-ART/SBA-15 (1:3 w/w) achieved drug release of only 9.3%, 25.3% and 31.1%, respectively. However, for the fco-spray dried samplesof ART/SBA-15 (1:3 w/w) and ART/SBA-15 (1:1 w/w) show improved drug release: by 15 min, an initial burst release of more than 90% ($p < 0.05$) was observed and by 2 h, 100% ($p < 0.05$) of ART had been released. Although the dissolution profiles obtained by using USP-II and USP-IV are not identical, the basic trend of difference among these samples is same. The ART co-spray dried with SBA-15 showed much higher dissolution rate than raw crystal ART or mixed with SBA-15.

Various mechanisms govern the rapid release of ART from SBA-15 encapsulated products, the first of which is the physical changes of ART by nano-confinement as revealed by PXRD and DSC (Ambrogi et al., 2013, Li-hong et al., 2013). Particles in the amorphous form are at the most energetic solid state and exhibit better dissolution and solubility compared with their

crystalline counterparts (Hancock and Parks, 2000, Hancock and Zografi, 1997). Therefore, no additional energy is required to dissolve the disordered ART since these drug particles inherently exhibit greater molecular motion with reduced binding energy and intermolecular interactions (Zhao et al., 2012a).

In addition, particle size reduction of the amorphous ART as determined by SEM images in Figure 5.7 also contributes to the dissolution enhancement. During co-spray drying, the ART drug particles are incorporated and homogeneously distributed inside the SBA-15 pore channels in amorphous forms with significantly reduced in particles size, which results in higher specific surface areas exposed to the dissolution medium compared with their crystalline counterpart. Thirdly, enhanced wettability of the solid dispersions due to the hydrophilic surface of silica carriers also leads to superior dissolution kinetics. The hydrophilicity of co-spray dried samples accelerate penetration rate of the water molecules into the capillaries of mesoporous silica and displace the ART molecules into the dissolution medium.

Finally, the enhanced drug release mechanism of ART from solid dispersions is also due to rapid desorption of drug molecules from pore channels of SBA-15, attributable to competitive interaction between water molecules and ART molecules because of the hydrophilicity of the silica pore walls (Ambrogi et al., 2013). Therefore, ART molecules bonded by weak van der Waal forces and hydrogen bonds are easily displaced by the influx of

water. Additionally, the mean pore diameter of SBA-15 which is in the mesoporous range of 8−9 nm and the short length of pore channels of SBA-15 (0.5−1 μm) also could facilitate the drug release. The relatively shorter pore channels of SBA-15 as publicized by the SEM and TEM images could further minimize the diffusion resistance and contribute for faster release of ART. Compared to microporous materials with pore size smaller than 2 nm, SBA-15 having considerably wider pores providing lesser steric hindrance to ART molecules to diffuse out of the pore channels, thus resulting in a greater amount of drug release (Van Speybroeck et al., 2009). The significance of pore diameter on dissolution kinetic was reported previously by Tarja Limnell et al. (2011a), who compared the performance of two mesoporous silica with different pore diameter (SBA-15 and MCM-41 with pore diameters of ~8 nm and ~2.5 nm, respectively). MCM-41, which has narrower pores than SBA-15, demonstrated slower release rate due to resistance that obstructs the diffusion of the drug molecules out of the pore channels.

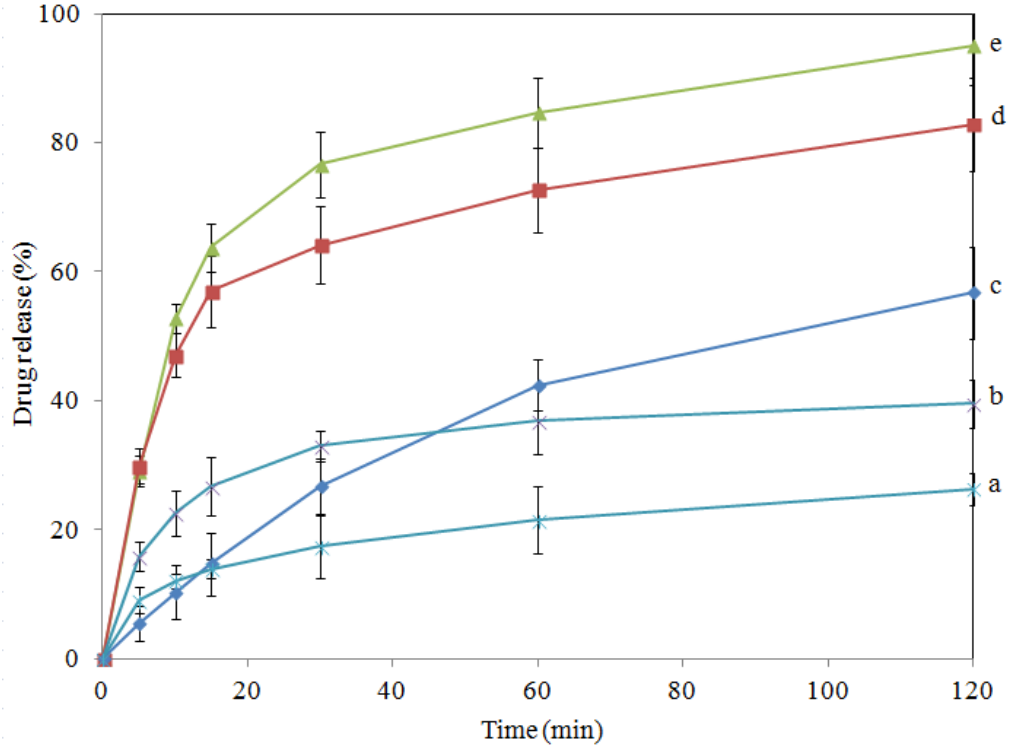

Figure 5.10 Dissolution profiles of (a) P.M.-ART/SBA-15 (1:3 w/w), (b) P.M.-ART/SBA-15 (1:1 w/w), (c) crystalline ART, (d) ART/SBA-15 (1:3 w/w) and (e) ART/SBA-15 (1:1 w/w) under sink condition using USP IV. n=3, $p < 0.05$ versus free ART.

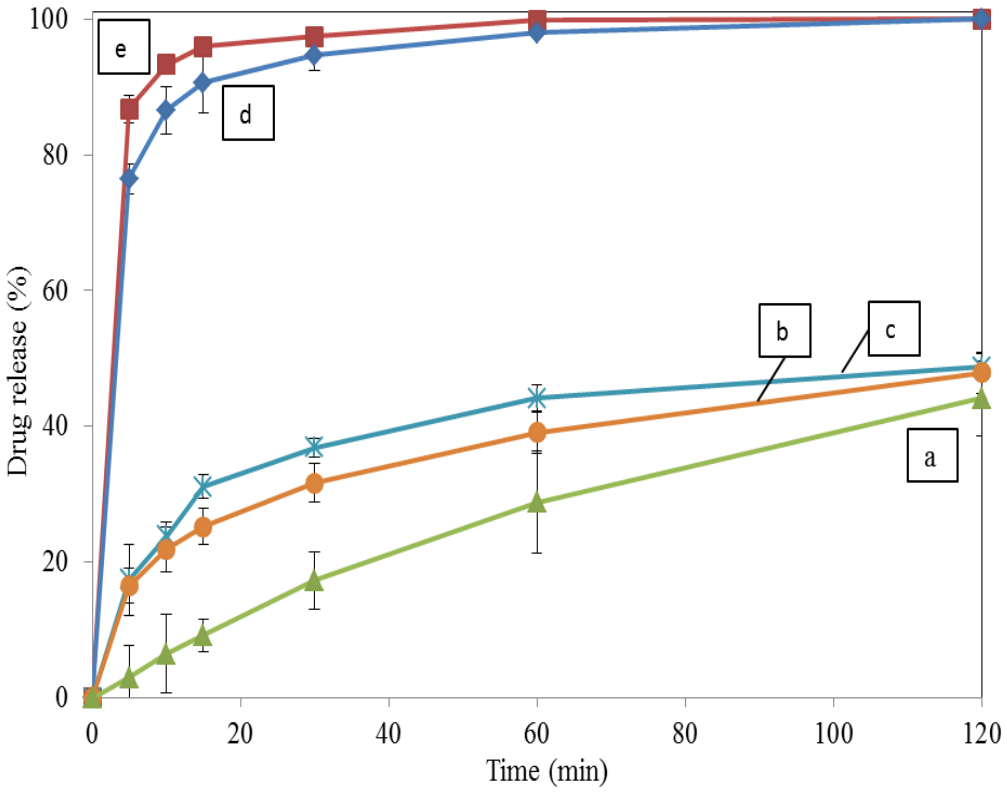

Figure 5.11 Dissolution profiles of (a) crystalline ART, (b) P.M.-ART/SBA-15 (1:1 w/w), (c) P.M.-ART/SBA-15 (1:3 w/w), (d) co-spray dried ART/SBA-15 (1:3 w/w) and (e) ART/SBA-15 (1:1 w/w) under sink condition using USP II. n=3, $p < 0.05$ versus free ART (this figure was not shown in the thesis).

5.8 Dissolution Profile (Non-Sink Condition)

Figure 5.12 depicts the dissolution profiles of crystalline ART and co-spray dried ART/SBA-15 samples. For crystalline ART, the amount dissolved in the first 5 min was 7.6 µg/mL and the concentration gradually increased throughout the experiment to 48.4 µg/mL in 2 h; nevertheless, equilibrium was not attained within the 2 h time period used in this study. For the co-spray dried ART/SBA-15 dispersions, an initial burst release was observed at the beginning of the dissolution and a supersaturation plateau was attained by 60 min with a drug concentration of 101 µg/mL ($p < 0.05$). The

thermodynamic solubility of crystalline ART in water at 37 °C is reported to be 48 µg/mL (Ferreira et al., 2013), whereas the apparent solubility of the formulated amorphous ART in dispersion was enhanced by two fold [101 µg/mL ($p < 0.05$)] and the supersaturation could be sustained for 120 min.

These results clearly indicate that the encapsulation of ART in mesoporous SBA-15 particles was able to circumvent the slow dissolution kinetics and low solubility of ART. Enhancing the apparent solubility is a vital step in improving the absorption and bioavailability of poorly water-soluble drugs. According to Fick's laws of diffusion, drug diffusion across the gastrointestinal epithelia can be improved by increasing the concentration gradient of the drug across the barriers (Van Speybroeck et al., 2010a). Hence, the enhanced apparent solubility of ART in this study would increase the availability of the drug across the gastrointestinal epithelia, thereby augmenting absorption and bioavailability.

Sustaining the enhanced supersaturation of drugs is a challenge faced in achieving optimal bioavailability. From a pharmaceutical perspective, besides improving the flux of drug across the intestinal membranes, supersaturation may also lead to rapid drug precipitation to energetically more favorable forms, which would affect the *in vivo* performance (Van Speybroeck et al., 2010a). This situation commonly necessitates precipitation inhibitors to delay the onset of crystallization and prolong the supersaturation. However, in *in vitro* aqueous solubility tests, the formulated co-spray dried ART/SBA-15

could sustain high supersaturation levels for at least 2 hours. Maintaining the supersaturation of ART is essential to ensure the dissolved drug to be absorbed across the intestinal lumen. Previous studies have also reported sustaining the supersaturation of itraconazole, but only for 30 min (Van Speybroeck et al., 2010b).

The change in physical state (from the crystalline form to the amorphous), the pore architecture (a wider pore size and shorter pore channels), host-guest chemical interactions (weak van der Waal forces and hydrogen bonds) and the properties of loaded drug (reduced particles size and improved wettability) contribute to the improvement of the apparent solubility of ART. All these advantages in co-spray dried formulations allow a rapid penetration of the dissolution medium that ensure the breaking of the hydrogen bonds between ART molecules and SBA-15 silanol groups to achieve rapid dissolution and a high apparent solubility. The correlation between particles size and supersaturation of pharmaceutically active ingredients is well demonstrated by the Ostwald-Freunlich equation (Ostwald, 1900, Freundlich, 1923).

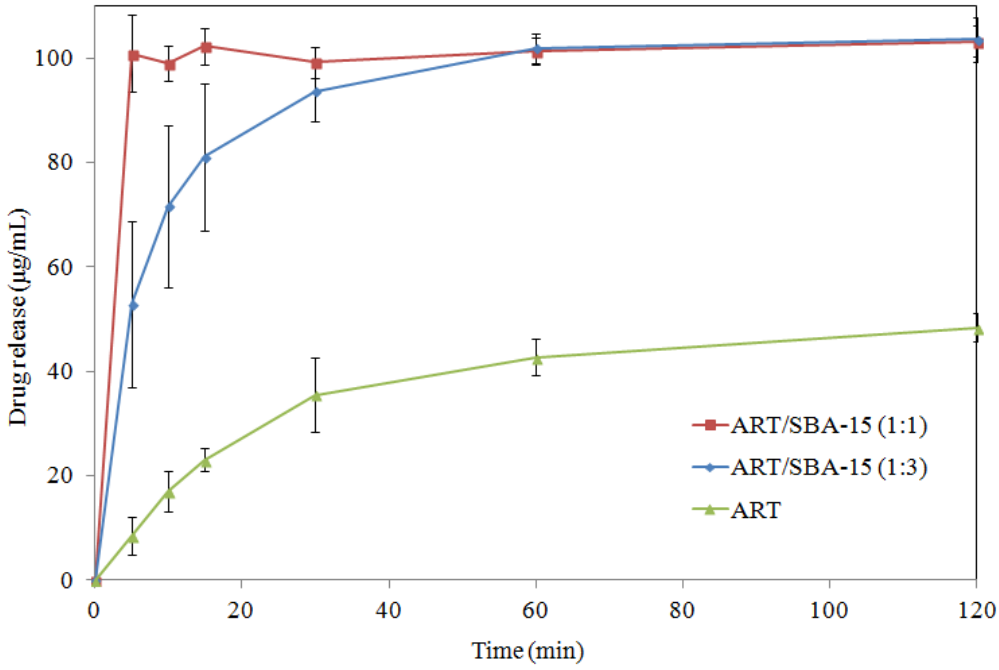

Figure 5.12 Supersaturation of crystalline ART, ART/SBA-15 (1:3 w/w) and ART/SBA-15 (1:1 w/w) under non-sink condition using USP II. *n*=3, $p < 0.05$ versus free ART.

5.9 Chemical Stability of Amorphous ART

Although the physical stability of formulated amorphous APIs has been investigated with different types of carriers, there is scarce literature on the chemical stability of APIs, especially with regard to ART. In order to address this gap, the chemical stability of amorphous ART under different storage conditions was examined. The chemical stabilities of co-spray dried ART/SBA-15 dispersions were analyzed by using HPLC after 3- and 6-months of storage. The percentages of ART preservation as a function of storage time at different temperatures and relative humidity are tabulated in Table 5.3. As a control, untreated ART and spray dried crystalline ART could preserve more than 99% of ART without degradation after stressed storage tests at 40 °C/75% RH in open pans for 12-month (Table 4.4). Similarly, the

co-spray dried samples of ART/SBA-15 (1:3 w/w) and ART/SBA-15 (1:1 w/w) stored in desiccators (25 °C/18% RH), Activ-vial® at 25 °C and 40 °C also displayed no or slight degradation of ART after 6-months of storage; more than 94% of ART was preserved in these samples. However, the samples in open pans at 25 °C/75% RH and 40 °C/75% RH started to degrade within the first-month of storage (data not shown) and ART degraded significantly after 6-months. In addition, it was observed that the ART/SBA-15 (1:3 w/w) exhibited a higher degradation rate than the ART/SBA-15 (1:1 w/w) samples.

In this study, 3 main factors that contribute to chemical degradation were investigated: storage temperature, relative humidity (% RH) and drug-carrier ratio (Hailu and Bogner, 2011). It can be deduced that hydrolytic degradation is predominant during the storage, given that the relative humidity (% RH) plays an important role in chemical instability of amorphous ART than the storage temperature. All the samples stored at a high relative humidity (75% RH), regardless of the storage temperature, degraded more easily compared with those stored in Activ-vial® and desiccators with a low humidity. The thermal stability of ART has been reported previously, as ART can remain stable without any decomposition even at its melting point (156–157 °C) and it starts to breakdown only at 190 °C (Li and Zhou, 2010, Lin et al., 1985). Accordingly, it can be concluded that the storage temperature did not exhibit significant effects on the degradation of ART.

The drug-carrier ratio of ART/SBA-15 also influenced the degree of degradation of ART through its impact on the specific area and the pore

volume on moisture content. ART/SBA-15 (1:3 w/w) is observed to exhibit a higher degradation rate compared with ART/SBA-15 (1:1 w/w). The lower drug loading in ART/SBA-15 (1:3 w/w) implies a larger specific area and a greater pore volume of SBA-15 for adsorption and condensation of vapour. Subsequently, the greater degree of vapor condensation accelerates the degradation of the encapsulated ART and impairs its chemical stability. As shown in Table 5.3, a lower extent of drug loading is associated with a higher moisture content and all ART/SBA-15 (1:3 w/w) samples have a higher moisture content than ART/SBA-15 (1:1 w/w) samples. In addition, for samples stored at 75% RH, the moisture content increases with duration of storage. Conversely, the moisture content for samples stored at a lower humidity was observed to be as low as 2%. Thus, it is recommended that products of ART/SBA-15 be formulated with a high extent of drug loading to maximally fill pore structures and be stored under conditions of low humidity to achieve a long shelf-life.

Table 5.3 Moisture content and amounts of ART remaining within ART/SBA-15 samples after storage under 5 different storage conditions for 3 and 6-months.

Storage period	Storage conditions	% of remaining ART		Moisture content (%)	
		ART/SBA-15 (1:3 w/w)	ART/SBA-15 (1:1 w/w)	ART/SBA-15 (1:3 w/w)	ART/SBA-15 (1:1 w/w)
Fresh		100.0 ± 1.5	100.0 ± 1.3	2.2 ± 0.1	1.7 ± 0.4
3-months	Desiccators (25 °C/18% RH)	98.2 ± 1.0	99.1 ± 0.8	2.0 ± 0.4	1.8 ± 0.4
	Activ-vial® (25 °C)	97.1 ± 1.8	99.7 ± 1.3	2.24 ± 0.2	1.41 ± 0. 5
	Open pan (25 °C/75% RH)	81.3 ± 0.3	94.2 ± 1.0	4.9 ± 0. 3	2.8 ± 0. 4
	Activ-vial® (40 °C)	96.4 ± 3.6	98.5 ± 1.0	2.1 ± 0.4	1.9 ± 0.3
	Open pan (40 °C/75% RH)	26.1 ± 0.1	59.8 ± 0.3	4.9 ± 0.9	2.6 ± 0.1
6-months	Desiccators (25 °C/18% RH)	97.9 ± 1.3	99.2 ± 0.7	2.2 ± 0.2	1.2 ± 0.4
	Activ-vial® (25 °C)	97.5 ± 0.8	98.5 ± 0.9	2.1 ± 0.2	1.67 ± 0.4

Storage period	Storage conditions	% of remaining ART		Moisture content (%)	
		ART/SBA-15 (1:3 w/w)	ART/SBA-15 (1:1 w/w)	ART/SBA-15 (1:3 w/w)	ART/SBA-15 (1:1 w/w)
	Open pan (25 °C/75% RH)	76.4 ± 0.5	80.9 ± 0.4	6.9 ± 1.1	3.9 ± 0.4
	Activ-vial® (40 °C)	96.0 ± 4.1	94.3 ± 6.0	2.1 ± 0. 5	1.6 ± 0. 6
	Open pan (40 °C/75% RH)	0	27.9 ± 2.0	8.8 ± 0. 6	4.3 ± 0. 3

Data represent mean ± S.D., *n*=3

5.10 Physical Stability of Amorphous ART

Despite the enhanced dissolution rate and supersaturation, amorphous drugs usually suffer from a poor thermodynamic stability as these drug particles tend to revert to the stable crystalline forms during transport and storage. Prolonging the physical stability of amorphous ART is one of the important considerations to preserve the enhanced physicochemical properties (Wang et al., 2013). Therefore, the physical stability of ART/SBA-15 formulations upon storage was investigated under three different storage conditions for up to 6-months. Those three conditions with a lower % RH in which amorphous ART/SBA-15 exhibited good chemical stability were used: desiccators (25 °C/18% RH), Activ-vial® (25 °C) and Activ-vial® (40 °C). The solid states of these samples were analyzed by PXRD and the results are displayed in Figure 5.13 (A) and (B). As aforementioned, the freshly co-spray dried solid dispersions exhibited typical amorphous characteristics. After storage, these ART/SBA-15 samples still exhibited flat patterns without evidence of PXRD peaks corresponding to crystalline ART. This indicates that the amorphous ART entrapped in the pore channels of SBA-15 remained physically unchanged during storage as no crystalline ART could be detected by PXRD after 6-months. It is accordingly suggested that SBA-15 confers a strong re-crystallization inhibition effect that stabilizes ART in the amorphous form during long-term storage periods.

SBA-15 confers physical stability upon amorphous ART via three mechanisms: the size-constraint effect on nucleation and crystal growth (Shen

et al., 2011, Shen et al., 2010); the thickness and rigidity of pore walls (Rengarajan et al., 2008); and the formation of hydrogen bonds through surface silanol groups (Watanabe et al., 2001, Watanabe et al., 2002). As regards the size-constraint effect of mesoporous silica, it has been reported that the nucleation will only take place if the ratio of pore diameter to drug molecular size exceeds 20 (Sliwinska-Bartkowiak et al., 2001, Qian and Bogner, 2012). The small and uniform pore size of SBA-15 in the range of only 8–9 nm is highly effective in inhibiting the nucleation of ART crystals by restricting molecular transport and re-arrangement. In addition, the thicker and rigid pore walls of SBA-15, as depicted by the TEM images, are able to separate the fine amorphous particles effectively and change the nucleation mechanism that can prevent the re-crystallization process. For example, those drug molecules entrapped in the pore channels of SBA-15 need to nucleate homogeneously since the rigid and non-nucleating pore walls will further delay the re-crystallization and crystal growth of amorphous particles (Rengarajan et al., 2008). Moreover, those confined ART molecules can form hydrogen bonds with the silanol groups on interfacial surface. The immobilization of drug molecules on the surfaces of SBA-15 could further prevent the movement and re-crystallization of ART. The importance of hydrogen bonding between drug and carrier in stabilizing the amorphous drug has been reported by Limnell et al. (2011a). According to the authors, SBA-15 is able to afford stability to amorphous indomethacin more effectively than MCM-41, due to the presence of larger number of silanol groups per unit area

of the former which provide better immobilization effect to the amorphous forms.

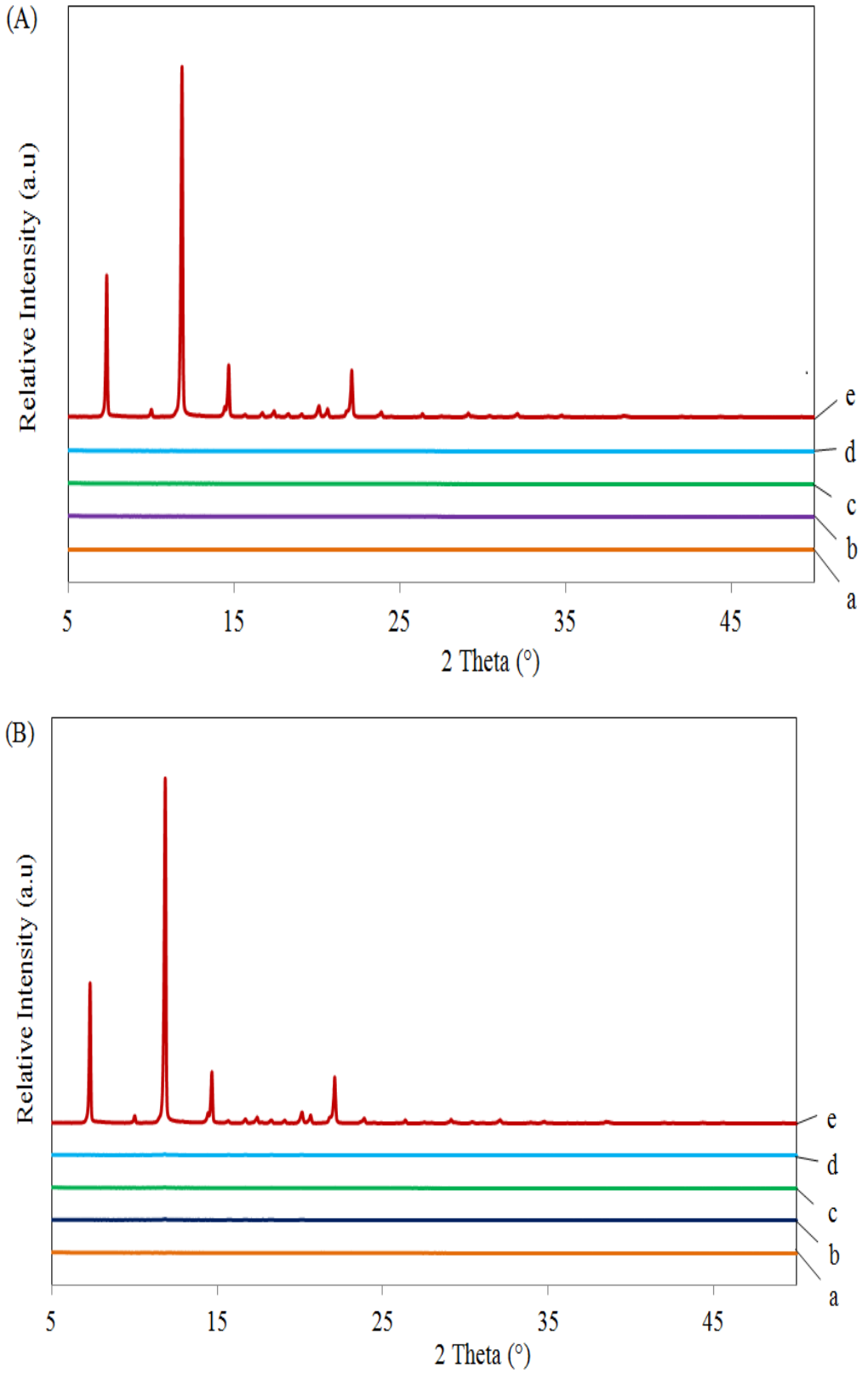

Figure 5.13 PXRD patterns of (A) ART/SBA-15 (1:3 w/w) and (B) ART/SBA-15 (1:1 w/w) that (a) freshly co-spray dried and after storage for 6-months in (b) desiccators (at 25 °C/18% RH), (c) Activ-vial® (at 25 °C) (d), Activ-vial® (at 40 °C) and (e) untreated ART crystals (fresh).

5.11 Dissolution after Storage using USP II

Those samples that exhibited adequate physical and chemical stability after 6-months of storage were subjected to dissolution tests (by using USP II) in order to assess the extent to which SBA-15 particles preserve the improved drug release of ART. Freshly co-spray dried samples were used as controls and the results are displayed in Figure 5.14. Approximately 90% ($p < 0.05$) of ART could be released to the dissolution medium in 2 h of dissolution. There are no significant changes in the drug release profile of the stored samples as compared with the freshly prepared samples. The long-term stability of amorphous ART in the dispersions and the hydrothermal stability of SBA-15 with unchanged pore structures mainly contribute to the improved and unchanged dissolution behavior of dosage forms.

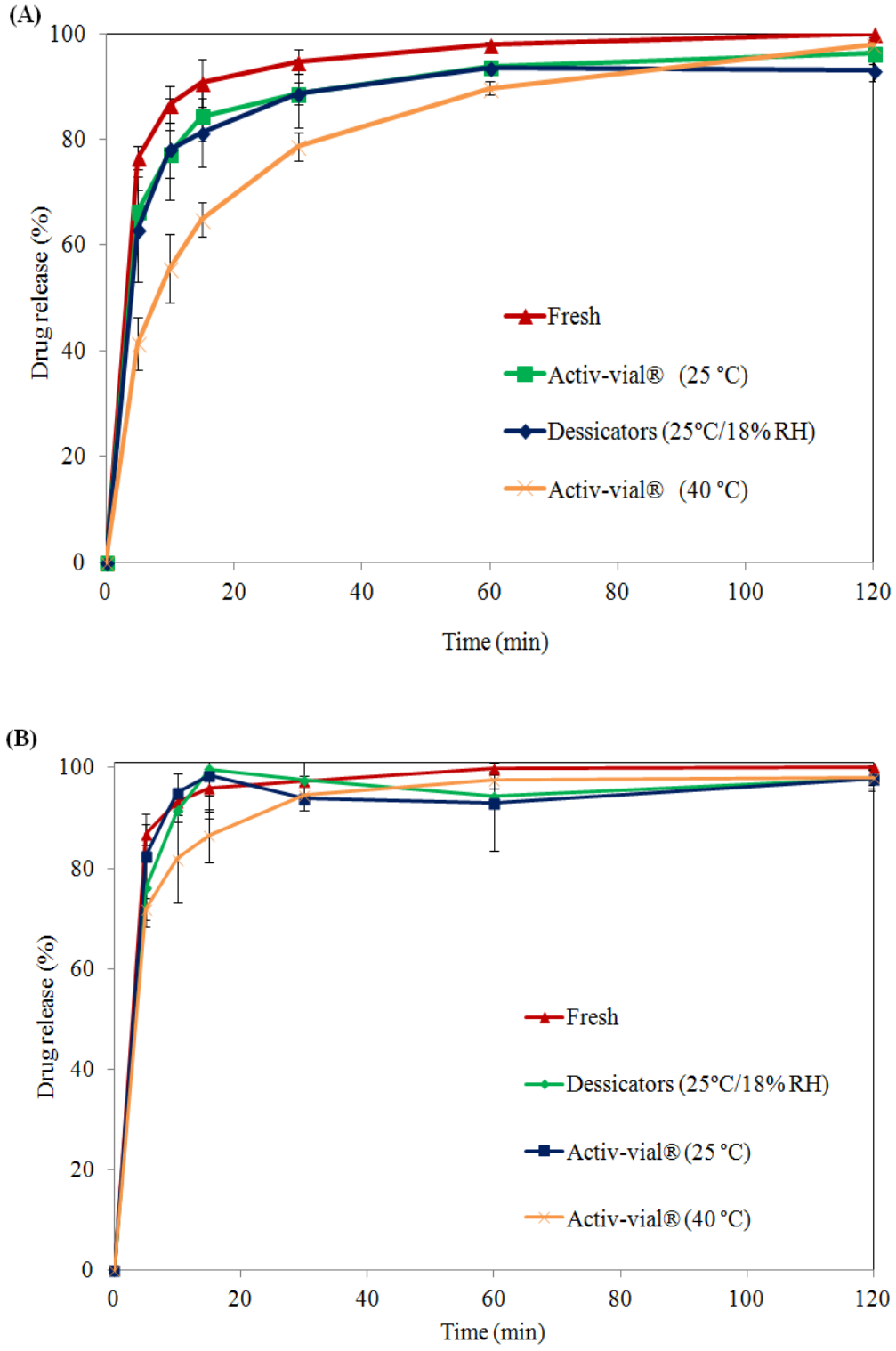

Figure 5.14 Dissolution profiles (USP II) of ART from co-spray dried (A) ART/SBA-15 (1:3 w/w) and (B) ART/SBA-15 (1:1 w/w) after storage at 3 different conditions for 6-months. n=3, $p < 0.05$ versus free ART.

5.12 *In vitro* Evaluation of Cytotoxicity

Cell viability is one of the most essential tools to evaluate the biocompatibility of oral drug delivery formulations. Therefore, in this study, the biocompatibility of the pure SBA-15 and equivalent concentrations of the free and encapsulated ART were quantified by assessing the effect of these samples on the survival rate of Caco-2 cells. Caco-2 cells were chosen as an *in vitro* model due to their morphological and physiological similarity to intestinal epithelial cells. Figure 5.15 presents the viability of Caco-2 cells after 24 h exposures to SBA-15 (0.25, 0.50, 1.0, 2.0 and 4.0 mg/mL), ART and ART/SBA-15 (25, 50, 100 and 200 µg/mL). The maximum concentration of the samples was limited to 200 µg/mL due to concerns with the formation of ART micro-crystals as observed with samples containing 400 µg/mL equivalent of ART as shown in Figure 5.16.

As seen in Figure 5.15, untreated ART, SBA-15 and formulated ART/SBA-15 samples exhibited neither harmful nor dose-dependent effects on the Caco-2 cells over the tested concentration range. Even at the highest concentration of samples, the cell survival rate remained above 90%, confirming little particle interference on cell integrity and negligible cytotoxicity. More importantly, no noticeable IC_{50} values were observed for any of the samples at any concentration after 24 h exposure. Several studies have reported the non-toxic nature of SBA-15 compared with other members of mesoporous silica such as MCM-41. It has also been reported that the entry of small and spherical particles into cells through endocytosis may be

responsible for cytotoxicity (Wang et al., 2013). Accordingly, it may be deduced that the non-toxic nature of SBA-15 in this study may be attributed to the inability of large particles to penetrate cell membranes. ART has likewise been reported to be safe for normal cells, despite its toxicity to various cancerous cells due to the higher iron influx rates of the latter (Nakase et al., 2008).

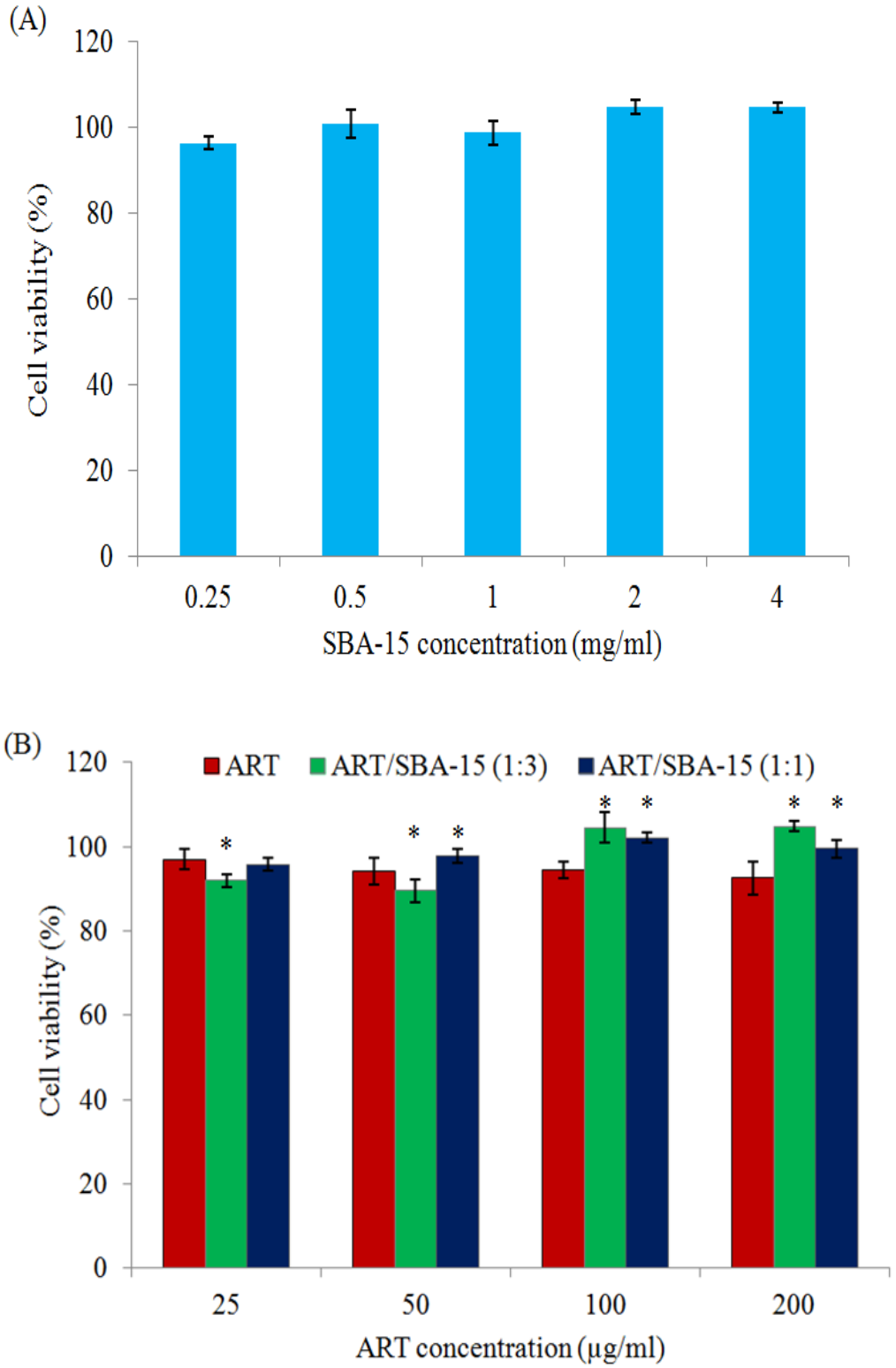

Figure 5.15 Caco-2 cell viability after 24 h incubation with (A) SBA-15 and (B) untreated ART and ART/SBA-15 solid dispersions at 37 ºC, as a function of the particle concentration. *n*=3, $p < 0.05$ versus free ART.

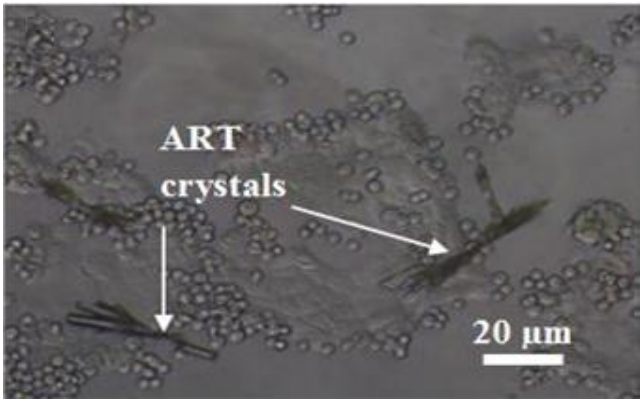

Figure 5.16 Optical microscopy of Caco-2 cells and ART.

5.13 Conclusion

SBA-15 particles with outstanding features such as high surface areas, large pore volumes, uniform pore size, short pore channels and hydrophilicity, were used as a drug vehicle for poorly soluble ART to enhance its biopharmaceutical properties via co-spray drying. Spatial confinement of amorphous ART within the pore channels of SBA-15 mainly contributed to the remarkably enhanced dissolution kinetics compared with the crystalline ART. The amorphous ART/SBA-15 achieved supersaturation of ART more than two-fold of the equilibrium solubility of ART, which can be sustained for 2 h without addition of any precipitation inhibitors. The ART/SBA-15 samples exhibited excellent chemical stability regardless of storage temperature under low humidity conditions. However, ART/SBA-15 showed obvious degradation when stored under conditions of high relative humidity. In addition, the amorphous state of ART/SBA-15 samples exhibited excellent physical stability lasting for 6-months with preserved enhanced dissolution properties. Meanwhile, as evident from the cell survival data, SBA-15,

untreated ART and formulated ART/SBA-15 samples show low cytotoxicity on Caco-2 cell line suggesting the biocompatibility of the samples. As comparison, non-porous silica was used a carrier to support the concenpt of nano-confinement of most of the ART drug particles inside the pore channel of SBA-15. Characteristic results such as PXRD, N_2 adsorption, SEM and TEM prove the encapsulation of most of the ART particles inside the pore channles of SBA-15.

Chapter 6 Encapsulation of ART in Functionalized Food Additives

In comparison with mesoporous carriers, the solubility of ART was enhanced by using water-soluble transglycosylated food additives, α-glucosyl hesperidin (Hsp-G) and α-glucosyl stevioside (Stevia-G), via co-spray drying. These two food additives have been chosen as potential drug carriers by virtue of their superior aqueous solubility, relative safety and cost-effectiveness. Additionally, Hsp-G has been reported to possess significant anti-inflammatory, hypotensive and analgesic effects; Stevia-G has been used as a sweetener for patients with diabetes and as a sugar substitute for hypoglycemia patients for more than 20 years. These functionalized foods have become an important ingredient in daily diets and play a vital role in preventing diseases in countries that face serious aging problem such as Japan (Tozuka et al., 2010). Therefore in this study the performance of transglycosylated food additives including drug loading capacity, drug release enhancement and storage stability will be studied and compared with SBA-15.

6.1 X-Ray Diffraction (XRD)

Initially, solid dispersions of ART/Hsp-G and ART/Stevia-G were formulated at two different ratios: 1:3 w/w and 1:10 w/w. However, the samples of 1:3 w/w exhibited a small PXRD peak at diffraction angles of 11.3° (Figure 6.1), although the 1:10 w/w samples showed halo patterns, suggesting the presence of the amorphous drug form. Since the presence of

crystal seeds in the solid dispersions can induce re-crystallization of the amorphous form and cause poor physical stability, the ART/Hsp-G (1:3 w/w) and ART/Stevia-G (1:3 w/w) samples were excluded in further analysis.

Comparison of X-ray diffraction of untreated ART, Hsp-G and Stevia-G, physical mixtures and co-spray dried solid dispersions with different vehicles are presented in

Figure 6.2 6.2. X-ray diffractions of untreated ART and spray dried ART (without carriers) have been discussed in Sections 4.3 and 5.3. Meanwhile, both the untreated hydrophilic carriers exist in the X-ray amorphous form as typical broad and halo amorphous band shown by the PXRD. The physical mixtures of ART with Hsp-G (1:10 w/w) and Stevia-G (1:10 w/w) show that the drug retained its original characteristic peaks though with reduced relative intensities. However, for spray dried solid dispersions of ART/Hsp-G (1:10 w/w) and ART/Stevia-G (1:10 w/w), halo diffraction patterns without characteristic peaks associated with the ART were observed, indicating that ART was no longer present in the crystalline form but might have been dispersed in an amorphous or monomolecular state. The non-crystalline forms of ART upon formulation can be attributed to the formation of micelle-like structure of Hsp-G and Stevia-G by encapsulating the ART molecules in hydrophobic cores (Figure 6.3) during co-spray drying inhibited the formation of long-range ordered molecular arrangement of ART.

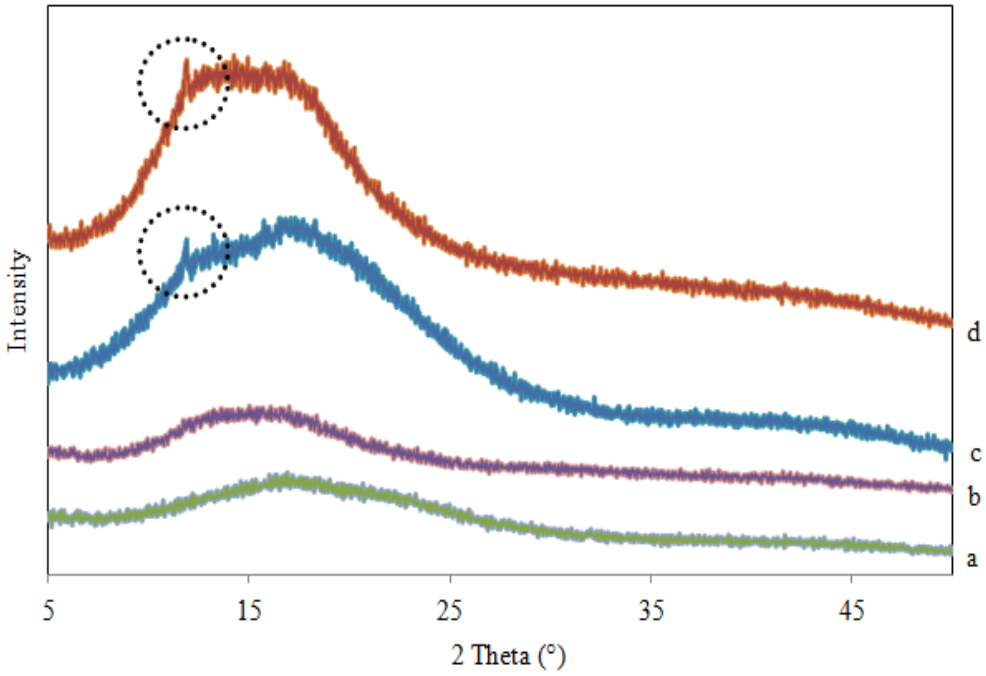

Figure 6.1 PXRD patterns of (a) ART/Hsp-G (1:10 w/w), (b) ART/Stevia-G (1:10 w/w), (c) ART/Hsp-G (1:3 w/w) and (d) ART/Stevia-G (1:3 w/w).

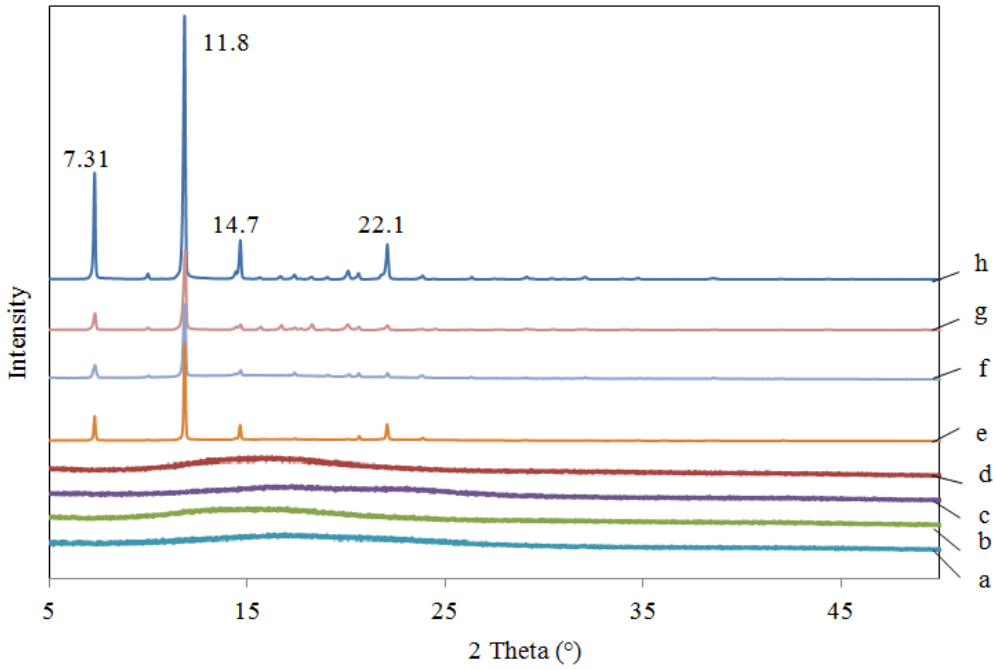

Figure 6.2 PXRD patterns of (a) ART/Hsp-G (1:10 w/w), (b) ART/Stevia-G (1:10 w/w), (c) Hsp-G, (d) Stevia-G, (e) physically mixed ART/Hsp-G (1:10 w/w), (f) physically mixed ART/Stevia-G (1:10 w/w), (g) spray dried ART and (h) untreated ART crystals. (Note: Intensity of PXRD peaks of (e), (f), (g) and (h) were reduced 20 time than that of the actual intensity).

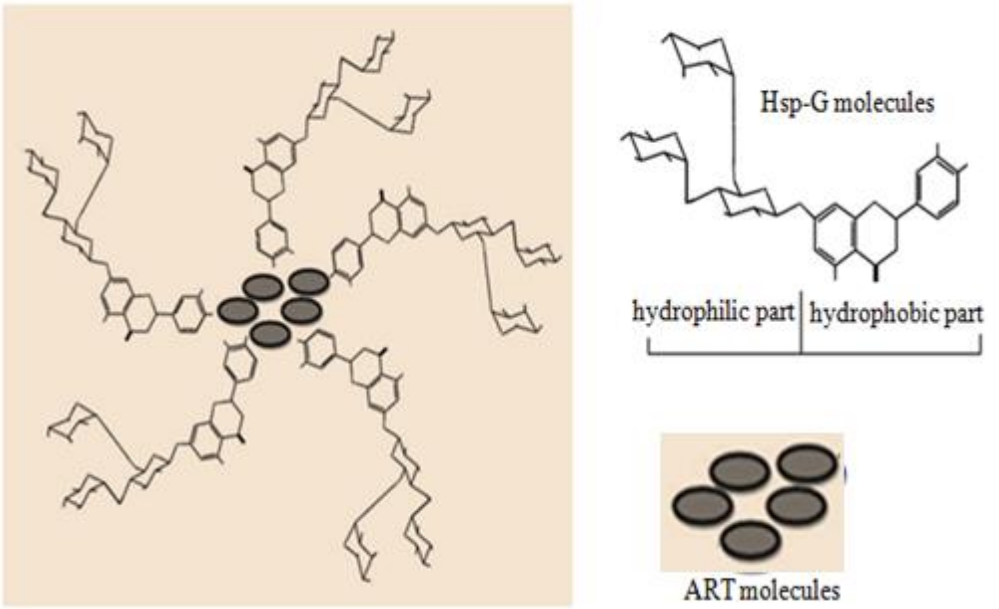

Figure 6.3 Schematic representation of the resultant micelle-like structures of Hsp-G in ethanol-water mixture solution [adapted from (Tozuka et al., 2010)].

6.2 Differential Scanning Calorimetry (DSC)

The thermal analysis of all the samples was performed by differential scanning calorimetric (DSC) and the results were presented in Figure 6.4. The melting point of crystalline ART at 153.4 °C as reported in Sections 4.2 and 5.4 was further corroborated by the results of hot stage microscope images (Figure 6.5). The melting point of the crystal as observed during hot stage microscopy was 153.4 °C, which is almost similar to the value obtained from the DSC peak (Figure 6.4) and the melting point of ART is size-dependent in that it varies from 153.0–157.8 °C. Meanwhile, no endothermic peak appeared for Hsp-G and Stevia-G, indicating their amorphous nature. In the thermograms of physical mixtures, the endothermic peaks of P.M.-ART/Hsp-G (1:10 w/w) and P.M.-ART/Stevia-G (1:10 w/w) were less intense, slightly broad and shifted towards to lower temperature (151.7 °C and 152.7 °C,

respectively). Once ART was co-spray dried with Hsp-G and Stevia-G, no peak corresponding to drug melting was observed, confirming the absence of ART crystals in the formulated samples. ART was successfully converted into the amorphous form upon encapsulation with the excipients, as the physical state was further confirmed by the powder X-ray diffraction results, indicating an amorphous form of the drug after co-spray dried with food additives.

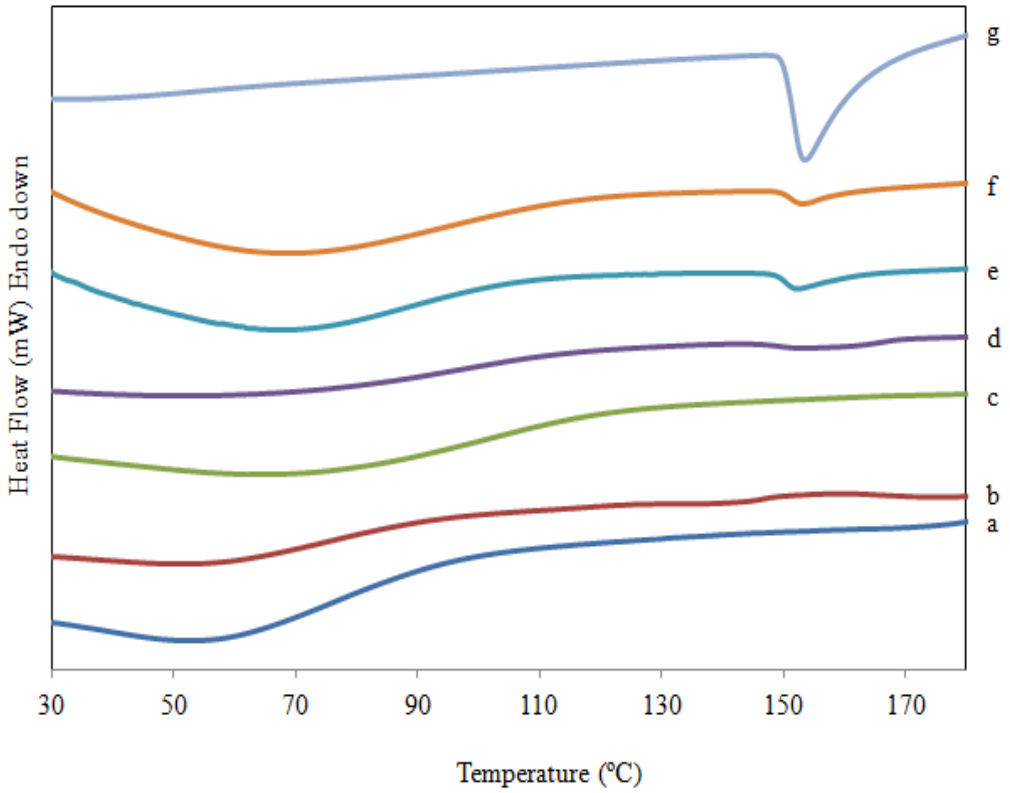

Figure 6.4 DSC curves of (a) Hsp-G, (b) ART/Hsp-G (1:10 w/w), (c) Stevia-G, (d) ART/Stevia-G (1:10 w/w), (e) physically mixed ART/Hsp-G (1:10 w/w), (f) physically mixed ART/Stevia-G (1:10 w/w) and (g) untreated ART crystals.

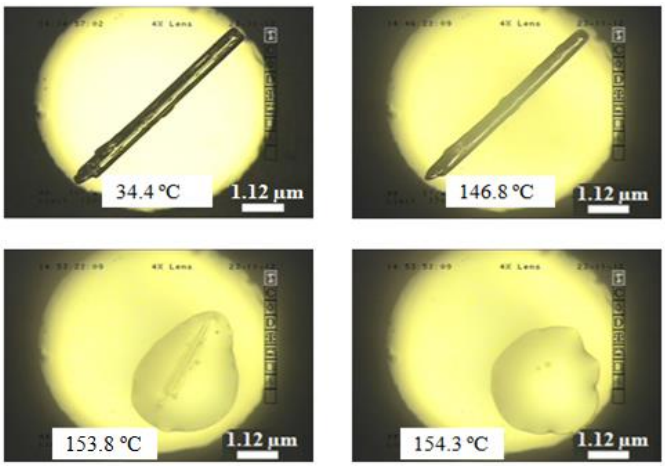

Figure 6.5 ART crystal images as observed from the microscope equipped with a hot stage.

6.3 Determination of Drug Loading

The encapsulation efficiency was quantified by measuring the ART loading in Hsp-G and Stevia-G after co-spray drying. ART-loaded samples weighing 5 mg were extracted with 50 mL of ethanol/water (1:1 v/v) with stirring for 24 h, followed by filtration and analysis by HPLC. Table 6.1 outlines the drug loading efficiency of ART/Hsp-G (1:10 w/w) and ART/Stevia-G (1:10 w/w) samples. The drug uptake by Hsp-G and Stevia-G particles was 8.04 wt% and 8.42 wt% respectively. It is shown that more than 88.6% and 92.7% of ART in the designed formulation were respectively encapsulated by Hsp-G and Stevia-G. However, when compared with drug loading of SBA-15 (48.8 wt%), the drug loading by functionalized food additives is considerably inferior. For SBA-15, the larger specific surface area and pore volume afforded accommodation of such large quantity of drug, which was difficult to achieve in food additives. Moreover, crystalline forms can be detected when the drug loading increased to 25 wt% (Figure 6.1).

Therefore, with respect to drug loading, SBA-15 has a better capacity compared with Hsp-G and Stevia-G.

Table 6.1 Drug loading of ART within Hsp-G and Stevia-G

Sample	Theoretical drug loading [wt%]	Drug Loading [wt%]	Drug Loading efficiency [%]
ART/Hsp-G (1:10 w/w)	9.09	8.04 ± 0.43	88.6 ± 4.74
ART/Stevia-G (1:10 w/w)	9.09	8.42 ± 0.13	92.7 ± 1.43

Data represent mean ± S.D., *n*=3

6.4 Scanning Electron Microscope (SEM)

The surface morphologies of all the samples were characterized by using SEM and the micrographs thus obtained were depicted in Figure 6.6

Figure 6.6. Refer to Sections 4.4 and 5.5 for more details about the physical state, polymorph and particle size of raw ART and spray dried ART. Figure 6.6(c) and (d) reveal that the morphology of Hsp-G and Stevia-G appeared to be in irregular shape with a relatively wide particle size distribution within a range of 0.7–75.6 μm for Hsp-G and 0.8–139.0 μm for Stevia-G. This morphology of the excipients has been reported previously (Uchiyama et al., 2011a, Tozuka et al., 2010). On the other hand, the spray dried additives [Figure 6.6(e) and (f)] show changes in morphology, whereby mixtures of irregular particles and shrank spheres can be observed. Meanwhile, the morphology of Hsp-G and Stevia-G were completely changed to shrunken spheres after co-spray dried with ART with a reduced particle size in the range of 0.5–14.2 μm [Figure 6.6(g) and (h)]. The disappearance of crystalline

particles of ART clearly indicates the encapsulation of ART by Hsp-G and Stevia-G and the final product appeared to be in non-crystalline forms. For the physical mixtures [Figure 6.6(g) and (h)], the drug and carriers appeared to be separate particles without changes in morphology or interactions between them. Conversely, for physical mixtures of ART/SBA-15 (Figure 7.7), SBA-15 appeared to adhere on the surface of ART due to interactions such as electrostatic or van der Waals forces.

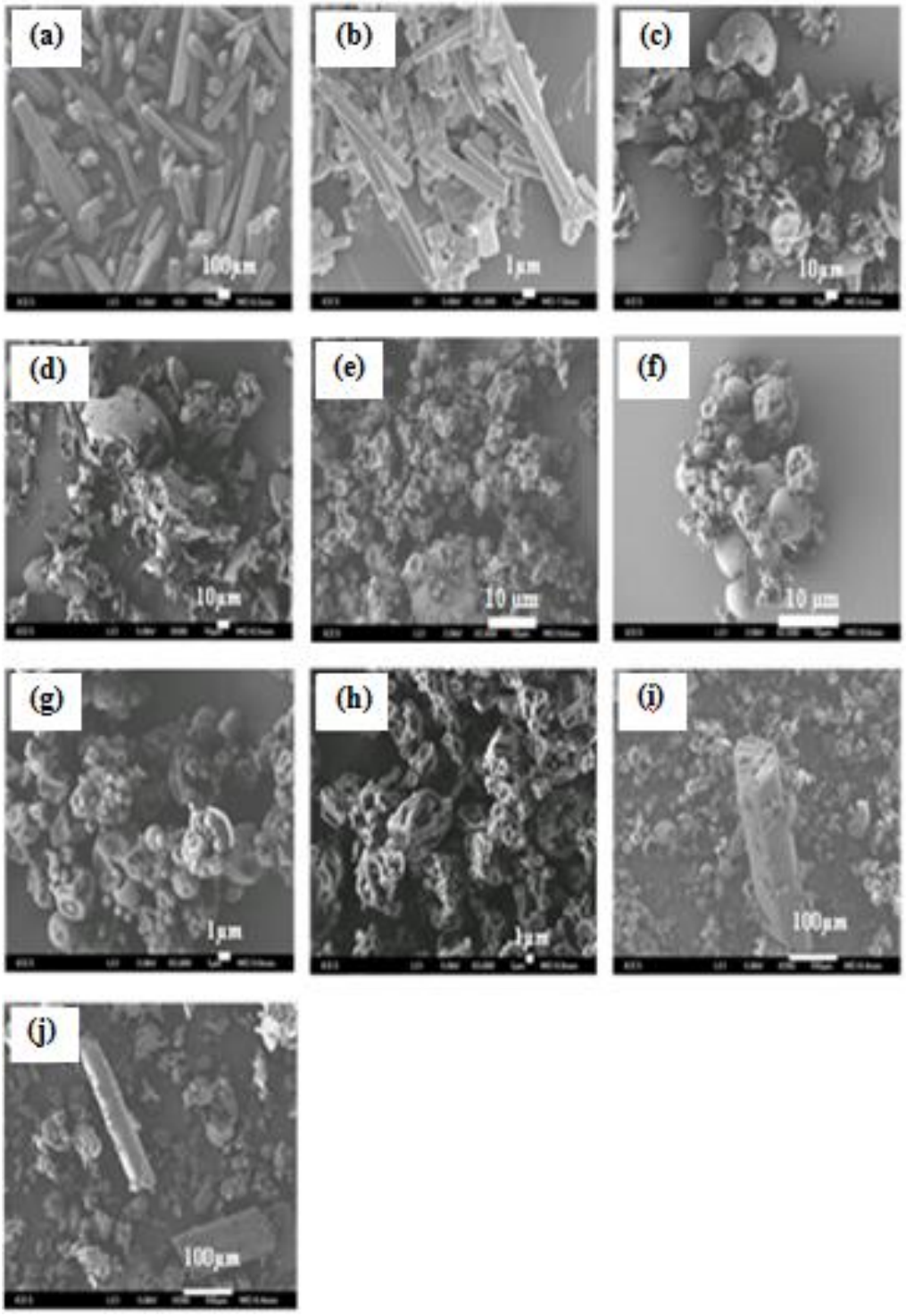

Figure 6.6 SEM images of (a) untreated ART crystal, (b) spray dried ART crystal, (c) Hsp-G, (d) Stevia-G, (e) spray dried Hsp-G, (f) spray dried Stevia-G, (g) ART/Hsp-G (1:10 w/w), (h) ART/Stevia-G (1:10 w/w), (i) physically mixed ART/Hsp-G (1:10 w/w) and (j) physically mixed ART/Stevia-G (1:10 w/w).

6.5 Dissolution Measurement

In this section, the dissolution profiles of co-spray dried solid dispersions and P.M.-ART/Hsp-G (1:10 w/w) and P.M.-ART/Stevia-G (1:10 w/w) were characterized and the results are depicted in Figure 6.7. As expected, both the untreated ART and physical mixtures have shown poor drug release rate. In the first 15 min, approximately 14.7% of the ART was released and it achieved 56.7% after 2 h. In the meantime, 54.9% of and 53.5% ART was dissolved after 2 h from P.M.-ART/Hsp-G (1:10 w/w) and P.M.-ART/Stevia-G (1:10 w/w), respectively. The poor dissolution of ART is mainly due to its crystalline and hydrophobic nature. Meanwhile, the lack of interaction between ART and Hsp-G and Stevia-G in the physical mixtures caused poor dissolution as untreated ART; hardly any differences were observed in the dissolution rate between untreated drug and physical mixtures.

It is found that the use of the hydrophilic Hsp-G and Stevia-G as carriers in solid dispersions for poorly water-soluble drugs produced a dramatic improvement in the dissolution rate of ART. As shown in Figure 6.7(d) and (e), ART loaded into functionalized food additives exhibited an initial burst of more than 94% ($p < 0.05$) within 5 min, in comparison with 4.0% for the untreated drug. The amounts of drug release in 5 min from ART/Hsp-G (1:10 w/w) and ART/Stevia-G (1:10 w/w) were 94.1% ($p < 0.05$) and 99.4% ($p < 0.05$), respectively and the final dissolved amounts of ART was 99% ($p < 0.05$) for both the samples at end of the dissolution. The possibility of the dissolved drug to re-crystallize in the sample holder due to

the minute amount of dissolution medium passing through the drug samples can be excluded for ART samples, since nearly 100% of ART dissolution was achieved in 5 min without any decrease in the measured dissolution.

Compared with mesoporous silica (Chapter 5), functionalized food additives have a remarkable role in enhancing dissolution rate, as attested to by an initial burst of almost 100% drug release within 5 min of dissolution test. The dissolution enhancement of treated ART was attributed to amorphization of ART alongside with particle size reduction and improved wettability by the hydrophilic carriers. The hydrophilic carriers could be rapidly wetted by water so that the drug molecules are surrounded with water, allowing fast drug dissolution. The impact of particle size reduction should be similar to that of spray dried ART that has been discussed in previous chapters.

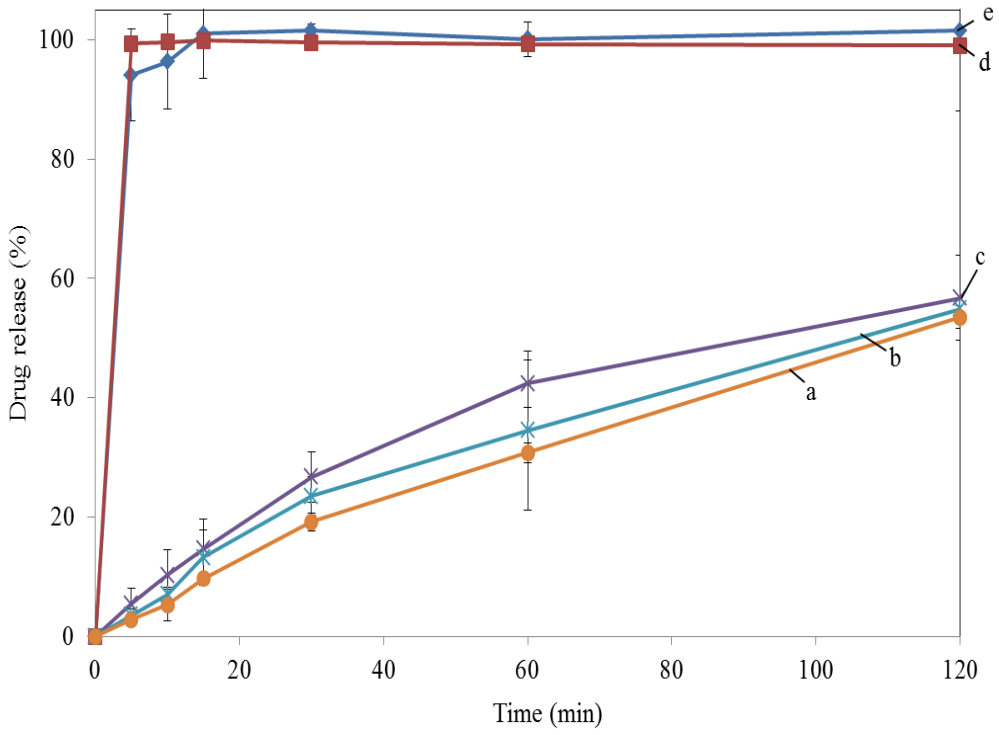

Figure 6.7 Dissolution profiles of (a) physically mixed ART/Stevia-G (1:10 w/w), (b) physically mixed ART/Hsp-G (1:10 w/w), (c) untreated ART, (d) ART/Stevia-G (1:10 w/w) and (e) ART/Hsp-G (1:10 w/w) using USP IV (sink condition). *n*=3, $p < 0.05$ versus free ART.

6.6 Solubility Measurement

Figure 6.8 shows the supersaturation of raw and formulated ART samples. The results indicated that the untreated ART possessed a very low aqueous solubility of 48.4 µg/mL, as was consistent with the reported literature (Ferreira et al., 2013). The supersaturation of the formulated solid dispersions was two-fold that of raw ART, i.e. the final solubility of ART/Hsp-G (1:10 w/w) and ART/Stevia-G (1:10 w/w) were 102.6 µg/mL ($p < 0.05$) and 95.6 µg/mL ($p < 0.05$), respectively. Both the formulated samples achieved a burst release with more than 98 µg/mL ($p < 0.05$) of drug dissolved within the first 5 min; in contrast, a release of only 8.5 µg/mL was observed

for raw ART during the same period. The maximum concentration was achieved at the 15th min of test, when the values of supersaturation achieved 102.9 μg/mL ($p < 0.05$) and 100.5 μg/mL ($p < 0.05$) for ART/Hsp-G (1:10 w/w) and ART/Stevia-G (1:10 w/w), respectively. The slight decrease in the solubility of ART/Stevia-G (1:10 w/w) at the end of the experiment compared with the initial 15 min might have been due to precipitation or re-crystallization of ART upon attainment of supersaturation.

The poor solubility of untreated ART is mainly owing to its stable and crystalline nature with a large crystal size as reported by Chan et al. (1997). According to them, ART exists in orthorhombic and triclinic forms, the former being more stable and less soluble than the latter. The formulation of solid dispersions of ART/Hsp-G and ART/Stevia-G afforded amorphous samples with rapid dissolution property which augmented the supersaturation of ART in the dissolution media. Binding energy between ART molecules become weaker upon conversion to the amorphous state, thereby necessitating no additional energy to break down the molecular structure during dissolution. Moreover, the particles size of drug loaded samples was reduced significantly, which can enlarge the contact area between the drug and the dissolution medium, as illustrated by the Noyes-Whitney equation (Noyes and Whitney, 1897).

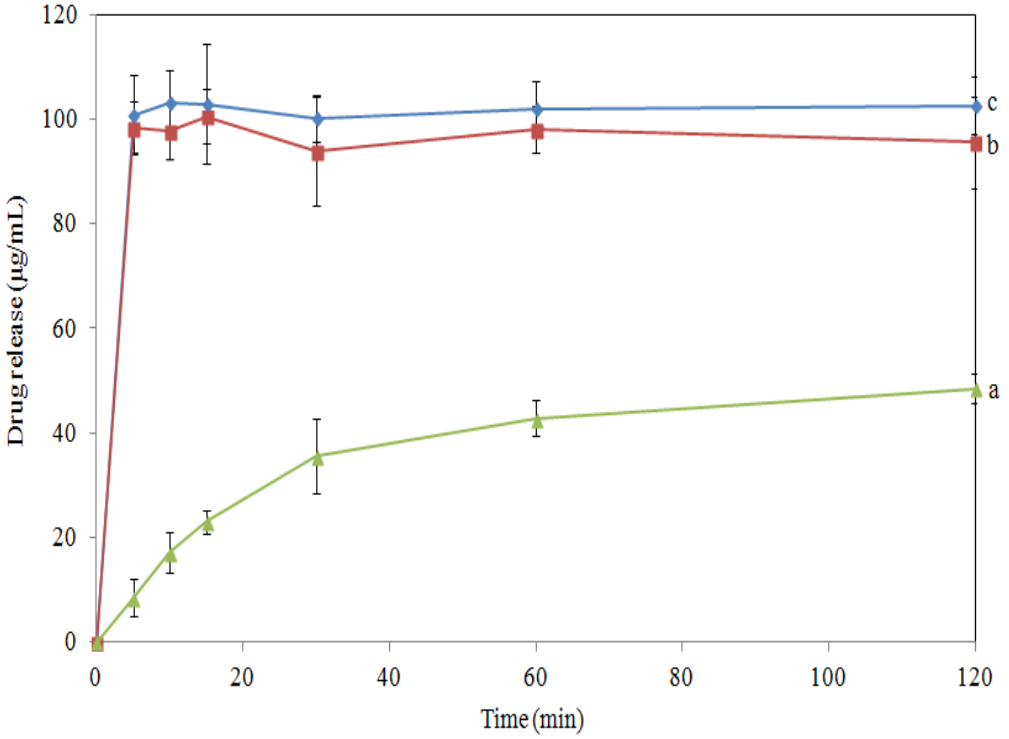

Figure 6.8 Supersaturation of (A) 200 mg of ART in solid dispersion of (a) untreated ART, (b) ART/Stevia-G (1:10 w/w) and (c) ART/Hsp-G (1:10 w/w). *n*=3, $p < 0.05$ versus free ART.

6.7 Chemical Stability Evaluation

The chemical stability of ART/Hsp-G (1:10 w/w) and ART/Stevia-G (1:10 w/w) samples was investigated for 6-months at 5 different storage conditions: desiccators (25 °C/18% RH), Activ-vial (25 °C/0% RH), open pan (25 °C/75% RH), Activ-vial (40 °C/0% RH) and open pan (40 °C/75% RH). Samples kept at higher temperatures including Activ-vial (40 °C/0% RH) and open pan (40 °C/75% RH) agglomerated to form hard lumps within two to three-weeks of storage as presented in Figure 6.9. High storage temperatures, moisture content and the presence of amorphous ART might induce the agglomeration and hardening of the food additive samples. Almost the same results were observed for ART/AC solid dispersions (agglomeration and

formation of sticky samples) after 3-months of storage under stressed conditions (Section 4.7). In contrast, previously, Tozuka et al. (2010) have conducted a similar type study on the physical stability of naringenin/Hsp-G (1:10 w/w) by storing the samples at 60 ºC for 3-months in a closed container; the samples showed a good physical stability throughout the storage.

The results of the chemical stability of the samples as a function of storage time at the remaining three conditions are presented in Table 6.2. Both the ART/Hsp-G (1:10 w/w) and ART/Stevia-G (1:10 w/w) exhibited excellent chemical stability with more than 95.8% of ART preserved for 6-months, at the end of which approximately 97.4–99.5% of ART could be preserved for ART/Hsp-G (1:10 w/w) and 95.8–99.8% for ART/Stevia-G (1:10 w/w). No appreciable changes in drug content were observed form 3-months to 6-months of storage under these three storage conditions. It was found that moderate conditions are suitable for the food additives to preserve the chemical stability of ART. Besides that, the good chemical stability of treated ART in open pan (25 ºC/75% RH) might also be attributed to the re-crystallization of ART as demonstrated by Figure 6.11.

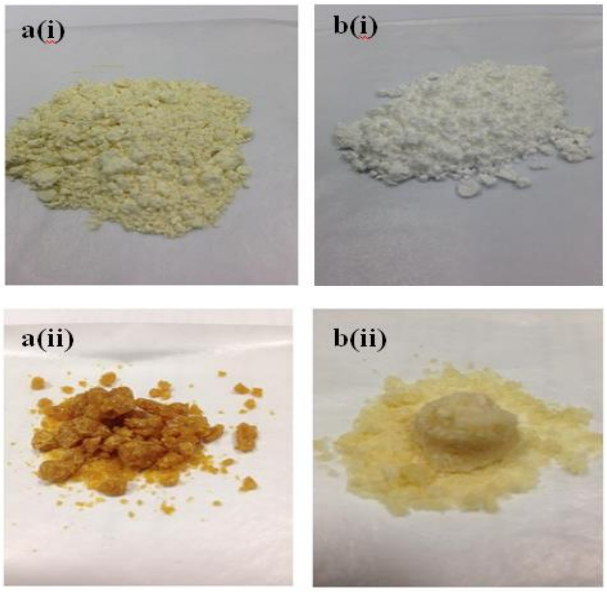

Figure 6.9 Physical appearances of (a) ART/Hsp-G (1:10 w/w) and (b) ART/Stevia-G (1:10 w/w) samples: (i) freshly co-spray dried and (ii) after 3-weeks of storage in open pan at 40 °C/75% RH.

Table 6.2 Percentage of ART remaining in solid dispersions without degradation after storage under 3 different storage conditions for 6-months.

Sample	Storage conditions	% of ART remain	
		3-month	6-month
ART/Hsp-G (1:10 w/w)	Desiccators (25 °C/18% RH)	99.5 ± 0.3	98.1 ± 0.5
	Activ-vial (25 °C/0% RH)	99.3 ± 1.0	97.4 ± 0.6
	Open pan (25 °C/75% RH)	98.0 ± 0.9	98.4 ± 1.0
ART/Stevia-G (1:10 w/w)	Desiccators (25 °C/18% RH)	99.1 ± 0.8	97.8 ± 0.9
	Activ-vial (25 °C/0% RH)	99.8 ± 0.7	95.8 ± 2.4
	Open pan (25 °C/75% RH)	97.6 ± 0.8	98.4 ± 0.5

Data represent mean ± S.D., *n*=3

6.8 Physical Stability Evaluation and Drug Release after Storage

Based on Figure 6.10 and Figure 6.11, all the co-spray dried samples show halo patterns throughout the storage periods, with the exception of the samples stored in the open pan at 25 °C/75% RH, for which a PXRD peak corresponding to crystalline ART was observed after 6-months (Figure 6.11). The reappearance of micron size ART crystals can be observed through SEM images as depicted in Figure 6.12 (yellow arrows). For the as prepared fresh samples, the halo patterns of ART/Hsp-G (1:10 w/w) and ART/Stevia-G (1:10 w/w) indicate the presence of amorphous ART incorporated within Hsp-G and Stevia-G. Molecular-level mixing and hydrophobic-hydrophilic interactions between ART and food additives in co-spray dried samples could inhibit the re-crystallization of ART by restricting the mobility of the encapsulated drug molecules. However, the samples stored in the open pans at 25 °C/75% RH were unstable and started to re-crystallize in 6-months duration. The re-crystallization of ART can be interpreted as a consequences of the plasticizing of food additives under a humid condition (75% RH), which allow elevated mobility of the amorphous ART molecules to trigger the onset of drug nucleation and to induce crystallization, as suggested by Zhang et al. (2014). Therefore, dry and low-temperature conditions would be recommended for solid dispersions formulated with transglycosylated food additives.

Nevertheless, all the samples stored under moderate conditions still showed almost the same and rapid dissolution profile as freshly spray dried

samples (Figure 6.13). This is due to the long term physicochemical stability of the samples at moderate conditions. More than 87–100% ($p < 0.05$) of ART could be released to the dissolution medium. Similar results were observed for the samples kept at 25 °C/75% RH, even though partially formulated ART was re-crystallized (Figure 6.12). The unchanged dissolution properties of the samples might have been due to several factors: (1) the percentage of crystalline ART formed is still very low (as represented by the intensity of the PXRD peaks) and the rest of the samples are in amorphous form; (2) the particles size of the re-crystallized ART is still in the range of 10 μm (similar size as spray dried ART); and (3) the presence of extremely water-soluble sugar additive molecules surrounding the crystalline ART.

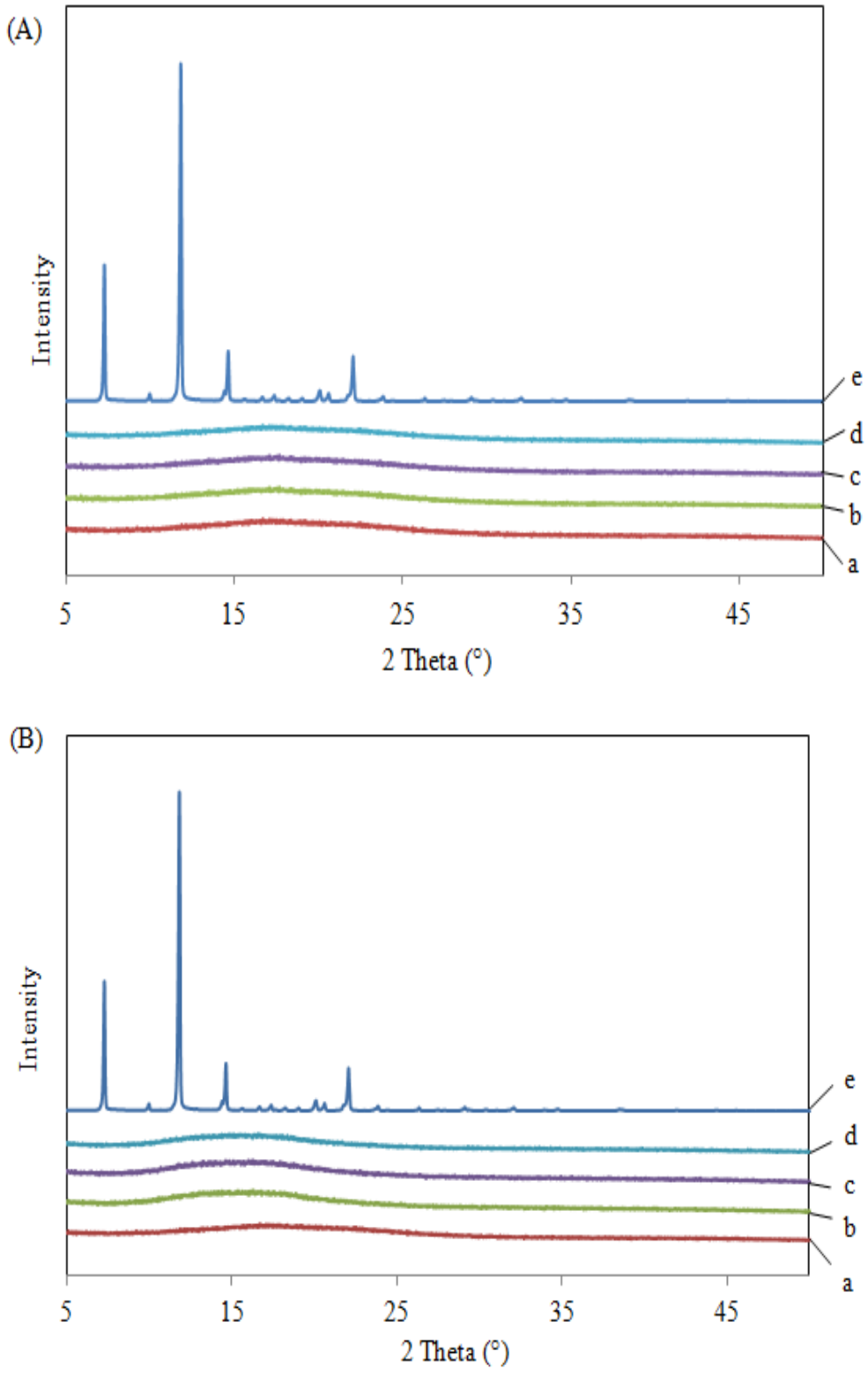

Figure 6.10 PXRD patterns of (A) ART/Hsp-G (1:10 w/w) and (B) ART/Stevia-G (1:10 w/w) after storage for 3-months: (a) fresh , (b) desiccators (25 °C/18% RH), (c) Activ-vial (25 °C/0% RH) (d) Activ-vial (25 °C/75% RH) and (e) untreated ART crystals.

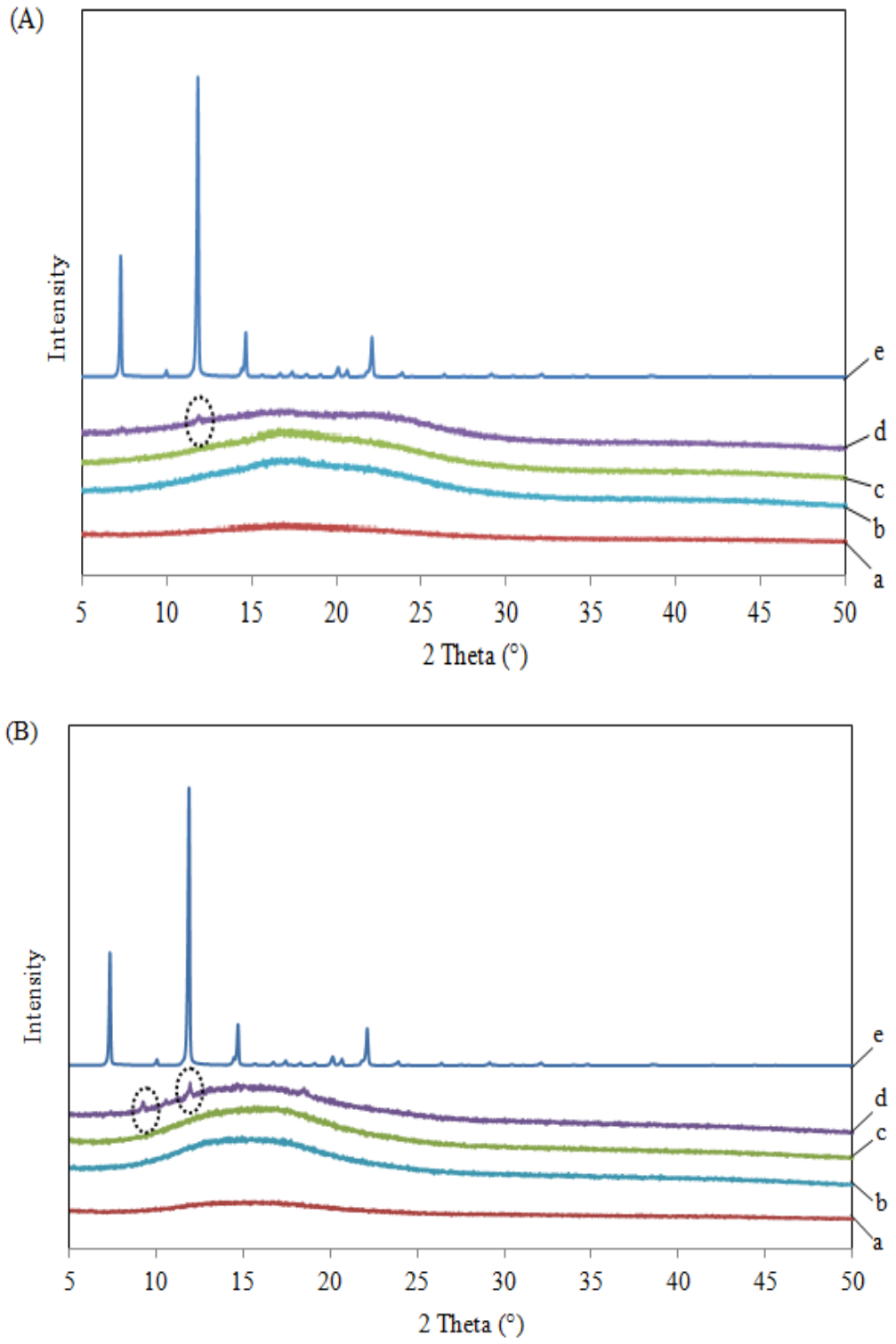

Figure 6.11 PXRD patterns of (A) ART/Hsp-G (1:10 w/w) and (B) ART/Stevia-G (1:10 w/w) after storage for 6-months: (a) fresh, (b) desiccators (25 °C/18% RH), (c) Activ-vial (25 °C/0% RH), (d) open pan (25 °C/75% RH) and (e) untreated ART crystals.

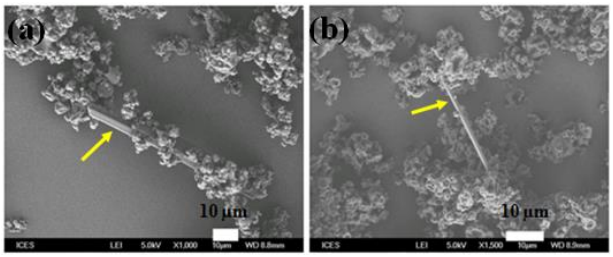

Figure 6.12 SEM images of (a) ART/Hsp-G (1:10 w/w) and (b) ART/Stevia-G (1:10 w/w) after 6-months of storage in open pan (25 °C/75% RH).

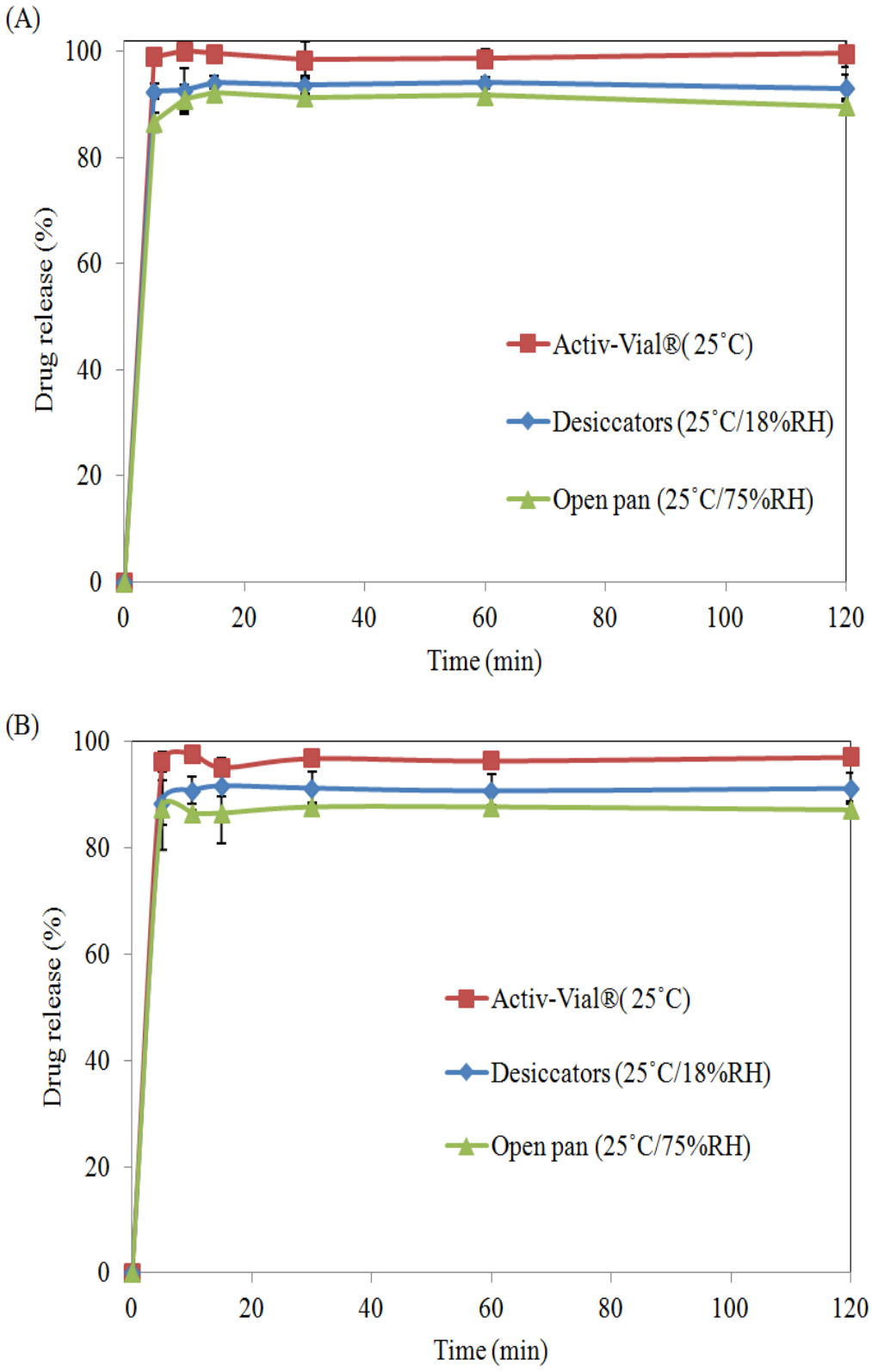

Figure 6.13 Dissolution profiles of ART from co-spray dried (A) ART/Hsp-G (1:10 w/w) and (B) ART/Stevia-G (1:10 w/w) after 6-months of storage. *n*=3, $p < 0.05$ versus free ART.

6.9 Conclusion

The formulation of solid dispersions of ART with transglycosylated food additives, α-glucosyl hesperidin (Hsp-G) and α-glucosyl stevioside (Stevia-G), via co-spray drying offers several advantages and disadvantages as compared with SBA-15 (Chapter 5). Similar to SBA-15, amorphization of ART could be accomplished with Hsp-G and Stevia-G by encapsulating the drug in micro-particles, though the loading capacity of the food additives (9.1 wt%) is inferior to that of SBA-15 (50 wt%). Both the Hsp-G and Stevia-G show a superior dissolution rate as a burst release of 100% of drug was achieved within 5 min, with the supersaturation enhanced by 2-fold. With regard to storage, dry conditions with a low temperature are suitable for solid dispersions of ART and food additives considering that elevated temperatures will cause drastic changes in the physical appearance of the samples and elevated relative humidity will induce re-crystallization.

Chapter 7 Formulation of Amorphous form of Combination of ART and MFQ using SBA-15

ACTs are recommended worldwide to combat malaria and have a high potential to reduce drug resistance. However, few studies have been reported regarding the solubility and bioavailability enhancement of antimalarial drugs in combination therapies. In this study, the solubility of two poorly water-soluble antimalarial drugs used in ACTs, ART and MFQ, was enhanced by encapsulating them in SBA-15 via co-spray drying. SBA-15, which showed a superior performance as compared with activated carbon and functionalized food additives, was chosen as the drug carrier for ACT formulation. Comparison between all the results obtained for all the carriers from previous chapters are summarized in Table 7.1. The storage conditions for stability study were based on the parameters that provide excellent storage stability to ART/SBA-15 and MFQ/SBA-15 solid dispersions.

Table 7.1 Comparison of the results obtained from Chapters 4, 5 and 6

Biopharmaceutical properties	ART	ART/AC (1:1 w/w)	ART/SBA-15 (1:1 w/w)	ART/Hsp-G & (1:10 w/w) ART/Stevia-G (1:10 w/w)
Physical state	C	A	A	A
Drug Loading (wt%)	−	50%	50%	9.1%
Dissolution (after 30 min)	23.1%	61.7%	76.6%	100%
Supersaturation (μg/mL)	48	90	103	96
Physical stability	−	−	✓	✓
Chemical stability	✓	✖	✓	✓

C: crystalline
A: amorphous

7.1 Structural Characterization and Degree of Drug Loading

The corresponding adsorption-desorption isotherms and pore size distributions of SBA-15 are respectively shown in Figure 7.1

Figure 7.1 and 7.2 whereas structural information about SBA-15 measured by the N_2 adsorption is summarized in Table 7.2. Mesoporous silica with extraordinary features such as large specific surface area, pore volume and wide pore size distributions are able to bond and store both the drug molecules with more than 47.9 wt% of drug loading (16.5 wt% of ART and 31.4 wt% of MFQ) (Table 7.3). There were two observations after drug loading: sharp decreases in the BET surface area and total pore volume, which implies the incorporation of ART and MFQ into the pores of the carrier due to capillary forces; and the narrowing of the hysteresis loop, which suggests limited

number of pores and pore size. Despite the reduction in the amount of adsorbed nitrogen, the shape of the hysteresis loop remained unchanged, indicating the unchanged pore channels of SBA-15 after the co-spray drying, a fact that is in agreement with the TEM analysis (Section 7.4). The tail in the pore size distribution of SBA-15 at small pore diameters corresponds to traces of 12% of micropores, which vanished upon loading due to either filling or obstruction by the presence of drug particles. A significant reduction in nitrogen adsorption, surface area and pore volume were also observed for the physical mixtures due to the presence of non-porous APIs in the mixtures [Figure 7.1 (B) and Figure 7.2 (B)]. In order to maximize the drug release, the APIs loaded onto the mesoporous carrier need to be in an amorphous state. Therefore, the physical state of ART and MFQ formulated with SBA-15 was assessed using PXRD in the next section.

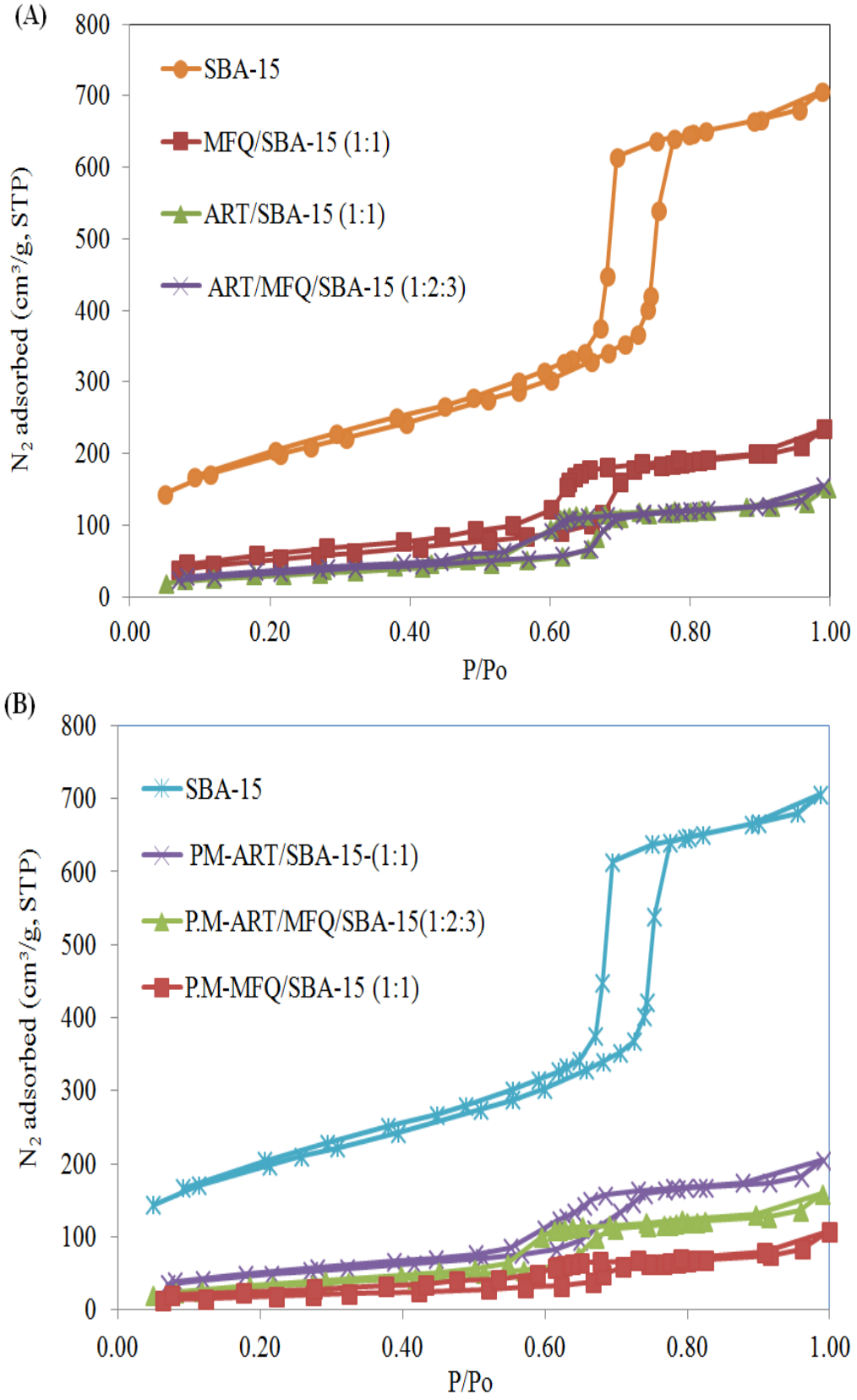

Figure 7.1 N_2 adsorption-desorption isotherms of SBA-15 before and after (A) co-spray drying and (B) physical mixing with ART and MFQ.

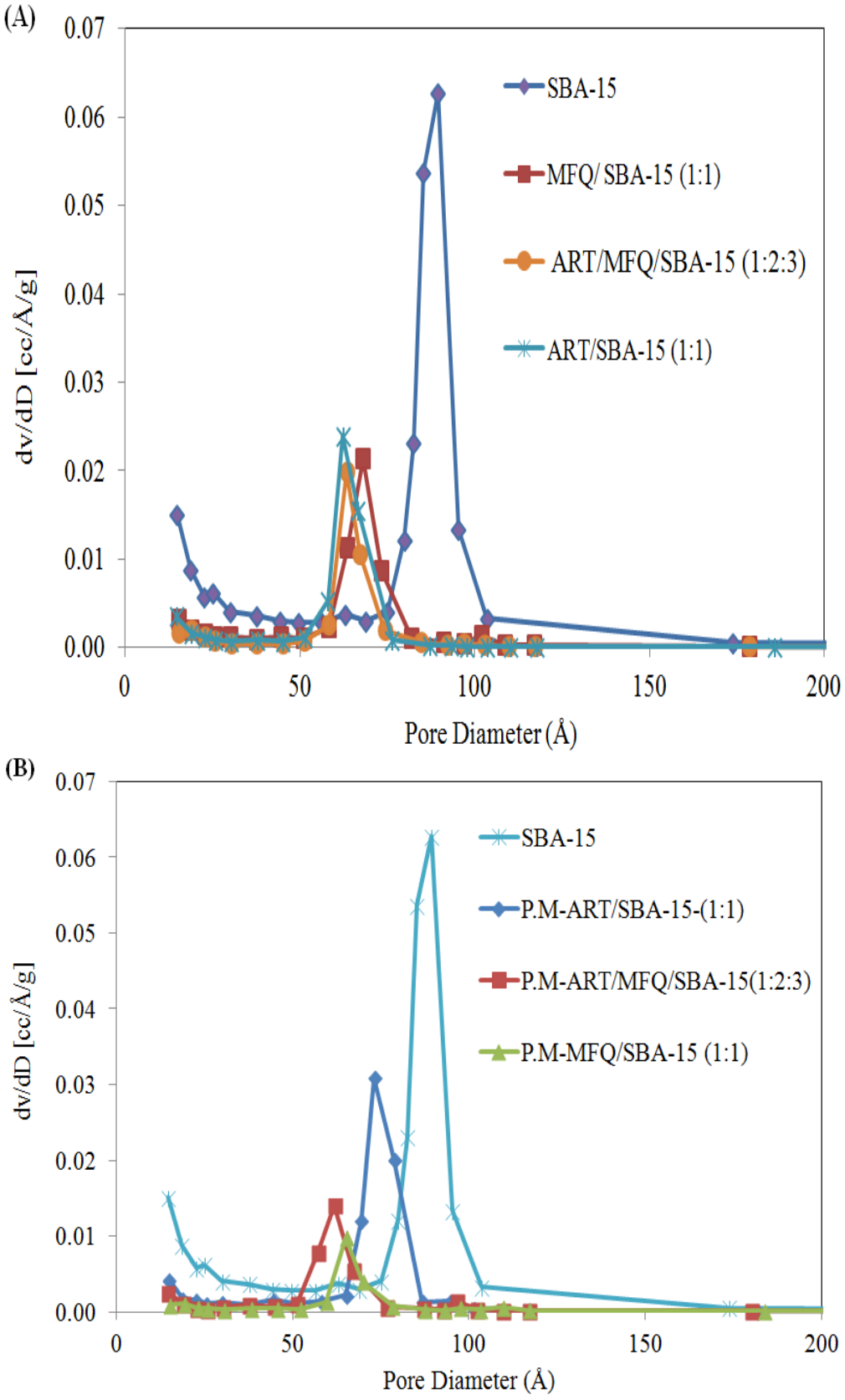

Figure 7.2 Pore size distributions of SBA-15 before and after (A) co-spray drying and (B) physical mixing with ART and MFQ.

Table 7.2 Pore volume, surface area and average pore size of SBA-15 before and after co-spray dried with ART and MFQ

Sample	Surface area (S_{BET}) [m^2/g]	Total pore volume (V_{pore}) [cc/g]	Average pore diameter (d) [nm]
SBA-15	809.0 ± 26.3	1.16 ± 0.04	8.70 ± 0.32
ART/SBA-15 (1:1 w/w)	112.8 ± 24.5	0.20 ± 0.04	6.40 ± 0.32
MFQ/SBA-15 (1:1 w/w)	188.3 ± 34.9	0.33 ± 0.07	6.80 ± 0.19
ART/MFQ/SBA-15 (1:2:3 w/w/w)	123.6 ± 10.1	0.21 ± 0.10	6.34 ± 0.40
P.M.-ART/SBA-15 (1:1 w/w)	251.20 ± 75.5	0.35 ± 0.30	7.32 ± 0.32
P.M.-MFQ/SBA-15 (1:1 w/w)	297.4 ± 85.9	0.43 ± 0.32	6.51 ± 0.96
P.M.-ART/MFQ/SBA-15 (1:2:3 w/w/w)	255.6 ± 61.1	0.31 ± 0.38	6.19 ± 0.40

Data represent mean ± S.D., *n*=3

Table 7.3 Drug loading of ART and MFQ within mesoporous silica

Sample	Theoretical drug loading [wt%]	Drug Loading [wt%]	Drug Loading efficiency [%]
ART/SBA-15 (1:1 w/w)	50	48.8 ± 1.1	97.6 ± 2.2
MFQ/SBA-15 (1:1 w/w)	50	47.1 ± 2.4	94.2 ± 4.8
ART/MFQ/SBA-15 (1:2:3 w/w/w)	17 [a]	16.5 ± 0.9 [a]	99.0 ± 1.7 [a]
	33 [b]	31.4 ± 1.8 [b]	94.2 ± 1.8 [b]

[a] refers to ART, [b] refers to MFQ
Data represent mean ± S.D., *n*=3

7.2 Physical Characterization

The physical-state of untreated drugs and freshly spray dried and physically mixed samples were analyzed with PXRD and the results are shown in Figure 7.3 and 7.4. Untreated ART was crystalline in nature as indicated by the highly intense PXRD peaks mostly between 7.0° and 25.0°, as discussed in Sections 4.3 and 5.3. The untreated MFQ shows PXRD peaks with relatively reduced intensity as compared with ART. Characteristic peaks at diffraction angles (2θ) of 10.9°, 11.3°, 14.1°, 15.3°, 21.2°, 23.2°, 25.0°, 25.3° indicate the crystalline nature of MFQ, which is most similar to the form D polymorph of the drug (Kitamura et al., 1994).

It can be observed that MFQ alone could be transformed into amorphous form upon spray drying; however, this was not possible for ART even when different processing routes (including spray drying) were applied (Figure 7.4(f) and Figure 7.5). Neither appearance of new peaks nor disappearance of existing peaks was detected for the spray dried ART. The locations of all PXRD peaks are almost identical, whereas the relative intensity of the peaks varies as compared with raw ART, indicating the decrease in the crystallinity of the drug. However, co-spray drying of ART and MFQ was able to produce amorphous ART due to co-amorphization. Nevertheless, a weak peak at 10.6° could be detected after one-week storage in desiccators at 25 °C/18% RH, suggesting the re-appearance of traces of crystalline drugs [Figure 7.6(a)]. This indicates that the amorphous ART/MFQ is physically unstable and has the propensity re-crystallize upon one-week of

storage. The re-crystallization of the sample is mainly attributed to the re-crystallization of ART since the PXRD peak corresponds to the characteristic peak of ART. Conversely, amorphous MFQ remains physically unchanged during the same storage period [Figure 7.6(a)].

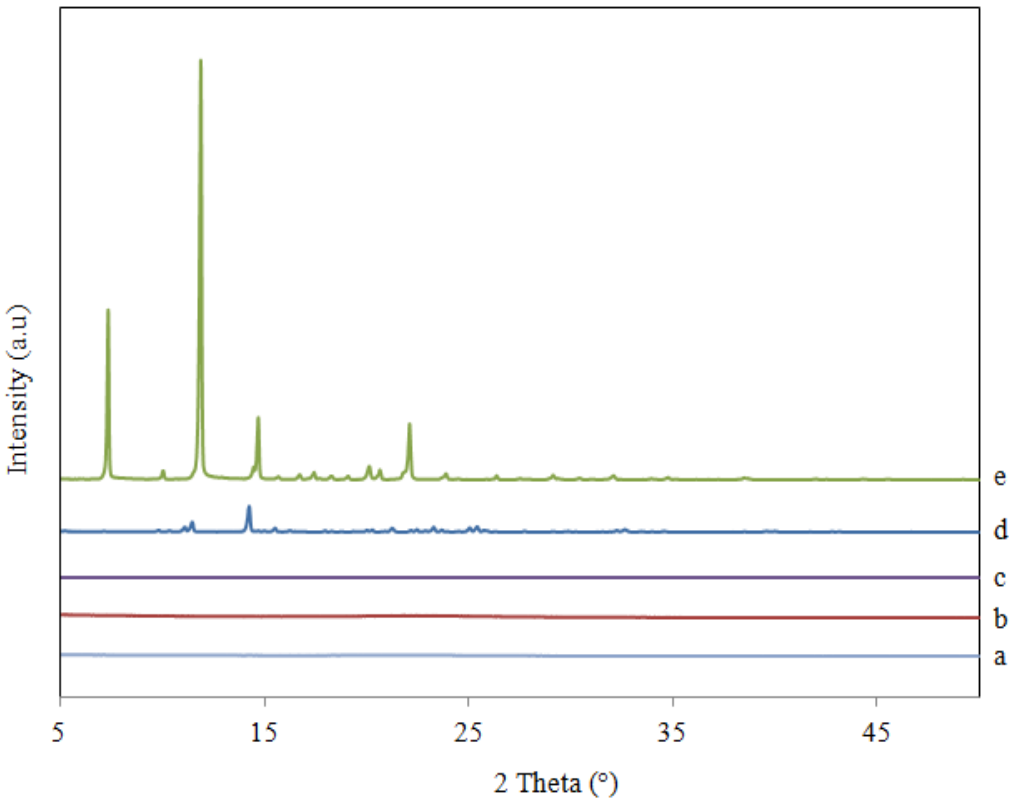

Figure 7.3 PXRD patterns of (a) ART/MFQ/SBA-15 (1:2:3 w/w/w), (b) MFQ/SBA-15 (1:1 w/w), (c) ART/SBA-15 (1:1 w/w), (d) MFQ and (e) ART.

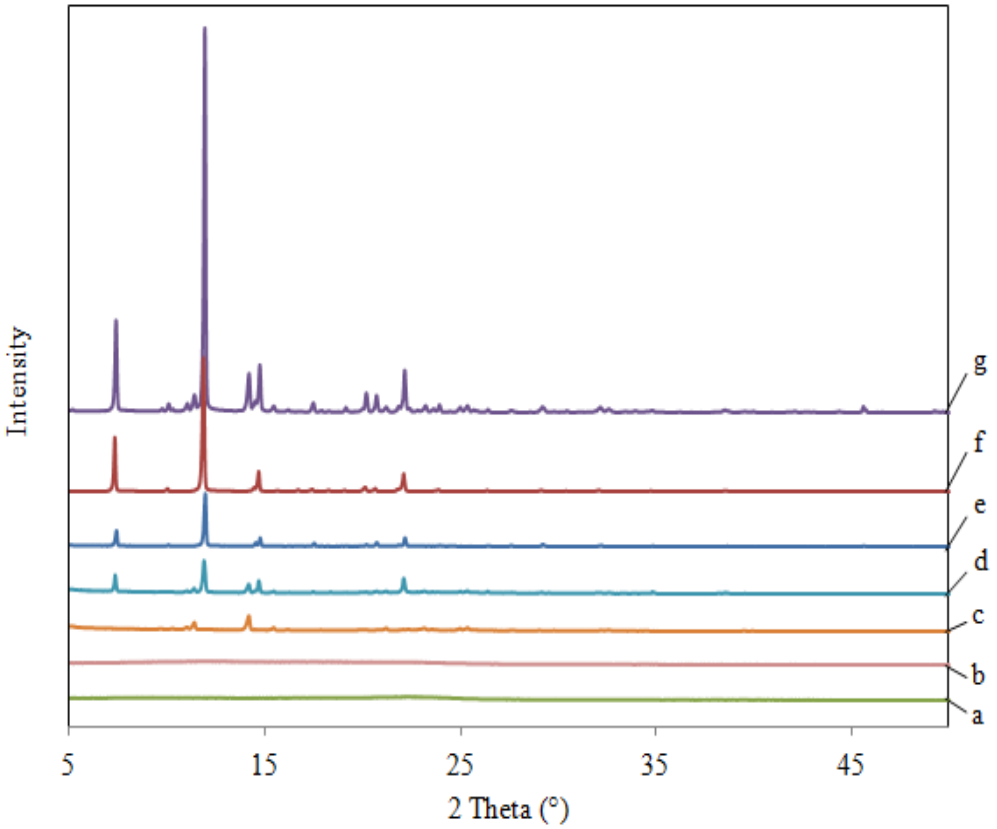

Figure 7.4 PXRD patterns of (a) spray dried MFQ, (b) co-spray dried ART/MFQ (1:2 w/w), (c) P.M.-MFQ/SBA-15 (1:1 w/w), (d) P.M.-ART/MFQ/SBA-15 (1:2:3 w/w/w), (e) P.M.-ART/SBA-15 (1:1 w/w), (f) spray dried ART and (g) P.M.-ART/MFQ (1:2 w/w).

For the P.M.-ART/MFQ (1:2 w/w), the diffraction pattern showed sharp and specific peaks from the original crystalline forms (Figure 7.4), with the main diffraction angles (2θ) at 10.9°, 11.3°, 14.1° and 15.3° attributed to the crystalline MFQ and those at 7.4°, 10.0°, 11.9°, 14.7°, 20.1°, 20.7° and 22.1° to the crystalline ART. The presence of both the characteristic peaks of MFQ and ART with unchanged peak intensity reflects the unchanged crystallinity with no strong interactions between the drugs in the physical mixtures. Conversely, for the physical mixtures of drug/SBA-15, the PXRD pattern exhibited the reflections relative to crystalline drugs with reduced intensity compared with untreated drugs and with P.M.-ART/MFQ (1:2 w/w).

On the other hand, all the spray dried solid dispersions of ART, MFQ and ART/MFQ with SBA-15 exhibit flat PXRD patterns. The characteristic peaks of ART and MFQ disappeared completely after incorporation into mesoporous silica, implying a non-crystalline or amorphous state of the confined drugs. Pore size of carriers (Zhao et al., 2012b), drug-carrier interactions (Takeuchi et al., 1987) and rapid evaporation of the solvent (Planinšek et al., 2011) during formulation appear to be responsible for the formation of amorphous particles. Sufficient space is required for the drug molecules to arrange themselves into an ordered structure and exist in the crystalline state. However, mesoporous silica with a narrow pore size distribution in the range of a few nanometers is effective in preventing the formation of crystals due to space confinement. Additionally, the drug molecules have less time to arrange into a crystal lattice due to the rapid evaporation of ethanol during spray drying, thereby predisposing the molecules into forming a disordered structure instead of an ordered one. Also, the tendency is high for the hydroxyl groups of drug molecules to form hydrogen bonds with the silanol groups of SBA-15. This enables thorough dispersion of drug molecules in the pore channels. Similarly, various studies such as those by Takeuchi et al. (2004, 1987) and Watanabe et al. (2001, 2002, 2003) have elucidated the interactions between drug molecules and silanol groups of silica.

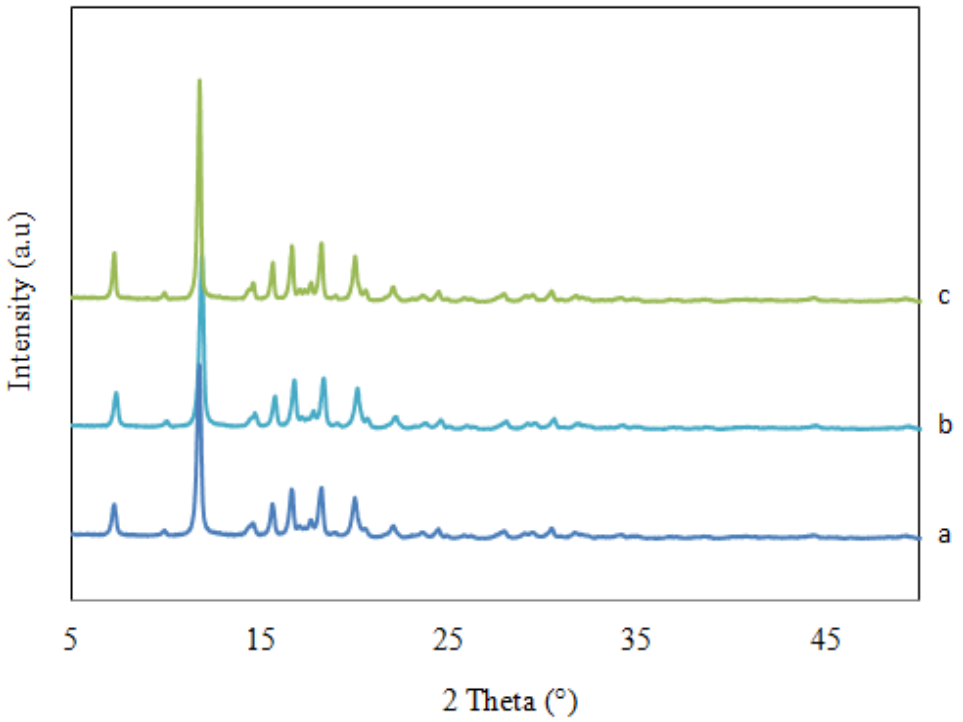

Figure 7.5 PXRD patterns of (a) melt quenched ART, (b) cryo milled ART and (c) ball milled ART.

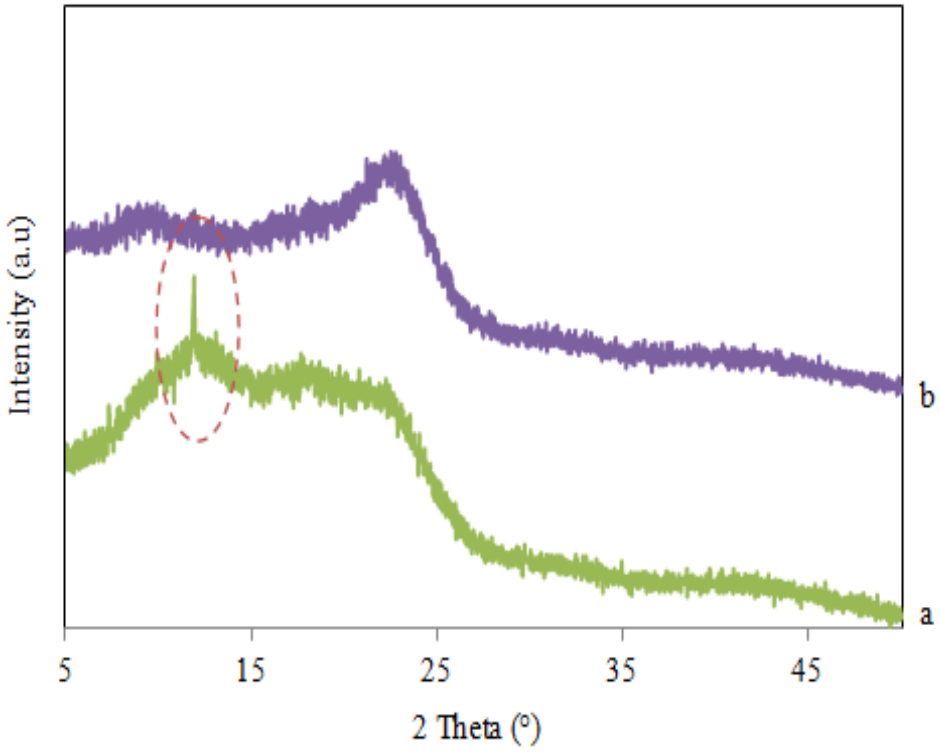

Figure 7.6 PXRD patterns of (a) co-spray dried ART/MFQ (1:2 w/w) and (b) spray dried MFQ after 1-week storage inside desiccators (25 °C/18% RH).

7.3 Morphology

SEM was employed to characterize the morphology of unprocessed and processed ART and MFQ as shown in Figure 7.7. The morphologies of untreated ART, spray dried ART and SBA-15 [Figure 7.7(b), (e) and (j)] have been discussed in Section 5.5. Figure 7.7(a) depicts the typical crystal habits of MFQ, which appears as a needle-shaped structure resembling the morphology of the polymorph form D. The form D is thermodynamically more stable than others at 37°C (Kitamura et al., 1994). The length of the MFQ crystals is in the range of 10–250 μm and the crystals are much smaller and thinner compared with untreated ART [Figure 7.7(b)]. The P.M.-ART/MFQ [Figure 7.7(c)] clearly illustrates the size difference of these two drugs. It can be observed that ART and MFQ exist as two separate particles in the physical mixture and only adhere to each other presumably due to the presence of weak forces such as electrostatic forces and van der Waals.

In contrast to the unchanged morphology of ART after spray drying [Figure 7.7(e)], the morphology of spray dried MFQ [Figure 7.7(d)] was completely changed to irregular and shrunken spherical particles, as attributed to the drug amorphization. The particles size was reduced to less than 5 μm, which was even smaller than the spray dried ART. The amorphization of MFQ was further supported by PXRD results (Figure 7.4). Importantly, the amorphization of MFQ could be achieved by spray drying without the presence of any carriers, which is difficult to achieve for ART. However, the co-amorphization of ART/MFQ was able to change the morphology of ART

together with MFQ without any trace of crystalline particles [Figure 7.7(f)]. The amorphous ART/MFQ particles are perfectly spherically-shaped with particle size less than 5 µm. The amorphization of ART might be accomplished due to the mixing at the molecular level and the presence of interactions, presumably hydrogen bonding between ART and MFQ.

The physical mixtures [Figure 7.7(g), (h) and (i)] showed a blend of drugs and SBA-15. The presence of both the carrier and the drugs can be seen since there are no significant changes to the crystalline morphology of the drugs. This also suggests that there is a lack of strong interactions between the drug and carrier particles in the physical mixtures. However, the SBA-15 particles adhered to the surface of ART and MFQ crystals may be due to electrostatic and van der Waals forces.

Meanwhile, the co-spray dried solid dispersions of drug/carriers are found to have conglomerated [Figure 7.7(k), (l) and (m)] and the morphology and the particles size of the samples are similar to SBA-15 particles [Figure 7.7(j)], which in the range of 0.5−1 µm. Moreover, the formulated solid dispersion particles are smaller and more homogeneous in size and morphology compared with the untreated drugs and the physical mixtures. Hardly any drug crystals were noticed on the surface of SBA-15 as most of the drug particles were dispersed and absorbed in the pore channels of SBA-15 in an amorphous form. The presence of SBA-15 micron particles during co-spray drying was able to inhibit the ART particle aggregation and crystal growth. On the other hand, the presence of extra particles on the surface of SBA-15

occurred by increasing the drug loading to 86 wt%. As illustrated in Figure 7.7(n), non-uniform particles can be observed on the surface of co-spray dried ART/MFQ/SBA-15 (2:4:1 w/w/w), due to the drug loading exceeding the capacity of the pore volume of SBA-15.

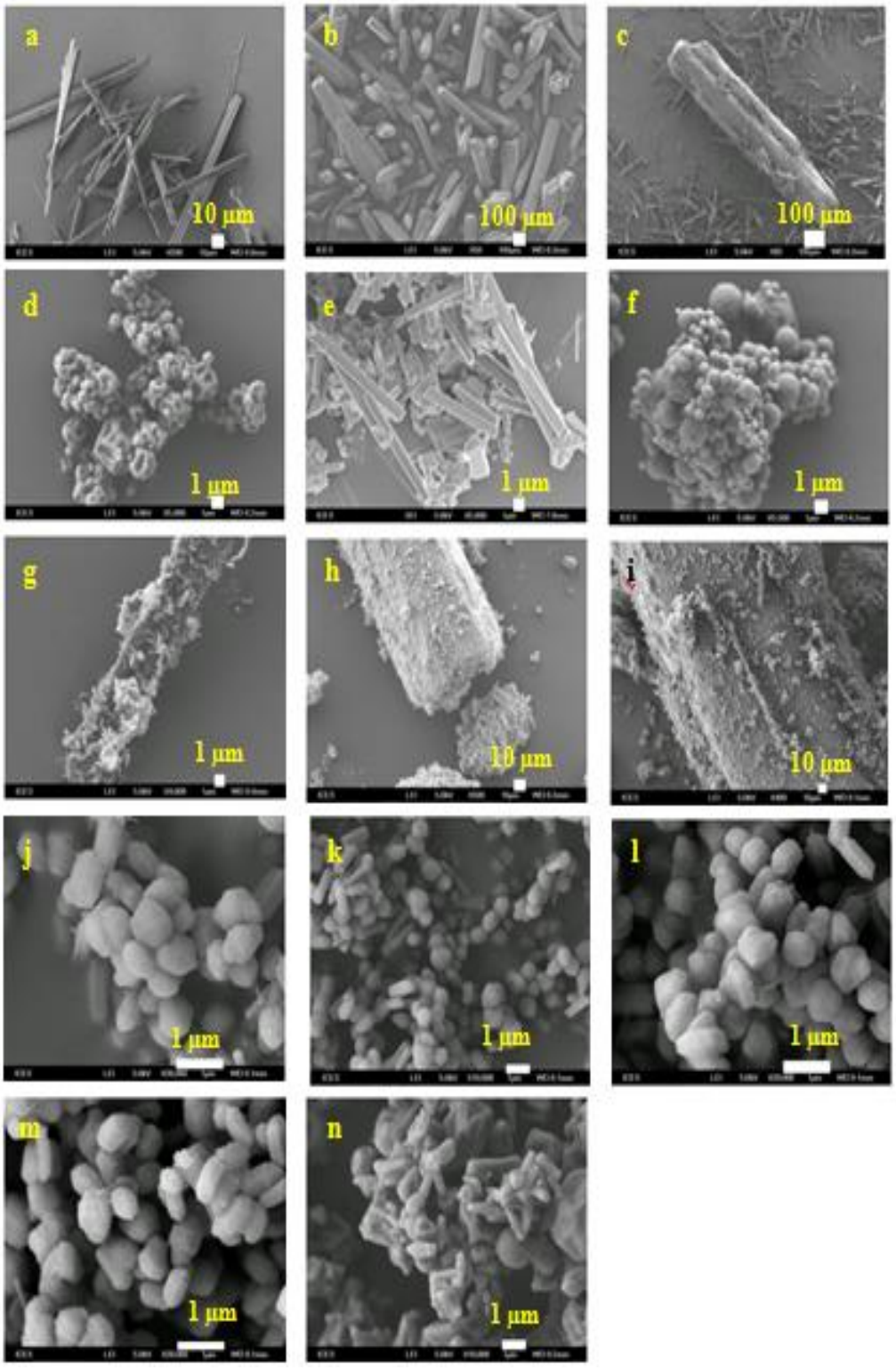

Figure 7.7 SEM images of (a) MFQ, (b) ART, (c) P.M.-ART/MFQ (1:2 w/w), (d) spray dried MFQ, (e) spray dried ART, (f) co-spray dried ART/MFQ (1:2 w/w), (g) P.M.-MFQ/SBA-15 (1:1 w/w), (h) P.M.-ART/SBA-15 (1:1 w/w), (i) P.M.-ART/MFQ/SBA-15 (1:2:3 w/w/w), (j) SBA-15, (k) MFQ/SBA-15 (1:1 w/w), (l) ART/SBA-15 (1:1 w/w), (m) ART/MFQ/SBA-15 (1:2:3 w/w/w) and (n) ART/MFQ/SBA-15 (2:4:1 w/w/w).

7.4 Transmission Electron Micrograph (TEM)

The structural features of the SBA-15 were examined by TEM and the results are presented in Figure 7.8. The TEM micrographs revealed the spherical and spheroid shape of SBA-15 micron-particles with a particle size of 0.5–1 μm [Figure 7.8(a)]; in agreement with the shape determined through SEM measurements [Figure 7.7(j)]. At higher magnifications, the ordered cylindrical pore channels of SBA-15 can be observed with an estimated uniform pore size in the range of 8–9 nm (in agreement with N_2 adsorption results) and thick pore walls. The thick pore walls and well-ordered pore channels are able to afford homogeneous drug distribution and restrict drug re-crystallization. In addition, the wider pore size and shorter pore channels are advantageous for the adsorption and desorption of drug molecules with minimum diffusion resistance, which is beneficial for dissolution and solubility enhancement (refer to Section 0). Please refer to Section 0 for more details about the internal pore structure of SBA-15. The unchanged pore channels and pore walls of SBA-15 after co-spray drying with ART and MFQ particles underscore the rigidity and unchanged internal pore structure of SBA-15 as reported previously.

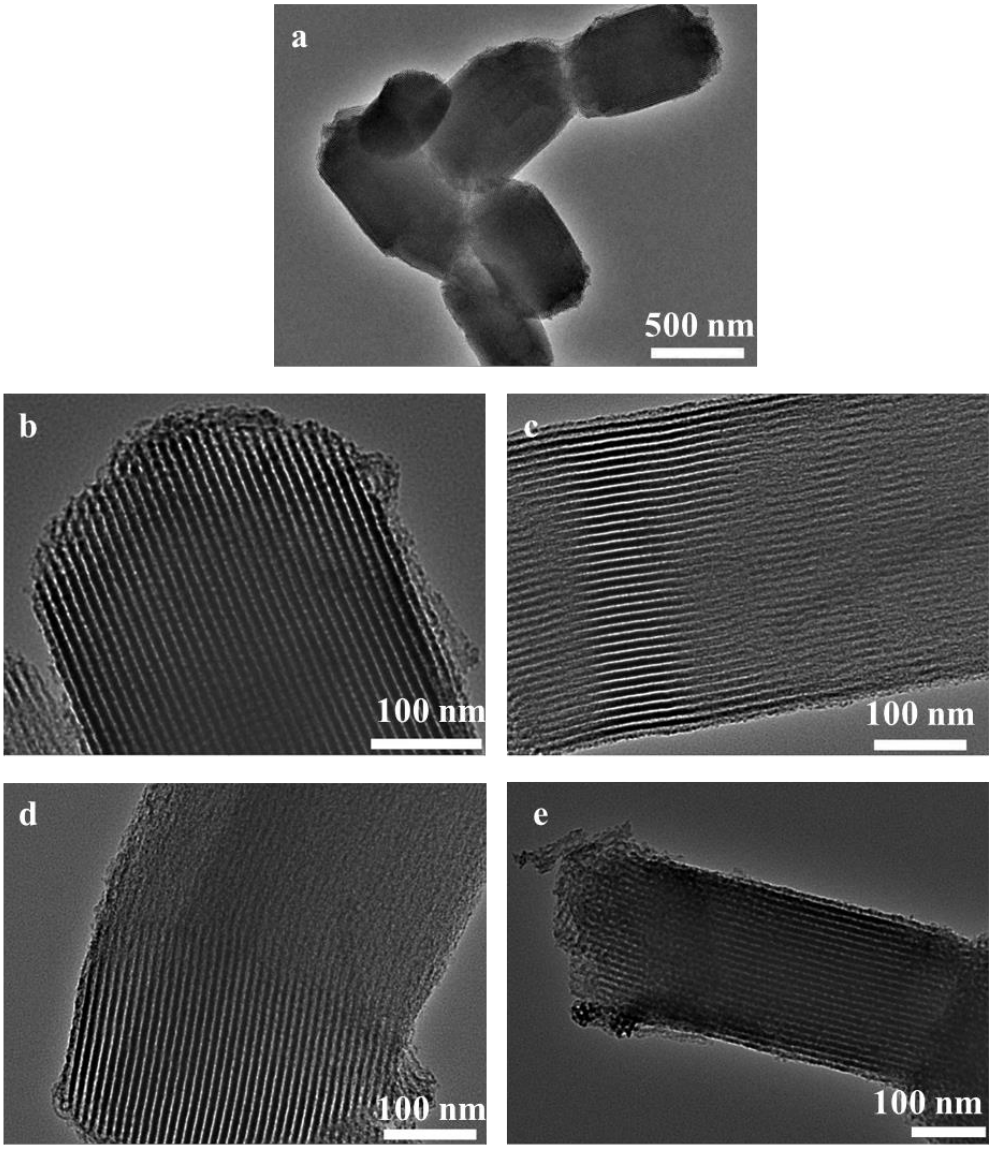

Figure 7.8 TEM images of SBA-15 at scale of (a) 500 nm and (b) 100 nm and (c) ART/SBA-15 (1:1 w/w), (d) MFQ/SBA-15 (1:1 w/w) and (d) ART/MFQ/SBA-15 (1:2:3 w/w/w).

7.5 Chemical and Physical Stability Evaluation

The physicochemical stability of ART/MFQ/SBA-15 (1:2:3 w/w/w) upon storage was investigated for 6-months in desiccators (25 °C/18% RH) and Activ-vial® (25 °C). These two conditions were chosen based on the previous screening studies on ART and MFQ. ART appears to be stable at low

humidity conditions despite the storage temperature as discussed in Section 5.9. Those storage conditions are desiccators (25 °C/18% RH), Activ-vial® (25 °C) and Activ-vial® (40 °C), which were used to investigate the chemical stability of MFQ/SBA-15 (1:1 w/w). The results are summarized in Table 7.4. The amorphous form of MFQ co-spray dried with SBA-15 exhibited good chemical stability against degradation in desiccators (25 °C/18% RH) and Activ-vial® (25 °C) with preservation of more than 98.0% of MFQ throughout the storage period. However, an obvious decrease was observed in the percentage of MFQ (86.4%) in Activ-vial® (40 °C), suggesting that high temperatures are not suitable for MFQ storage; hence, this particular condition was excluded for the ART/MFQ combination stability study. The results of physicochemical stability of ART/SBA-15 and MFQ/SBA-15 were summarized in Table 7.5.

The results of chemical stability of ART/MFQ/SBA-15 (1:2:3 w/w/w) solid dispersion are summarized in Table 7.6. The percentage of ART and MFQ in solid dispersions stored in desiccators (25 °C/18% RH) and Activ-vial® (25 °C) remains almost unchanged without degradation after 6-months. Approximately 97–98% of drugs in desiccators (25 °C/18% RH) and 99% in Activ-vial® (25 °C) were preserved, indicating that the process of spray drying and used storage conditions and storage periods did not affect the chemical stability of the drugs.

The solid dispersions also exhibited excellent physical stability as the samples retained their amorphous forms throughout the storage periods

without any traces of crystals. All the stored samples showed the halo PXRD pattern, as freshly co-spray dried samples, without the presence of PXRD peaks assigned to the crystalline ART or MFQ after 6-months (Figure 7.9). The ability of SBA-15 to inhibit re-crystallization through the size-constraint effect (Shen et al., 2011, Shen et al., 2010), thickness and rigidity of pore walls (Rengarajan et al., 2008) and interaction with silanol groups (Watanabe et al., 2001, Watanabe et al., 2002) not only play an important role in producing amorphous forms but also stabilizing the amorphous forms during long-term storage periods. Please refer to Section 5.10 for more details. In addition, the hydrothermal stability of SBA-15 also contributes to the maintenance of the dispersed state of amorphous drug molecules, since the stability of solid dispersions is also expected to be a function of the stability of the carrier (Mellaerts et al., 2010, Cassiers et al., 2002).

Table 7.4 Amounts of MFQ remaining within MFQ/SBA-15 (1:1 w/w) samples after storage under 3 different storage conditions for 3 and 6-months.

Storage conditions	Percentage of remaining MFQ	
	3-months	6-months
Desiccators (25 °C/18% RH)	100.0 ± 0.3	99.2 ± 1.0
Activ-vial® (25 °C)	98.8 ± 1.1	98.0 ± 1.7
Activ-vial® (40 °C)	94.5 ± 3.5	86.4 ± 7.1

Data represent mean ± S.D., *n*=3

Table 7.5 Summary of the results of chemical stability of ART and MFQ

Condition	Samples	
	ART/SBA-15 (1:1 w/w)	MFQ/SBA-15 (1:1 w/w)
Desiccators (25 °C/18% RH)	✓	✓
Activ-vial® (25 °C)	✓	✓
Open pan (25 °C/75% RH)	×	-
Activ-vial® (40 °C)	✓	×
Open pan (40 °C/75% RH)	×	–

Table 7.6 Amounts of ART and MFQ remaining in ART/MFQ/SBA-15 (1:2:3 w/w/w) samples after storage at 2 different storage conditions for 3 and 6-months.

Storage conditions	Percentage of drug	
	3-month	6-month
Desiccators (25 °C/18% RH)	97.7 ± 2.1[a]	97.1 ± 2.7[a]
	97.7 ± 1.8[b]	98.2 ± 1.5[b]
Activ-vial® (25 °C)	99.8 ± 0.3[a]	99.5 ± 0.2[a]
	99.7 ± 0.8[b]	99.6 ± 0.6[b]

[a]ART, [b]MFQ
Data represent mean ± S.D., *n*=3

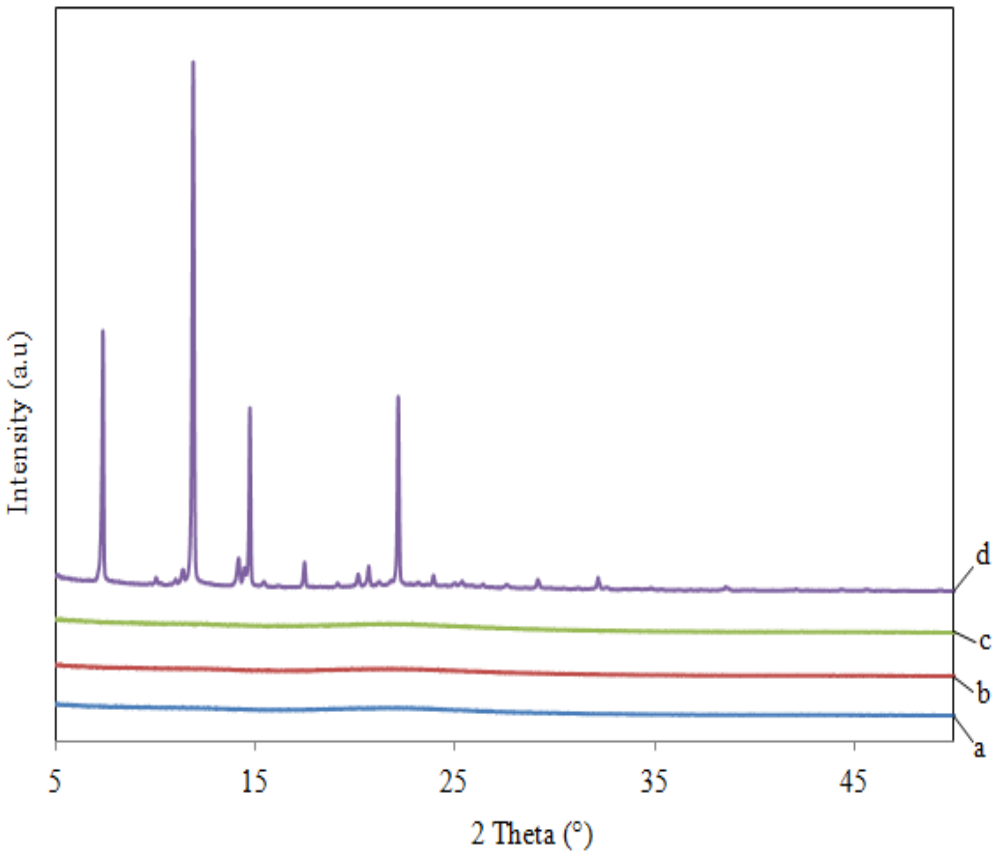

Figure 7.9 PXRD patterns of ART/MFQ/SBA-15 (1:2:3 w/w/w) after storage for 6-months: (a) fresh, (b) desiccators (25 °C/18% RH), (c) Activ-vial® (25 °C) and (d) P.M.-ART/MFQ (1:2 w/w).

7.6 *In vitro* Drug Release

Figure 7.10, 7.11 and 7.12 illustrate the *in vitro* drug release profiles of solid dispersions of ART and MFQ with SBA-15 at various conditions using 1× phosphate buffered saline (PBS) as a dissolution medium. Figure 7.10 and Figure 7.11 depict the drug release under sink condition using USP IV and non-sink condition using USP II, respectively, to study the dissolution rate and supersaturation of the drugs, respectively. Shown in Figure 7.12 is the effect of aging on the dissolution rate, as the drug release of the samples was analyzed after 6-months of storage using USP II. The drug release behaviors

of all the formulated samples were compared with that of the co-spray dried ART/MFQ (1:2 w/w) and P.M.-ART/MFQ (1:2 w/w).

As shown in Figure 7.10, the P.M.-ART/MFQ (1:2 w/w) achieved only marginal dissolution rates: the amount of drugs dissolved in the first 15 min were only 10.1% of ART and 21.1% of MFQ and in 2 h were only 26.8% of ART and 54.6% of MFQ. This finding indicates the poor dissolution of the untreated drugs due to their hydrophobic and crystalline nature. In contrast, the co-spray dried ART/MFQ (1:2 w/w) sample exhibited an improved dissolution rates compared with the untreated drugs: the amount of drugs dissolved in the first 15 min were 24.5% of ART and 37.7% of MFQ and in 2 h were 75.4% ($p < 0.05$) of ART and 89.6% ($p < 0.05$) of MFQ. A markedly superior drug release is observed for co-formulated ART/MFQ/SBA-15 (1:2:3 w/w/w) sample: by 15 min, initial burst release of 76.0% ($p < 0.05$) of ART and 87.3% ($p < 0.05$) of MFQ was observed; by 2 h, 100% ($p < 0.05$) of ART and MFQ had been released.

Figure 7.11 shows the supersaturation of untreated ART of 48.4 µg/mL, which is similar to the value reported by Ferreira et al. (2013). For crystalline MFQ, no equilibrium was observed within the 2 h dissolution period and the amount of MFQ dissolved after 2 h was 90.2 µg/mL. However, the apparent solubility of the drugs from mesoporous silica formulation was significantly higher than that of untreated drugs. Co-formulated ART achieved a supersaturation of 124.8 µg/mL ($p < 0.05$), which could be sustained for

120 min whereas the MFQ showed an apparent solubility of 282.1 µg/mL ($p < 0.05$) with no attainment of equilibrium after 2 h.

The enhanced dissolution rate and apparent solubility of ART and MFQ (both BCS class II drugs) by nano-confinement are expected to improve their absorption in the gastrointestinal tract and thereby improve their bioavailability. Several factors contribute to the dissolution and supersaturation enhancement: (1) a lack of crystallinity due to amorphization, (2) augmented surface area of the drug via particle size reduction, (3) host-guest interactions such as weak van der Waal forces and hydrogen bonds, (4) enhanced wettability caused by hydrophilic carrier and (5) pore architecture such as pore size and length of pore channels.

Two processes are involved in drug release from the pores of the carrier into the dissolution medium: first, penetration of water molecules to dissolve the entrapped drugs; and second, diffusion of the dissolved drugs through the pore channel into the dissolution medium. Factors such as the hydrophilicity of carriers and host-guest interactions facilitate the rapid penetration of dissolution medium influx through the pore channels to break the hydrogen bonds between drug molecules and silanol groups to displace them drug molecules. The rapid displacement of drug molecules by the dissolution medium attributes to the competitive interaction between water and ART because of the hydrophilicity of the silica pore walls (Ambrogi et al., 2013).

The dissolution and the apparent solubility are enhanced by their amorphous forms with reduced particles size. Drugs incorporated into the pores channels of SBA-15 within the nanometer range will be in the amorphous form (Figure 7.3) and the formation of the highly ordered crystalline forms may be restricted by the confined space of the nanopores. This culminates in a reduction in the lattice energy of the drug molecules compared with the crystalline forms, thereby dramatically increasing the apparent solubility and dissolution rate of the drugs. The effects of amorphization and particle size reduction on the drug release were further reflected by the dissolution enhancement of the co-spray dried ART/MFQ (1:2 w/w) sample.

Finally, the relatively wider pore size and shorter pore channels accelerate the diffusion of the dissolved drug by minimizing the diffusion distance and the pore restriction. The mean pore diameter of SBA-15 is in the range of 8–9 nm (Table 7.1) and the length of the pore channels is in the range of 0.5–1 μm (Figure 7.7 and Figure 7.8). The considerably wider pore opening and shorter pore channels of SBA-15 provide lesser steric hindrance to ART and MFQ molecules to diffuse out of the pore channels, thus resulting in a rapid desorption of a greater amount of drug molecules without any obstructions (Van Speybroeck et al., 2009).

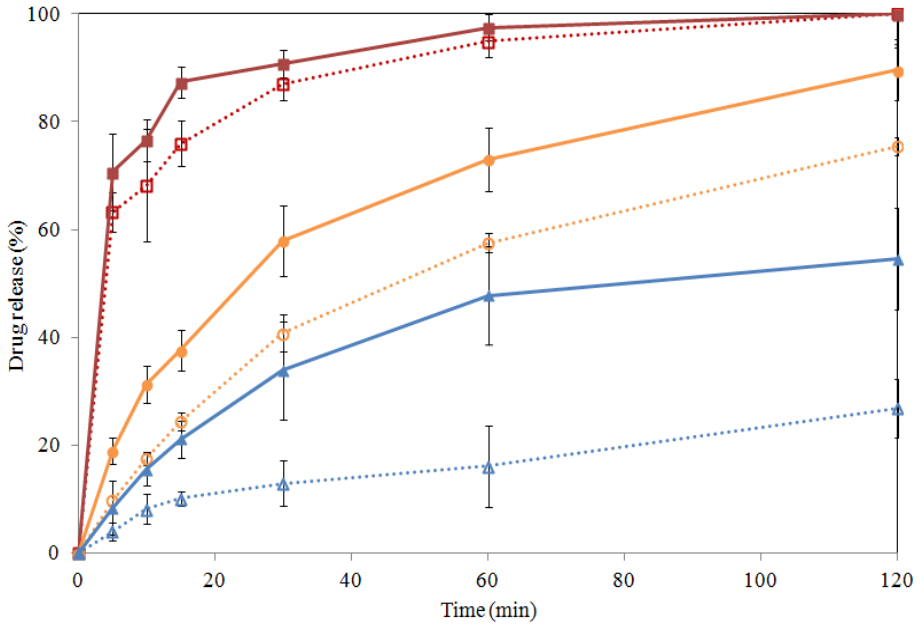

Figure 7.10 Dissolution profiles (under sink condition using USP IV) of (▲) P.M.-ART/MFQ (1:2 w/w), (●) co-spray dried ART/MFQ (1:2 w/w) and (■) ART/MFQ/SBA-15 (1:2:3 w/w/w). The dotted lines with hollow markers refer to ART and the solid lines with solid markers refer to MFQ. n=3, $p < 0.05$ versus free drugs.

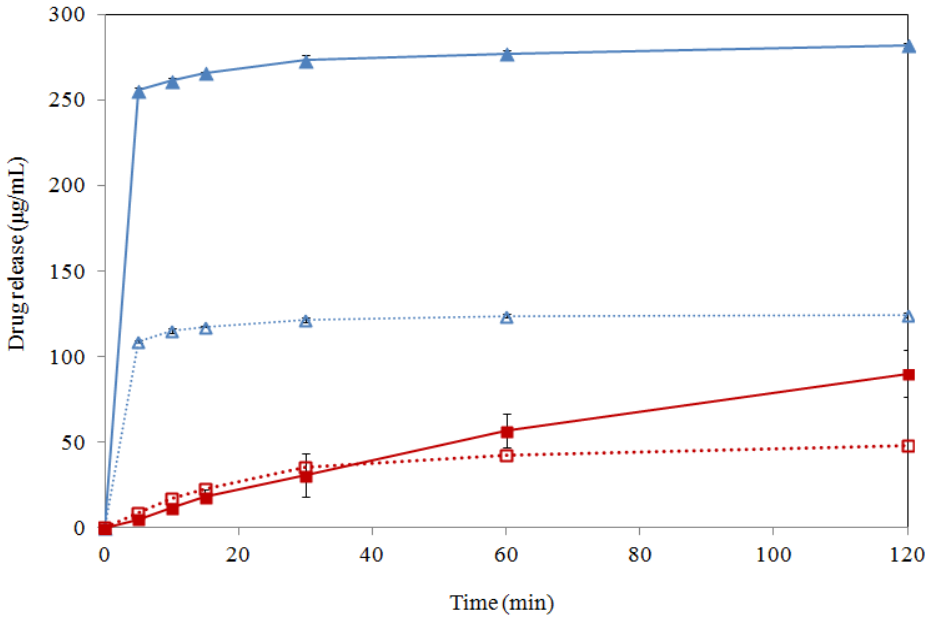

Figure 7.11 Supersaturation (under non-sink condition using USP II) of (■) P.M.-ART/MFQ (1:2 w/w) and (▲) ART/MFQ/SBA-15 (1:2:3 w/w/w). The dotted lines with hollow markers refer to ART and the solid lines with solid markers refer to MFQ. n=3, $p < 0.05$ versus free drugs.

Depicted in Figure 7.12 are the *in vitro* dissolution rate profiles of the ART/MFQ/SBA-15 (1:2:3 w/w/w) sample after 6-months of storage with fresh P.M.-ART/MFQ (1:2 w/w) sample as a control. An initial burst release of the drugs is observed for almost all the samples with approximately 91.1–97.6% ($p < 0.05$) of drugs released to the dissolution medium in 2 h upon dissolution. In addition, there are significant differences in the drug release profiles of the stored samples as compared with the untreated drugs because only 35.6% of ART and 59.7% of MFQ were dissolved at the end of the assay. The long-term stability of amorphous ART and MFQ in the solid dispersions and the hydrothermal stability of SBA-15 with unchanged pore structures contribute to an excellent shelf life with preserved dissolution behavior of dosage forms for 6-months.

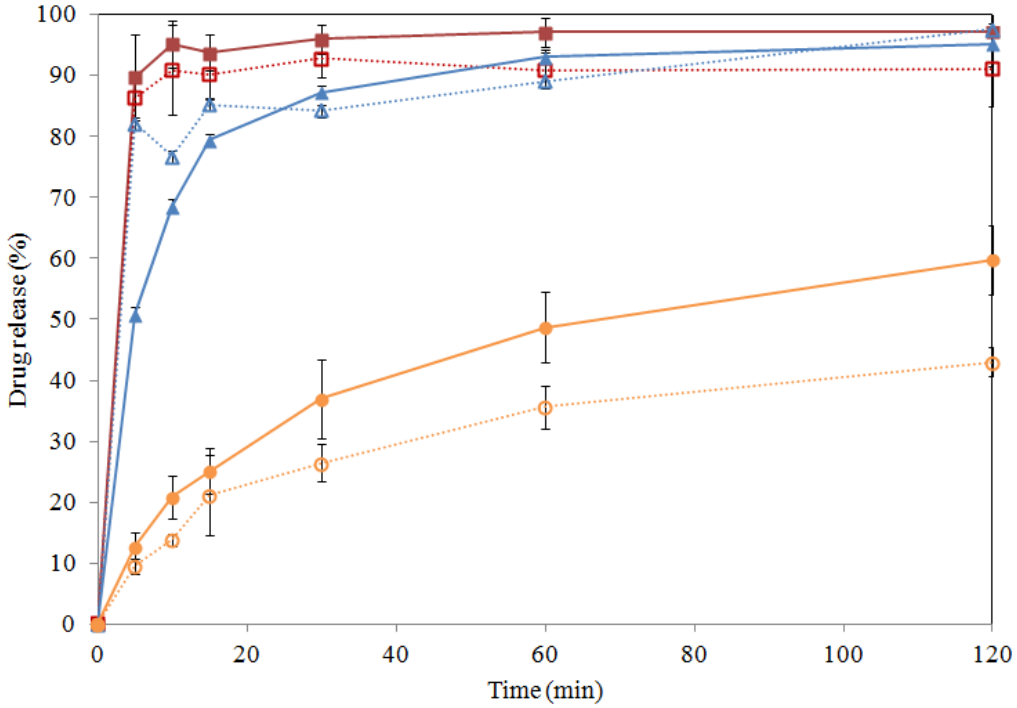

Figure 7.12 Dissolution profiles (under sink condition using USP II) of (—●—) fresh P.M.-ART/MFQ (1:2 w/w) and ART/MFQ/SBA-15 (1:2:3 w/w/w) stored in (—▲—) desiccators (25 °C/18% RH) and (—■—) Activ-vial® (25 °C) after storage for 6-months. The dotted lines with hollow markers refer to ART and the solid lines with solid markers refer to MFQ. n=3, $p < 0.05$ versus free drugs.

7.7 Conclusion

The results have revealed that it is technically feasible to generate X-ray amorphous ART and MFQ combinative solid dispersions using mesoporous carriers via co-spray drying. The significance of the mesoporous carriers is reflected by the fact that the amorphous ART could be stabilized by the presence of SBA-15. Although amorphous ART/MFQ could be achieved without any excipients, this amorphous form has been found to be physically unstable and would revert to the crystalline form within one week of storage in desiccators (Figure 7.6).

The remarkably enhanced dissolution kinetics of amorphous ART/SBA-15 and MFQ/SBA-15 compared with the crystalline counterpart and its physical mixtures are attributed to the advantageous structural properties and hydrophilicity of SBA-15. Moreover, the particle size reduction and amorphization of ART and MFQ due to spatial confinement in the pore structure of SBA-15 also contributed to the enhanced dissolution. The elucidation of the physicochemical stability of ART and MFQ is vital to prolonging the shelf life of the formulated amorphous antimalarial drugs with preserved drug release profile. Given the excellent chemical and physical stability of co-spray dried ART/MFQ/SBA-15 at moderate and dry storage conditions for 6-months, it is accordingly recommended that the solid dispersions of combination of these two drugs be stored at low humidity and temperature for maximal preservation of the physical and chemical forms of the APIs.

Chapter 8 Overall Conclusions

The aim of this research is to examine the feasibility of porous and biocompatible excipients in enhancing the biopharmaceutical properties of BCS class II antimalarial drugs, ART and MFQ. Based on our knowledge, studies on the stability of formulated ART have been rarely reported despite the abundance of studies on *in vitro* drug release. Additionally, mesoporous carriers and functionalized food additives have not been used in generating solid dispersions of antimalarial drugs. Most importantly, combinations of ART and MFQ have never been studied before. Our results have revealed that it is technically feasible to generate amorphous solid dispersions of ART using mesoporous carriers and functionalized food additives via co-spray drying. The significance of the carriers in amorphization of ART is reflected by the fact that the drug was unable to amorphize by spray drying in their absence. Co-spray drying of MFQ and ART nonetheless was able to produce amorphous ART without any excipients, albeit this amorphous form was physically unstable and reverted to the crystalline form within one-week of storage even in desiccators.

The application of mesoporous carriers and functionalized food additives, coupled with spray drying, to enhance the solubility of poorly water-soluble ART and MFQ may impart numerous advantages. SBA-15 with a large drug loading capacity will diminish materials and energy consumption by minimizing wastage of raw materials. Meanwhile, Hsp-G and Stevia-G are extremely water-soluble, safe and cost-effective materials. Moreover, the

single-step co-spray drying of ART and MFQ with excipients will translate into a reduced number of energy-intensive secondary manufacturing steps such as milling, micronization and blending. Additionally, the elucidation of the physical and chemical stability of ART and MFQ with suitable storage conditions will enable the prolongation of the shelf-life of the amorphous drugs.

Initially, activated carbon (AC) was selected as the mesoporous carrier for ART since AC is an industrially available, cost-effective porous material at a large scale and has been widely used in medical applications. ART/AC at 5 different weight ratios were prepared through co-spray drying: ART/AC (1:3 w/w), ART/AC (1:1 w/w), ART/AC (2:1 w/w), ART/AC (3:1 w/w) and ART/AC (4:1 w/w). Solid dispersions with drug loading up to 80 wt% were formulated in order to study the encapsulation capacity of AC to form amorphous forms. It was expected that AC would be able to form amorphous solid dispersions even at higher drug loading due to its large pore volume and specific surface area with strong adsorption capacity. However, only co-spray drying of ART/AC samples below 50 wt% drug loading (ART/AC $\leq$ 1:1 w/w) result in amorphous ART; at high drug loading (ART/AC > 1:1 w/w), formation of partially crystalline ART in orthorhombic and triclinic forms could be observed. Nonetheless, formulation of both the amorphous and partially crystalline forms contributed to the enhancement in dissolution rate and supersaturation of ART. Although the supersaturation of the treated ART was enhanced 2-fold compared with untreated ART, the drug release profile of

treated ART was affected by the strong adsorption capacity and catalytic activity of AC.

Mesoporous silica (SBA-15) with outstanding features such as high specific surface area, large pore volume, uniform pore size, short pore channels and hydrophilic nature was chosen as a drug vehicle to replace AC. Amorphization and particles size reduction of ART via spatial confinement contributes to the remarkable dissolution kinetics and supersaturation. The dissolution rates of the formulated ART/SBA-15 are significantly improved than that of the untreated drug and the supersaturation is enhanced by 2-fold of the equilibrium solubility of crystalline drug. Strikingly, the enhanced supersaturation could be sustained for 120 min without addition of any precipitation inhibitors. The ART/SBA-15 samples exhibited excellent chemical stability in desiccators (25 °C/18% RH), Activ-vial® (25 °C) and Activ-vial® (40 °C), indicating that the degradation of ART could be prevented under low humidity conditions under the storage temperature of 25°C and 40 °C. In addition, the amorphous state of ART/SBA-15 samples also exhibited excellent physical stability for 6-months with preserved enhanced dissolution properties of ART. Therefore, the conditions of desiccators (25 °C/18% RH), Activ-vial® (25 °C) and Activ-vial® (40 °C) were used for further analysis. Finally, the low cytotoxicity effect of untreated ART, SBA-15 and formulated ART/SBA-15 on Caco-2 cells after 24 hours incubation proves the biocompatibility of SBA-15 and ART.

Additionally, the investigation of non-porous silica as a control and characteristic studies such as SEM, TEM, PXRD and N2 adsorption clearly demonstrate that most of the ART drug particles entrapped inside the pore channel of SBA-15 and not on the external surfaces. SBA-15 able to appear in amorphous form even at high drug loading of 50 wt.% as compared with non-porous silica which is unable to accommodate even 10 wt.% of ART in amorphous forms. However, ART/SBA-15 only appeared to be in crystalline form with additional particles on the external surface once the pore volume was fully occupied at drug loading of 75 wt.%. Based on these results, a conclusion that most of the ART molecules are entrapped in the pore channels of SBA-15 can be drawn.

On the other hand, the performance of inorganic and water-insoluble material (SBA-15) as a drug carrier was compared with that of the water-soluble carriers, α-glucosyl hesperidin (Hsp-G) and α-glucosyl stevioside (Stevia-G). Relative to SBA-15, both the food additives exhibited extraordinary dissolution profiles, for which 100% of drug release was achieved within 5 min mainly due to the amorphization of the ART and extreme aqueous solubility of the carriers. Meanwhile, the enhanced supersaturation of ART from Hsp-G and Stevia-G was almost two-fold as achieved by the solid dispersion of SBA-15, although a slight decrease in supersaturation could be observed after 2 h. However, the drug loading achieved through ART/Hsp-G and ART/Stevia-G was very low (9.1 wt%) and solid dispersions at 25 wt% of drug loading formed crystalline samples. In addition, only dry and low-temperature conditions were suitable for the

storage of these samples given that formation of micro-crystals at 25 °C/75% RH and changes in the physical state in Activ-vial® (40 °C) and open pan (40 °C/75% RH) were observed after the 6-month storage.

Biopharmaceutical properties	ART/AC	ART/SBA-15	ART/Hsp-G & ART/Stevia-G
Physical state	amorphous and crystalline	amorphous	amorphous
Drug Loading (wt%)	high	high	low
Dissolution (after 30 min)	61.7%	76.6%	100%
Supersaturation (μg/mL)	90	103	96
Storage stability	poor	good	good

Therefore, based on the previous screening study as summarized in the table above, SBA-15 was chosen as the carrier for the formulation of ART and MFQ combination. Storage test was conducted under two storage conditions with desiccators (25 °C/18% RH) and Activ-vial® (25 °C); Activ-vial® (40 °C) was excluded since it caused degradation of MFQ/SBA-15 solid dispersions. As expected, it was technically feasible to formulate amorphous solid dispersions of combination of ART and MFQ using SBA-15 at weight ratio of 1:1 (w/w) via co-spray drying. The formulated solid dispersions exhibited superior performance in drug loading efficiency, drug release and storage stability for ART and MFQ drugs. Based on the obtained results, it is

recommended that the formulated solid dispersions of ART/MFQ/SBA-15 be stored at low humidity and low temperature to prolong the shelf-life of the dosage forms. Extensive studies on ART and ART/MFQ could provide a practical reference in understanding the physicochemical stability of these two drugs during the formulation and development of pharmaceutical dosage forms.

Chapter 9 Recommendations and Future Work

Notwithstanding the advantages of the formulation of solid dispersions with mesoporous silica and functionalized food additives in enhancing the biopharmaceutical properties of poorly water-soluble drugs, some limitations remain that need to be addressed. For example, although the bioavailability of BCS class II drugs is expected to be enhanced through solubility enhancement, the caveat is that the acceptable methods to quantify the bioavailability and therapeutic effect of the drugs are through *in vivo* studies. Therefore, it would be recommended that *in vitro* cellular studies (such cell permeability) and *in vivo* experiments be conducted to completely evaluate the bioavailability enhancement of formulated antimalarial drugs. *In vivo* studies such as pharmacokinetics analysis, biodistribution analysis through imaging and antimalarial efficacy studies are recommended to evaluate the bioavailability of formulated solid dispersions.

Apart from that, additional works are required in order to furnish more data for validation and to corroborate the claim in our research. Below are some recommendations for future work.

1. To compare the efficiency of spray drying with that of other formulation techniques. Although spray drying has been found to been a remarkable technique to formulate antimalarial drugs in solid dispersions, other techniques such freeze drying, ball milling, hot melt extrusion and supercritical fluid technique are appealing in this

context. Therefore, it is recommended that comparison be made between all such formulation techniques.

2. To evaluate the effects of nano-confinement of SBA-15 on other antimalarial drug combinations such as artemisinin-naphthoquine or artesunate-mefloquine, which are available in the market and widely used in ACTs. The performance of the formulated samples can be compared with that of the commercialized products of either fixed-dose combination tablets or co-blistered tablets.
3. To evaluate the co-formulations of ART/MFQ/SBA-15 solid dispersions with functionalized food additives. Since both the Hsp-G and Stevia-G have the ability to act as a drug carrier and sugar substitute, these two materials can be exploited. They not only able to enhance the biopharmaceutical properties of ART and MFQ but also to suppress the bitterness of the formulated dosage forms and increase their palatability and, in turn, patient compliance. There are two different approaches to co-formulate the samples: co-spray drying both the drugs (ART and MFQ) and both the carriers (SBA-15 and Hsp-G or Stevia-G) together; or coating the formulated solid dispersions of ART/MFQ/SBA-15 with Hsp-G or Stevia-G.
4. To elucidate the effects of MFQ in co-amorphization with other antimalarial drugs. It has been shown in this research that MFQ has the ability to form co-amorphous samples when co-spray dried with ART. Therefore, it is recommended study the effect of co-amorphization of MFQ.

5. To identify the feasibility and biocompatibility of all the formulations by extending the *in vitro* cytotoxicity studies to food additives and ACTs related formulations.

REFERENCES

Abdelbary AA, Li X, El-Nabarawi M, Elassasy A, Jasti B. Comparison of nanomilling and coprecipitation on the enhancement of in vitro dissolution rate of poorly water-soluble model drug aripiprazole. Pharma Dev Technol, 2014;19:491-500.

Abdelwahed W, Degobert G, Stainmesse S, Fessi H. Freeze-drying of nanoparticles: formulation, process and storage considerations. Adv Drug Deliv Rev, 2006;58:1688-1713.

Adjuik M, Agnamey P, Babiker A, Baptista J, Borrmann S, Brasseur P, Carnevale P, et al. Artesunate combinations for treatment of malaria: meta-analysis. Lancet, 2004;363:9-17.

Agharkar S, Lindenbaum S, Higuchi T. Enhancement of solubility of drug salts by hydrophilic counterions: properties of organic salts of an antimalarial drug. J Pharm Sci, 1976;65:747-749.

Agrawal U, Sharma R, Gupta M, Vyas SP. Is nanotechnology a boon for oral drug delivery? Drug Discov Today, 2014;19:1530-1546.

Aguiar AJ, Krc J, Kinkel AW, Samyn JC. Effect of polymorphism on the absorption of chloramphenicol from chloramphenicol palmitate. J Pharm Sci, 1967;56:847-853.

Aguinaco A, Pocostales JP, García-Araya JF, Beltrán FJ. Decomposition of hydrogen peroxide in the presence of activated carbons with different characteristics. J Chem Technol Biotechnol, 2011;86:595-600.

Ahola M, Kortesuo P, Kangasniemi I, Kiesvaara J, Yli-Urpo A. Silica xerogel carrier material for controlled release of toremifene citrate. Int J Pharm, 2000;195:219-227.

Ahuja M, Verma P, Bhatia M. Preparation and evaluation of chitosan-itraconazole co-precipitated nanosuspension for ocular delivery. J Exp Nanosci, 2015;10:209-221.

Ahuja N, Katare OP, Singh B. Studies on dissolution enhancement and mathematical modeling of drug release of a poorly water-soluble drug using water-soluble carriers. Eur J Pharm Biopharm, 2007;65:26-38.

Aiache JM, Islasse M, Beyssac E, Aiache S, Renoux R, Kantelip JP. Kinetics of indomethacin release from suppositories - in vitro in vivo correlation. Int J Pharm, 1987;39:235-242.

Ajibade PA, Kolawole GA. Synthesis, characterization, antiplasmodial and antitrypanosomal activity of some metal(iii) complexes of sulfadiazine. Bull Chem Soc Ethiop, 2008;22:261-268.

Akbuga J, Gursoy A, Kendi E. The preparation and stability of fast release furosemide-PVP solid dispersion. Drug Dev Ind Pharm, 1988;14:1439-1464.

Al-Obaidi H, Lawrence MJ, Shah S, Moghul H, Al-Saden N, Bari F. Effect of drug-polymer interactions on the aqueous solubility of milled solid dispersions. Int J Pharm, 2013;446:100-105.

Alavijeh MS, Chishty M, Qaiser MZ, Palmer AM. Drug metabolism and pharmacokinetics, the blood-brain barrier and central nervous system drug discovery. NeuroRx, 2005;2:554-571.

Ambrogi V, Marmottini F, Pagano C. Amorphous carbamazepine stabilization by the mesoporous silicate SBA-15. Microporous and Mesoporous Mater, 2013;177:1-7.

Ambrogi V, Perioli L, Marmottini F, Giovagnoli S, Esposito M, Rossi C. Improvement of dissolution rate of piroxicam by inclusion into MCM-41 mesoporous silicate. Eur J Pharm Sci, 2007;32:216-222.

Ameri M, Maa Y-F. Spray drying of biopharmaceuticals: stability and process considerations. Drying Technol, 2006;24:763-768.

Amidon G, Lennernäs H, Shah V, Crison J. A theoretical basis for a biopharmaceutic drug classification: the correlation of in vitro drug product dissolution and in vivo bioavailability. Pharm Res, 1995;12:413-420.

Andersson J, Rosenholm J, Areva S, Linden M. Influences of material characteristics on ibuprofen drug loading and release profiles from ordered micro- and mesoporous silica matrices. Chem Mater, 2004;16:4160-4167.

Anonymous. List of malaria pharmaceutical products classified according to the Global Fund Quality Assurance Policy [Online]. Available: http://www.theglobalfund.org/documents/psm/PSM_ProductsMALARIA_List_en/ [Accessed 28th February 2015]

Anwer MK, Jamil S, Ansari MJ, Al-Shdefat R, Ali BE, Ganaie MA, Abdel-Kader MS, Shakeel F. Water soluble binary and ternary complexes of diosmin with β-cyclodextrin: spectroscopic characterization, release studies and anti-oxidant activity. J Mol Liq, 2014;199:35-41.

Arndt M, Stannarius R, Groothues H, Hempel E, Kremer F. Length scale of cooperativity in the dynamic glass transition. Phys Rev Lett, 1997;79:2077-2080.

Attaran A, Barnes KI, Curtis C, D'alessandro U, Fanello CI, Galinski MR, Kokwaro G, et al. WHO, the Global Fund and medical malpractice in malaria treatment. Lancet, 2004;363:237-240.

Bagshaw SA, Prouzet E, Pinnavaia TJ. Templating of mesoporous molecular sieves by nonionic polyethylene oxide surfactants. Science, 1995;269:1242-4.

Bajaj H, Bisht S, Yadav M, Singh V. Biovailability enhancement: a review. Int J Pharma and Bio Sci, 2011;2:202-216.

Balducci AG, Magosso E, Colombo G, Sonvico F, Khan NaK, Yuen KH, Bettini R, Colombo P, Rossi A. Agglomerated oral dosage forms of artemisinin/β-cyclodextrin spray-dried primary microparticles showing increased dissolution rate and bioavailability. AAPS PharmSciTech, 2013;14:911-918.

Bandarkar FS, Vavia PR. An optimized commercially feasible milling technique for molecular encapsulation of meloxicam in β-cyclodextrin. Drug Dev Ind Pharm, 2011;37:1318-1328.

Barnes KI, White NJ. Population biology and antimalarial resistance: the transmission of antimalarial drug resistance in Plasmodium falciparum. Acta Trop, 2005;94:230-240.

Bate R, Coticelli P, Tren R, Attaran A. Antimalarial drug quality in the most severely malarious parts of Africa - a six country study. PLos One, 2008;3:e2132

Bernkop-Schnurch A, Kast CE. Chemically modified chitosans as enzyme inhibitors. Adv Drug Deliv Rev, 2001;52:127-137.

Bérubé F, Kaliaguine S. Calcination and thermal degradation mechanisms of triblock copolymer template in SBA-15 materials. Microporous and Mesoporous Mater, 2008;115:469-479.

Bhakay A, Merwade M, Bilgili E, Dave RN. Novel aspects of wet milling for the production of microsuspensions and nanosuspensions of poorly water-soluble drugs. Drug Dev Ind Pharm, 2011;37:963-976.

Bhattachar SN, Wesley JA, Fioritto A, Martin PJ, Babu SR. Dissolution testing of a poorly soluble compound using the flow-through cell dissolution apparatus. Int J Pharm, 2002;236:135-143.

Billon A, Bataille B, Cassanas G, Jacob M. Development of spray-dried acetaminophen microparticles using experimental designs. J Pharm Sci, 2000;203:159-168.

Blagden N, De Matas M, Gavan PT, York P. Crystal engineering of active pharmaceutical ingredients to improve solubility and dissolution rates. Adv Drug Deliv Rev, 2007;59:617-630.

Boahene PE, Soni KK, Dalai AK, Adjaye J. Application of different pore diameter SBA-15 supports for heavy gas oil hydrotreatment using FeW catalyst. Appl Catal A Gen, 2011;402:31-40.

Bobe KR, Subrahmanya CR, Suresh S, Gaikwad DT, Patil MD, Khade TS, Gavitre BB, Kulkarni VS, Gaikwad UT. Formulation and evaluation of solid dispersion of atorvatstatin with various carrier. Int J Compr Pharma, 2011;2:1-6.

Boersen AC. Spray drying technology. J Society Dairy Technol, 1990;43:5-7.

Bouchal F, Skiba M, Fatmi S, Chaffai N, Lahiani-Skiba M. Influence of the preparation method on the dissolution properties of piroxicam - cyclodextrins systems. Lett Drug Des Discov, 2014;11:786-808.

Brayden DJ, O'mahony DJ. Novel oral drug delivery gateways for biotechnology products: polypeptides and vaccines. Pharm Sci Technol Today, 1998;1:291-299.

Breitenbach J. Melt extrusion: from process to drug delivery technology. Eur J Pharm Biopharm, 2002;54:107-117.

Breman J.G., Daily J., E.L. B. Epidemiology, prevention and control of malaria in endemic areas [Online]. UpToDate. Available: http://www.united-academics.org/magazine/health-medicine/historic-accidental-finding-now-produced-promising-malaria-vaccine/ [Accessed 28th February 2015].

Brewster DR, Kwiatkowski D, White NJ. Neurological sequelae of cerebral malaria in children. Lancet, 1990;336:1039-1043.

Brion M, Jaspart S, Perrone L, Piel G, Evrard B. The supercritical micronization of solid dispersions by Particles from Gas Saturated Solutions using experimental design. J Supercrit Fluids, 2009;51:50-56.

Brockman A, Price RN, Van Vugt M, Heppner DG, Walsh D, Sookto P, Wimonwattrawatee T, et al. Plasmodium falciparum antimalarial drug susceptibility on the north-western border of Thailand during five years of extensive use of artesunate-mefloquine. Trans R Soc Trop Med Hyg, 2000;94:537-544.

Bromberg L. Polymeric micelles in oral chemotherapy. J Control Release, 2008;128:99-112.

Cabral-Marques H, Almeida R. Optimisation of spray-drying process variables for dry powder inhalation (DPI) formulations of corticosteroid/cyclodextrin inclusion complexes. Eur J Pharm Biopharm, 2009;73:121-129.

Calvo P, Vilajato JL, Alonso MJ. Comparative in vitro evaluation of several colloidal systems, nanoparticles, nanocapsules and nanoemulsions, as ocular drug carriers. J Pharm Sci, 1996;85:530-536.

Cao F, Guo JX, Ping QN. The physicochemical characteristics of freeze-dried scutellarin-cyclodextrin tetracomponent complexes. Drug Dev Ind Pharm, 2005;31:747-756.

Carrio A, Schwach G, Coudane J, Vert M. Preparation and degradation of surfactant-free PLAGA microspheres. J Control Release, 1995;37:113-121.

Cassiers K, Linssen T, Mathieu M, Benjelloun M, Schrijnemakers K, Van Der Voort P, Cool P, Vansant EF. A detailed study of thermal, hydrothermal and mechanical stabilities of a wide range of surfactant assembled mesoporous silicas. Chem Mater, 2002;14:2317-2324.

Chan KL, Yuen KH, Takayanagi H, Janadasa S, Peh KK. Polymorphism of artemisinin from Artemisia annua. Phytochemistry, 1997;46:1209-1214.

Charnay C, Begu S, Tourne-Peteilh C, Nicole L, Lerner DA, Devoisselle JM. Inclusion of ibuprofen in mesoporous templated silica: drug loading and release property. Eur J Pharm Biopharm, 2004;57:533-540.

Charoenchaitrakool M, Dehghani F, Foster NR, Chan HK. Micronization by rapid expansion of supercritical solutions to enhance the dissolution rates of poorly water-soluble pharmaceuticals. Ind Eng Chem Res, 2000;39:4794-4802.

Chen T-H, Chen S-C, Chan P, Chu Y-L, Yang H-Y, Cheng J-T. Mechanism of the hypoglycemic effect of stevioside, a glycoside of Stevia rebaudiana. Planta Med, 2005;71:108-113.

Chen Y, Lu Y, Chen J, Lai J, Sun J, Hu F, Wu W. Enhanced bioavailability of the poorly water-soluble drug fenofibrate by using liposomes containing a bile salt. J Pharm Sci, 2009;376:153-160.

Chiou WL, Riegelma.S. Pharmaceutical applications of solid dispersion systems. J Pharm Sci, 1971;60:1281-1302.

Cloete TT, Wilma Breytenbach J, Kock CD, Smith PJ, Breytenbach JC, N'da DD. Synthesis, antimalarial activity and cytotoxicity of 10-aminoethylether derivatives of artemisinin. Bioorg Med Chem, 2012;20:4701-4709.

Cockburn R, Newton PN, Agyarko EK, Akunyili D, White NJ. The global threat of counterfeit drugs: why industry and governments must communicate the dangers. PLos Med, 2005;2:302-308.

Crowley MM, Zhang F, Repka MA, Thumma S, Upadhye SB, Battu SK, Mcginity JW, Martin C. Pharmaceutical applications of hot-melt extrusion: part I. Drug Dev Ind Pharm, 2007;33:909-926.

Cserháti T, Forgács E, Szejtli J. Inclusion complex formation of antisense nucleotides with hydroxypropyl-β-cyclodextrin. Int J Pharm, 1996;141:1-7.

Da Costa M, Seiceira R, Rodrigues C, Hoffmeister C, Cabral L, Rocha H. Efavirenz dissolution enhancement I: co-micronization. Pharmaceutics, 2012;5:1-22.

Dahlberg C, Millqvist-Fureby A, Schuleit M. Surface composition and contact angle relationships for differently prepared solid dispersions. Eur J Pharm Biopharm, 2008;70:478-485.

Das SK, Bhunia MK, Bhaumik A. Highly ordered Ti-SBA-15: Efficient H2 adsorbent and photocatalyst for eco-toxic dye degradation. J Solid State Chem, 2010;183:1326-1333.

Datta S, Grant DJW. Crystal structures of drugs: advances in determination, prediction and engineering. Nat Rev Drug Discov, 2004;3:42-57.

Daughton CG, Ruhoy IS. Lower-dose prescribing: Minimizing "side effects" of pharmaceuticals on society and the environment. Sci Total Environ, 2013;443:324-337.

De Donno A, Grassi T, Idolo A, Guido M, Papadia P, Caccioppola A, Villanova L, et al. First-time comparison of the in vitro antimalarial activity of Artemisia annua herbal tea and artemisinin. Trans R Soc Trop Med Hyg, 2012;106:696-700.

Derendorf H, Drehsen G, Rohdewald P. In vivo-in vitro correlations of salicylate saliva levels and continuous flow cell dissolution rates. Int J Pharm, 1983;15:167-175.

Desai KGH, Kulkarni AR, Aminabhavi TM. Solubility of rofecoxib in the presence of methanol, ethanol and sodium lauryl sulfate at (298.15, 303.15 and 308.15) K. J Chem Eng Data, 2003;48:942-945.

Desai KGH, Park HJ. Solubility studies on valdecoxib in the presence of carriers, cosolvents and surfactants. Drug Dev Res, 2004;62:41-48.

Ding H, Sun H, Shan Y. Preparation and characterization of mesoporous SBA-15 supported dye-sensitized TiO2 photocatalyst. J Photochem Photobiol A: Chem, 2005;169:101-107.

Dobry DE, Settell DM, Baumann JM, Ray RJ, Graham LJ, Beyerinck RA. A model-based methodology for spray-drying process development. J Pharm Innov, 2009;4:133-142.

Dondorp AM, Nosten F, Yi P, Das D, Phyo AP, Tarning J, Lwin KM, et al. Artemisinin resistance in Plasmodium falciparum malaria. N Engl J Med, 2009;361:455-467.

Du Plessis LH, Helena C, Van Huysteen E, Wiesner L, Kotzé AF. Formulation and evaluation of pheroid vesicles containing mefloquine for the treatment of malaria. J Pharm Pharmacol, 2014;66:14-22.

Dutt GB. Rotational diffusion of hydrophobic probes in Brij-35 micelles: effect of temperature on micellar internal environment. The J Phys Chem B, 2003;107:10546-10551.

Eastman RT, Fidock DA. Artemisinin-based combination therapies: a vital tool in efforts to eliminate malaria. Nat Rev. Microbiol, 2009;7:864-74.

Ekvall H, Premji Z, Bjorkman A. Chloroquine treatment for uncomplicated childhood malaria in an area with drug resistance: early treatment failure aggravates anaemia. Trans R Soc Trop Med Hyg, 1998;92:556-560.

Elshaboury MH. Physical properties and dissolution profiles of tablets directly compressed with β-cyclodextrin. Int J Pharm, 1990;63:95-100.

Emara LH, Badr RM, Abd Elbary A. Improving the dissolution and bioavailability of nifedipine using solid dispersions and solubilizers. Drug Dev Ind Pharm, 2002;28:795-807.

Emara LH, Taha NF, Mursi NM. Investigation of the Effect of Different Flow-Through Cell Designs on the Release of Diclofenac Sodium SR Tablets. Dissolut Technol, 2009;16:23-31.

Esmaili M, Ghaffari SM, Moosavi-Movahedi Z, Atri MS, Sharifizadeh A, Farhadi M, Yousefi R, et al. Beta casein-micelle as a nano vehicle for solubility enhancement of curcumin; food industry application. Food Sci Technol, 2011;44:2166-2172.

Esposito E, Roncarati R, Cortesi R, Cervellati F, Nastruzzi C. Production of Eudragit microparticles by spray-drying technique: influence of experimental parameters on morphological and dimensional characteristics. Pharm Dev Technol, 2000;5:267-278.

FDA. Center for Drug Evaluation and Research (CDER), Guidance for Industry Dissolution Testing of Immediate Release Solid Oral Dosage Forms: U.S. Department of Health and Human Services Food and Drug Administration August 1997. 1997.

Ferreira JFS, Zheljazkov VD, Gonzalez JM. Artemisinin concentration and antioxidant capacity of Artemisia annua distillation byproduct. Ind Crops Prod, 2013;41:294-298.

Forster A, Hempenstall J, Rades T. Characterization of glass solutions of poorly water-soluble drugs produced by melt extrusion with hydrophilic amorphous polymers. J Pharm Pharmacol, 2001a;53:303-315.

Forster A, Hempenstall J, Tucker I, Rades T. The potential of small-scale fusion experiments and the Gordon-Taylor equation to predict the suitability of drug/polymer blends for melt extrusion. Drug Dev Ind Pharm, 2001b;27:549-560.

Freundlich H. Colloid and capillary chemistry, 1923.

Frizon F, Eloy JDO, Donaduzzi CM, Mitsui ML, Marchetti JM. Dissolution rate enhancement of loratadine in polyvinylpyrrolidone K-30 solid dispersions by solvent methods. Powder Technol, 2013;235:532-539.

Fu JJ, Zhang LL, Guan TT, Tang X, He HB. Stable nimodipine tablets with high bioavailability containing NM-SD prepared by hot-melt extrusion. Powder Technol, 2010;204:214-221.

Gachot B, Wolff M, Nissack G, Veber B, Vachon F. Acute lung injury complicating imported Plasmodium falciparum malaria. Chest, 1995;108:746-749.

Gahoi S, Jain GK, Tripathi R, Pandey SK, Anwar M, Warsi MH, Singhal M, Khar RK, Ahmad FJ. Enhanced antimalarial activity of lumefantrine nanopowder prepared by wet-milling DYNO MILL technique. Colloids Surf B Biointerfaces, 2012;95:16-22.

Galarneau A, Cambon H, Di Renzo F, Fajula F. True Microporosity and Surface Area of Mesoporous SBA-15 Silicas as a Function of Synthesis Temperature. Langmuir, 2001;17:8328-8335.

Gaucher G, Satturwar P, Jones M-C, Furtos A, Leroux J-C. Polymeric micelles for oral drug delivery. Eur J Pharm Biopharm, 2010;76:147-158.

Ghebremeskel AN, Vernavarapu C, Lodaya M. Use of surfactants as plasticizers in preparing solid dispersions of poorly soluble API: selection of polymer-surfactant combinations using solubility parameters and testing the processability. J Pharm Sci, 2007;328:119-129.

Goldberg M, Gomez-Orellana I. Challenges for the oral delivery of macromolecules. Nat Rev Drug Discov, 2003;2:289-295.

Gouin S. Microencapsulation: industrial appraisal of existing technologies and trends. Trends Food Sci Technol, 2004;15:330-347.

Greenwood BM, Bojang K, Whitty CJM, Targett GaT. Malaria. The Lancet, 2005;365:1487-1498.

Grunenberg A, Henck JO, Siesler HW. Theoretical derivation and practical application of energy temperature diagrams as an instrument in preformulation studies of polymorphic drug substances. J Pharm Sci, 1996;129:147-158.

Guerin PJ, Olliaro P, Nosten F, Druilhe P, Laxminarayan R, Binka F, Kilama WL, Ford N, White NJ. Malaria: current status of control, diagnosis, treatment and a proposed agenda for research and development. Lancet Infect Dis, 2002;2:564-573.

Guo Z, Liu X-M, Ma L, Li J, Zhang H, Gao Y-P, Yuan Y. Effects of particle morphology, pore size and surface coating of mesoporous silica on naproxen dissolution rate enhancement. Colloids Surf B Biointerfaces, 2013;101:228-235.

Gupta AK, Sehrawat SK. Bioavailability enhancement of poorly water soluble drugs: a review. Int J Pharm Life Sci, 2011;2:640-650.

Gupta NK, Dixit VK. Bioavailability enhancement of curcumin by complexation with phosphatidyl choline. J Pharm Sci, 2011;100:1987-1995.

Hailu SA, Bogner RH. Complex effects of drug/silicate ratio, solid-state equivalent pH and moisture on chemical stability of amorphous quinapril hydrochloride coground with silicates. J Pharm Sci, 2011;100:1503-1515.

Hammond RB, Pencheva K, Roberts KJ, Auffret T. Quantifying solubility enhancement due to particle size reduction and crystal habit modification: case study of acetyl salicylic acid. J Pharm Sci, 2007;96:1967-1973.

Hancock BC, Parks M. What is the true solubility advantage for amorphous pharmaceuticals. Pharm Res, 2000;17:397-404.

Hancock BC, Zografi G. Characteristics and significance of the amorphous state in pharmaceutical systems. J Pharm Sci, 1997;86:1-12.

Hartmann M. Ordered mesoporous materials for bioadsorption and biocatalysis. Chem Mater, 2005;17:4577-4593.

He HB, Yang R, Tang X. In vitro and in vivo evaluation of fenofibrate solid dispersion prepared by hot-melt extrusion. Drug Dev Ind Pharm, 2010;36:681-687.

Heikkila T, Salonen J, Tuura J, Kumar N, Salmi T, Murzin DY, Hamdy MS, et al. Evaluation of mesoporous TCPSi, MCM-41, SBA-15 and TUD-1 materials as API carriers for oral drug delivery. Drug Deliv, 2007;14:337-347.

Heng D, Cutler DJ, Chan HK, Yun J, Raper JA. What is a suitable dissolution method for drug nanoparticles? Pharm Res, 2008;25:1696-1701.

Heng D, Ogawa K, Cutler D, Chan H-K, Raper J, Ye L, Yun J. Pure drug nanoparticles in tablets: what are the dissolution limitations? J Nanopart Res, 2010;12:1743-1754.

Hezave AZ, Aftab S, Esmaeilzadeh F. Micronization of creatine monohydrate via Rapid Expansion of Supercritical Solution (RESS). J Supercrit Fluids, 2010;55:316-324.

Hoa NT, Michoel A, Kinget R. Dissolution testing of artemisinin solid oral dosage forms. Int J Pharm, 1996;138:185-190.

Hombhanje FW, Huang Q. Artemisinin-naphthoquine combination (ARCO®): an overview of the progress. Pharmaceuticals, 2010;3:3581-3593.

Hombhanje FW, Linge D, Saweri A, Kuanch C, Jones R, Toraso S, Geita J, et al. Artemisinin-naphthoquine combination (ARCO®) therapy for uncomplicated falciparum malaria in adults of Papua New Guinea: a preliminary report on safety and efficacy. Malar J, 2009;8:196.

Horcajada P, Ramila A, Perez-Pariente J, Vallet-Regi M. Influence of pore size of MCM-41 matrices on drug delivery rate. Microporous and Mesoporous Mater, 2004;68:105-109.

Hu L, Jia Y, Niu F, Jia Z, Yang X, Jiao K. Preparation and enhancement of oral bioavailability of curcumin using microemulsions vehicle. J Agric Food Chem, 2012a;60:7137-7141.

Hu Y, Zhi Z, Zhao Q, Wu C, Zhao P, Jiang H, Jiang T, Wang S. 3D cubic mesoporous silica microsphere as a carrier for poorly soluble drug carvedilol. Microporous and Mesoporous Mater, 2012b;147:94-101.

Hu Z, Srinivasan MP. Mesoporous high-surface-area activated carbon. Microporous and Mesoporous Mater, 2001;43:267-275.

Illum L. Nasal drug delivery: new developments and strategies. Drug Discov Today, 2002;7:1184-1189.

Impéror-Clerc M, Davidson P, Davidson A. Existence of a Microporous Corona around the Mesopores of Silica-Based SBA-15 Materials Templated by Triblock Copolymers. J Am Chem Soc, 2000;122:11925-11933.

Isacchi B, Arrigucci S, Marca GL, Bergonzi MC, Vannucchi MG, Novelli A, Bilia AR. Conventional and long-circulating liposomes of artemisinin: preparation, characterization and pharmacokinetic profile in mice. J Liposome Res, 2011;21:237-244.

Isacchi B, Bergonzi MC, Grazioso M, Righeschi C, Pietretti A, Severini C, Bilia AR. Artemisinin and artemisinin plus curcumin liposomal formulations: enhanced antimalarial efficacy against Plasmodium berghei-infected mice. Eur J Pharm Biopharm, 2012;80:528-534.

Jiang H, Wang T, Wang L, Sun C, Jiang T, Cheng G, Wang S. Development of an amorphous mesoporous TiO2 nanosphere as a novel carrier for poorly water-soluble drugs: effect of different crystal forms of TiO2 carriers on drug loading and release behaviors. Microporous and Mesoporous Mater, 2012a;153:124-130.

Jiang H, Yang Z, Zhou X, Fang Y, Ji H. Immobilization of β-cyclodextrin as insoluble β-cyclodextrin polymer and its catalytic performance. Chin J Chem Eng, 2012b;20:784-792.

Jinno J, Kamada N, Miyake M, Yamada K, Mukai T, Odomi M, Toguchi H, et al. Effect of particle size reduction on dissolution and oral absorption of a poorly water-soluble drug, cilostazol, in beagle dogs. J Control Release, 2006;111:56-64.

Johari GP, Kim S, Shanker RM. Dielectric studies of molecular motions in amorphous solid and ultraviscous acetaminophen. J Pharm Sci, 2005;94:2207-2223.

Jones MC, Leroux JC. Polymeric micelles - a new generation of colloidal drug carriers. Eur J Pharm Biopharm, 1999;48:101-111.

Kakran M, Sahoo NG, Li L, Judeh Z. Dissolution enhancement of artemisinin with β-cyclodextrin. Chem Pharm Bull, 2011;59:646-652.

Kamble PR, Shaikh KS, Chaudhari PD. Application of liquisolid technology for enhancing solubility and dissolution of rosuvastatin. Adv Pharm Bull, 2014;4:197-204.

Kantele A, Jokiranta TS. Review of cases with the emerging fifth human malaria parasite, Plasmodium knowlesi. Clin Infect Dis, 2011;52:1356-1362.

Kapoor S, Hegde R, Bhattacharyya AJ. Influence of surface chemistry of mesoporous alumina with wide pore distribution on controlled drug release. J Control Release, 2009;140:34-39.

Kato Y, Kohketsu M. Relationship between polymorphism and bioavailability of amobarbital in the rabbit. Chem Pharm Bull, 1981;29:268-272.

Kawabata Y, Wada K, Nakatani M, Yamada S, Onoue S. Formulation design for poorly water-soluble drugs based on biopharmaceutics classification system: basic approaches and practical applications. J Pharm Sci, 2011;420:1-10.

Kawakami K, Miyoshi K, Ida Y. Solubilization behavior of poorly soluble drugs with combined use of gelucire 44/14 and cosolvent. J Pharm Sci, 2004;93:1471-1479.

Kawakami K, Oda N, Miyoshi K, Funaki T, Ida Y. Solubilization behavior of a poorly soluble drug under combined use of surfactants and cosolvents. Eur J Pharm Sci, 2006;28:7-14.

Keating GM. Dihydroartemisinin/piperaquine a review of its use in the treatment of uncomplicated plasmodium falciparum malaria. Drugs, 2012;72:937-961.

Keck CM, Muller RH. Drug nanocrystals of poorly soluble drugs produced by high pressure homogenisation. Eur J Pharm Biopharm, 2006;62:3-16.

Kermode M. Unsafe injections in low-income country health settings: need for injection safety promotion to prevent the spread of blood-borne viruses. Health Promot Int, 2004;19:95-103.

Khalafallah N, Khalil SA, Moustafa MA. Bioavailability determination of two crystal forms of sulfameter in humans from urinary excretion data. J Pharm Sci, 1974;63:861-864.

Khanfar M, Fares MM, Salem MTS, Qandil AM. Mesoporous silica based macromolecules for dissolution enhancement of Irbesartan drug using pre-adjusted pH method. Microporous and Mesoporous Mater, 2013;173:22-28.

Kiekens F, Eelen S, Verheyden L, Daems T, Martens J, Van Den Mooter G. Use of ordered mesoporous silica to enhance the oral bioavailability of ezetimibe in dogs. J Pharm Sci, 2012;101:1136-1144.

Kim M-S, Lee S, Park J-S, Woo J-S, Hwang S-J. Micronization of cilostazol using supercritical antisolvent (SAS) process: effect of process parameters. Powder Technol, 2007;177:64-70.

Kinnari P, Mäkilä E, Heikkilä T, Salonen J, Hirvonen J, Santos HA. Comparison of mesoporous silicon and non-ordered mesoporous silica materials as drug carriers for itraconazole. Int J Pharm, 2011;414:148-156.

Kitamura S, Chang LC, Guillory JK. Polymorphism of mefloquine hydrochloride. J Pharm Sci, 1994;101:127-144.

Kleitz F, Schmidt W, Schuth F. Calcination behavior of different surfactant-templated mesostructured silica materials. Microporous and Mesoporous Mater, 2003;65:1-29.

Kolasinac N, Kachrimanis K, Homsek I, Grujic B, Duric Z, Ibric S. Solubility enhancement of desloratadine by solid dispersion in poloxamers. Int J Pharm, 2012;436:161-170.

Kometani T, Fukuda T, Kakuma T, Kawaguchi K, Tamura W, Kumazawa Y, Nagata K. Effects of α-glucosylhesperidin, a bioactive food material, on collagen-induced arthritis in mice and rheumatoid arthritis in humans. Immunopharmacol Immunotoxicol, 2008;30:117-134.

Kometani T, Nishimura T, Nakae T, Takii H, Okada S. Synthesis of neohesperidin glycosides and naringin glycosides by cyclodextrin glucanotransferase from an alkalophilic bacillus species. Biosci Biotechnol Biochem, 1996;60:645-649.

Kometani T, Takashi K, Takahisa N, Takashi N, Hiroshi T. A method for preparation of soluble carthamin, red pigment from safflower, using glycosyl hesperidin. Food Sci Technol Res, 1999;5:265.

Kortesuo P, Ahola M, Kangas M, Kangasniemi I, Yli-Urpo A, Kiesvaara J. In vitro evaluation of sol-gel processed spray dried silica gel microspheres as carrier in controlled drug delivery. Int J Pharm, 2000;200:223-229.

Kotta S, Khan AW, Pramod K, Ansari SH, Sharma RK, Ali J. Exploring oral nanoemulsions for bioavailability enhancement of poorly water-soluble drugs. Expert Opin Drug Deliv, 2012;9:585-598.

Kresge CT, Leonowicz ME, Roth WJ, Vartuli JC, Beck JS. Ordered mesoporous molecular-sieves synthesized by a liquid-crystal template mechanism. Nature, 1992;359:710-712.

Kruk M, Jaroniec M, Ko CH, Ryoo R. Characterization of the porous structure of SBA-15. Chem Mater, 2000;12:1961-1968.

Kutty RV, Feng S-S. Cetuximab conjugated vitamin E TPGS micelles for targeted delivery of docetaxel for treatment of triple negative breast cancers. Biomaterials, 2013;34:10160-10171.

Lachheb H, Ahmed O, Houas A, Nogier JP. Photocatalytic activity of TiO2–SBA-15 under UV and visible light. J Photochem Photobiol A: Chem, 2011;226:1-8.

Lachman L, Lieberman HA, Kanig JL 1986. The theory and practice of industrial pharmacy third edition.

Lai CS, Nair NK, Mansor SM, Olliaro PL, Navaratnam V. An analytical method with a single extraction procedure and two separate high performance liquid chromatographic systems for the determination of artesunate, dihydroartemisinin and mefloquine in human plasma for application in clinical pharmacological studies of the drug combination. J Chromatogr B Analyt Technol Biomed Life Sci, 2007;857:308-14.

Lalatsa A, Schatzlein AG, Garrett NL, Moger J, Briggs M, Godfrey L, Iannitelli A, Freeman J, Uchegbu IF. Chitosan amphiphile coating of peptide nanofibres reduces liver uptake and delivers the peptide to the brain on intravenous administration. J Control Release, 2015;197:87-96.

Langenbucher F, Benz D, Kurth W, Moller H, Otz M. Standardized flow-cell method as an alternative to existing pharmacopoeial dissolution testing. Pharm Ind, 1989;51:1276-1281.

Lapenna S, Bilia AR, Morris GA, Nilsson M. Novel artemisinin and curcumin micellar formulations: drug solubility studies by NMR spectroscopy. J Pharm Sci, 2009;98:3666-3675.

Lee B-J, Lee J-R. Enhancement of solubility and dissolution rate of poorly water-soluble naproxen by complexation with 2-hydroxypropyl-β-cyclodextrin. Arch Pharm Res (Seoul), 1995;18:22-26.

Lee IC, He JS, Tsai MT, Lin KC. Fabrication of a novel partially dissolving polymer microneedle patch for transdermal drug delivery. J Mater Chem B, 2015;3:276-285.

Leuner C, Dressman J. Improving drug solubility for oral delivery using solid dispersions. Eur J Pharm Biopharm, 2000;50:47-60.

Li-Hong W, Xin C, Hui X, Li-Li Z, Jing H, Mei-Juan Z, Jie L, et al. A novel strategy to design sustained-release poorly water-soluble drug mesoporous silica microparticles based on supercritical fluid technique. Int J Pharm, 2013;454:135-142.

Li J, Zhou B. Biological actions of artemisinin: insights from medicinal chemistry studies. Molecules, 2010;15:1378-1397.

Lim RTY, Ng WK, Tan RBH. Dissolution enhancement of indomethacin via amorphization using co-milling and supercritical co-precipitation processing. Powder Technol, 2012;240:79-87.

Limnell T, Heikkilä T, Santos HA, Sistonen S, Hellstén S, Laaksonen T, Peltonen L, et al. Physicochemical stability of high indomethacin payload ordered mesoporous silica MCM-41 and SBA-15 microparticles. Int J Pharm, 2011a;1:242-251.

Limnell T, Riikonen J, Salonen J, Kaukonen AM, Laitinen L, Hirvonen J, Lehto VP. Surface chemistry and pore size affect carrier properties of mesoporous silicon microparticles. J Pharm Sci, 2007;343:141-147.

Limnell T, Santos HA, Mäkilä E, Heikkilä T, Salonen J, Murzin DY, Kumar N, et al. Drug delivery formulations of ordered and nonordered mesoporous silica: comparison of three drug loading methods. J Pharm Sci, 2011b;100:3294-3306.

Lin AJ, Klayman DL, Hoch JM, Silverton JV, George CF. Thermal rearrangement and decomposition products of artemisinin (qinghaosu). J Org Chem, 1985;50:4504-4508.

Lindenberg M, Kopp S, Dressman JB. Classification of orally administered drugs on the World Health Organization Model list of Essential Medicines according to the biopharmaceutics classification system. Eur J Pharm Biopharm, 2004;58:265-278.

Lipinski CA, Lombardo F, Dominy BW, Feeney PJ. Experimental and computational approaches to estimate solubility and permeability in drug discovery and development settings. Adv Drug Deliv Rev, 1997;23:3-25.

Liu CS, Desai KG. Characteristics of rofecoxib-polyethylene glycol 4000 solid dispersions and tablets based on solid dispersions. Pharm Dev Technol, 2005;10:467-477.

Liu CS, Desai KGH, Liu CG. Solubility of valdecoxib in the presence of ethanol and sodium lauryl sulfate at (298.15, 303.15 and 308.15) K. J Chem Eng Data, 2004;49:1847-1850.

Liu NQ, Choi YH, Verpoorte R, Van Der Kooy F. Comparative quantitative analysis of artemisinin by chromatography and qNMR. Phytochem Anal, 2010a;21:451-456.

Liu Y, Sun C, Hao Y, Jiang T, Zheng L, Wang S. Mechanism of dissolution enhancement and bioavailability of poorly water soluble celecoxib by preparing stable amorphous nanoparticles. J Pharm Pharm Sci, 2010b;13:589-606.

Liversidge GG, Cundy KC. Particle-size reduction for improvement of oral bioavailability of hydrophobic drugs .1. Absolute oral bioavailability of nanocrystalline danazol in beagle dogs. J Pharm Sci, 1995;125:91-97.

Lobenberg R, Amidon GL. Modern bioavailability, bioequivalence and biopharmaceutics classification system. New scientific approaches to international regulatory standards. Eur J Pharm Biopharm, 2000;50:3-12.

Lu GW, Hawley M, Smith M, Geiger BM, Pfund W. Characterization of a novel polymorphic form of celecoxib. J Pharm Sci, 2006;95:305-317.

Malaria S. Severe malaria. Trop Med Int Health, 2014;19:7-131.

Maniruzzaman M, Rana MM, Boateng JS, Mitchell JC, Douroumis D. Dissolution enhancement of poorly water-soluble APIs processed by hot-melt extrusion using hydrophilic polymers. Drug Dev Ind Pharm, 2013;39:218-227.

Manzano M, Vallet-Regi M. New developments in ordered mesoporous materials for drug delivery. J Mater Chem, 2010;20:5593-5604.

Marconi G, Monti S, Manoli F, Degli Esposti A, Mayer B. A circular dichroism and structural study of the inclusion complex artemisinin-β-cyclodextrin. Chem Phys Lett, 2004;383:566-571.

Martin FJ, Grove C. Microfabricated drug delivery systems: concepts to improve clinical benefit. Biomed Microdevices, 2001;3:97-107.

Matson DW, Fulton JL, Petersen RC, Smith RD. Rapid expansion of supercritical fluid solutions - solute formation of powders, thin-films and fibers. Ind Eng Chem Res, 1987;26:2298-2306.

Matsuda H, Matsumoto S, Kaguragi K, Kurihara K, Tochigi K, Tomono K. Determination and correlation of solubilities of famotidine in water plus co-solvent mixed solvents. Fluid Phase Equilib, 2011;302:115-122.

Mellaerts R, Houthoofd K, Elen K, Chen H, Van Speybroeck M, Van Humbeeck J, Augustijns P, et al. Aging behavior of pharmaceutical

formulations of itraconazole on SBA-15 ordered mesoporous silica carrier material. Microporous and Mesoporous Mater, 2010;130:154-161.

Mellaerts R, Mols R, Jammaer JaG, Aerts CA, Annaert P, Van Humbeeck J, Van Den Mooter G, Augustijns P, Martens JA. Increasing the oral bioavailability of the poorly water soluble drug itraconazole with ordered mesoporous silica. Eur J Pharm Biopharm, 2008;69:223-230.

Meynen V, Cool P, Vansant EF. Verified syntheses of mesoporous materials. Microporous and Mesoporous Mater, 2009;125:170-223.

Miyako Y, Khalef N, Matsuzaki K, Pinal R. Solubility enhancement of hydrophobic compounds by cosolvents: role of solute hydrophobicity on the solubilization effect. J Pharm Sci, 2010;393:48-54.

Montaner JS, Montessori V, Harrigan R, O'shaughnessy M, Hogg R. Antiretroviral therapy: 'the state of the art'. Biomed Pharmacother, 1999;53:63-72.

Moretti MDL, Gavini E, Juliano C, Pirisino G, Giunchedi P. Spray-dried microspheres containing ketoprofen formulated into capsules and tablets. J. Microencapsul, 2001;18:111-121.

Murdande S, Pikal M, Shanker R, Bogner R. Solubility advantage of amorphous pharmaceuticals: II. Application of quantitative thermodynamic relationships for prediction of solubility enhancement in structurally diverse insoluble pharmaceuticals. Pharm Res, 2010a;27:2704-2714.

Murdande SB, Pikal MJ, Shanker RM, Bogner RH. Solubility advantage of amorphous pharmaceuticals: I. A thermodynamic analysis. J Pharm Sci, 2010b;99:1254-1264.

Murphy GS, Oldfield EC. Falciparum malaria. Infect Dis Clin North Am, 1996;10:747-775.

Mutabingwa TK. Artemisinin-based combination therapies (ACTs): Best hope for malaria treatment but inaccessible to the needy! Acta Trop, 2005;95:305-315.

Nagarsenker MS, Meshram RN, Ramprakash G. Solid dispersion of hydroxypropyl-β-cyclodextrin and ketorolac: enhancement of in-vitro dissolution rates, improvement in anti-inflammatory activity and reduction in ulcerogenicity in rats. J Pharm Pharmacol, 2000;52:949-956.

Nakase I, Lai H, Singh NP, Sasaki T. Anticancer properties of artemisinin derivatives and their targeted delivery by transferrin conjugation. Int J Pharm, 2008;354:28-33.

Nekkanti V, Muniyappan T, Karatgi P, Hari MS, Marella S, Pillai R. Spray-drying process optimization for manufacture of drug-cyclodextrin complex

powder using design of experiments. Drug Dev Ind Pharm, 2009;35:1219-1229.

Newton PN, Green MD, Mildenhall DC, Plancon A, Nettey H, Nyadong L, Hostetler DM, et al. Poor quality vital anti-malarials in Africa - an urgent neglected public health priority. Malar J, 2011;10:352.

Ngo Thu H, Michoel A, Kinget R. Dissolution testing of artemisinin solid oral dosage forms. Int J Pharm, 1996;138:185-190.

Nicklasson M, Orbe A, Lindberg J, Borgå B, Magnusson AB, Nilsson G, Ahlgren R, Jacobsen L. A collaborative study of the in vitro dissolution of phenacetin crystals comparing the flow through method with the USP Paddle method. Int J Pharm, 1991;69:255-264.

Niu X, Wan L, Hou Z, Wang T, Sun C, Sun J, Zhao P, Jiang T, Wang S. Mesoporous carbon as a novel drug carrier of fenofibrate for enhancement of the dissolution and oral bioavailability. Int J Pharm, 2013;452:382-389.

Nosten F, Brasseur P. Combination therapy for malaria: the way forward? Drugs, 2002;62:1315-1329.

Nosten F, Luxemburger C, Terkuile FO, Woodrow C, Eh JP, Chongsuphajaisiddhi T, White NJ. Treatment of multidrug-resistant Plasmodium falciparum malaria with 3-day artesunate mefloquine combination. J Infect Dis, 1994;170:971-977.

Nosten F, Van Vugt M, Price R, Luxemburger C, Thway KL, Brockman A, Mcgready R, et al. Effects of artesunate-mefloquine combination on incidence of Plasmodium falciparum malaria and mefloquine resistance in western Thailand: a prospective study. Lancet, 2000;356:297-302.

Noyes AA, Whitney WR. The rate of solution of solid substances in their own solutions. J Am Chem Soc, 1897;19:930-934.

Okonogi S, Oguchi T, Yonemochi E, Puttipipatkhachorn S, Yamamoto K. Improved dissolution of ofloxacin via solid dispersion. Int J Pharm, 1997;156:175-180.

Okumu A, Dimaso M, Loebenberg R. Dynamic Dissolution Testing To Establish In Vitro/In Vivo Correlations for Montelukast Sodium, a Poorly Soluble Drug. Pharm Res, 2008;25:2778-2785.

Ostwald W. On the assumed isomerism of red and yellow mercury oxide and the surface-tension of solid bodies. Z Phys Chem (N F), 1900;34:495-503.

Ozeki T, Kano Y, Takahashi N, Tagami T, Okada H. Improved bioavailability of a water-insoluble drug by inhalation of drug-containing maltosyl-β-cyclodextrin microspheres using a four-fluid nozzle spray drier. AAPS PharmSciTech, 2012;13:1130-1137.

Pan L, Ho Q, Tsutsui K, Takahashi L. Comparison of chromatographic and spectroscopic methods used to rank compounds for aqueous solubility. J Pharm Sci, 2001;90:521-529.

Pandit JK, Gupta SK, Gode KD, Mishra B. Effect of crystal form on the oral absorption of phenylbutazone. J Pharm Sci, 1984;21:129-132.

Park JW. Kinetics and mechanism of cyclodextrin inclusion complexation incorporating bidirectional inclusion and formation of orientational isomers. J Phys Chem B, 2006;110:24915-24922.

Park K, Kwon IC, Park K. Oral protein delivery: current status and future prospect. React Funct Polym, 2011;71:280-287.

Pasquali I, Bettini R, Giordano F. Supercritical fluid technologies: an innovative approach for manipulating the solid-state of pharmaceuticals. Adv Drug Deliv Rev, 2008;60:399-410.

Patton JS, Byron PR. Inhaling medicines: delivering drugs to the body through the lungs. Nat Rev Drug Discov, 2007;6:67-74.

Paudel A, Worku ZA, Meeus J, Guns S, Van Den Mooter G. Manufacturing of solid dispersions of poorly water soluble drugs by spray drying: formulation and process considerations. J Pharm Sci, 2013;453:253-84.

Phillips J, Chen Y, Wakeling I. A Flow-Through Dissolution Approach to In Vivo/In Vitro Correlation of Adinazolam Release from Sustained Release Formulations. Drug Dev Ind Pharm, 1989;15:2177-2195.

Phyo AP, Nkhoma S, Stepniewska K, Ashley EA, Nair S, Mcgready R, Moo CL, et al. Emergence of artemisinin-resistant malaria on the western border of Thailand: a longitudinal study. Lancet, 2012;379:1960-1966.

Pitha J, Milecki J, Fales H, Pannell L, Uekama K. Hydroxypropyl-β-cyclodextrin: preparation and characterization; effects on solubility of drugs. Int J Pharm, 1986;29:73-82.

Planinšek O, Kovačič B, Vrečer F. Carvedilol dissolution improvement by preparation of solid dispersions with porous silica. Int J Pharm, 2011;406:41-48.

Pokharkar VB, Mandpe LP, Padamwar MN, Ambike AA, Mahadik KR, Paradkar A. Development, characterization and stabilization of amorphous form of a low T_g drug. Powder Technol, 2006;167:20-25.

Ponchel G, Irache JM. Specific and non-specific bioadhesive particulate systems for oral delivery to the gastrointestinal tract. Adv Drug Deliv Rev, 1998;34:191-219.

Prakash J, Gupta A, Kumar O, Rout SB, Malhotra V, Srivastava PK. Acute renal failure in Falciparum malaria - Increasing prevalence in some areas of India - A need for awareness. Nephrol Dial Transplant, 1996;11:2414-2416.

Prasad R, Lele S. Stabilization of the amorphous phase inside carbon nanotube - solidification in a constrained geometry. Philos Mag Lett, 1994;70:357-361.

Price RN. Artemisinin drugs: novel antimalarial agents. Expert Opin Investig Drugs, 2000;9:1815-1827.

Procházka J, Kavan L, Zukalová M, Frank O, KalbáČ M, Zukal AT, Klementová M, Carbone D, Graetzel M. Novel synthesis of the TiO2 (B) multilayer templated films. Chem Mater, 2009;21:1457-1464.

Qian KK, Bogner RH. Application of mesoporous silicon dioxide and silicate in oral amorphous drug delivery systems. J Pharm Sci, 2012;101:444-463.

R. P. Patel, M. P. Patel, A. M. Suthar. Spray drying technology: an overview. Indian J Sci Technol, 2009;2:44-47.

Rabinow BE. Nanosuspensions in drug delivery. Nat Rev Drug Discov, 2004;3:785-796.

Rahmat N, Abdullah AZ, Mohamed AR. A review: mesoporous santa barbara amorphous-15, types, synthesis and its applications towards biorefinery production. Am J Appl Sci, 2010;7:1579-1586.

Rao AB, Murthy RSR. A rapid spectrophotometric method for the determination of mefloquine hydrochloride. J Pharm Biomed Anal, 2002;27:959-965.

Rasenack N, Hartenhauer H, Müller BW. Microcrystals for dissolution rate enhancement of poorly water-soluble drugs. Int J Pharm, 2003;254:137-145.

Rasenack N, Muller BW. Dissolution rate enhancement by in situ micronization of poorly water-soluble drugs. Pharm Res, 2002;19:1894-1900.

Ré M-I. Formulating Drug Delivery Systems by Spray Drying. Drying Technol, 2006;24:433-446.

Rengarajan GT, Enke D, Steinhart M, Beiner M. Stabilization of the amorphous state of pharmaceuticals in nanopores. J Mater Chem, 2008;18:2537-2539.

Rey A, Zazo JA, Casas JA, Bahamonde A, Rodriguez JJ. Influence of the structural and surface characteristics of activated carbon on the catalytic decomposition of hydrogen peroxide. Appl Catal A Gen, 2011;402:146-155.

Ridley RG. Medical need, scientific opportunity and the drive for antimalarial drugs. Nature, 2002;415:686-693.

Ruenraroengsak P, Cook JM, Florence AT. Nanosystem drug targeting: facing up to complex realities. J Control Release, 2010;141:265-276.

Ruthstein S, Frydman V, Kababya S, Landau M, Goldfarb D. Study of the formation of the mesoporous material SBA-15 by EPR spectroscopy. J Phys Chem B, 2003;107:1739-1748.

Ryoo R, Kim JM, Ko CH, Shin CH. Disordered Molecular Sieve with Branched Mesoporous Channel Network. J Phys Chem, 1996;100:17718-17721.

Ryoo R, Ko CH, Kruk M, Antochshuk V, Jaroniec M. Block-copolymer-templated ordered mesoporous silica: Array of uniform mesopores or mesopore-micropore network? J Phys Chem B, 2000;104:11465-11471.

Sa JM, Chong JL, Wellems TE 2011. Malaria drug resistance: new observations and developments. Essays Biochem: 2011;51:137-160.

Saharan VA, Kukkar V, Kataria M, Gera M, Choudhury PK. Dissolution Enhancement of drugs. Part 1: technology and effect of carriers. Int J Health Res, 2009;2:107-124.

Sahoo NG, Abbas A, Judeh Z, Li CM, Yuen KH. Solubility enhancement of a poorly water-soluble anti-malarial drug: experimental design and use of a modified multifluid nozzle pilot spray drier. J Pharm Sci, 2009;98:281-96.

Sahoo NG, Kakran M, Abbas A, Judeh Z, Li L. Preparation, characterization and dissolution behavior of artemisinin microparticles. Adv Powder Technol, 2011a;22:458-463.

Sahoo NG, Kakran M, Li L, Judeh Z. Fabrication of composite microparticles of artemisinin for dissolution enhancement. Powder Technol, 2010;203:277-287.

Sahoo NG, Kakran M, Li L, Judeh Z, Müller RH. Dissolution enhancement of a poorly water-soluble antimalarial drug by means of a modified multi-fluid nozzle pilot spray drier. Mater Sci Eng C, 2011b;31:391-399.

Santos HA, Riikonen J, Salonen J, Mäkilä E, Heikkilä T, Laaksonen T, Peltonen L, Lehto V-P, Hirvonen J. In vitro cytotoxicity of porous silicon microparticles: Effect of the particle concentration, surface chemistry and size. Acta Biomater, 2010;6:2721-2731.

Salonen J, Kaukonen AM, Hirvonen J, Lehto VP. Mesoporous silicon in drug delivery applications. J Pharm Sci, 2008;97:632-53.

Salonen J, Laitinen L, Kaukonen AM, Tuura J, Bjorkqvist M, Heikkila T, Vaha-Heikkila K, Hirvonen J, Lehto VP. Mesoporous silicon microparticles for oral drug delivery: loading and release of five model drugs. J Control Release, 2005;108:362-374.

Sarode AL, Malekar SA, Cote C, Worthen DR. Hydroxypropyl cellulose stabilizes amorphous solid dispersions of the poorly water soluble drug felodipine. Carbohydr Polym, 2014;112:512-519.

Savjani KT, Gajjar AK, Savjani JK. Drug solubility: importance and enhancement techniques. ISRN Pharm, 2012;2012:1-10.

Schreier S, Malheiros SVP, De Paula E. Surface active drugs: self-association and interaction with membranes and surfactants. Physicochemical and biological aspects. Biochim Biophys Acta Acta-Biomembranes, 2000;1508:210-234.

Seedher N, Kanojia M. Micellar solubilization of some poorly soluble antidiabetic drugs: a technical note. AAPS PharmSciTech, 2008;9:431-436.

Seedher N, Kanojia M. Co-solvent solubilization of some poorly-soluble antidiabetic drugs. Pharm Dev Technol, 2009;14:185-192.

Sekiguchi K, Obi N. Studies on absorption of eutectic mixture .1. Comparison of behavior of eutectic mixture of sulfathiazole and that of ordinary sulfathiazole in man. Chem Pharm Bull, 1961;9:866-872.

Semalty A, Tanwar YS, Semalty M. Preparation and characterization of cyclodextrin inclusion complex of naringenin and critical comparison with phospholipid complexation for improving solubility and dissolution. J Therm Anal Calorim, 2014;115:2471-2478.

Serajuddin ATM. Solid dispersion of poorly water-soluble drugs: early promises, subsequent problems and recent breakthroughs. J Pharm Sci, 1999;88:1058-1066.

Shah PP, Mashru RC, Rane YM, Thakkar A. Design and optimization of mefloquine hydrochloride microparticles for bitter taste masking. AAPS PharmSciTech, 2008;9:377-89.

Shahidi F, Han XQ. Encapsulation of food ingredients. Crit Rev Food Sci Nutr, 1993;33:501-547.

Shahzad Y, Shah SNH, Ansari MT, Riaz R, Safdar A, Hussain T, Malik M. Effects of drug-polymer dispersions on solubility and in vitro diffusion of artemisinin across a polydimethylsiloxane membrane. Chin Sci Bull, 2012;57:1685-1692.

Shakeel F, Alanazi FK, Alsarra IA, Haq N. Solubility of antipsychotic drug risperidone in Transcutol plus water co-solvent mixtures at 298.15 to 333.15 K. J Mol Liq, 2014;191:68-72.

Sharma A, Jain CP. Solid dispersion: a promising technique to enhance solubility of poorly water soluble drug. Int J Drug Deliv 3, 2011;149-170.

Shen S-C, Ng WK, Chia L, Hu J, Tan RBH. Physical state and dissolution of ibuprofen formulated by co-spray drying with mesoporous silica: effect of pore and particle size. Int J Pharm, 2011;410:188-195.

Shen SC, Ng WK, Chia L, Dong YC, Tan RB. Stabilized amorphous state of ibuprofen by co-spray drying with mesoporous SBA-15 to enhance dissolution properties. J Pharm Sci, 2010;99:1997-2007.

Shete AS, Yadav AV, Murthy MS. Evaluation of performance of co crystals of mefloquine hydrochloride in tablet dosage form. Drug Dev Ind Pharm, 2013;39:716-723.

Shiraki K, Takata N, Takano R, Hayashi Y, Terada K. Dissolution improvement and the mechanism of the improvement from cocrystallization of poorly water-soluble compounds. Pharm Res, 2008;25:2581-2592.

Shono Y, Jantratid E, Kesisoglou F, Reppas C, Dressman JB. Forecasting in vivo oral absorption and food effect of micronized and nanosized aprepitant formulations in humans. Eur J Pharm Biopharm, 2010;76:95-104.

Shugarts S, Benet LZ. The role of transporters in the pharmacokinetics of orally administered drugs. Pharm Res, 2009;26:2039-2054.

Sigfridsson K, Lundqvist AJ, Strimfors M. Particle size reduction for improvement of oral absorption of the poorly soluble drug UG558 in rats during early development. Drug Dev Ind Pharm, 2009;35:1479-1486.

Sigurðoardóttir AM, Loftsson T. The effect of polyvinylpyrrolidone on cyclodextrin complexation of hydrocortisone and its diffusion through hairless mouse skin. Int J Pharm, 1995;126:73-78.

Simpson JA, Aarons L, Collins WE, Jeffery GM, White NJ. Population dynamics of untreated Plasmodium falciparum malaria within the adult human host during the expansion phase of the infection. Parasitology, 2002;124:247-263.

Sing KSW, Everett DH, Haul RaW, Moscou L, Pierotti RA, Rouquerol J, Siemieniewska T. Reporting physisorption data for gas solid systems with special reference to the determination of surface-area and porosity (recommendations 1984). Pure Appl Chem, 1985;57:603-619.

Singh MMC, Sayyad AB, Sawant DSD. Review on various techniques of solubility enhancement of poorly soluble drugs with special emphasis on solid dispersion. J Pharm Res, 2010;3:2494-2501.

Skolnik S, Lin X, Wang J, Chen X-H, He T, Zhang B. Towards prediction of in vivo intestinal absorption using a 96-well Caco-2 assay. J Pharm Sci, 2010;99:3246-3265.

Sliwinska-Bartkowiak M, Dudziak G, Gras R, Sikorski R, Radhakrishnan R, Gubbins KE. Freezing behavior in porous glasses and MCM-41. Colloids Surf A Physicochem Eng Asp, 2001;187-188:523-529.

Slowing II, Vivero-Escoto JL, Wu C-W, Lin VSY. Mesoporous silica nanoparticles as controlled release drug delivery and gene transfection carriers. Adv Drug Deliv Rev, 2008;60:1278-1288.

Snow RW, Guerra CA, Noor AM, Myint HY, Hay SI. The global distribution of clinical episodes of Plasmodium falciparum malaria. Nature, 2005;434:214-217.

Snow RW, Peshu N, Forster D, Mwenesi H, Marsh K. The role of shops in the treatment and prevention of childhood malaria on the coast of Kenya. Trans R Soc Trop Med Hyg, 1992;86:237-239.

Song SW, Hidajat K, Kawi S. Functionalized SBA-15 materials as carriers for controlled drug delivery: influence of surface properties on matrix-drug interactions. Langmuir, 2005;21:9568-9575.

Ståhl K, Claesson M, Lilliehorn P, Lindén H, Bäckström K. The effect of process variables on the degradation and physical properties of spray dried insulin intended for inhalation. J Pharm Sci, 2002;233:227-237.

Stein A. Advances in microporous and mesoporous solids - Highlights of recent progress. Adv Mater, 2003;15:763-775.

Strauch S, Jantratid E, Dressman JB, Junginger HE, Kopp S, Midha KK, Shah VP, Stavchansky S, Barends DM. Biowaiver monographs for immediate release solid oral dosage forms: mefloquine hydrochloride. J Pharm Sci, 2011;100:11-21.

Strickley RG. Solubilizing excipients in oral and injectable formulations. Pharm Res, 2004;21:201-230.

Stringham RW, Lynam KG, Mrozinski P, Kilby G, Pelczer I, Kraml C. High performance liquid chromatographic evaluation of artemisinin, raw material in the synthesis of artesunate and artemether. J Chromatogr A, 2009;1216:8918-8925.

Subramaniam B, Rajewski RA, Snavely K. Pharmaceutical processing with supercritical carbon dioxide. J Pharm Sci, 1997;86:885-890.

Sugano K, Okazaki A, Sugimoto S, Tavornvipas S, Omura A, Mano T. Solubility and dissolution profile assessment in drug discovery. Drug Metab Pharmacokinet, 2007;22:225-254.

Sun M, Si L, Zhai X, Fan Z, Ma Y, Zhang R, Yang X. The influence of co-solvents on the stability and bioavailability of rapamycin formulated in self-

microemulsifying drug delivery systems. Drug Dev Ind Pharm, 2011;37:986-994.

Sunesen VH, Pedersen BL, Kristensen HG, Mullertz A. In vivo in vitro correlations for a poorly soluble drug, danazol, using the flow-through dissolution method with biorelevant dissolution media. Eur J Pharm Sci, 2005;24:305-313.

Takagi T, Ramachandran C, Bermejo M, Yamashita S, Yu LX, Amidon GL. A provisional biopharmaceutical classification of the top 200 oral drug products in the United States, Great Britain, Spain and Japan. Mol Pharm, 2006;3:631-643.

Takeuchi H, Handa T, Kawashima Y. Spherical solid dispersion containing amorphous tolbutamide embedded in enteric coating polymers or colloidal silica prepared by spray-drying technique. Chem Pharm Bull, 1987;35:3800-3806.

Takeuchi H, Nagira S, Yamamoto H, Kawashima Y. Solid dispersion particles of tolbutamide prepared with fine silica particles by the spray-drying method. Powder Technol, 2004;141:187-195.

Takeuchi H, Nagira S, Yamamoto H, Kawashima Y. Solid dispersion particles of amorphous indomethacin with fine porous silica particles by using spray-drying method. J Pharm Sci, 2005;293:155-164.

Taylor SM, Molyneux ME, Simel DL, Meshnick SR, Juliano JJ. Does this patient have malaria? Jama, 2010;304:2048-2056.

Thu Hoa N, Vertommen J, Kinget R. Formulation of artemisinin tablets. Int J Pharm, 1997;146:271-274.

Thybo P, Hovgaard L, Lindelov JS, Brask A andersen SK. Scaling up the spray drying process from pilot to production scale using an atomized droplet size criterion. Pharm Res, 2008;25:1610-20.

Torchilin VP. Structure and design of polymeric surfactant-based drug delivery systems. J Control Release, 2001;73:137-172.

Tozuka Y, Imono M, Uchiyama H, Takeuchi H. A novel application of α-glucosyl hesperidin for nanoparticle formation of active pharmaceutical ingredients by dry grinding. Eur J Pharm Biopharm, 2011;79:559-565.

Tozuka Y, Kishi J, Takeuchi H. Anomalous dissolution property enhancement of naringenin from spray-dried particles with α-glucosylhesperidin. Adv Powder Technol, 2010;21:305-309.

Trampuz A, Jereb M, Muzlovic I, Prabhu RM. Clinical review: severe malaria. Crit Care, 2003;7:315-323.

Trape JF, Pison G, Preziosi MP, Enel C, Du Lou AD, Delaunay V, Samb B, et al. Impact of chloroquine resistance on malaria mortality. C R Acad Sci III, 1998;321:689-697.

Uchiyama H, Tozuka Y, Asamoto F, Takeuchi H. Fluorescence investigation of a specific structure formed by aggregation of transglycosylated stevias: solubilizing effect of poorly water-soluble drugs. Eur J Pharm Sci, 2011a;43:71-77.

Uchiyama H, Tozuka Y, Asamoto F, Takeuchi H. α-Glucosyl hesperidin induced an improvement in the bioavailability of pranlukast hemihydrate using high-pressure homogenization. Int J Pharm, 2011b;410:114-117.

Uchiyama H, Tozuka Y, Imono M, Takeuchi H. Improvement of dissolution and absorption properties of poorly water-soluble drug by preparing spray-dried powders with α-glucosyl hesperidin. J Pharm Sci, 2010a;392:101-6.

Uchiyama H, Tozuka Y, Imono M, Takeuchi H. Transglycosylated stevia and hesperidin as pharmaceutical excipients: dramatic improvement in drug dissolution and bioavailability. Eur J Pharm Biopharm, 2010b;76:238-44.

Uekama K, Hirayama F, Irie T. Cyclodextrin drug carrier systems. Chem Rev, 1998;98:2045-2076.

Unger K, Rupprecht H, Valentin B, Kircher W. The use of porous and surface modified silicas as drug delivery and stabilizing agents. Drug Dev Ind Pharm, 1983;9:69-91.

Valizadeh H, Nokhodchi A, Qarakhani N, Zakeri-Milani P, Azarmi S, Hassanzadeh D, Lobenberg R. Physicochemical characterization of solid dispersions of indomethacin with PEG 6000, Myrj 52, lactose, sorbitol, dextrin and Eudragit (R) E100. Drug Dev Ind Pharm, 2004;30:303-317.

Vallet-Regi M, Rámila A, Del Real RP, Pérez-Pariente J. A new property of MCM-41: drug delivery system. Chem Mater, 2000;13:308-311.

Van Den Mooter G. The use of amorphous solid dispersions: a formulation strategy to overcome poor solubility and dissolution rate. Drug Discov Today: Technologies, 2012;9:e79-e85.

Van Drooge DI, Hinrichs WLJ, Frijlink HW. Incorporation of lipophilic drugs in sugar glasses by lyophilization using a mixture of water and tertiary butyl alcohol as solvent. J Pharm Sci, 2004;93:713-725.

Van Eerdenbrugh B, Vermant J, Martens JA, Froyen L, Humbeeck JV, Van Den Mooter G, Augustijns P. Solubility increases associated with crystalline drug nanoparticles: methodologies and significance. Mol Pharm, 2010;7:1858-1870.

Van Nijlen T, Brennan K, Van Den Mooter G, Blaton N, Kinget R, Augustijns P. Improvement of the dissolution rate of artemisinin by means of supercritical fluid technology and solid dispersions. Int J Pharm, 2003;254:173-181.

Van Speybroeck M, Barillaro V, Thi TD, Mellaerts R, Martens J, Van Humbeeck J, Vermant J, et al. Ordered mesoporous silica material SBA-15: a broad-spectrum formulation platform for poorly soluble drugs. J Pharm Sci, 2009;98:2648-2658.

Van Speybroeck M, Mellaerts R, Mols R, Thi TD, Martens JA, Van Humbeeck J, Annaert P, Van Den Mooter G, Augustijns P. Enhanced absorption of the poorly soluble drug fenofibrate by tuning its release rate from ordered mesoporous silica. Eur J Pharm Sci, 2010a;41:623-630.

Van Speybroeck M, Mellaerts R, Thao Do T, Martens JA, Van Humbeeck J, Annaert P, Van Den Mooter G, Augustijns P. Preventing release in the acidic environment of the stomach via occlusion in ordered mesoporous silica enhances the absorption of poorly soluble weakly acidic drugs. J Pharm Sci, 2011;100:4864-4876.

Van Speybroeck M, Mols R, Mellaerts R, Thi TD, Martens JA, Humbeeck JV, Annaert P, Mooter GVD, Augustijns P. Combined use of ordered mesoporous silica and precipitation inhibitors for improved oral absorption of the poorly soluble weak base itraconazole. Eur J Pharm Biopharm, 2010b;75:354-365.

Vasanthavada M, Tong WQ, Joshi Y, Kislalioglu MS. Phase behavior of amorphous molecular dispersions I: Determination of the degree and mechanism of solid solubility. Pharm Res, 2004;21:1598-1606.

Vasconcelos T, Sarmento B, Costa P. Solid dispersions as strategy to improve oral bioavailability of poor water soluble drugs. Drug Discov Today, 2007;12:1068-1075.

Vemula VR, Lagishetty V, Lingala S. Solubility enhancement techniques. Int J Pharm Sci Rev Res, 2010;5:41-51.

Vialpando M, Aerts A, Persoons J, Martens J, Van Den Mooter G. Evaluation of ordered mesoporous silica as a carrier for poorly soluble drugs: influence of pressure on the structure and drug release. J Pharm Sci, 2011;100:3411-3420.

Vinu A, Hossain KZ, Ariga K. Recent advances in functionalization of mesoporous silica. J Nanosci Nanotechnol, 2005;5:347-371.

Viscomi GC, Campana M, Barbanti M, Grepioni F, Polito M, Confortini D, Rosini G, et al. Crystal forms of rifaximin and their effect on pharmaceutical properties. CrystEngComm, 2008;10:1074-1081.

Vogt M, Kunath K, Dressman JB. Dissolution enhancement of fenofibrate by micronization, cogrinding and spray-drying: comparison with commercial preparations. Eur J Pharm Biopharm, 2008a;68:283-288.

Vogt M, Vertzoni M, Kunath K, Reppas C, Dressman JB. Cogrinding enhances the oral bioavailability of EMD 57033, a poorly water soluble drug, in dogs. Eur J Pharm Biopharm, 2008b;68:338-345.

Waehling C, Schroeter C, Hanefeld A. Flow-Through Cell Method and IVIVR for Poorly Soluble Drugs. Dissolut Technol, 2011;18:15-24.

Wan S, Sun Y, Qi X, Tan F. Improved bioavailability of poorly water-soluble drug curcumin in cellulose acetate solid dispersion. AAPS PharmSciTech, 2011;13:159-166.

Wan Y, Zhao DY. On the controllable soft-templating approach to mesoporous silicates. Chem Rev, 2007;107:2821-2860.

Wang F, Hui H, Barnes TJ, Barnett C, Prestidge CA. Oxidized mesoporous silicon microparticles for improved oral delivery of poorly soluble drugs. Mol Pharm, 2010;7:227-236.

Wang SB. Ordered mesoporous materials for drug delivery. Microporous and Mesoporous Mater, 2009;117:1-9.

Wang X, Liu P, Tian Y. Ordered mesoporous carbons for ibuprofen drug loading and release behavior. Microporous and Mesoporous Mater, 2011a;142:334-340.

Wang X, Liu P, Tian Y, Zang L. Novel synthesis of Fe-containing mesoporous carbons and their release of ibuprofen. Microporous and Mesoporous Mater, 2011b;145:98-103.

Wang Y, Zhao Q, Hu Y, Sun L, Bai L, Jiang T, Wang S. Ordered nanoporous silica as carriers for improved delivery of water insoluble drugs: a comparative study between three dimensional and two dimensional macroporous silica. Int J of Nanomedicine, 2013;8:4015-4031.

Wang YM, Sato H, Adachi I, Horikoshi I. Preparation and characterization of poly(lactic-co-glycolic acid) microspheres for targeted delivery of a novel anticancer agent, Taxol. Chem Pharm Bull, 1996;44:1935-1940.

Warrell DA, Looareesuwan S, Warrell MJ, Kasemsarn P, Intaraprasert R, Bunnag D, Harinasuta T. Dexamethasone proves deleterious in cerebral malaria - a double-blind trial in 100 comatose patients. N Engl J Med, 1982;306:313-319.

Watanabe T, Hasegawa S, Wakiyama N, Kusai A, Senna M. Comparison between polyvinylpyrrolidone and silica nanoparticles as carriers for indomethacin in a solid state dispersion. J Pharm Sci, 2003;250:283-286.

Watanabe T, Ohno I, Wakiyama N, Kusal A, Senna M. Controlled dissolution properties of indomethacin by compounding with silica. Stp Pharma Sci, 2002;12:363-367.

Watanabe T, Wakiyama N, Usui F, Ikeda M, Isobe T, Senna M. Stability of amorphous indomethacin compounded with silica. J Pharm Sci, 2001;226:81-91.

Watkins WM, Mberu EK, Winstanley PA, Plowe CV. The efficacy of antifolate antimalarial combinations in Africa: a predictive model based on pharmacodynamic and pharmacokinetic analyses. Parasitol Today, 1997;13:459-464.

Wells S, Diap G, Kiechel J-R. The story of artesunate-mefloquine (ASMQ), innovative partnerships in drug development: case study. Malar J, 2013;12:68.

Wen X, Tan F, Jing Z, Liu Z. Preparation and study the 1:2 inclusion complex of carvedilol with β-cyclodextrin. J Pharm Biomed Anal, 2004;34:517-523.

Wernsdorfer WH. Epidemiology of drug-resistance in malaria. Acta Trop, 1994;56:143-156.

White N. Antimalarial drug resistance and combination chemotherapy. Philos Trans R Soc Lond B Biol Sci, 1999a;354:739-49.

White NJ. Assessment of the pharmacodynamic properties of antimalarial drugs in vivo. Antimicrob Agents Chemother, 1997;41:1413-1422.

White NJ. Preventing antimalarial drug resistance through combinations. Drug Resist Updat, 1998;1:3-9.

White NJ. Delaying antimalarial drug resistance with combination chemotherapy. Parassitologia (Rome), 1999b;41:301-308.

White NJ. Antimalarial drug resistance. J Clin Invest, 2004;113:1084-1092.

White NJ, Olliaro PL. Strategies for the prevention of antimalarial drug resistance: rationale for combination chemotherapy for malaria. Parasitol Today, 1996;12:399-401.

White NJ, Pukrittayakamee S, Hien TT, Faiz MA, Mokuolu OA, Dondorp AM. Malaria. Lancet, 2014;383:723-735.

Wong JW, Yuen KH. Improved oral bioavailability of artemisinin through inclusion complexation with β- and γ-cyclodextrins. Int J Pharm, 2001;227:177-185.

Wu C, Wang, Chen B, Quan, Li, Wu, Dian, Dong. Increasing the oral bioavailability of poorly water-soluble carbamazepine using immediate-release pellets supported on SBA-15 mesoporous silica. Int J of Nanomedicine, 2012;7:5807-5818.

Xi J, Qiu X, Ma X, Cui M, Yang J, Tang X, Zhu W, Chen L. Composite polymer electrolyte doped with mesoporous silica SBA-15 for lithium polymer battery. Solid State Ionics, 2005;176:1249-1260.

Xia X, Zhou C, Ballell L, Garcia-Bennett AE. In vivo enhancement in bioavailability of atazanavir in the presence of proton-pump inhibitors using mesoporous materials. Chemmedchem, 2012;7:43-48.

Xu W, Gao Q, Xu Y, Wu D, Sun Y, Shen W, Deng F. Controllable release of ibuprofen from size-adjustable and surface hydrophobic mesoporous silica spheres. Powder Technol, 2009;191:13-20.

Yadav AV, Dabke AP, Shete AS. Crystal engineering to improve physicochemical properties of mefloquine hydrochloride. Drug Dev Ind Pharm, 2010;36:1036-1045.

Yalkowsky SH, Rubino JT. Solubilization by cosolvents .1. Organic solutes in propylene-glycol water mixtures. J Pharm Sci, 1985;74:416-421.

Yamanaka YJ, Leong KW. Engineering strategies to enhance nanoparticle-mediated oral delivery. J Biomater Sci Polym Ed, 2008;19:1549-1570.

Yaméogo JBG, Gèze A, Choisnard L, Putaux J-L, Gansané A, Sirima SB, Semdé R, Wouessidjewe D. Self-assembled biotransesterified cyclodextrins as artemisinin nanocarriers – I: formulation, lyoavailability and in vitro antimalarial activity assessment. Eur J Pharm Biopharm, 2012;80:508-517.

Yang B, Lin J, Chen Y, Liu Y. Artemether/hydroxypropyl-β-cyclodextrin host-guest system: characterization, phase-solubility and inclusion mode. Bioorg Med Chem, 2009;17:6311-6317.

Yang B, Wang J, Huang R, Zhao Y-L, Yang J. Binding behavior of artemether/sulfobutyl ether β-cyclodextrin in solution and the solid state. Monatsh Chem, 2011;143:235-241.

Yang CC, Zheng YR. Improved the performance of dye-sensitized solar cells by incorporating mesoporous silica (SBA-15) materials in scattering layer. J Power Sources, 2012;201:387-394.

Yasuji T, Takeuchi H, Kawashima Y. Particle design of poorly water-soluble drug substances using supercritical fluid technologies. Adv Drug Deliv Rev, 2008;60:388-398.

Yoshioka S, Aso Y. Correlations between molecular mobility and chemical stability during storage of amorphous pharmaceuticals. J Pharm Sci, 2007;96:960-81.

Yu BG, Okano T, Kataoka K, Kwon G. Polymeric micelles for drug delivery: solubilization and haemolytic activity of amphotericin B. J Control Release, 1998;53:131-136.

Yu CZ, Yu YH, Zhao DY. Highly ordered large caged cubic mesoporous silica structures templated by triblock PEO-PBO-PEO copolymer. Chem Commun, 2000;575-576.

Yu H, Zhao X, Zu Y, Zhang X, Zu B, Zhang X. Preparation and characterization of micronized artemisinin via a Rapid Expansion of Supercritical Solutions (RESS) method. Int J Mol Sci, 2012a;13:5060-5073.

Yu LX. Use and Limitations of In Vitro Dissolution Testing: Topic Introduction and Overview. 2012b.

Yu LX, Amidon GL, Polli JE, Zhao H, Mehta MU, Conner DP, Shah VP, et al. Biopharmaceutics classification system: the scientific basis for biowaiver extensions. Pharm Res, 2002;19:921-925.

Zeng A-G, Pang X-L, Wu N, Wang D, Nan G-J, Yang G-D, Bian X-L. Solubility of daidzein in propylene glycol plus water cosolvent mixtures. Fluid Phase Equilib, 2014;366:127-133.

Zeng W, Qian X-F, Zhang Y-B, Yin J, Zhu Z-K. Organic modified mesoporous MCM-41 through solvothermal process as drug delivery system. Mater Res Bull, 2005;40:766-772.

Zhang F, Aaltonen J, Tian F, Saville D, Rades T. Influence of particle size and preparation methods on the physical and chemical stability of amorphous simvastatin. Eur J Pharm Biopharm, 2009a;71:64-70.

Zhang H, Sun J, Ma D, Bao X, Klein-Hoffmann A, Weinberg G, Su D, Schlögl R. Unusual Mesoporous SBA-15 with Parallel Channels Running along the Short Axis. J Am Chem Soc, 2004;126:7440-7441.

Zhang H-X, Wang J-X, Zhang Z-B, Le Y, Shen Z-G, Chen J-F. Micronization of atorvastatin calcium by antisolvent precipitation process. Int J Pharm, 2009b;374:106-113.

Zhang P, Forsgren J, Stromme M. Stabilisation of amorphous ibuprofen in Upsalite, a mesoporous magnesium carbonate, as an approach to increasing the aqueous solubility of poorly soluble drugs. J Pharm Sci, 2014;472:185-191.

Zhang Y, Wang J, Bai X, Jiang T, Zhang Q, Wang S. Mesoporous silica nanoparticles for increasing the oral bioavailability and permeation of poorly water soluble drugs. Mol Pharm, 2012;9:505-513.

Zhang Y, Zhang J, Jiang T, Wang S. Inclusion of the poorly water-soluble drug simvastatin in mesocellular foam nanoparticles: drug loading and release properties. Int J Pharm, 2011;410:118-124.

Zhao DY, Feng JL, Huo QS, Melosh N, Fredrickson GH, Chmelka BF, Stucky GD. Triblock copolymer syntheses of mesoporous silica with periodic 50 to 300 angstrom pores. Science, 1998;279:548-552.

Zhao P, Jiang H, Jiang T, Zhi Z, Wu C, Sun C, Zhang J, Wang S. Inclusion of celecoxib into fibrous ordered mesoporous carbon for enhanced oral bioavailability and reduced gastric irritancy. Eur J Pharm Sci, 2012a;45:639-647.

Zhao P, Wang L, Sun C, Jiang T, Zhang J, Zhang Q, Sun J, Deng Y, Wang S. Uniform mesoporous carbon as a carrier for poorly water soluble drug and its cytotoxicity study. Eur J Pharm Biopharm, 2012b;80:535-543.

Zhao Q, Wang T, Wang J, Zheng L, Jiang T, Cheng G, Wang S. Fabrication of mesoporous hydroxycarbonate apatite for oral delivery of poorly water-soluble drug carvedilol. J Non Cryst Solids, 2012c;358:229-235.

Zhu S, Chen C, Chen Z, Liu X, Li Y, Shi Y, Zhang D. Thermo-responsive polymer-functionalized mesoporous carbon for controlled drug release. Mater Chem Phys, 2011;126:357-363.

APPENDICES

A1. List of Publications

1. Kumaran Letchmanan, Shou-Cang Shen, Wai Kiong Ng, Reginald B.H. Tan, Enhancing Solubility and Physical Stability of Poorly Aqueous Soluble Artemisinin via Co-spray Drying with Activated Carbon. Tropical Journal of Pharmaceutical Research. (Accepted on Feb 2015)
2. Letchmanan K, S-C Shen, WK Ng, RBH Tan. Enhanced dissolution and stability of artemisinin by nano-confinement in ordered mesoporous SBA-15 particles. J Microencapsul, 2015; 32: 1-11.

A2. Conferences

1. Kumaran Letchmanan, Shou-Cang Shen, Wai Kiong Ng, Reginald B.H. Tan, Enhancing bioavailability through formulating amorphous forms with porous biocompatible excipients. Inaugural GSK-Singapore Partnership for Green and Sustainable Manufacturing (GSM) Symposium 2013, 12–13 Mar 2013
2. Kumaran Letchmanan, Shou-Cang Shen, Wai Kiong Ng, Reginald B.H. Tan, Enhancing bioavailability through formulating amorphous forms with porous biocompatible excipients. ISPE Singapore Student Poster Competition at ISPE Singapore Conference in association with Interphex Asia 2013, 1 July 2013
3. Kumaran Letchmanan, Shou-Cang Shen, Wai Kiong Ng, Reginald B.H. Tan, bioavailability enhancement of artemisinin through amorphization by

nano-confinement via co-spray drying with ordered mesoporous silica. The European Summit for Clinical Nanomedicine and Targeted Medicine 2014 (7^{th} CLINAM 2014), Basel, Switzerland, June 23-25, 2014